TEMPERATURE DEPENDENCE OF THE OPTICAL PROPERTIES OF Au AND Ag

P. WINSEMIUS

STELLINGEN

1. Vestigingen van zogenaamde multinationale ondernemingen vormen een veelal onmisbare bijdrage tot een spoedige ontplooiing van de economie der ontwikkelingslanden.

2. De ruwheid van het oppervlak van gloeiende metalen ten gevolge van thermisch etsen leidt tot fouten in de bepaling van de temperatuur van het massieve metaal met behulp van optische pyrometers.

L.K. Thomas; 1968, J.Appl.Phys. 39, 3737.

3. De metingen betreffende de temperatuurafhankelijkheid van de uittreepotentiaal van niobium en lood zoals uitgevoerd door respectievelijk De Waele en Kunz zijn ten gevolge van oxydatie van en adsorptie aan de preparaten eerder representatief voor de oppervlaktelaag dan voor het zuivere metaal.

A.Th.A.M. de Waele; proefschrift Leiden, 1972, deel II.
L.W. Kunz; 1971, Phys.Rev.Letters 26, 1311.

4. Bij de verandering van de eigenschappen van opgedampte laagjes SiO_x ($0 < x < 2$) ten gevolge van bestraling met ultraviolet licht en/of verhitting speelt behalve de binding van - bij het opdampen - ingevangen zuurstof, zoals voorgesteld door Philipp, ook diffusie van zuurstof van buiten af een rol.

H.R. Philipp; 1971, J.Phys.Chem.Solids 32, 1935.

5. De uitleg door Pétrakian et al. van de absorptiestruktuur waargenomen aan yttrium bij een fotonenergie van ongeveer 5,6 eV is foutief. Deze struktuur wordt veroorzaakt door overgangen van elektronen vanuit begintoestanden met een energieniveau van ongeveer 3.2 eV beneden het Fermi niveau.

J.P. Pétrakian, J.P. Palmari, G. Rasigni;
1970, Appl.Optics 9, 2115.

6. De definitie van de absorptiecoëfficiënt van licht in metalen als zijnde $4\pi nk/\lambda$ (n: brekingsindex, k: uitdovingscoëfficiënt, λ: golflengte van het licht in vacuüm), zoals o.a. gegeven door Mott en Jones en door Ziman, berust veeleer op een intuïtieve dan op een theoretische basis.

N.F. Mott, H. Jones; "The Theory of the Properties of Metals and Alloys" (Dover, New York, 1958), p. 108.
J.M. Ziman; "Principles of the Theory of Solids" (Cambridge University Press, Cambridge, 1965), p. 221.

7. De metingen van Pells en Montgomery aan de legeringssystemen CuZn, CuGa, CuGe, CuAs kunnen beter worden uitgelegd met behulp van een legeringsmodel zoals voorgesteld door Miedema dan met het "rigid band" model zoals door hen gesuggereerd.

G.P. Pells, H. Montgomery; 1970, J.Phys.C3: Suppl. Metal Physics 3, S330.
A.R. Miedema; 1973, Philips techn. T. 33, 157, 204.

8. Voor een berekening van de toestandsdichtheid met behulp van de coherente potentiaal benadering (C.P.A.) is het legeringssysteem AgCu meer aan te bevelen dan de tot nu toe gekozen systemen.

bijv. S. Kirkpatrick, B. Velický, H. Ehrenreich; 1970, Phys.Rev. B 1, 3250.
G.M. Stocks; 1971, Intern. J. Quantum Chem. 5, 533.

9. Meting van de temperatuurafhankelijkheid van optische eigenschappen kan een belangrijke bijdrage leveren tot de oplossing van het z.g. $AuGa_2$ dilemma.

bijv. J.E. Schirber, A.C. Switendick; 1970, Solid State Comm. 8, 1383.
W.W. Warren et al.; 1973, Phys.Rev. B 7, 1247.

P. Winsemius

Leiden, 4 september 1973

TEMPERATURE DEPENDENCE OF THE OPTICAL PROPERTIES OF Au AND Ag

PROEFSCHRIFT

TER VERKRIJGING VAN DE GRAAD VAN DOCTOR IN DE WISKUNDE EN NATUURWETENSCHAPPEN AAN DE RIJKSUNIVERSITEIT TE LEIDEN, OP GEZAG VAN DE RECTOR MAGNIFICUS DR. A. E. COHEN, HOOGLERAAR IN DE FACULTEIT DER LETTEREN, VOLGENS BESLUIT VAN HET COLLEGE VAN DEKANEN TE VERDEDIGEN OP DINSDAG 4 SEPTEMBER 1973 TE KLOKKE 14.15 UUR

DOOR

PIETER WINSEMIUS

GEBOREN TE VOORBURG IN 1942

1973

DRUKKERIJ J. H. PASMANS, 'S-GRAVENHAGE

Promotor : Prof. dr. C.J. Gorter
Co-promotor : Prof. dr. W.J. Huiskamp
Co-referent : dr. G.J. van den Berg

This investigation is part of the research program of the "Stichting voor Fundamenteel Onderzoek der Materie (F.O.M.)", which is financially supported by the "Nederlandse Organisatie voor Zuiver-Wetenschappelijk Onderzoek (Z.W.O.)" and by the "Centrale Organisatie voor Toegepast-Natuurwetenschappelijk Onderzoek (T.N.O.)".

aan *hannah*
albert
gijs

Table of Contents

Guide to reading.

Vectors are underlined, e.g. $\underline{E}$.

Complex quantities are indicated a tilde, e.g. $\tilde{E}$.

Complex conjugates are indicated by an asterisk, e.g. $\tilde{E}^*$.

Some abbreviations are frequently used in the text; for easy reference they are listed below:

APW : augmented plane wave (section 2.2.1.),

RAPW : relativistic augmented plane wave (section 2.2.1.),

DOS : density of states (sections 2.2.5., 2.5.1.3.),

JDOS : joint density of states (sections 2.2.5., 2.5.1.3.),

PJDOS : partial joint density of states (sections 2.2.5., 2.5.1.3.),

EDJDOS: energy distribution of the JDOS (section 2.7.2.1.),

XPS : X-ray photoelectron spectroscopy (section 2.9.3.).

CHAPTER I: PREFACE

1.1.1. *Why.*

Knowledge of the electron structure of matter is of fundamental importance in the evaluation of its properties and its possibilities. Going from one element to the next in the periodic system the essential change is in the number of electrons. Still the characteristic physical properties of two neighbouring elements may be considerably different, a good example being the variation of the magnetic properties of the transition metals. Study of such properties clearly yields information on the electron structure.

Theoretical calculations of the electron energy band structure depend largely upon the choice of a suitable crystal potential. In the case of the noble metals the energy bands directly at the Fermi level are not very sensitive to the choice of potential and consequently Fermi surface experiments (transport properties, specific heat, magnetic properties, De Haas-Van Alphen effect, cyclotron resonance, etc.) yield little discrimininative data. Knowledge of the width and position of the much more critical *d* bands and of the unoccupied conduction bands does provide such information. Only by "optical" means is it possible to probe sufficiently far below and above the Fermi level.

The noble metals are of particular importance in this respect. Cu has served as a test case for theory and experiment and recently the agreement has been rather convincing. Ag and especially Au proved to be more troublesome. Being heavier metals relativistic effects had to be included in the energy band calculations. The results of such calculations first appeared about five years ago. Apart from spin-orbit splitting effects the major change with respect to non-relativistic calculations was in the $L_{2'} \rightarrow L_1$ separation that was found to decrease by as

much as 3 eV. As pointed out in section 1.1.3. the experimental determination of this energy gap has been one of the main objectives of this research.

1.1.2. *When.*

For a long time the optical properties have made a major contribution to the development of physics. As a matter of fact Leiden has played a prominent part in the early stages. In 1875, when attention was concentrated on electromagnetic foundations, Lorentz wrote his thesis on the theory of reflection and diffraction of light. His subsequent work in this field (a.o. optical properties of moving media, magneto-optics) has been of major importance (e.g. Lorentz, Collected Papers (1935)). The first issue of the Communications of the (at that time) Laboratory of Physics opens with a summary of the thesis of Sissingh (1885) on the temperature dependence of the optical properties of Ag and Fe. This work was continued and expanded by Zeeman who after finishing his thesis on magneto-optical effects in metals (1893) side-stepped to discover the Zeeman effect. With the theoretical contribution of Lorentz and amongst others the theoretical and experimental pioneering work of Drude these efforts culminated in the classical electron theory.

In a second period of major theoretical progress in the understanding of the electron structure of matter Kronig (1929,1931) bridged the gap between the new quantum mechanics and the analysis of the optical properties (a.o. direct transitions). The first attempts at band calculations were predestined to remain primitive in the absence of suitable calculating facilities.

However, an explosive expansion of activities in this field can be noted during the last decade. The detailed calculation of electron energy band structures is made possible through extensive use of computers, whereas mathematical techniques (e.g. interpolation schemes, relativistic calculation) were further developed. Experimentally progress was made both in established techniques (lock-in amplification, ultra high vacuum, vacuum ultraviolet spectroscopy using a.o. synchrotron radiation) and in the opening of new fields (modulation spectroscopy, photoemission, ESCA).

In 1966 Dr. C. van Baarle took the initiative to a re-awakened interest at the Kamerlingh Onnes Laboratory in the optical properties. Originally intended as part of a research program on alloys it was later found that highly accurate measurements on the temperature dependence of the optical properties of pure metals provide valuable information on the band structure.

1.1.3. *How.*

Rather infrequent use has been made of the tool "temperature variation". Still from band calculations it is known that temperature changes can have a pronounced effect on the band structure. Schematically this may be visualized as in figure 1-1: at higher temperatures the interatomic spacing increases and the band stucture becomes more "atom-like". The "*s* bands" narrow, whereas the "*d* bands" in addition are shifted to lower energy. More specifically band calculations performed for varying lattice spacings predict an extreme sensitivity of transitions between the partially occupied lower conduction band (band 6) and the unoccupied "upper" conduction band (band 7). These transitions are expected to occur in the vicinity of the ΓL symmetry axis of the Brillouin zone, interest being centered on the critical interband point $L_4^- \rightarrow L_4^+$ (non-relativistic = $L_{2'} \rightarrow L_1$). The location of this energy gap yields one of the most

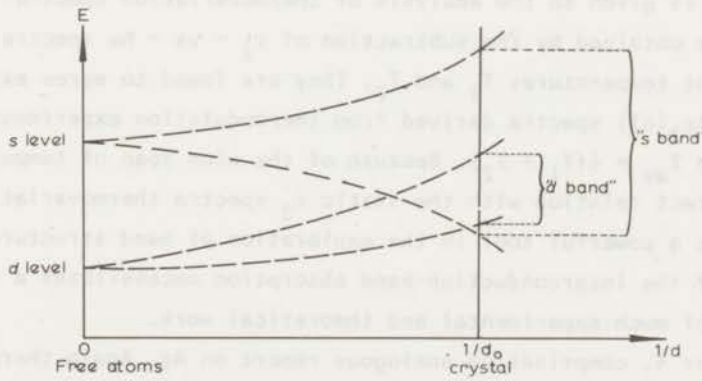

Fig. 1-1: Origin of the band structure in noble metals. Energy levels versus 1/d, d being the interatomic spacing.

valuable tests for the accuracy of band calculations - as a matter of fact semi-empirical calculations often rely heavily of knowledge of this parameter. It is with this in mind that the analysis of the temperature dependence of the optical properties of Au and Ag is concentrated to a large extent on the interconduction-band structure.

1.2 *Organization.*

In chapter 2. an introduction is given to the general backgrounds of this type of experiment and the analysis thereof. By no means this introduction pretends to provide a rigid theoretical foundation; wherever necessary references are given to more complete literature. The one--electron approach, that is used almost exclusively throughout this thesis, is known to have its limitations. It excludes electron-electron and electron-phonon interactions and necessitates a somewhat phenomenological treatment of intraband transitions. In this chapter a choice is made from the bewildering assortment of terminologies, basical concepts are introduced, possible sources of temperature dependence are evaluated and some models of general use are discussed.

Chapter 3. gives an account of very extensive series of measurements on Au. Some fine structure in the ε_2/λ spectra is reported, most notably a "splitting" of the absorption edge at low temperatures. However, most importance is given to the analysis of thermovariation spectra. These spectra are obtained by the subtraction of ε_2 - vs - $\hbar\omega$ spectra measured at different temperatures T_1 and T_2. They are found to agree extremely well with $\Delta\varepsilon_2(\Delta T)$ spectra derived from thermodulation experiments at a temperature $T_{av} = \frac{1}{2}(T_1 + T_2)$. Because of the wide span of temperatures and the direct relation with the static ε_2 spectra thermovariation is found to be a powerful tool in the exploration of band structures. The analysis of the interconduction-band absorption necessitates a re-interpretation of much experimental and theoretical work.

Chapter 4. comprises an analogous report on Ag. Again thermovariation results suggest an alternative explanation of interconduction-band absorption. Very interestingly they also cast some doubt on the usual analysis of transitions involving final states near the Fermi surface.

In chapter 5. we give a critical assessment of the experimental set--up that is required to perform ellipsometric measurements (Beattie's method) on bulk samples and to do so with a high accuracy. It is hoped that the information gathered in this chapter will be of help to other people entering this or a related field.

CHAPTER 2: BASIS

2.1. *Electromagnetism: optical properties.*

A brief introduction is given to demonstrate the relation of the measurable parameters to the macroscopic theory of electromagnetism. A great many textbooks deal with this matter, our preference going to the review article by F. Stern (1963). Throughout this thesis we will use mks units: it should be noted that the nomenclature differs from that used by Stern.

2.1.1. *Modified Muller Nebraska Convention.*

Understanding of the electromagnetic backgrounds of the optical properties of metals dawned only long after the practical need for a terminology had taken charge. Almost every stage of theoretical progress brought along new definitions. This has led to a great deal of confusion and has made much literature difficult to read.

At the 1969 Symposium on Recent Developments in Ellipsometry held at Lincoln, Nebraska R.H. Muller (1969a) gave a critical survey of definitions and conventions in ellipsometry. His indicated preferences were modified through a contribution by H.E. Bennett, the name Muller Nebraska Convention being proposed by J. Kruger. This convention is used throughout this thesis.

2.1.2. *Maxwell's equations.*

An electromagnetic field may be represented by an electric field vector $\underline{E}$ and a magnetic field vector $\underline{B}$. The interaction of such a field with an infinite conducting medium is described by Maxwell's equations, which in the absence of free charge or current sources may be written (Stratton (1941), p. 268)

$$\underline{\nabla}\cdot\underline{B} = 0 \quad , \tag{2-1a}$$

$$\underline{\nabla}\cdot\underline{E} = 0 \quad , \tag{2-1b}$$

$$\underline{\nabla} \times \underline{E} = -\partial\underline{B}/\partial t \quad , \tag{2-1c}$$

$$\underline{\nabla} \times \underline{B} = \mu\sigma\underline{E} + \mu\varepsilon(\partial\underline{E}/\partial t) \quad . \tag{2-1d}$$

The physical parameters of the medium are characterized by the values of the dielectric constant ε, the magnetic permeability μ, and the specific conductivity σ. These then are the fundamental quantities, that are to be measured from experimental observation of the electromagnetic wave motion.

The dielectric constant and magnetic permeability in vacuum - respectively ε_0 and μ_0 - are related by

$$c = (\varepsilon_0 \mu_0)^{-\frac{1}{2}} \tag{2-2}$$

where c is the velocity of propagation of light in vacuum. One can distinguish the effect of matter on an electromagnetic wave by writing

$$\varepsilon \underline{E} = \varepsilon_0 \underline{E} + \underline{P} = \varepsilon_0 \varepsilon_r \underline{E},$$

$$\underline{B}/\mu = \underline{B}/\mu_0 - \underline{M} = \underline{B}/(\mu_0 \mu_r).$$

In these formulas $\underline{P}$ is the polarization (the electric dipole moment per unit volume) and $\underline{M}$ is the magnetization (the magnetic moment per unit volume). Also introduced are the dimensionless relative dielectric constant $\varepsilon_r = \varepsilon/\varepsilon_0$ and the relative magnetic permeability $\mu_r = \mu/\mu_0$.

2.1.3. *Dispersion.*

In the range covered by optical means the field frequencies usually are of the order of magnitude of the eigenfrequencies of the electronic vibrations that lead to electric polarization. Any microscopic model - whether classical or quantum-mechanical - predicts a phase-shift between the polarization $\underline{P}$ and the electric field $\underline{E}$. The dielectric constant will be a function not only of the properties of the medium but also of the frequency (Landau and Lifshitz (1960), p. 249). The relation expressing this frequency dependence is called its dispersion law.

Similar arguments hold for the magnetic permeability and the specific conductivity. It might be noted, however, that the eigenfrequencies responsible for magnetization usually are quite different from those

causing polarization. Actually at optical frequencies the magnetization processes will not be able to follow the variation of the field at all. Therefore - even for ferromagnetic metals - the dispersion will be such, that one may assume (Landau (1960) and Lifshitz, p. 188, 251)

$$\mu_r = 1. \tag{2-3}$$

For anisotropic materials the dispersion relations become quite complicated, e.g. the dielectric constant is a tensor. However, our specimens are either cubic crystals or fine-grain polycrystalline ones, and are therefore considered to be homogeneous and isotropic (i.e. the physical properties at each point are independent of place and direction). We will refer only to this type of materials.

2.1.4. *Complex dielectric constant; complex refractive index.*

From eqs. 2-1c, 1d, 3 and the vector identity $\underline{\nabla} \times (\underline{\nabla} \times \underline{E}) = \underline{\nabla}(\underline{\nabla}\cdot\underline{E}) - \nabla^2\underline{E}$ follows since $\underline{\nabla}\cdot\underline{E} = 0$:

$$\nabla^2\underline{E} = \mu_0\sigma(\partial\underline{E}/\partial t) + \mu_0\varepsilon(\partial^2\underline{E}/\partial t^2) \quad .^{\dagger)} \tag{2-4}$$

The simplest solution of this wave-equation is that of a plane, time-harmonic wave

$$\underline{E} = \mathrm{Re}[\tilde{\underline{E}}] = \mathrm{Re}[\tilde{\underline{E}}_0 \exp i(\omega t - \tilde{\underline{K}}\cdot\underline{r})]$$

$$= \mathrm{Re}[\tilde{\underline{E}}_0 \exp i(\omega t - \underline{K}_1\cdot\underline{r})] \exp(-\underline{K}_2\cdot\underline{r}) \tag{2-5}$$

where $\omega = 2\pi\nu$ is the angular frequency of the field and $\tilde{\underline{E}}_0$ is the polarization vector. Generally the wave vector will be complex : $\tilde{\underline{K}} = \underline{K}_1 - i\underline{K}_2$. From eqs. 2-4, 5, 2 one obtains

†) It is assumed that ε, μ and σ are constant. As indicated in the previous section, however, one has to take into account frequency dispersion. A more correct derivation of the dispersion equations - making use of Fourier transformed Maxwell's equations - is given by Agranovich (1966) and Ginzburg.

$$\tilde{\underline{K}}\cdot\tilde{\underline{K}} = [\varepsilon_r(\omega) - i\sigma(\omega)/\varepsilon_0\omega](\omega/c)^2$$

$$= K_1^2 - K_2^2 - 2i\underline{K}_1\cdot\underline{K}_2 \qquad (2\text{-}6)$$

The optical properties of metals thus are completely described by a complex relative dielectric constant

$$\tilde{\varepsilon}_r(\omega) = \varepsilon_r(\omega) - i\sigma(\omega)/\varepsilon_0\omega$$

$$= \varepsilon_{r_1}(\omega) - i\varepsilon_{r_2}(\omega) \quad . \qquad (2\text{-}7)$$

Alternatively one often introduces a complex refractive index $\tilde{n}(\omega)$ such that $\tilde{\underline{K}}\cdot\tilde{\underline{K}} = \tilde{n}^2\omega^2/c^2$, an expression very similar to that found in the treatment of dielectrics. Eqs. 2-6, 7 show

$$\tilde{n}(\omega) = (\tilde{\varepsilon}_r)^{\frac{1}{2}}$$

$$= n(\omega) - ik(\omega) \qquad (2\text{-}8)$$

Here we also define the so-called optical constants the refractive index n and the extinction coefficient k. From eqs. 2-7, 8 one obtains the following relations for the real and imaginary parts of the relative dielectric constant:

$$\varepsilon_{r_1}(\omega) = n^2 - k^2 = \varepsilon_r \quad , \qquad (2\text{-}9a)$$

$$\varepsilon_{r_2}(\omega) = 2nk \qquad = \sigma(\omega)/\varepsilon_0\omega. \qquad (2\text{-}9b)$$

2.1.5. *Power dissipation.*

The amount of work needed to displace a charge q in time Δt over a distance Δs is equal to $\Delta W = q\underline{E}\cdot\underline{\Delta s}$. For a surface A that is perpendicular to $\underline{\Delta s}$ the associated current density is $\underline{J} = q/(A\Delta t)$. Hence the dissipated power is $\Delta W/\Delta t = \underline{E}\cdot(q/\Delta t)\underline{\Delta s} = \underline{E}\cdot\underline{J}(A\Delta s)$ or, alternatively, the power dissipation per unit volume is $\underline{E}\cdot\underline{J}$.

The current $\underline{J}$ should include all displacements of charge (Stern (1963), p. 301 f.f.). From eqs. 2-1d, 4 follows

$$\underline{\nabla} \times \underline{B} = \mu_0 \underline{J}_{tot} = \mu_0(\sigma \underline{E} + \varepsilon_0 \varepsilon_r \partial \underline{E}/\partial t).$$

For monochromatic waves of frequency ω one obtains on substituting eq. 2-7

$$\underline{J}_{tot} = \mathrm{Re}\tilde{\underline{J}}_{tot} = \mathrm{Re}[(i\omega\varepsilon_0\varepsilon_r + \sigma)\tilde{\underline{E}}]$$

$$= \mathrm{Re}[i\omega\varepsilon_0\tilde{\varepsilon}_r\tilde{\underline{E}}].$$

The time-averaged power dissipation per unit volume of the material then is

$$\overline{\underline{E}\cdot\underline{J}_{tot}} = \tfrac{1}{2}\mathrm{Re}[\tilde{\underline{E}}^*\cdot\tilde{\underline{J}}_{tot}] = \tfrac{1}{2}\mathrm{Re}[i\omega\varepsilon_0\tilde{\varepsilon}_r|\tilde{\underline{E}}|^2]$$

$$= \tfrac{1}{2}\omega\varepsilon_0\varepsilon_{r_2}(\omega)|\tilde{\underline{E}}|^2.$$

Introducing the vacuum wavelength λ such that $\omega\lambda = 2\pi c$ and using eqs. 2-2, 9b one can optionally write

$$\tfrac{1}{2}\varepsilon_0|\tilde{\underline{E}}|^2[\omega\varepsilon_{r_2}(\omega)] = \pi(\varepsilon_0/\mu_0)^{\frac{1}{2}}|\tilde{\underline{E}}|^2[\varepsilon_{r_2}(\omega)/\lambda] = \tfrac{1}{2}|\tilde{\underline{E}}|^2[\sigma(\omega)].$$

The power dissipation per unit volume thus is proportional to $\omega\varepsilon_{r_2}(\omega)$ or alternatively $\varepsilon_{r_2}(\omega)/\lambda$ or $\sigma(\omega)$. These then are the quantities of primary interest in the interpretation of the absorption of metals.

2.1.6. *Other parameters of practical interest.*

For the case of a plane wave with a single frequency as treated here one can reformulate Maxwell's equations in complex notation, using eqs. 2-1, 5, 7, 2 ;

$$\tilde{\underline{K}}\cdot\tilde{\underline{B}} = 0 \quad , \quad \tilde{\underline{K}}\cdot\tilde{\underline{E}} = 0$$

$$\tilde{\underline{K}} \times \tilde{\underline{E}} = \omega\tilde{\underline{B}} \quad , \quad \tilde{\underline{K}} \times \tilde{\underline{B}} = -\omega\tilde{\varepsilon}_r\tilde{\underline{E}}/c^2$$

The amount of energy, which crosses per unit time a unit area in a direction, that is perpendicular to the directions of $\underline{E}$ and $\underline{B}$, is given by the Poynting vector (Landau (1960) and Lifshitz, p. 253)

$$\underline{S} = \underline{E} \times \underline{B}/\mu_0 \ .$$

The time-averaged energy flow is

$$\begin{aligned}\overline{\underline{S}} &= \overline{\underline{E} \times \underline{B}/\mu_0} = \mathrm{Re}[\tilde{\underline{E}}^* \times \tilde{\underline{B}}/2\mu_0] = \mathrm{Re}[\tilde{\underline{E}}^* \times (\tilde{\underline{K}} \times \tilde{\underline{E}})/2\omega\mu_0] \\ &= \mathrm{Re}\{[(\tilde{\underline{E}}^* \cdot \tilde{\underline{E}})\tilde{\underline{K}} - (\tilde{\underline{E}}^* \cdot \tilde{\underline{K}})\tilde{\underline{E}}]/2\omega\mu_0\} = \mathrm{Re}[(\tilde{\underline{E}}^* \cdot \tilde{\underline{E}})\tilde{\underline{K}}/2\omega\mu_0] \\ &= [(\tilde{\underline{E}}^* \cdot \tilde{\underline{E}})|\underline{K}_1|/2\omega\mu_0]\hat{\underline{K}}_1 \\ &= [(\tilde{\underline{E}}_0^* \cdot \tilde{\underline{E}}_0)\exp(2\underline{K}_2 \cdot \underline{r})|\underline{K}_1|/2\omega\mu_0]\hat{\underline{K}}_1 \ . \end{aligned} \tag{2-10}$$

The time-averaged Poynting vector is of great practical interest; its direction (in the formula indicated by the unit vector $\hat{\underline{K}}_1$) represents the direction of propagation of the light, while its magnitude is usually defined as being the light intensity

$$I = |\tilde{\underline{E}}|^2|\underline{K}_1|/2\omega\mu_0 = |\tilde{\underline{E}}_0|^2 \exp(2\underline{K}_2 \cdot \underline{r})|\underline{K}_1|/2\omega\mu_0. \tag{2-11}$$

Further quantities of interest can be expressed in the optical constants. In eq. 2-5 $\underline{K}_1$ is perpendicular to the planes of constant phase whereas $\underline{K}_2$ is perpendicular to the planes of constant amplitude. For a wave, that is incident normal to the surface (e.g. parallel to the z-axis), the field amplitudes in the wave are damped according to the factor $\exp(K_2 z)$. From eqs. 2-6, 9 $K_2 = k\omega/c = 2\pi k/\lambda$. As a practical measure one defines the penetration or skin depth

$$\delta_0 = 1/K_2 = c/(k\omega) = \lambda/(2\pi k). \tag{2-12}$$

Also, defining the reflectivity as the ratio of the intensities of the reflected and the incident light waves, one can derive for the

reflectivity at normal incidence (e.g. Wooten (1972), p. 232 f.f.)

$$R = [(n - 1)^2 + k^2]/[(n + 1)^2 + k^2] \ . \qquad (2\text{-}13)$$

2.2. *Electron energy band structure.*

2.2.1. *Band structure calculations.*

The fundamentals of band structure calculations have been treated in a number of books (Callaway (1964), Loucks (1967), Altmann (1970), Fletcher (1971)). For the present purpose it suffices to make some general comments that will facilitate the interpretation of the results.

Au and Ag possess an f.c.c. crystal structure with a first Brillouin zone as shown in figure 2-1. Band calculations are generally performed along symmetry axes in the irreducible 1/48 zone denoted by ΓKWXUL. Thus the typical "folding maps" of band structure are obtained such as shown in figure 2-2 for an APW calculation on Au by Christensen (1971).

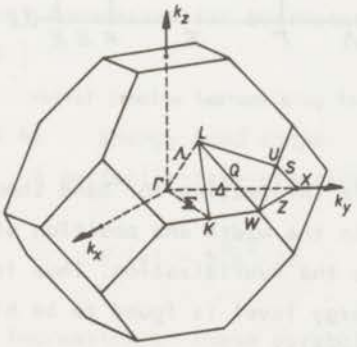

Fig. 2-1: Symmetry points in the f.c.c. Brillouin zone and the irreducible 1/48 zone.

of band structure are obtained such as shown in figure 2-2 for an APW calculation on Au by Christensen (1971).

For energies near the Fermi energy E_F (i.e. of the order of magnitude of the usual photon energies) the energy bands of the noble metals are quite similar: a broad *sp* band is crossed by and hybridizes with a narrow *d* band. The essential differences between the metals are to be found in the position of the *d*-band with respect to the *sp* band, and the width of this *d* band (Andersen (1970)). It are these two parameters that are very sensitive to the particular choice of crystal potential, and therefore experi-

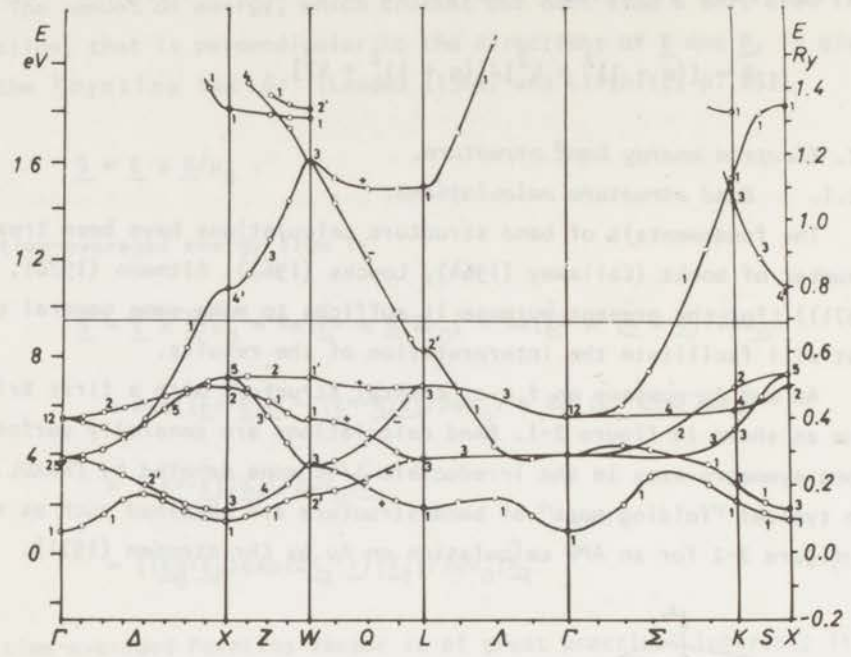

Fig. 2-2: APW energy bands (nonrelativistic) of gold (normal volume) (after Christensen (1971)).

mental data concerning them yield valuable information for band theory. However, it must be stated that changes in the width and position of the *d* band also influence the *sp* bands due to the hybridization. Thus in the noble metals the position of the $L_1^{(u)}$ energy level is found to be highly critical to the choice of the crystal potential.

2.2.2. *Relativistic vs. non-relativistic calculations.*

In heavy metals such as Au one must include relativistic effects. Essentially two effects may be distinguished: the distortion of the *d* band mainly due to spin-orbit coupling, and a lowering of the *sp* band relative to the *d* band caused by mass-velocity and Darwin correction terms (e.g. Andersen (1970), Christensen (1971)).

From comparison of non-relativistic band structures (figure 2-2) with results obtained by relativistic calculations (e.g. figure 3-1) it can be seen that these corrections may cause sizeable changes. Spin-orbit split-

ting of energy levels sometimes reaches values of the order of magnitude of energy gaps. For instance, the non-relativistic $\Gamma_{25'}$ level develops into Γ_7^+ and Γ_8^+ that are separated by more than 1 eV. Extremely critical results are obtained, however, for the conduction band shifts near L. For the $L_{2'} \rightarrow L_1$ energy gap Christensen (1971) obtained a non-relativistic APW value of 6.82 eV, whereas a relativistic calculation (RAPW) yielded 3.72 eV. Similar corrections in Ag are smaller but should not be neglected (Christensen (1972b)).

2.2.3. *Expanded lattice.*

Generally band calculations are performed for a crystal structure corresponding to T = 0 K. At higher temperatures results may be approximated by choosing a crystal potential for an expanded lattice (e.g. Davis (1968), Jacobs (1968), Christensen (1971)). Reversing the technique, compressing a room temperature lattice in band calculations yields a theoretical foundation for hydrostatic pressure experiments. (See also section 2.6.)

2.2.4. *Energy band shape.*

A perfectly-free-electron band is described by

$$E_n(\underline{k}) = \hbar^2 k^2/2m.$$

On increasing $\underline{k}$ these parabola will cross the boundary of the first Brillouin zone and the $E_n(\underline{k})$ - vs. - $\underline{k}$ curves will deviate from the parabola shape (e.g. Mott (1958) and Jones, p. 68), creating band gaps at the zone boundary. Still one can describe the energy band shape by relations reminiscent of free-electron formulas by introducing the concept of the effective mass (e.g. Altmann (1970), p. 107). The free-electron mass m is replaced by an effective mass tensor $\underline{\underline{m}}^x$ such that $(\underline{\underline{m}}^x)^{-1} = \hbar^{-2}(\partial^2 E/\partial\underline{k}\cdot\partial\underline{k})$: flat bands have a heavy effective mass. Also it can be shown (e.g. Callaway (1964), p. 29-43) that one may assume that the band energies depend quadratically on the distance in $\underline{k}$-space from a symmetry point $\underline{k}_0$. Thus the energy near the symmetry point can be expanded

$$E_n(\underline{k}) = E_n(\underline{k}_0) + \sum_{i=1}^{3} \hbar^2 (k_i - k_{0i})^2 / 2m_i^*. \qquad (2\text{-}14)$$

Looking at figure 2-2 one sees that one (or more) m_i^* can be negative. Actually one classifies these symmetry points $\underline{k}_0$ - called the (analytic) critical points or Van Hove points - according to the number of negative m_i^x values:

$P_0 = m_1^x, m_2^x, m_3^x$ all negative $\rightarrow E_n(\underline{k}_0)$ is a maximum

$P_1 = m_1^x, m_2^x$ negative, m_3^x positive $\rightarrow E_n(\underline{k}_0)$ is a saddle-point

$P_2 = m_1^x$ negative, m_2^x, m_3^x positive $\rightarrow E_n(\underline{k}_0)$ is a saddle-point

$P_3 = m_1^x, m_2^x, m_3^x$ all positive $\rightarrow E_n(\underline{k}_0)$ is a minimum

2.2.5. *(Joint) density of states.*

Of primary importance in the evaluation of optical measurements are the density of states (DOS) and the joint density of states (JDOS). The DOS - defined more properly in section 2.5.1.3. - "counts" the number of one-electron states per unit energy interval. The number of points $\underline{k}$ at which the energy values are directly calculated usually is rather small: 89 in the 1/48 zone is considered a high number (Christensen (1970), p. 84). Therefore it is necessary to interpolate the energy bands over a large number of $\underline{k}$ points between the regions of high symmetry in order to obtain reasonable accuracy in the literature. The derived DOS generally exhibits many sharp peaks and some empirical broadening must be introduced to take into account the effects of for instance electron-electron and electron--phonon interaction. Thus more "realistic" pictures are obtained that can be compared to experiment.

Particularly interesting for the analysis of the optical properties are the partial (or band-to-band) joint density of states (PJDOS) as obtained by Christensen (1970b, 1971). These functions $J_{lu}(\hbar\omega)$ represent the densities of allowed transitions of energy $\hbar\omega$ from the part of band l, that is below the Fermi level, to the part of band u, that is above E_F. The total JDOS is the sum of all $J_{lu}(\hbar\omega)$ (see section 2.5.3.).

A wealth of information on this subject is gathered in the proceedings of the 1969 conference on Electronic Density of States (Bennett (1971)).

2.2.6. *Momentum matrix elements.*

Matrix elements are known to have an important part in determining the probability of a transition and thus the strength of absorption (section 2.5.1.). In the absence of calculations it generally is assumed that the matrix elements are the same for all transitions in $\underline{k}$ space (section 2.5.7.). This rough approximation is found to be reasonable for transitions originating from *d* bands within about 5 eV below E_F (e.g. Christensen (1971), Shirley (1972a), Hüfner (1972)). However, it is also shown for Cu (Mueller (1967), Williams (1972)) and to some extent for Ag (Nilsson (1973a)) that the matrix elements vary considerably for inter-conduction-band transitions in the vicinity of L. In Cu they are known to be considerably enhanced for these transitions. To our knowledge no "wave function band structure" has been calculated for Au.

The $\underline{k}$ dependence of the matrix elements is also reported to be quite significant in other metals, for example Al (Dresselhaus (1971)) and K (Ching (1973)).

2.3. *Intraband transitions.*

As shown in section 2.1. for optical frequencies the power dissipation of an electromagnetic field in a homogeneous, isotropic metal is proportional to $\varepsilon_2(\omega)\omega$ (or alternatively $\varepsilon_2(\omega)/\lambda$ or $\sigma(\omega)$).[†] Generally $\varepsilon_2(\omega)$ is split into two assumedly independent components that are due to absorption by "nearly free" conduction electrons within one band (intraband absorption) and by "bound" electrons from one band to another (interband absorption). Using Kramers-Kronig analysis to relate the real and imaginary parts of the dielectric constant

$$\tilde{\varepsilon}(\omega) = \varepsilon_1(\omega) - i\varepsilon_2(\omega)$$

[†] Because of practical considerations we will refrain from using the more correct writing $\tilde{\varepsilon}_r$ for the complex relative dielectric constant and omit the subscript r.

one can separate the two contributions (Ehrenreich (1962)):

$$\tilde{\varepsilon}(\omega) = [\varepsilon_1^{(f)}(\omega) - i\varepsilon_2^{(f)}(\omega)] + [\varepsilon_1^{(b)}(\omega) - i\varepsilon_2^{(b)}(\omega)]. \qquad (2.15)$$

As will be discussed in section 2.3.3. only limited information on the intraband parameters can be obtained from our experiments. Thus, principally we will refrain from an extensive intraband analysis of the data. However, in order to clarify the interband structure by subtracting the intraband contribution it is of importance to use a reasonable model for the latter. A survey of such models is presented in the following sections.

2.3.1. *Intraband dielectric constant.*

The "free" electron term may tentatively be described by the classical Drude relations, the main characteristics of which later were confirmed quantum-mechanically:

$$\varepsilon_1^{(f)}(\omega) = 1 - \omega_{pf}^2/(\omega^2 + \tau^{-2}) + \delta\varepsilon_1^{(b)}, \qquad (2\text{-}16a)$$

$$\varepsilon_2^{(f)}(\omega) = \omega_{pf}^2/[\omega\tau(\omega^2 + \tau^{-2})] \qquad (2\text{-}16b)$$

$$\text{or} \quad \varepsilon_2^{(f)}(\omega)/\lambda = \omega_{pf}^2/[2\pi c\tau(\omega^2 + \tau^{-2})] .$$

Here ω_{pf} is the free-electron plasma frequency, τ the intraband relaxation time and $\delta\varepsilon_1^{(b)}$ an assumedly constant interband contribution to $\varepsilon_1^{(f)}(\omega)$. This last term can be understood from the fact that in deriving $\varepsilon_1^{(b)}(\omega)$ from $\varepsilon_2^{(b)}(\omega)$ by means of Kramers-Kronig dispersion relations the integration has to be performed over <u>all</u> frequencies. Thus, although $\varepsilon_2^{(b)}(\omega)$ has a rather sharp onset frequency (the absorption threshold), $\varepsilon_1^{(b)}(\omega)$ contributes to $\varepsilon_1(\omega)$ over the total frequency range. Alternatively to ω_{pf} one often uses the so-called optical mass

$$m_0 = Ne^2/\varepsilon_2\omega_{pf}^2$$

2.3.1.1. *Model I: d.c. conductivity (Drude).*

From a plot of ε_1 - vs. - ε_2/λ (a so-called Argand diagram) one derives a value of τ. Knowing $\sigma_{dc} = \varepsilon_0\omega_{pf}^2\tau$ the d.c. conductivity (obtained from resistivity measurements) is used to calculate the intraband optical properties.

Because external parameters (σ_{dc}) are incorporated one can hardly speak of fitting the data. The Drude model is assumed to be exact, which acutally is a matter of considerable controversy. Any remaining structure is attributed to other physical mechanisms (section 2.4.).

References: Bennett (1966), Lenham (1966), Powell (1970).

2.3.1.2. *Model II: optical conductivity.*

Again values of τ and $\delta\varepsilon_1^{(b)}$ are obtained from an Argand diagram. Evaluation of either $\varepsilon_1(\omega)$ or $\varepsilon_2(\omega)/\lambda$ then yields ω_{pf}. The greater freedom of having two adjustable parameters improves the fit. From ω_{pf} and τ one now computes an optical conductivity σ_{opt} that usually differs considerably from σ_{dc} (e.g. Otter). The physical interpretation of σ_{opt} is uncertain though.

Reference: Otter (1961a).

2.3.1.3. *Model III:* $\omega\tau >> 1$.

Eventually it will be found that for most experiments of the type described in this thesis $\omega\tau >> 1$. Using this result from the start the Drude relations may be simplified:

$$\varepsilon_1^{(f)} = \delta\varepsilon_1^{(b)} - \omega_{pf}^2/\omega^2 = 1 + \delta\varepsilon_1^{(b)} - (\omega_{pf}^2/4\pi^2c^2)\lambda^2 \quad , \qquad (2\text{-}17a)$$

$$\varepsilon_2^{(f)}/\lambda = \omega_{pf}^2/(2\pi c\omega^2\tau) = (\omega_{pf}^2/8\pi^3c^3\tau)\lambda^2 \quad . \qquad (2\text{-}17b)$$

Plotting ε_1 - vs. - λ^2 one thus obtains a value of ω_{pf}. A subsequent plot of ε_2/λ - vs. - λ^2 and substitution of ω_{pf} yields a value of τ.

Reference: Johnson (1972).

2.3.1.4. *Model IV: frequency-dependent relaxation time.*

On extrapolation of the ε_1 - vs. - λ^2 graph to zero wavelength the cut-off of the vertical axis gives an estimate of the contribution of the interband transitions, $\delta\varepsilon_1^{(b)}$. However a similar cut-off, that is sometimes found in the ε_2/λ - vs. - λ^2 graphs, is less obvious. The observed behaviour is:

$$\varepsilon_2/\lambda = A\lambda^2 + B \quad . \tag{2-17c}$$

Physically one may assume the Drude model to be valid and introduce an effective relaxation time (Thèye (1970)) that is no longer constant

$$(1/\tau_{eff}) = (1/\tau_{opt}) + b\omega^2 \quad .$$

Here the optical relaxation time at zero frequency, τ_{opt}, still differs from the d.c. relaxation time (e.g. Abelès (1966b)).

Because of its practical value much energy has been devoted to improving the theoretical background of the frequency dependence of τ, most notable being the reference to the work of Gurzhi (1966) who shows that electron-electron interaction may be the relevant mechanism.

References: Roberts (1955), Lenham (1967), Bennett (1968), Thèye (1970).

2.3.1.5. *Model V: two-or-more relaxation times.*

Roberts obtained a good fit to the experimental data by assuming different types of "free" electrons and summing their Drude contributions. Physically the anisotropy of the Fermi surface, that touches the Brillouin zone boundaries thus creating "bellies" and "necks" with different relaxation times (e.g. Ziman (1961a,b), Rayne (1961), Van Baarle (1967), Brown (1971)), provides some foundation for this model. Questionable then is the discontinuous transition from one type to the other in moving from a belly to a neck. The d.c. conductivity is obtained as the sum of the contributions of the various classes of electrons.

References: Roberts (1955, 1959, 1960), Lenham (1966), Powell (1970).

2.3.1.6. *Model VI: anomalous skin effect corrections.*

The anomalous skin effect is extensively treated by Sokolov (1967, chapter 8). The main correction to the Drude model is through the introduction of a parameter p that is related to the probability that a conduction electron is reflected specularly at the specimen surface. Thus for perfectly specular reflection p = 1, for diffuse reflection p = 0. The evaluation of the relaxation time has to be reconsidered

$$(1/\tau_{experiment}) = (1/\tau_{dc})[1 + 3(1 - p)L/8\delta_0]$$

where L is the mean free path of the electrons and δ_0 is the penetration depth of the light (Abelès (1966)). The correction thus becomes important only when $p \neq 1$ and $L \geq \delta_0$. As δ_0 is independent of temperature and L increases considerably at low temperatures, special attention is called for under these circumstances. For temperatures below the Debye temperature the relaxation time may be modified further (Holstein (1954)).

References: Bennett (1968), Thèye (1970).

2.3.1.7. *Model VII:* $\varepsilon_2/\lambda = A\lambda^{\alpha}$.

A simple fitting procedure without theoretical foundation was proposed by Lenham:

$$\varepsilon_2/\lambda = A\lambda^{\alpha} \quad .$$

Purely empirical it provides an easy and fairly accurate way to get rid of the intraband absorption structure.

References: Lenham (1967), Steel (1972), Beaglehole (1972).

2.3.2. *Comments.*

A great amount of work has been done on this subject and little agreement has been reached. We will limit ourselves to some general comments.

The division between the physical backgrounds of the various models is not sharp. For instance the anomalous skin effect correction leads

to an optical conductivity that is different from the d.c. conductivity. Quite possibly this is related to the higher surface resistance that Otter (1961a) suggests to be the cause for this difference. Also Roberts (1959,1960) shows how a separate class of electrons with very short relaxation time contributes an essentially constant term to ε_2/λ (see figure 2-3: V), thus providing a link between methods V and IV and giving an alternative to the frequency dependence of τ.

With due care one may conclude that the better the specimen, the better the Drude model. This improvement has been observed by Bennett (1966) using method I; in method IV the term B is reduced (Roberts (1955), Thèye (1970)); the surface parameter p goes to 1 ultimately eliminating the anomalous skin effect correction in method VI; the value of α in method VII is found to be closer to the Drude-predicted 2.

2.3.2.1. *Surface inhomogeneities.*

Deviations from the Drude theory may be expected due to non-ideal reflections on the specimen surface of

(1) the incident light (lower reflectance due to scattering),

(2) conduction electrons ($p \to 0$; electron-surface relaxation times [†]) (e.g. Meessen (1968), Smith (1969,1970), Dujardin (1971), Palmer (1972)).

In both cases surface inhomogeneities (roughness, adsorbed layers) are the main culprit. A complete analysis of such effects is possible only when a satisfactory model of the surface is known together with quantitative data obtained on the actual specimen. In studies on evaporated films one most commonly assumes a Gaussian surface roughness distribution (e.g. Bennett (1961,1968)). Endriz (1971) obtained much better results, however, using the general theory of Elson (1971) and Ritchie. Further work of interest is due to Hunderi (1970) and Beaglehole. It must be expected that the success is much less for bulk metals where polishing might introduce preferential directions to the surface roughness.

[†]) Electron-surface interaction can introduce a "new" class of electrons with an apparent (i.e. experimentally observed in the surface layer where the light penetrates) relaxation time that is much smaller than the bulk relaxation time of the conduction electrons (see section 3.6.4.). This possibly accounts for the success of Roberts' model V.

2.3.2.2. *Bulk inhomogeneities.*

Intraband structure is also greatly affected by imperfections of the bulk of the specimen (relaxation time!). Numerous investigations have been made on the influence of lattice defects such as grain boundaries, dislocations, vacancies or impurities (e.g. Shkliarevskii (1966), Hodgson (1968), Bispinck (1970), Hunderi (1973a,b,c)). Similarly the damaged crystal structure caused by (especially mechanical) polishing has been shown to have drastic effects (e.g. Köster (1967), Pells (1969)). Frequent attention has been paid to the differing density of evaporated films and bulk specimens (e.g. Cottin (1967), Nilsson (1967), Hodgson (1968)).

2.3.2.3. *Physical influences.*

A number of more physical - that is, not directly related to the specimen condition - influences have been proposed. Most renowned amongst these are the many-body effects (electron-electron and electron-phonon interactions). A treatment is beyond the scope of this thesis; instead one is referred to the literature, e.g. Abelès (1966b,1972a) and Thèye (1970) and references cited there. Frequently the solution of indirect transitions has been suggested (e.g. Rayne (1961), Otter (1961a)) and discarded (e.g. Biondi (1968)).

Biondi (1968) points at the frequency dependence of the penetration depth δ_0. As $\delta_0 = \lambda/2\pi k$ (e.g. 2-12) and k reaches a minimum for a photon energy just below the absorption edge, the deeper penetration of the electromagnetic field may lead to deviations. For instance, this frequency dependence is not taken into account in the usual anomalous skin effect theory.

2.3.3. *Conclusions.*

Very different values have been published for the "free electron" parameters (e.g. Schulz (1957), Lenham (1967b), Smith (1969)) causing serious doubts about their physical significance[†]. We hesitate to be-

[†] As shown in section 3.6., table 3-2 the values of ω_{pf} and m_o also vary when different methods of analysis are used.

lieve in quantitative analyses of physical mechanisms if these analyses are based on values of the optical mass derived from measurements at relatively high photon energies (e.g. Mathewson (1972)). Discrepancies in the experimentally determined values of τ are still considerably larger; only qualitative evaluation is permissible (see also sections 3.6. and 4.6.).

Only through systematic research can one expect to make progress in this field. To verify the physical meaning of the models I, II, IV, V, VI the experiments should be extended to lower photon energies, farther away from interband contributions. To study the relaxation time one has to vary the temperature; also the belly-neck hypothesis of the two-or-more-τ model should be very sensitive to alloying, causing an increase of the necks of the Fermi surface (experiments of this type have been done by Rayne (1961)). Above all, specimen surface preparation must be perfected - both for bulk samples and films - and analyzed quantitatively (e.g. surface roughness). Experiments of this type are at present being done by D.L. Decker and Stanford at China Lake, California (private communication).

The answers, that are to be expected from our experiments, are of limited value in this respect. Limited attention will therefore be given to the analysis of the results.

2.4. *Anomalous absorption.*

On subtracting $\tilde{\varepsilon}^{(f)}(\omega)$ from the measured values of $\tilde{\varepsilon}$ one obtains $\tilde{\varepsilon}^{(b)}(\omega)$. However, quite often additional structure is found at photon energies below that of the onset of interband absorption. As no satisfactory intra- or interband explanation is available, these absorptions are classified as "anomalous". Two types of structure can be distinguished:

(1) one (or more) absorption peaks;

(2) a tailing of the absorption edge to lower photon energies.

2.4.1. *Absorption peaks.*

Although most (in-)famous of the type is the so-called Mayer-El Naby peak found in the alkali metals (Mayer (1966)), we mainly limit ourselves to the noble metals.

2.4.1.1. *Broad absorption peaks.*

In our opinion one must distinguish the broad peak reported by Pells (1969) from most other bumps found in the literature. The width and height of Pells' structure follow directly from the use of method I (section 2.3.1.); it disappears almost completely when using method IV or VII.

The analysis of broad absorption structure is bothersome. With the usual spread in data and the limited wavelength intervals it is difficult to distinguish between

(1) a Drude-like contribution of a separate class of electrons with a very short relaxation time (method V),

(2) a constant term B due to a frequency dependence of τ (method IV),

(3) an additional broad absorption (VIII).

This is demonstrated in fig. 2-3. Extreme care should be taken in the physical evaluation of any below-the-absorption-edge structure.

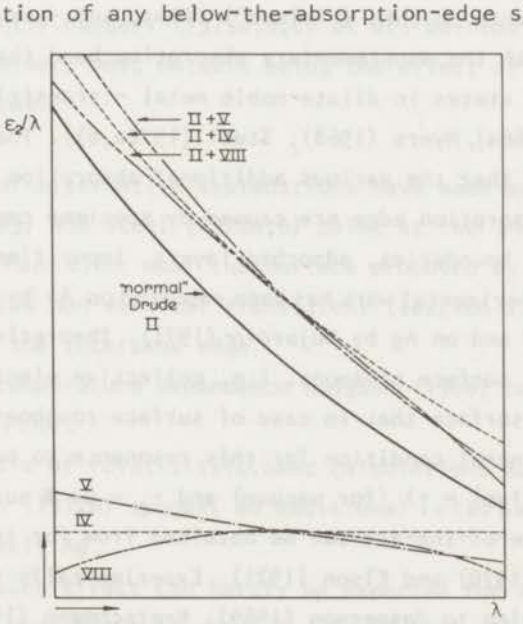

Fig. 2-3: Intraband absorption: superimposed on a Drude absorption (II) are contributions (IV, V, VIII) typical of various models.

2.4.1.2. *Narrow absorption peaks.*

Much speculation has been done regarding the much smaller, usually

more localized bumps reported by various authors (sections 3.6.2, 4.6, 4.9.1.). The analysis is considerably complicated by the possibility of having different physical mechanisms that cause absorption peaks at the same time.

(1) *Specimen conditions*. Strong indications suggest that for improving sample preparation the additional structure diminishes or disappears altogether (e.g. Roberts (1955), Bennett (1966), Shkliarevskii (1966), Devant (1967), Thèye (1970), Dujardin (1971), Palmer (1971), Hunderi (1973a,b,c)). It is difficult to reconcile this pattern with absorption due to interband transitions that is known to become stronger for improving specimen quality (see sections 3.14., 4.11.). Much structure shows a marked similarity with the anomalous absorption that has been found in experiments on thin ("island") films, and - as noted by Thèye (1970) - also with the supplementary absorption band that is attributed to virtual bound states in dilute noble metal - transition metal alloys (e.g. Abelès (1966a), Myers (1968), Steel (1972a,b)). These considerations strongly suggest that the various additional absorption peaks noted below the interband absorption edge are caused by specimen conditions (surface roughness, grain boundaries, adsorbed layers, impurities, defects).

Relevant experimental work has been reported on Au by Devant (1967) and Thèye (1970) and on Ag by Dujardin (1971). Theoretically most work has been done on surface plasmons, i.e. collective electron resonances parallel to the surface that in case of surface roughness can cause absorption. The general condition for this resonance to occur is $\varepsilon_1 \approx -\varepsilon_1$ (surrounding medium) = -1 (for vacuum) and $\varepsilon_2 \approx 0$. A survey of the theoretical state-of-the-art can be obtained from for instance Economou (1969), Melnyk (1970) and Elson (1971). Experimentally this purpose may be served referring to Jasperson (1969), Kretschmann (1969a,b), Stanford (1970), Daudé (1972) and especially Endriz (1971). Anomalous structure in thin granular films has been reported many times and explained by a variety of models (e.g. Carlan (1969), Rouard (1969), Yoshida (1971), Bedeaux (1973) and Vlieger). Recently Meessen (1972) - supported by Rasigni (1972) - tried to bridge the gap between these island films and a surface roughness on bulk metals by postulating an "island layer"

on top of the bulk. The resulting resonance absorption, that also can be caused by adsorbed layers, could possibly explain the Mayer-El Naby peak in the alkali metals. It may arise in all metals, however, expecially in spectral ranges of low absorption (ε_2 small).

Further theoretical models for anomalous absorption and scattering due to spherical and hemispherical surface inhomogeneities are proposed by Berreman (1970a,b) and Hunderi (1970) and Beaglehole. Berreman finds that absorption may occur when both ε_1 and $-\varepsilon_2$ are small, between -2 and 0. Galeener (1971) shows that submicroscopic voids inside a specimen may introduce additional structure resembling that caused by surface plasmons. As the condition for this "volume roughness" absorption is $\varepsilon_1 \simeq -\frac{1}{2}$ and $\varepsilon_2 \simeq 0$, the new structure will be near, probably even overlap the surface roughness induced absorption.

More recently Hunderi (1973a,b,c) et al. pointed at the influence of structural disorder, most notable being the effect of grain boundary plasma resonances.

A number of alternative explanations have been proposed.

(2) Pells (1969) and Steel (1972a,b) point at the evanescent parts to the wave function near the surface proposed by Stern (1967), that in Au could allow non-vertical transitions (section 2.5.4.) to cause absorption below the interband edge.

(3) From the temperature dependence Hodgson (1968) concludes to indirect transitions.

(4) On the basis of relativistic band calculations Kupratakuln (1970) and Christensen (1972b) suggest an additional interband absorption in Au respectively Ag.

(5) Although such effect can hardly be expected for Au, It has been pointed at the possible influence of oxidation (Garfinkel (1966), Mueller (1967)). For Ag this suggestion perhaps finds some support from measurements by Huebner (1965) et al., who note the growth of structure in $n - vs. - \hbar\omega$ spectra upon oxidation.

2.4.1.3. *Mini absorption peaks.*

Additional mini-peaks at the very onset of the absorption edge of Ag can be related to the bulk plasma frequency ω_p. Lindau (1971c) and Nilsson interpret very small anomalous absorptions just above ω_p as being due to the excitation of longitudinal plasmons, whereas Hopfield (1965) suggests a minor enhancement of ε_2 near ω_p arising from electron-electron interactions (scattering caused by thermal or structural disorder). Such structure has possibly been measured for potassium by Palmer (1971).

2.4.1.4. *Conclusions.*

Most probably absorption peaks in the "intraband" photon energy range are related to specimen conditions. The analysis is complicated due to the possible contributions of different mechanisms. Essential to a satisfactory decomposition is an accurate measurement of the surface roughness, experimentally a difficult problem. A condition for all these absorption mechanisms is that both ε_1 and ε_2 are small. This situation is found in the noble metals - especially so in Ag - just below the interband absorption edge. Therefore all structure in this spectral region must be handled with care.

2.4.2. *Tailing of the absorption edge to lower energies.*

An exponential tailing of the absorption edge has been found in Au (Shkliarevskii (1966), Nilsson (1967), Thèye (1970)) and Ag (Yarovaya (1965), Dujardin (1971)). The magnitude of this effect is dependent on the Drude analysis technique. Various causes have been proposed.

(1) Indirect transitions cannot account for the width of the tail.

(2) Deformation of electronic bands due to lattice defects (Nilsson) is eliminated by Thèye who shows that the tail is independent of film structure.

(3) Lifetime broadening of the absorption edge (Nilsson) cannot account for the width of the tail, especially in Ag.

(4) Auger-type broadening of the edge (Thèye, Dujardin) (e.g. Friedel (1972, p. 18).

(5) RAPW calculations on Au by Christensen (1971) indicate a tailing of interband absorption due to transitions in the vicinity of X. A similar

explanation cannot account for the tail in Ag though. Also see sections 3.8.3. and 4.9.2..

2.5. *Interband transitions: dielectric constant.*

The relationship between the (theoretically calculated) band structure and the (experimentally determined) interband optical properties has been extensively treated in the literature (e.g. Stern (1963, chapter 5), Bassani (1966), Sokolov (1967, chapters 3 and 4)). In this section therefore some general concepts are introduced; no derivations are given.

2.5.1. *Interband absorption:* $\varepsilon_2^{(b)}$.

The interband part of the spectrum is due to transitions of electrons from occupied states in lower band to unoccupied states in upper bands. In the independent-particle model the interaction of the many-electron system with the electromagnetic radiation can be approximated (Ehrenreich (1959,1966), p. 133). by the response of one-electron wave functions in a self-consistent field. In the ground state, the total wave function ψ then is the Slater determinant of these one-electron wave functions ϕ_n that in a periodic lattice in turn can be described by Bloch functions.

In section 2.1.5. it is shown that the time-averaged power dissipation from an electromagnetic wave $\underline{E} = \mathrm{Re}[\tilde{\underline{E}}]$ of angular frequency ω per unit volume of the material is equal to $\frac{1}{2}\omega\varepsilon_o\varepsilon_2(\omega)|\tilde{\underline{E}}|^2$. On the other hand this absorption is equal to the total transition probability at photon energy $\hbar\omega$, W_{tot}, multiplied by that photon energy

$$(\hbar\omega)W_{tot} = \tfrac{1}{2}\omega\varepsilon_o\varepsilon_2(\omega)|\tilde{\underline{E}}|^2 .$$

In the one-electron model the term W_{tot} is determined by the following factors (transitions from a lower band l to an upper band u):

(1) matrix elements for transitions from l to u;

(2) Fermi distribution functions of initial and final states;

(3) (joint) density of states.

2.5.1.1. *Transition matrix elements.*

From time-dependent perturbation theory the probability (per unit time) of an electronic transition from an initial state $\phi_{\underline{k}_l}$ with energy $E_l(\underline{k}_l)$ to a final state $\phi_{\underline{k}_u}$ with energy $E_u(\underline{k}_u)$ is:

$$P_{lu}(\hbar\omega) = (2\pi e^2|\tilde{A}_0|^2/4m^2\hbar)|M_{lu}|^2\delta(E_u(\underline{k}_u) - E_l(\underline{k}_l) - \hbar\omega). \quad (2\text{-}18)$$

In this expression $\tilde{A}_0$ is the amplitude of the complex vector potential whereas M_{lu} is the matrix element for transitions from band l to band u (see section 2.2.6.). Furthermore -e is the charge and m the mass of the electron.

2.5.1.2. *Fermi distribution of initial and final states.*

From Fermi-Dirac statistics the probability for occupation of a state with energy E_n is given by the Fermi distribution function:

$$f(E_n) = \{\exp[(E_n - E_F)/k_BT] + 1\}^{-1} \quad (2\text{-}19)$$

(E_F = Fermi energy; k_B = Boltzmann's constant). Thus the transition probability has to be multiplied by factor $f(E_l)[1 - f(E_u)]$ to account for the degree of occupation of initial and final states. For transitions at T = 0 K with $E_l < E_F < E_u$ this factor becomes 1. †)

2.5.1.3. *(Joint) density of states.*

The number of one-electron states per unit with energies between E and E + dE is specified by the density of states (DOS) per unit energy interval (e.g. Fletcher (1971), p. 31):

$$N(E) = [2/(2\pi)^3] \int dS_E/|\nabla_{\underline{k}}[E(\underline{k})]| \quad . \quad (2\text{-}20)$$

†) Strictly speaking the Fermi energy E_F is only defined at T = 0 K. At higher temperatures one should rather use the thermodynamical potential ζ such as for instance introduced by Mott (1958) and Jones (p. 175). However, conforming to general usage we will employ "Fermi energy" and "E_F" for all temperatures.

The integral in eq. 2-20 is over the surface of constant energy E.

Similarly one can introduce the band-to-band or partial joint density of states (PJDOS) $J_{lu}(\hbar\omega)$ that specifies the number of allowed relations between the occupied part of band l and the unoccupied part of band u for photon energies between $\hbar\omega$ and $\hbar(\omega + d\omega)$. In analogy with eq. 2-20 one obtains:

$$J_{lu}(\hbar\omega) = [2/(2\pi)^3] \int dS_{\hbar\omega} f(E_l(\underline{k}))[1-f(E_u(\underline{k}))]/|\nabla_{\underline{k}}[E_u(\underline{k})-E_l(\underline{k})] \quad , \tag{2-21}$$

where the integral now is over surfaces of constant interband energy $\hbar\omega$. To obtain the total joint density of states (JDOS) $J(\hbar\omega)$ one has to sum the PJDOS contributions from all possible combinations of bands.

$$J(\hbar\omega) = \sum_{l,u} J_{lu}(\hbar\omega) \quad . \tag{2-21b}$$

2.5.1.4. $\varepsilon_2^{(b)}(\omega)$ *related to absorption.*

Using the foregoing one obtains an expression for $\varepsilon_2^{(b)}(\omega)$

$$\varepsilon_2^{(b)}(\omega) = (C/\varepsilon_0\omega^2)_{l,u} \int dS_{\hbar\omega}|M_{lu}|^2 f(E_l(\underline{k})[1-f(E_u(\underline{k}))]/$$

$$|\nabla_{\underline{k}}[E_u(\underline{k})-E_l(\underline{k})] \tag{2-22}$$

with $C = (e/2\pi m)^2$.

2.5.2. *Interrelation of optical constants: rules-of-thumb.*

The optical constants are related to one another by Kramers-Kronig dispersion formulas (Stern (1963, chapter 3)). The integration in these expressions is over the whole frequency range from 0 to ∞. From our point of view the most important equations relate $\varepsilon_1(\omega)$ to $\varepsilon_2(\omega)$ (or $\varepsilon_1^{(b)}(\omega)$ to $\varepsilon_2^{(b)}(\omega)$).

As shown by Velický (1961) the qualitative relations between the structural details of the frequency dependence of optical constants are local. One can use the ensuing rules-of-thumb to great profit in the analysis of optical spectra. The most useful relations are (Tauc (1966,

p. 67), Green (1965, p. 16)):

maximum in $\varepsilon_1(\omega)$ [or $n(\omega)$] $\leftrightarrow$ $d\varepsilon_2/d\omega$ large and positive [resp.$dk/d\omega$],

minimum in $\varepsilon_1(\omega)$ [or $n(\omega)$] $\leftrightarrow$ $d\varepsilon_2/d\omega$ large and negative [resp.$dk/d\omega$],

$d\varepsilon_1/d\omega$ large and negative [or $dn/d\omega$)] $\leftrightarrow$ maximum in $\varepsilon_2(\omega)$ [resp. k],

$d\varepsilon_1/d\omega$ large and positive [or $dn/d\omega$)] $\leftrightarrow$ minimum in $\varepsilon_2(\omega)$ [resp. k].

It should be noted in this respect that a peak position of $\varepsilon_1^{(b)}(\omega)$ is sometimes used to locate the position of an absorption edge (e.g. Ehrenreich (1966), Steel (1972b); see section 2.5.6.).

2.5.3. *Lifetime broadening.*

After a certain lifetime in the excited state an electronic excitation will decay through various scattering processes such as interaction with lattice imperfections or with another electron or phonon. As a consequence of the uncertainty principle this limited lifetime leads to a broadening of the energy levels corresponding to the initial or final states. The effect on $\tilde{\varepsilon}$ can be described somewhat phenomenologically using a Lorentzian broadening parameter Γ (e.g. Batz (1972), p. 348).

2.5.4. *Conservation laws.*

2.5.4.1. *Conservation of energy.*

A second selection rule based on conservation of energy follows from the delta-function in eq. 2-18:

$$E_u(\underline{k}) - E_l(\underline{k}) = \hbar\omega \ . \qquad (2\text{-}23)$$

2.5.4.2. *Direct transitions.*

Due to the translation symmetry the probability of a transition involving a phonon of wave vector $\underline{K}$ vanishes unless (e.g. Sokolov (1967), p. 101):

$$-\underline{k}_u + \underline{K} + \underline{k}_l = 0.$$

In the optical frequency region the wave vector of the incident wave $K = 2\pi/\lambda \approx 10^5 cm^{-1}$ is negligibly small compared to the dimensions of the Brillouin zone, $\pi/a \approx 10^8 cm^{-1}$ (a = lattice spacing). One thus obtains a selection rule based on conservation of crystal momentum:

$$\underline{k}_u = \underline{k}_l \quad . \tag{2-24}$$

In the reduced zone scheme this implies that only vertical or <u>direct</u> transitions occur.

2.5.4.3. *Nondirect and indirect transitions.*

Based on photoemission work Spicer et al. (e.g. Spicer (1972), p. p. 831 f.f.) suggested the possibility of <u>nondirect</u> transitions, where <u>k</u> is not conserved. These transitions lack a satisfactory theory. It has been pointed at the inadequacies of the one-electron model. Possible explanations therefore include the perturbation of the lattice (through static imperfections, alloying, etc.), the influence of the surface in taking up momentum, electron-electron interactions. The controversy on the importance of <u>k</u>-conservation is very important in the interpretation of photoemission data (section 2.9.2.).

Nondirect transitions should not be interchanged with <u>indirect</u> transitions, that involve contributions of the lattice vibrations (phonons). The distinction can be made by means of temperature variation: indirect transitions vanish at low temperatures.

2.5.5. *Constant matrix elements.*

In a rough approximation one might assume the matrix elements to be constant. It then follows from eqs. 2-21, 22 that

$$\varepsilon_2^{(b)}(\omega)\omega^2 = C'J(\hbar\omega) \quad , \tag{2-25}$$

where C' is a constant containing the matrix elements.

2.5.6. *Absorption edge.*

The major rise in $\varepsilon_2^{(b)}(\omega)$, that is related to the low-energy onset

of interband absorption in the noble metals, is generally named the (interband) absorption edge. As minor structure of $\varepsilon_2^{(b)}(\omega)$ sometimes preceeds this steep rise, care must be taken in comparing literature values of this parameter. Preferably we define the threshold energy $\hbar\omega^*$ as being the spectral position of the parabolic footpoint of the $\varepsilon_2^{(b)}(\omega)\omega^2$ function (Cooper (1965), Miloslavskii (1967)) (see section 2.7.2.1.). However, Liljenvall (1970b) chooses the position of the onset to be the place of zero slope on the ε_2 - vs. - $\hbar\omega$ curve, a procedure which may lead to inaccuracies due to the superposition of intra- and interband contributions. Ehrenreich (1966, p. 143) locates the absorption edge using the photon energy $\hbar\omega_a$ at which $\varepsilon_1^{(b)}(\omega)$ peaks. This definition is directly related (section 2.5.2.) to the one of $\hbar\omega_a$ as being the photon energy of steepest slope of $\varepsilon_2^{(b)}$ (i.e. $d\varepsilon_2^{(b)}/d\omega$ maximal)(e.g. Beaglehole (1969), Steel (1972b)).

2.6. *Interband transitions: temperature dependence.*

To facilitate the analysis the dielectric constant may be thought to consist of a static part $\tilde{\varepsilon}$ (static) and a contribution induced by temperature changes $\Delta\tilde{\varepsilon}$

$$\tilde{\varepsilon} = \tilde{\varepsilon}(\text{static}) + \Delta\tilde{\varepsilon}$$

Separating intraband and interband contributions to $\tilde{\varepsilon}$ as before one obtains for the temperature dependent part

$$\Delta\tilde{\varepsilon} = \Delta\tilde{\varepsilon}^{(f)} + \Delta\tilde{\varepsilon}^{(b)} = [\Delta\varepsilon_1^{(f)} - i\Delta\varepsilon_2^{(f)}] + [\Delta\varepsilon_1^{(b)} - i\Delta\varepsilon_2^{(b)}] .$$

Although the free-electron contribution is described by fairly simple formulas, the physical background is subject to doubt (see section 2.3.). Apart from a dilatation effect (Scouler (1967)) the temperature dependences of the various relaxation times (electron-electron, electron-phonon) cause rather undetermined effects. Once again therefore the analysis will be limited to an empirical subtraction. Work of interest in this field is reported by Otter (1961b) and Rosei (1972).

Temperature dependence of the interband dielectric constant is caused by

(1) lattice expansion;

(2) lifetime broadening;

(3) Fermi distribution broadening;

(4) shift of Fermi level.

Adding the contributions from all pairs of band one obtains a first-order approximation for small ΔT:

$$\Delta\tilde{\varepsilon}^{(b)}(\omega) = \sum_{u,l} [(\partial\tilde{\varepsilon}^{(b)}/\partial E_{ul})(dE_{ul}/da)(da/dT) \quad \text{:lattice expansion}$$

$$+ \{(\partial\tilde{\varepsilon}^{(b)}/\partial E_{ul})(dE_{ul}/dT) + (\partial\tilde{\varepsilon}^{(b)}/\partial\Gamma)(d\Gamma/dT)\} \text{:lifetime broadening}$$

$$+ (\partial\tilde{\varepsilon}^{(b)}/\partial f)(df/dT) \quad \text{:Fermi distribution}$$

$$+ (\partial\tilde{\varepsilon}^{(b)}/\partial E_{ul})(dE_{ul}/dE_F)(dE_F/dT)] \quad \text{:shift of Fermi level}$$

$$\times \Delta T \ . \qquad (2\text{-}26)$$

Here a is the lattice spacing.

Tentatively eq. 2-26 can be used in the analysis of the temperature dependence of the interband optical properties. No general expression can be given for the partial derivatives of $\tilde{\varepsilon}^{(b)}$ with respect to E_{ul} and Γ. Only a model-wise description of $\tilde{\varepsilon}^{(b)}(\omega)$ (or alternatively the JDOS; see section 2.5.5.) allows a prediction to be made of the expected line shape. Discussion of such models is put off to section 2.7. Rather we will first try to estimate the magnitude and type of temperature dependence (linear, quadratic, etc.) of the energy shifts $((dE_{ul}/da)(da/dT), (dE_{ul}/dT)$ and broadening terms $(d\Gamma/dT, df/dT)$.

2.6.1. *Energy shift due to lattice expansion $(dE_{ul}/da)(da/dT)$.*

As the interatomic distance increases, the crystal potential changes. The shift of energy band structure is in the direction of free atoms (figure 1-1): the *sp* bands are narrowed, the *d* bands are narrowed and lowered (e.g. Watson (1970)). Any detailed prediction of the shift of in-

terband transitions therefore is difficult without actual band calculations for the expanded lattice. Davis et al. (1968) suggested and demonstrated in a band calculation of Cu that for small changes in lattice spacing, variations in the resulting band structure are linear.

Note that the thermal volume expansion coefficient dV/dT, which in a first order approximation is proportional to the lattice expansion term da/dT, is approximately constant for $T >> \theta_D$ (the Debye temperature) and proportional to T^3 for $T << \theta_D$.

2.6.2. *Lifetime broadening: electron-phonon interaction.*

Several scattering processes can contribute to the lifetime broadening of energy levels. One may expect that the most important mechanism - especially with regard to temperature dependence - will be electron--phonon interaction.

Knowledge of this type of interaction has been reviewed by Sham and Ziman (Sham (1963)). In the presence of especially acoustical phonons electrons can reach higher or lower states by phonon absorption or phonon emission. The transition probability of phonon absorption is proportional to the phonon occupation number:

$$f_B = [\exp(h\omega_{\underline{q}}/k_B T) - 1]^{-1} , \qquad (2\text{-}27)$$

($\omega_{\underline{q}}$: frequency associated with the longitudinal acoustic mode $\underline{q}$), whereas the probability of phonon emission follows ($f_B + 1$) (Ziman (1960), p. 182).

2.6.2.1. *Electron-phonon interaction: dE_{ul}/dT.*

The magnitude of the energy shifts due to a smearout of the potential caused by thermal vibration can be estimated using principles outlined by Ziman (1965, p. 54 f.f.). The matrix element for scattering is split into an atomic factor (the Fourier transform of the atomic potential) and a structure factor. To account for the electron-phonon interaction it now suffices (Kasowski (1969)) to multiply the structure factor by the appropriate Debye-Waller factor, exp(-W) (Ziman (1965), p. 60 f.f.), which can be derived from knowledge of the phonon spectrum.

For the *sp* bands of Au and Ag a rough estimate of the temperature--dependent Debye-Waller exponent W has been obtained by Christensen (1971). Using an OPW-LCAO[†)] scheme he found that with a temperature rise from 0 K to 750 K the largest energy shift in Au is of the order of 27 meV. For Ag the calculated W is approximately a factor 1.3 smaller than in Au.

Interesting work in this field is also due to Sak (1968), Mitra (1969) and Das (1973).

2.6.2.2. *Electron-phonon interaction: $d\Gamma/dT$.*

Batz (1972, p. 361) showed that for acoustical phonons at $T >> \theta_D$ the broadening of a level is proportional to the density of states and to the temperature. Thus $d\Gamma/dT$ is a constant, the magnitude of which is found to be much smaller than dE_{ul}/dT. Tentatively therefore in nonpolar crystals it may be neglected in the analysis of the temperature dependence of the optical properties (also Cardona (1969), p. 117).

2.6.3. *Fermi distribution broadening df/dT.*

From eq. 2-19 it follows

$$df(E_n)/dT = (E_n-E_F)\exp[(E_n-E_F)/k_BT]/[k_BT^2\{\exp[(E_n-E_F)/k_BT]+1\}^2]$$

Some typical curves are shown in figure 2-4.

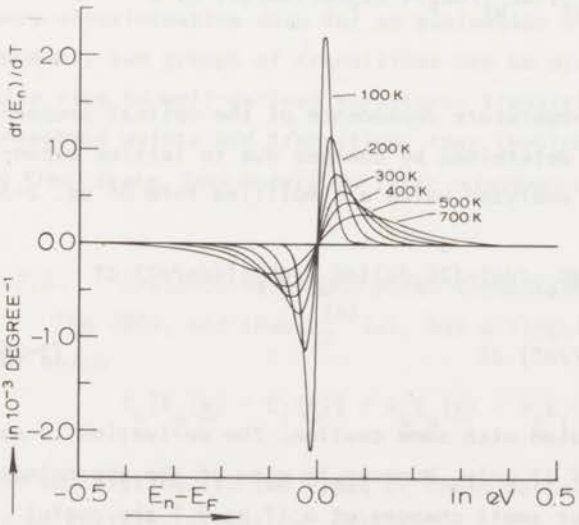

Fig. 2-4: $df(E_n)/dT$ at various temperatures between 0 and 700 K.

†) Orthogonalized Plane Wave - Linear Combination of Atomic Orbitals.

2.6.4. *Shift of Fermi level.*

The shift of E_F due to the change of the Fermi distribution function is given by Mott (1958) and Jones (p. 178):

$$\Delta E_F = -(\pi^2/6)(k_B T)^2 (d \log N/dE)_{E=E_F(0\,K)} \quad ,$$

where N is the total number of electrons per unit volume. For free electrons one has E_F = constant x $(N/V)^{2/3}$ (e.g. Kittel (1968), p. 208) and therefore

$$\Delta E_F = -(\pi^2/4)(k_B T)^2/E_F \quad .$$

Similarly the effect of lattice expansion is

$$\Delta E_F = -\frac{2}{3} E_F \Delta V/V \approx -2E_F\, a/\Delta a \quad .$$

Substituting "realistic" values of E_F = 5.5 eV, T = 300 K, $\Delta a/a = 3 \times 10^{-3}$ (for ΔT = 300 K) it is found that the effect due to lattice expansion is larger by two orders of magnitude. Thus for the noble metals one may substitute for the appropriate part in eq. 2-26

$$\Delta\tilde{\varepsilon}^{(b)} = (\partial\tilde{\varepsilon}^{(b)}/\partial E_{ul})(dE_{ul}/dE_F)(-2E_F/a)(da/dT)\,\Delta T \quad .$$

2.6.5. *Summary.*

It is found that the temperature dependence of the optical properties of Au and Ag is mainly determined by changes due to lattice expansion. It can tentatively be analyzed using a simplified form of eq. 2-26

$$\Delta\tilde{\varepsilon}^{(b)} = (\partial\tilde{\varepsilon}^{(b)}/\partial E_{ul})[(dE_{ul}/da) - (2E_F/a)(dE_{ul}/dE_F)](da/dT)\,\Delta T$$

$$+ (\partial\tilde{\varepsilon}^{(b)}/\partial f)(df/dT)\,\Delta T \quad . \qquad (2\text{-}28)$$

Eq. 2-28 should be treated with some caution. The derivation is appropriate to small values of ΔT only. However, in view of the approximately linear dependence on T for small changes of a ($T \gg \theta_D$) the useful range of the formula may be more extended. A non-linear temperature depen-

dence is expected for structure due to transitions involving the Fermi surface as initial or final state.

It should be noted that - apart from Fermi surface transitions - structure described by eq. 2-28 should be directly related to that caused by a wavelength variation (Batz (1972))

$$\Delta\tilde{\varepsilon}^{(b)} = -(\partial\tilde{\varepsilon}^{(b)}/\partial E_{ul})\Delta(\hbar\omega) \qquad (2\text{-}29a)$$

or even more so to that due to hydrostatic pressure on the specimen

$$\Delta\tilde{\varepsilon}^{(b)} = (\partial\tilde{\varepsilon}^{(b)}/\partial E_{ul})[(dE_{ul}/da) - (2E_F/a)(dE_{ul}/dE_F)]\Delta a \ . \qquad (2\text{-}29b)$$

Very interestingly shear strain (directional stress) will yield quite different results as the crystal symmetry is reduced. According to Gerhardt (1968) resulting shifts of structure are mainly caused by changes in the band structure near symmetry points.

2.7. *Transitions at critical interband points.*

Most structure in optical spectra of metals is expected to be relatively smooth (e.g. section 2.7.3.) and therefore will not yield very discriminative data for an evaluation of band structures etc. However, two groups of transitions can be distinguished that possibly do give rise to well-defined structure: transitions taking place at critical interband points and transitions that involve the Fermi surface as initial or final state. Some models for later reference are introduced in this section.

2.7.1. *Critical interband point transitions.*

The JDOS, and thus $\varepsilon_2^{(b)}(\omega)$, has a singular character at frequencies for which

$$\nabla_{\underline{k}}[E_u(\underline{k}) - E_l(\underline{k})] = \nabla_{\underline{k}}E_u(\underline{k}) - \nabla_{\underline{k}}E_l(\underline{k}) = 0 \qquad (2\text{-}30)$$

One can distinguish two types of these so-called critical interband points (e.g. Phillips (1966), p. 67):

$$\text{symmetry interband points: } \nabla_{\underline{k}} E_u(\underline{k}) = \nabla_{\underline{k}} E_l(\underline{k}) = 0 \quad , \tag{2-30a}$$

$$\text{general interband points : } \nabla_{\underline{k}} E_u(\underline{k}) = \nabla_{\underline{k}} E_l(\underline{k}) \neq 0 \quad . \tag{2-30b}$$

A qualitative analysis is possible through a Taylor series expansion of the interband energy near a critical interband point at $\underline{k}_0$:

$$E_{ul}(\underline{k}) = E_u(\underline{k}) - E_l(\underline{k}) = E_0(\underline{k}_0) + \sum_{i=1}^{3} a_i (k_i - k_{0i})^2 \tag{2-31}$$

where $a_i = \hbar^2/2m_i'$. In analogy with eq. 2-1 we here introduced the interband effective mass tensor $\underline{\underline{m}}'$ such that $(\underline{\underline{m}}')^{-1} = \hbar^{-2}(\partial^2 E/\partial\underline{k}\partial\underline{k})$. As before one can distinguish four types of critical interband points M_0, M_1, M_2, M_3; the index indicates the number of negative a_i (i.e. m_i') in eq. 2-31. Knowing the shape of $E_u(\underline{k}) - E_l(\underline{k})$ one may now calculate the PJDOS in the vicinity of these critical points (Batz (1972), p. 344). Results are summarized in table 2-1.

Table 2-1

Behaviour of the band-to-band joint density of states (PJDOS) in the vicinity of critical interband points

Type	a_1	a_2	a_3	$2\pi^2\lvert a_1a_2a_3\rvert^{\frac{1}{2}} J_{lu}(E_{ul})$ $E_{ul}<E_0$	$E_{ul}>E_0$
Minimum M_0	+	+	+	0	$(E_{ul}-E_0)^{\frac{1}{2}}$
Saddle point M_1	+	+	-	$C-(E_0-E_{ul})^{\frac{1}{2}}$	C
Saddle point M_2	-	-	+	C	$C-(E_{ul}-E_0)^{\frac{1}{2}}$
Maximum M_3	-	-	-	$(E_0-E_{ul})^{\frac{1}{2}}$	0

In the neighbourhood of $\underline{k}_0$ the matrix elements do not vary to a great extent. Thus very simple relations may be obtained for $\varepsilon_2^{(b)}$ by substituting the appropriate JDOS into eq. 2-25. Kramers-Kronig analysis once again yields expressions to model $\varepsilon_1^{(b)}$ for transitions near $\underline{k}_0$ (Cardona, (1969), p. 18). The results are gathered in figure 2-5a. As a rule of thumb one may state that a square root singularity arises in all cases; the singularity in $\varepsilon_1^{(b)}$ occurs below E_0 when that of $\varepsilon_2^{(b)}$ is above E_0 and vice versa.

2.7.1.1. *Temperature dependence.*

Referring to section 2.6.5. the partial derivatives of $\tilde{\varepsilon}^{(b)}$ may be described using a function (Batz (1972), p. 331)

$$F(x) = [(x^2+1)^{\frac{1}{2}} + x]^{\frac{1}{2}}/(x^2+1)^{\frac{1}{2}} = \exp(\tfrac{1}{2}x)/\cosh x \quad . \qquad (2\text{-}32)$$

where $x = (\hbar\omega - E_0)/\Gamma$. Substituting the appropriate relations for $\varepsilon_1^{(b)}$ and $\varepsilon_2^{(b)}$ near a critical point, Batz (p. 350) obtained the results summarized in table 2-2 and figure 2-5b. Also included in the table is the derivative of $\varepsilon^{(b)}$ with respect to the phonon energy $\hbar\omega$.

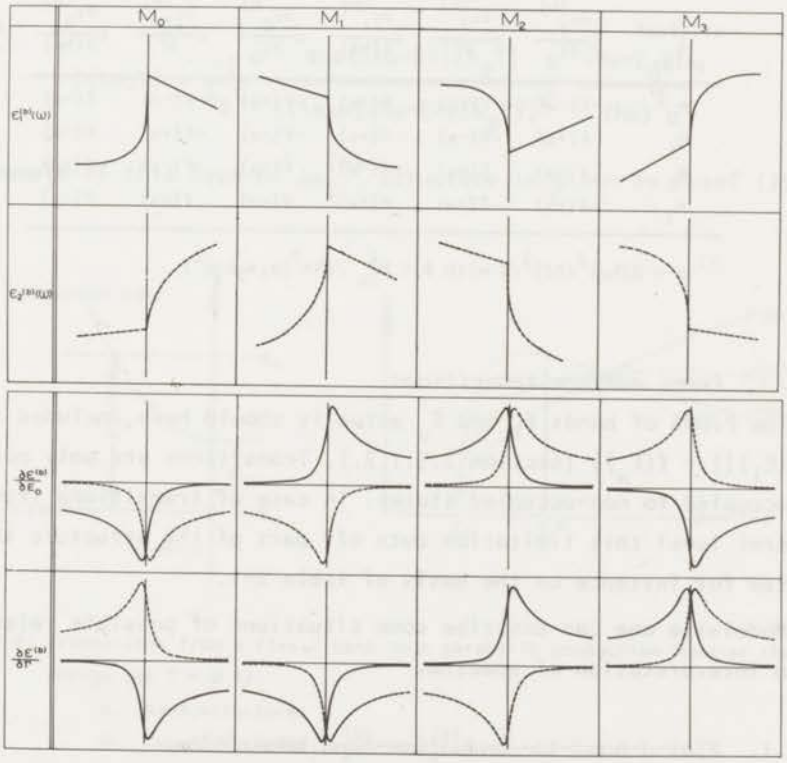

Fig. 2-5: The four types of three-dimensional critical interband points.
a: ε_1 and ε_2 plotted against $\hbar\omega$ in the vicinity of E_0.
b: $\delta\varepsilon_1^{(b)}/\delta E_0$, $\delta\varepsilon_1^{(b)}/\delta\Gamma$ (solid lines) and $\delta\varepsilon_2^{(b)}/\delta E_0$, $\delta\varepsilon_2^{(b)}/\delta\Gamma$ (broken lines) plotted against $x = (\hbar\omega - E_0)/\Gamma$.

Structure observed in optical spectra is often tentatively identified on the basis of theoretically predicted critical interband transitions. This procedure is not without serious criticism (section 2.7.3.).

It should be noted that in these deviations it was quietly assumed that $f(E_l) = 1$ and $f(E_u) = 0$, that is no account was taken of the possible influence of the Fermi distribution functions.

Table 2-2

The behaviour of the derivatives of $\varepsilon_1^{(b)}$ and $\varepsilon_2^{(b)}$ with respect to the critical point gap energy E_0, the Lorentzian broadening parameter Γ, and the photon energy $\hbar\omega$ near the critical points †).

critical point	$c\frac{\partial\varepsilon_1^{(b)}}{\partial E_0}$	$c\frac{\partial\varepsilon_1^{(b)}}{\partial\Gamma}$	$c\frac{\partial\varepsilon_1^{(b)}}{\partial(\hbar\omega)}$	$c\frac{\partial\varepsilon_2^{b)}}{\partial E_0}$	$c\frac{\partial\varepsilon_2^{(b)}}{\partial\Gamma}$	$c\frac{\partial\varepsilon_2^{(b)}}{\partial(\hbar\omega)}$
M_0	$-F(-x)$	$-F(+x)$	$F(-x)$	$-F(+x)$	$F(-x)$	$F(+x)$
M_1	$F(+x)$	$-F(-x)$	$-F(+x)$	$-F(-x)$	$-F(+x)$	$F(-x)$
M_2	$F(-x)$	$F(+x)$	$-F(-x)$	$F(+x)$	$-F(-x)$	$-F(+x)$
M_3	$-F(+x)$	$F(-x)$	$F(+x)$	$F(-x)$	$F(+x)$	$-F(-x)$

†) $c = 2(\hbar\omega)^2(2\Gamma)^{\frac{1}{2}}/B$ with $B = M_{lu}^2/(4\pi^2|a_1a_2a_3|^{\frac{1}{3}})$.

2.7.2. *Fermi surface transitions.*

The PJDOS of bands E_l and E_u actually should have included the factor $f(E_l)[1 - f(E_u)]$ (section 2.5.1.2.). Transitions are only possible from occupied to non-occupied states. In case of transitions from or to the Fermi level this limitation cuts off part of the structure that was expected for instance on the basis of table 2-1.

Modelwise one can describe some situations of possible relevance in the interpretation of spectra.

2.7.2.1. *Flat-d-band-to-conduction-band transition.*

(1) *Roseť (1972).*

Transitions from a relatively flat *d* band to a more or less parabolic conduction band (figure 2-6) may be described with a PJDOS of type M_0. However, part of the conduction band is filled such that transitions

are only possible for $\hbar\omega \geq E_F - E_d = E^* > E_0$, where E_d is the top of the d band. Assuming constant matrix elements table 2-1 yields an admittedly rough model for $\varepsilon_2^{(b)}(\omega)$.

$$\varepsilon_2^{(b)}(\omega) \propto (\hbar\omega - E_0)^{\frac{1}{2}} (\hbar\omega)^{-2} [1 - \{1 + \exp[(E_d + \hbar\omega - E_F)/k_B T]\}^{-1}]$$

$$(\text{for } \hbar\omega \geq E_0)^{\dagger)} \qquad (2\text{-}28a)$$

The temperature dependence of $\varepsilon_2^{(b)}$ follows upon substitution in eq. 2-28

$$\Delta\varepsilon_2^{(b)} \propto C(\hbar\omega, T)\{[(dE_{ul}/da) - (2E_F/a)](da/dT) + (\hbar\omega - E^*)/T\}\Delta T \qquad (2\text{-}28b)$$

where

$$C(\hbar\omega, T) = \frac{-1}{k_B T} \frac{\exp[(\hbar\omega - E^*)/k_B T]}{\{1 + \exp[(\hbar\omega - E^*)/k_B T]\}^2} \frac{(\hbar\omega - E_0)^{\frac{1}{2}}}{(\hbar\omega)^2} .$$

An example of this type of $\Delta\varepsilon_2^{(b)}$ structure is given by Rosei (1972; figure 4).

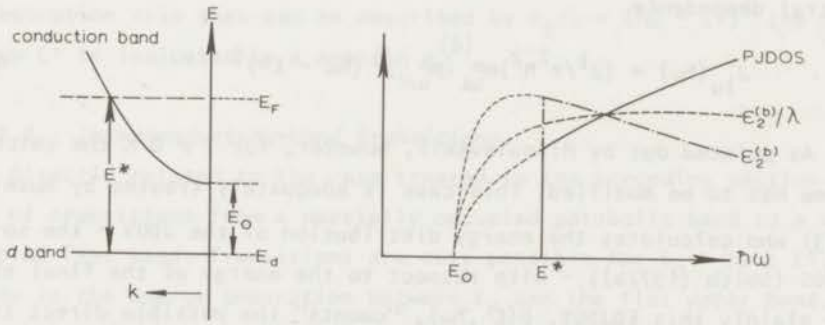

Fig. 2-6: Transitions from a flat d band to a parabolic conduction band at the Fermi energy (at T = 0 K):

a. band structure;

b. resulting PJDOS, $\varepsilon_2^{(b)}/\lambda$, $\varepsilon_2^{(b)}$.

†) The analogous formula given by Rosei (1972, p. 3887) is in error.

(2) *Cooper (1965), Miloslavskii (1967).*

Because of the possible relevance in the analysis of the absorption edge in the noble metals model calculations have been carried to greater detail (also Haga (1965)). Choosing a new coordinate system with origin at L one tries to model the band structure near L by parabolic bands making use of appropriate effective band masses (section 2.2.4.). Thus an energy surface near L is represented by

$$E_n = E_{L,n} + \hbar^2 k_{//}^2 / 2m^*_{n//} + \hbar^2 k^2 / 2m^*_{n\perp} \quad , \tag{2-29}$$

where $E_{L,n}$ is the energy at L and // and $\perp$ are used to denote band structure quantities which are appropriate, respectively, parallel and perpendicular to the ΓL direction (see e.g. figure 2-6). The formulas derived by Cooper (1965) and Miloslavskii (1967) are applicable at T = 0 K. They predict a parabolic behaviour of the PJDOS above the edge. The Fermi surface condition enters in the equations through an additional factor containing the effective band and interband masses. For the simplified case of a perfectly flat *d* band ($m^*_L = \infty$) both authors predict the same spectral dependence

$$J_{lu}(\hbar\omega) = (2^{\frac{1}{2}}/\pi^2\hbar^2) m^*_{u\perp} (m^*_{u//})^{\frac{1}{2}} (\hbar\omega - E^*)^{\frac{1}{2}} \tag{2-30}$$

As pointed out by Miloslavskii, however, for T $\neq$ 0 K the calculation scheme has to be modified. This case is adequately treated by Rosei (1973) who calculates the energy distribution of the JDOS - the so-called EDJDOS (Smith (1972a)) - with respect to the energy of the final state. More plainly this EDJDOS, $D(E_u, \hbar\omega)$, "counts" the possible direct transitions at a photon energy $\hbar\omega$ to final states with energy E_u. Only final states in the neighbourhood of the Fermi surface are affected by a change of the Fermi distribution; the initial states are sufficiently far below E_F to be occupied permanently. Substituting the appropriate Fermi distribution factor $[1 - f(E_u)]$ (section 2.5.1.) and assuming constant matrix elements (section 2.5.5.) Rosei obtains the expected line shape of $\Delta\varepsilon_2$:

$$\Delta\varepsilon_2 \propto -\Delta T (\hbar\omega)^{-2} \int D(E_u, \hbar\omega) \frac{\partial f(E_u, T)}{\partial T} \, dE_u \quad . \tag{2-31}$$

The EDJDOS is calculated from the model of Cooper, Ehrenreich and Phillip. Using feasible values of the band parameters Rosei obtained a striking similarity between the theoretical and experimental (i.e. thermomodulation) line shape of Au. The problem is complicated somewhat by contributions from other temperature dependent mechanisms (shift of one of the bands, shift of E_F, etc.).

(3) *"Type M_0 critical interband point".*

Looking at table 2-1 a parabolic dependence of the PJDOS $J_{1u}(\hbar\omega) \propto (\hbar\omega - E^*)^{\frac{1}{2}}$ as obtained by Cooper and Miloslavskii (eq. 2-30) is well described as that of a type M_0 critical interband point. Disregarding the physics behind this analogy the expected line shape of $\partial\varepsilon_2^{(b)}/\partial E^*$ follows from figure 2-5b.

Summarizing, if the absorption edge is due to Fermi surface transitions in a rather localized area of $\underline{k}$-space in the vicinity of L, one can expect to find an almost parabolic behaviour of $\varepsilon_2^{(b)}$ as a function of photon energy $\hbar\omega$. It has been shown by Miloslavskii (1966) that for an absorption rise that can be described by $\varepsilon_2/\lambda \propto (\hbar\omega - E^*)^{\frac{1}{2}}$ the onset energy E^* is indicated by a peak in $\varepsilon_1^{(b)}$.

2.7.2.2. *Interconduction-band transitions.*

Directly related to the case treated in the preceding section is that of transitions from a partially occupied parabolic band to a non-occupied flat band. Transitions are only possible for $E_0 > \hbar\omega \geq E^*$, where E^* now is the energy separation between E_F and the flat upper band. The critical interband gap E_0 is of the type M_3. Thus in analogy to eq. 2-28:

$$\varepsilon_2^{(b)}(\omega) \propto (E_0 - \hbar\omega)^{\frac{1}{2}} (\hbar\omega)^{-2} \{1+\exp[(E_L(\underline{k}) - E_F)/k_B T]\}^{-1} \qquad (2\text{-}32)$$

$$(\text{for } \hbar\omega < E_0) \quad .$$

As before the model can be extended to describe a typical situation encountered in all noble metals. This description is particularly relevant as the situation - sketched in figure 2-7a - occurs at the L gap

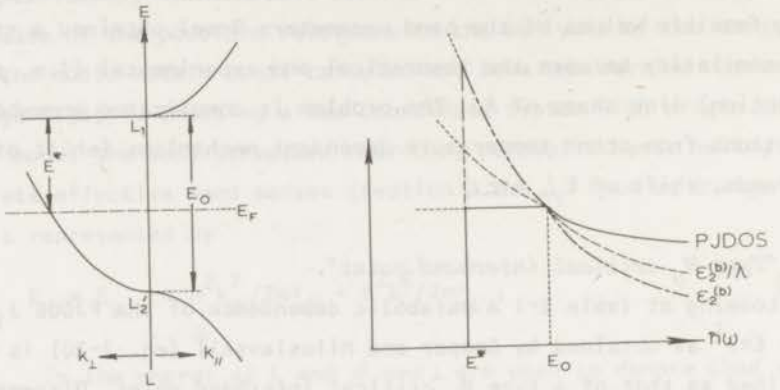

Fig. 2-7: Interconduction-band transitions to the Fermi energy (at T = 0 K) :
a. band structure;
b. resulting PJDOS, $\varepsilon_2^{(b)}/\lambda$, $\varepsilon_2^{(b)}$.

(nonrelativistic: $L_2' \rightarrow L_1$), the theoretical value of which was found to be highly sensitive to the choice of crystal potential (section 2.2.).

Again eq. 2-29 is used to describe the upper and lower conduction bands around L. In view of the band shape in the $\underline{k}_{//}$ direction the critical interband point is of the type M_2. Using table 2-1 it follows

$$\varepsilon_2^{(b)}(\omega) \propto C(\hbar\omega)^{-2}\{1+\exp[(E_L(k_\perp)-E_F)/k_BT]\}^{-1} \quad \text{for } \hbar\omega < E_0,$$

$$\varepsilon_2^{(b)}(\omega) \propto C(\hbar\omega)^{-2} - (\hbar\omega-E_0)^{\frac{1}{2}}(\hbar\omega)^{-2} \quad \text{for } \hbar\omega > E_0 . \qquad (2\text{-}33)$$

The resulting structure is sketched in figure 2-7b. Somewhat more refined versions of this so-called box model have been proposed in the analysis of piezoreflectance (Morris (1969)) and photoemission work (Koyama (1970), Lindau (1971b), Nilsson (1973a)).

The temperature dependence can be evaluated by procedures similar to those indicated in the preceding section.

2.7.3. *Transitions in extended regions.*

On the basis of band calculations Kane (1966) suggested for the case

of Si that absorption due to transitions in extended rather than in localized regions of $\underline{k}$-space contributes the main structure to ε_2 spectra. For the noble metals this has been supported by the band calculations of Fong (1970; Cu) and Williams (1972; Cu) and Christensen (1971, 1972a,b; Au,Ag). Good agreement was obtained between calculated and experimental spectra; the main features of the absorption spectra could then be assigned to specific band-to-band transitions over extended regions of $\underline{k}$-space. Christensen (1972a) shows photoemission structure in Au to originate from extended regions; however, he explains modulation spectra by means of localized transitions treated in section 2.7.2. (Christensen (1971)).

In this respect most attention has been concentrated on the absorption edge. In section 2.7.2.1. it was suggested that flat *d* band → parabolic *sp* band at E_F in the vicinity of L would provide a good explanation for the absorption edge. However, Ehrenreich (1962) (also Cooper (1965), Cardona (1969, p. 83)) showed that relatively sharp edges in the absorption spectrum can be expected from transitions between two bands over extended regions of $\underline{k}$-space, if one of the bands is flat whereas the other crosses the Fermi level. As such it belongs to the class of Fermi surface transitions. As shown in eq. 2-22 $\varepsilon_2^{(b)}(\omega)$ is more or less determined by the integral over surfaces of constant interband energy $\hbar\omega$ with the condition that $E_L < E_F < E_u$. Assuming a perfectly flat lower band $E_L(\underline{k})$ is constant for all $\underline{k}$. Then, in view of eq. 2-23 $\hbar\omega = E_u(\underline{k}) - E_l(\underline{k})$, in $\underline{k}$-space the surfaces of constant interband energy $\hbar\omega$ coincide with the surfaces of constant E_u. If the upper band "crosses" the Fermi level such that $E_u^{(1)} = E_F$, one of the surfaces of constant interband energy, $\hbar\omega^{(1)}$, coincides with the Fermi surface: $\hbar\omega^{(1)} + \text{constant} = E_u^{(1)} = E_F$. A slightly larger energy $\hbar\omega^{(2)}$ corresponds with $\hbar\omega^{(2)} + \text{constant} = E_u^{(2)} > E_F$; a smaller energy $\hbar\omega^{(3)}$ with $\hbar\omega^{(3)} + \text{constant} = E_u^{(3)} < E_F$. Thus, as $\varepsilon_2^{(b)}(\omega)$ is dependent on the surface integral over that part of the surface of constant interband energy at which $E_l < E_F$ and $E_u > E_F$, in case of a flat and occupied lower band a sharp rise in $\varepsilon_2^{(b)}$ will be observed when the whole surface of constant $\hbar\omega$ is activated. In practice this structure will be broadened and weakened by the temperature dependence of the Fermi distribution function and especially by the sloping of the lower band.

Such an explanation of the absorption edge has been strongly sup-

ported for Au by Christensen (1971) who showed that at the onset of strong interband absorption a large portion of the constant interband energy surface coincides with the Fermi surface. The shape of the absorption edge thus is determined by the JDOS (and possibly matrix elements); that it is found to be parabolic must be considered somewhat coincidental

2.7.3.1. *Temperature dependence.*

Accurate knowledge of the EDJDOS would in principle allow the determination of the temperature induced changes of ε_2 according to eq. 2-28. In the absence of such quantitative information a few general statements can be made regarding the expected structure of $\Delta\varepsilon_2(\Delta T)$ or $[\varepsilon_2(T_2) - \varepsilon_2(T_1)]$. In principle Fermi surface transitions can be distinguished from transitions that do not involve the Fermi surface by the differing temperature dependence of $\Delta\varepsilon_2$. From eq. 2-28 and figure 2-4 it may be expected that $\Delta\varepsilon_2$ (Fermi surface transitions) will increase and sharpen at low temperatures (decrease and broaden at high T). For non-F.S. transitions, however, lattice expansion is the expected dominating factor (section 2.6.4.) and consequently the ensuing $\Delta\varepsilon_2$ structure is small at low T and increases at high T.

2.8. *The X-point.*

In studies of the temperature dependence of the optical properties frequent attention has been paid to the so-called X-points. The physical background of these points - characterized by the temperature independence of a specific parameter (e.g. reflectivity, emissivity, ε_1, ε_2) at a certain photon energy - has been subject to speculation. However, in a separate publication (Winsemius (1973b)) we conclude on the basis of the results on Ag presented in chapter 4. that - as also suggested by Latyev (1970) et al. - the existence of X-points is determined by the relative invariance of transitions originating from initial states in the *d* bands. In the noble metals the temperature induced shift of the upper *d* bands, the lower conduction band near E_F and E_F is approximately the same. Absorption structure between these bands (see section 2.7.2.1.) therefore is little temperature dependent leading to the observation of X--points (actually more probably X-regions). No such effect is found for

interconduction-band transitions (section 2.7.2.2.) where the X-point is spoiled by the larger shift of the upper conduction band.

A fairly complete introduction to the subject is given by Verch (1967), Latyev (1970) and Winsemius (1973b). More extensive discussion of our results is given in the latter article; we therefore refrain from further discussion on this subject. In our opinion the importance of X-points as a characteristic optical constant should not be overemphasized (Otter (1961b)).

2.9. *Related techniques for band structure spectroscopy.*

2.9.1. *Modulation spectroscopy.*

Principles and techniques of modulation spectroscopy are outlined in a number of reviews (Cardona (1969), Seraphin (1970,1972), Willardson (1972)). By a small a.c. variation of a sample parameter the optical properties are modulated. Analysis of the a.c. modulation - usually measured as a change in the reflection - yields a derivative spectrum of the dielectric constant with respect to the variable parameter: hydrostatic or uniaxial strain (piezoreflectance), temperature (thermoreflectance), electric field (electroreflectance), magnetic field (magnetoreflectance), alloy concentration (alloy modulation). In one of the best-known techniques, one changes the wavelength of the light, i.e. not an internal sample parameter. As such wavelength modulation does not belong to the same group of methods; it yields a direct derivative of the static spectra. In the case of thermomodulation the formulas derived in section 2.6. apply (e.g. eq. 2-26,28) to the analysis of line shape and magnitude of $\Delta\varepsilon_2$. Strongly related expressions for wavelength and hydrostatic pressure modulation are given in eqs. 2-29a,b. Kramers-Kronig analysis is generally used to obtain $\Delta\varepsilon_1$.

Very generally it is stressed that modulation spectroscopy is a particularly strong tool in lifting out structure due to critical points transitions from a more or less structureless background. This would be a major advantage over the results obtained by direct measurement of the optical properties, where the sharp features due to discontinuities of the JDOS at critical points (section 2.7.1.) will drown in the broad structure originating from extended regions of the Brillouin zone. Thus

the various modulation techniques would provide exactly that information which is required by band theorists for the choice of a suitable crystal potential.

The arguments underlying the critical point assumption - if given at all - are somewhat hand-waving. Seraphin (1972, p. 171) points at the following:

(1) The entirely different line shapes of static and modulated reflectance.

(2) On a qualitative basis, the modulated response can be approximated by the differential of the predicted ε_2 line shapes at critical points (e.g. section 2.7.1., figure 2-5), whereas the approximation calls for considerable imagination in the case of static reflectance.

(3) The spectral width of modulated response is typically 20 to 50 times smaller than the width of reflectance structure.

(4) No response is obtained over large regions of the spectrum, suggesting that only limited areas of the Brillouin zone are affected by the modulation.

Seraphin (1972, p. 194) suggests a probable explanation for this critical point selectivity of modulation techniques. Using the constant matrix elements approximation (section 2.5.5.) modulation of E_0 causes a variation of $\varepsilon_2^{(b)}$:

$$\Delta\varepsilon_2^{(b)}/\Delta E_0 = (C'/\omega^2)(\Delta J/\Delta E_0).$$

At all types of symmetry interband points the $J_{1u}(\hbar\omega)$ varies as the square root of the spectral distance from E_0 (section 2.7.1., table 2-1). Hence the derivative with respect to E_0 has a singularity of the type $(E_0-\hbar\omega)^{-\frac{1}{2}}$ at the critical point. The response disappears as the spectral distance from E_0 increases. Noncritical areas with a smooth JDOS function contribute very little to the modulation spectrum.

Although possibly true for semiconductors considerable care should be taken in applying this model to metals. As shown in preceding sections much structure both in $\varepsilon_2^{(b)}(\omega)$ and the JDOS is probably due to transitions involving the Fermi surface. The cut-off or cut-on of $J_{1u}(E_{u1})$ (e.g. sections 2.7.2., 2.7.3.) may cause equally sharp structure in the

$\Delta\varepsilon_2^{(b)}$ spectrum. Also it will be seen in chapters 3. and 4. that the four more or less qualitative arguments given by Seraphin are not very compelling in the case of Au and Ag. Thus a critical point analysis of modulation spectra of the noble metals should be performed with some reservation.

A state-of-the-art report on progress in this field will appear in the Proceedings of the First International Conference on Modulation Spectroscopy (Seraphin (1973)).

2.9.2. *Ultraviolet photoemission spectroscopy.*

A very powerful tool for the study of band structures is ultraviolet photoelectron spectroscopy (UPS) or, shortly, photoemission. Light of photon energy $\hbar\omega$ is incident on a metal, exciting an electron from an initial state with energy E_l to a final state with energy E_u. If $E_u - E_F$ is larger than the work function ϕ and if the electron moves (in principle unscattered) in the right direction, the electron can escape from the metal. Analysis of the kinetic energy of the escaped electron together with a knowledge of the work function and of the incident photon energy allows the determination of the initial and final state energies relative to the Fermi energy E_F:

$$E_F - E_l = \hbar\omega - E_{kin} - \phi \ , \qquad (2\text{-}34a)$$

$$E_u - E_F = E_{kin} + \phi \ . \qquad (2\text{-}34b)$$

Thus the photoemission experiment allows the measurement of both E_l and E_u. This clearly is an advantage over the optical properties where one can only determine $E_u - E_l$.

Experimentally one measures the energy distribution curve (EDC; i.e. the number of photoemitted electrons with a certain kinetic energy against that kinetic energy) for a fixed incident photon energy. Comparing the shift of peaks in the EDC's obtained at various photon energies one can distinguish

(1) $\Delta E(\text{peak}) = 0$ indicating a maximum in the DOS at final states;

(2) $\Delta E(\text{peak}) = \Delta(\hbar\omega)$ indicating a maximum in the DOS at final states:

$$E(\text{peak}) = E_1 + \hbar\omega \ ;$$

(3) $\Delta E(\text{peak}) \neq \Delta(\hbar\omega)$.

The first two types of structure can most easily be explained assuming nondirect transitions (section 2.5.4.3.). Assuming constant matrix elements one thus obtains direct experimental evidence of the DOS which in view of the uncertainties involved is usually called the optical density of states (ODS). It would provide a very attractive feature of photoemission.

To explain (1) and (2) by means of direct transitions (section 2.5.4.3 2.5.4.2.) one has to assume a flat upper respectively a flat lower band (many states with energy $E(\underline{k})$). In such cases no difference can be seen between direct and nondirect transitions. For sloping initial and final state bands, $E_l(\underline{k})$ and $E_u(\underline{k})$, the peak in the EDC's may move to higher and lower energies nonproportionally to the steps in $\hbar\omega$. Thus shift of type (3) is usually explained by direct transitions. The discussion on the direct - vs. - nondirect transitions is still wide open. Lately the tendency has been towards a reconfirmation of the theoretically more satisfying direct transition model (e.g. Smith (1969b,1971,1972a), Nilsson (1970), Lindau (1971b), Christensen (1972a,b)).

Theoretically and technically the photoemission experiment is considerably more difficult than the measurement of the optical properties in the same wavelength region. The range of final state energies is limited at the low energy side by the work function of the metal or of a coating (Cs). More importantly, various interaction mechanisms lead to scattering of the electrons thus influencing the escape probability and resulting a.o. in secondary electron emission. At high photon energies the scattering length of the excited electron becomes very small, for Au typically 20 or 30 Å for an electron 5 ot 10 eV above E_F (Spicer (1972), p. 796 f.f.). Thus only a very thin surface layer of the specimen is "active" in the photoemission process, causing an extreme sensitivity to surface conditions. Also the determination of the work function (from the lowest photon energy at which one still detects a signal due to photo-

emitted electrons) is somewhat problematic as demonstrated by the major discrepancies in the literature values. Still with the improving experimental possibilities (ultrahigh vacuum $\leq 10^{-10}$ torr; detection techniques; higher derivative techniques; angular dependence spectroscopy) photoemission undoubtedly will continue to provide greatly interesting data. Recent review articles have been written by Spicer (1972) and Eastman (1972a).

2.9.3. *Other techniques.*

1. X-ray photoelectron spectroscopy (XPS).
   Electron spectroscopy for chemical analysis (ESCA).

X-ray emission of electrons is followed by analysis of the kinetic energy of the emitted electrons (see section 2.9.2.). Techniques and possibilities are reviewed by Siegbahn et al. (1967); see also the Proceedings of the Conference on Electron Spectroscopy (Shirley, 1972).

2. Soft X-ray emission spectroscopy (SXS).

X-ray excitation of a core electron is followed by a jump of an outer electron to the hole state. The emitted light gives information about the energy difference between the occupied states. Alternatively Auger transitions may occur: the energy is transferred to another electron that is emitted. For light metals this latter process is dominant.

3. X-ray absorption spectroscopy.

Core electrons are excited by X-ray radiation to states just above E_F. Analysis of the transmitted radiation together with knowledge of its photon energy and the energy of the core states yields information on the unoccupied final states.

4. Ion neutralization spectroscopy (INS).

An incident ion is neutralized by attracting an electron from a higher energy level. The freed energy is transferred to another electron that is emitted. The principles are outlined by Hagstrum (1971).

CHAPTER 3: GOLD

3.1. *Motivation.*

The motivation of the choice of Au is two-fold.

Initially plans were to measure the optical properties of dilute alloys of Au with transition metals. In view of the favourable properties of Au (no oxidation, little adsorption) it was thought profitable to calibrate the apparatus on the pure metal. Numerous reports on the optical properties of Au have appeared in the literature. However, especially at low temperatures we found new structure ("splitting") in the absorption edge (section 3.8.4.).

In the meantime relativistic band calculations for normal (T = 0 K) and expanded lattices (Christensen (1971)) indicated the possible interest of measurements over extended temperature regions especially so in regard to the highly temperature sensitive interconduction-band transitions in the vicinity of L. Analysis of this type of structure has mostly been the privilege of modulation spectroscopists and people working on photoemission. In view of the expected dominance of lattice expansion in temperature induced changes of the band structure and the approximately linear temperature dependence of this expansion for $T \gg \theta_D$, a discussion with Dr. Christensen suggested the possible relevance of "thermovariation" spectra. Thermovariation - a word that we introduced to distinguish the effect from thermomodulation [†)] - actually consists of the subtraction of static spectra obtained at different temperatures. It is shown in section 3.5. that indeed a very good agreement is found with thermomodulation results. As the latter experiment essentially has to be performed on thin evaporated films, the highest temperature that can be reached is limited to about 400 K. A major advantage of thermovariation therefore is the larger temperature range that permits a more extensive analysis of shifts of structure. The main part of this chapter is devoted to this type of analysis that is shown to provide a powerful tool in the exploration of band structure.

As the possibilities of thermovariation became known after the completion of our experiments we had to incorporate data from other sources

[†)] Actually the terms "difference" and "differential" would be more appropriate than "variation" and "modulation".

into our analysis. Generally this was associated with a decrease of accuracy causing an uncertainty in some evaluations. Measurements on a single-crystal Au specimen, that hopefully will answer some of the questions posed in this chapter, are being undertaken at the time of writing.

3.2. *Band structure.*

Results of a RAPW calculation (normal volume: T = 0 K) by Christensen (1971) are presented in figure 3-1. Comparing with his nonrelativistic APW band structure (figure 2-2) it is obvious that important differences arise (also section 2.2.2.). Similar conclusions have been reported by Ramchandani (1970) and Smith (1972b). Some representative data concerning spin-orbit splitting in Au have been given by Christensen (1972a, table I). Noting that a number of nonrelativistic calculations have appeared (Ballinger (1969), Chatterjee (1967b, 1968), Jacobs (1968), Kupratakuln

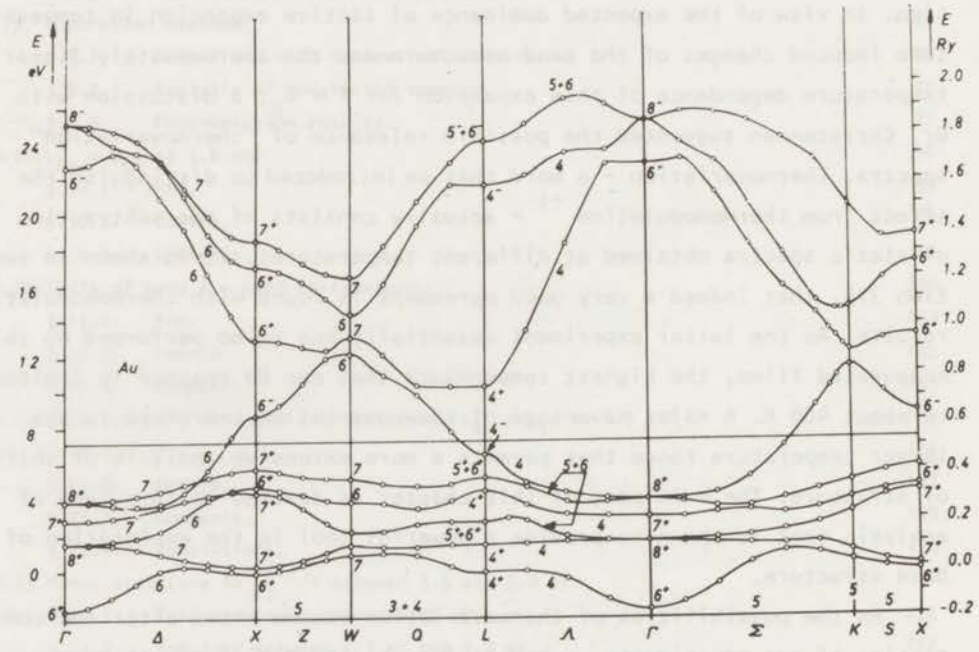

Fig. 3-1: RAPW energy bands of gold (normal volume: T = 0 K) obtained by Christensen (1971).

(1969), O'Sullivan (1970), Schlosser (1970)), we will limit ourselves to the relativistic results.

Considerably different values of the energy levels at high symmetry points in the reciprocal lattice have been obtained in the relativistic calculations on Au by Sommers (1969), Connolly (1970), Kupratakuln (1970), Ramchandani (1970, 1971), Christensen (1971) and Smith (1972a). The best agreement is obtained by Connolly, Kupratakuln and Christensen. The results by Sommers, Ramchandani and Smith can be criticized on theoretical-computational grounds (Christensen (1971, 1972a)).

Assuming constant matrix elements (section 2.5.5.) one can calculate the contributions of the various pairs of bands to $\varepsilon_2^{(b)}/\lambda$ from the PJDOS as obtained by Christensen †). Such "partial $\varepsilon_2^{(b)}/\lambda$" spectra are shown in figure 3-2 for normal (T = 0 K) and expanded lattice (T ≈ 920 K) calculations.

3.3. *Literature review.*

Numerous reports on the optical properties of Au have been published. A review of the experimental and theoretical knowledge in the pre-band--calculation era has been given by Suffczynski (1964). From the older experimental work one should mention that on vacuum-grown single-crystals by Otter (1961a). A major step forward in the interpretation as related to band structure was due to Cooper (1965), Ehrenreich and Philipp. A survey of publications that have appeared since that time on optical work with a direct relevance to the study of band structure comprises over 40 titles. These articles are spread out rather evenly over four major fields - optical properties, photoemission, alloys and modulation spectroscopy - with quantitatively smaller contributions from other disciplines such as ESCA. Rather than listing these references here we will introduce them whenever relevant. Furthermore one is referred to the forthcoming review article on the optical properties of metals by Nilsson (1973b).

For a long time the standard work on the temperature dependence of

†) We wish to thank Dr. Christensen for providing us with the otherwise unpublished PJDOS of the expanded lattice band calculations.

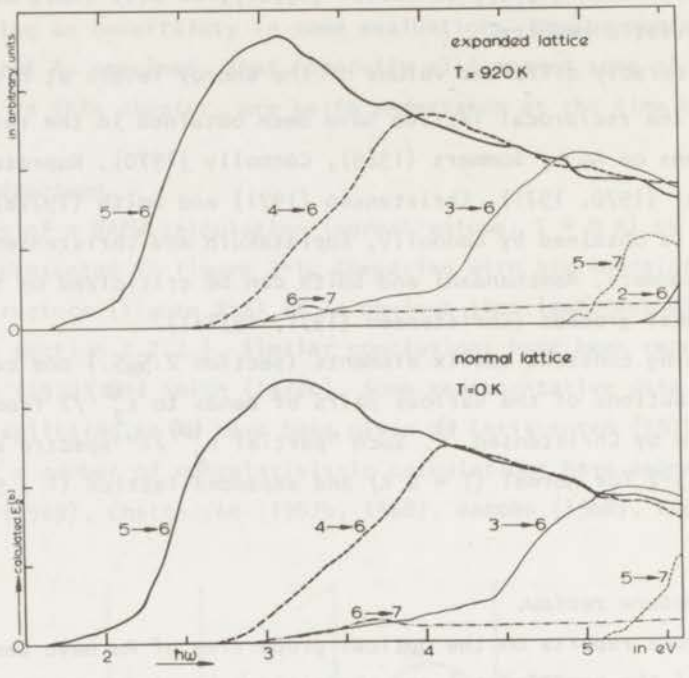

Fig. 3-2: Partial $\varepsilon_2^{(b)}/\lambda$ - vs. - $\hbar\omega$ spectra of Au at T = 0 K and T = 920 K ††).

the optical properties of the noble metals was due to Joos (1954) and Klopfer. The later work of Otter (1961b) - more accurate and spanning a much larger temperature interval between 283 K and the melting point - has somehow escaped attention. Further work has been reported by Hodgson (1968) and Stahl (1968). The first ones to use the temperature dependence as a serious tool to study the interband transitions, however, were Pells (1969) and Shiga who obtained spectra at photon energies between 0.5 and 5.9 eV and temperatures ranging from 295 to 770 K.

††) Actually Christensen's calculation was made for an expanded lattice (a = 7.7820 a.u.; private communication). Using literature values of the lattice expansion (Nix (1941), Corruccini (1961)) and the normal volume (T = 0 K) value of the lattice constant (a = 7.6813 a.u.) the expanded lattice is found to correspond with a temperature of about 920 K. This is considerably higher than the 750 K estimated by Christensen using a rougher approach. It should be noted that in figures 3-2 no account is taken of Fermi distribution broadening.

3.4. *Experiment.*

3.4.1. *Sample.*

A polycrystalline Au sample (purity 5N+; average grain diameter 1.5 mm) was cut and planed into its required shape (diameter 27 mm, thickness 3.5 mm) by spark erosion. Mechanical polishing was done by an etch-attack technique (Samuels (1971), p. 145): Al_2O_3 powder (final stage 0.05 micron) is made into an abrasive slurry by adding a 10% CrO_3 solution. Subsequently the specimen was electrolytically polished on the rotating wheel machine (see section 5.3.1.); best results were obtained using an electrolyte consisting of

9.6	g.	$Na_2S_2O_3$
4.2	g.	NH_4CNS
5	ml.	H_2SO_4 (96%)
5	ml.	HF (40%)
285	ml.	butylcellosolve
55	ml.	deionized H_2O.

The current density was 3.5 mA/cm^2.
The surfaces thus obtained were shiny, flat except for a rounding at the edges, and did not show any relief structure due to preferential attack of some crystallites. Polishing was continued until all traces of mechanical polishing were removed. This was confirmed by a sharpening of X-ray patterns; very minor differences only are noted after annealing the electropolished sample.

Directly after polishing the specimen was mounted in the sample holder and the vacuum chamber was pumped down. At all further stages the vacuum was of the order of 10^{-7} mm/Hg or better.

Unless stated otherwise the specimen was heated in vacuum for periods of at least 4 hours and a temperature of 700 K or higher. This heat treatment serves to anneal remaining surface distortion due to the mechanical treatment (also spark erosion) (e.g. Köster (1967)) and in addition it cleans the surface (e.g. Fane (1968)). A distinct disadvantage is due to thermal etching that results in a roughening and faceting of the surface (e.g. Moore (1963), p. 176 f.f.) thus increasing the amount of scattered

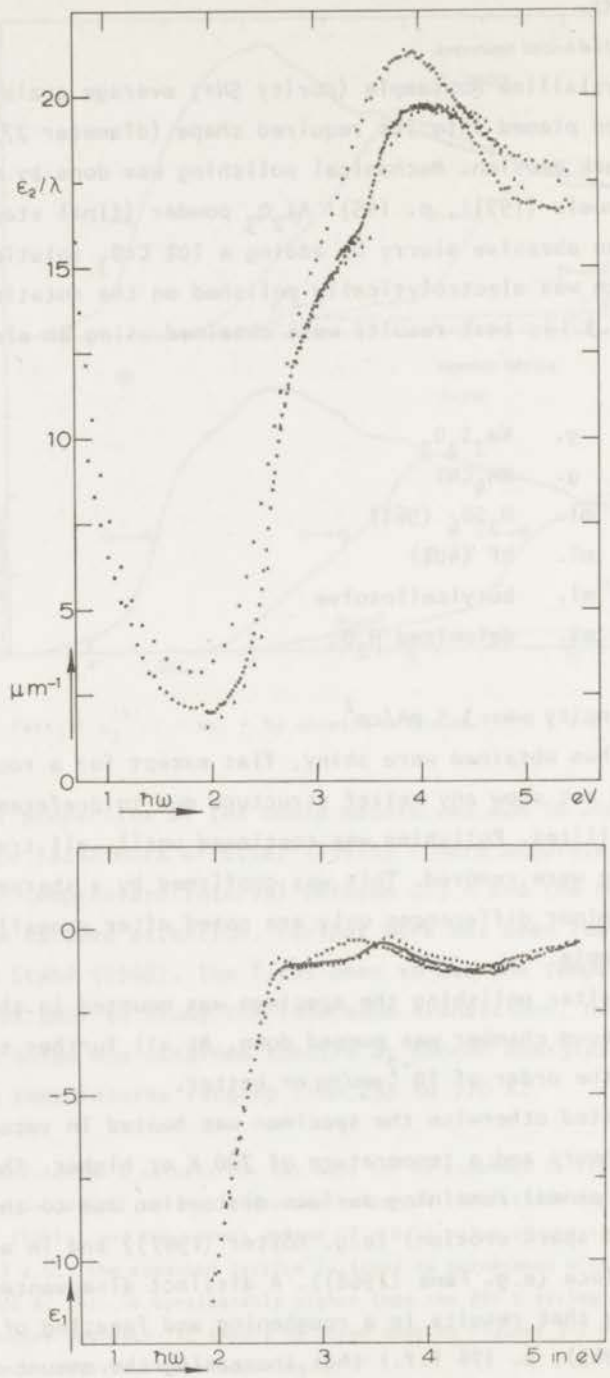
20
15
10
5
0
ε_2/λ
μm^{-1}
1 $\hbar\omega$ 2 3 4 5 eV
0
-5
-10
ε_1
1 $\hbar\omega$ 2 3 4 5 in eV

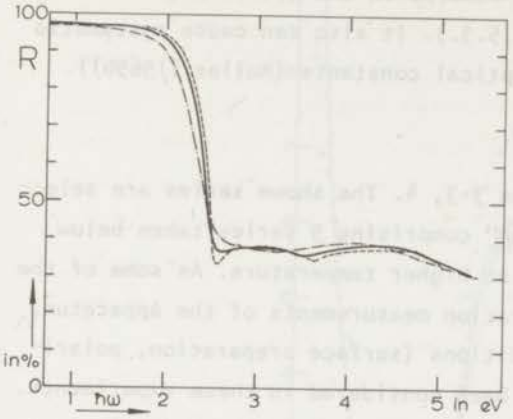

Fig. 3-3: Optical properties of Au for T = 40 K (▲), 295 K (●) and 725 K (■):

a. ε_2/λ - vs. - $\hbar\omega$

b. $-\varepsilon_1$ - vs. - $\hbar\omega$

for T = 40 K (dash-dash), 295 K (solid) and 725 K (dash-dot):

c. R - vs. - $\hbar\omega$

d. n - vs. - $\hbar\omega$

e. k - vs. - $\hbar\omega$

f. $\mathrm{Im}(1/\tilde{\varepsilon})$ - vs. - $\hbar\omega$

g. $\mathrm{Im}[1/(\tilde{\varepsilon}+1)]$ - vs. - $\hbar\omega$

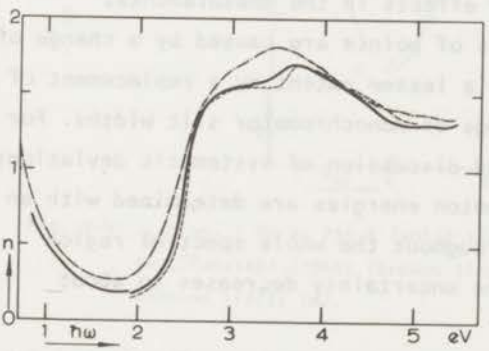

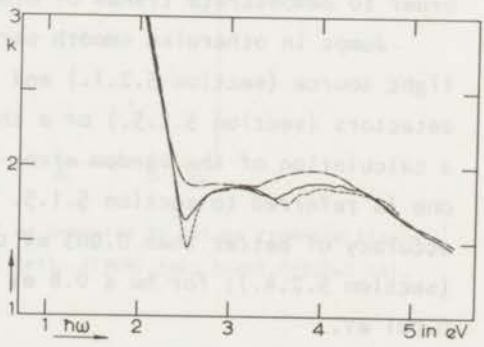

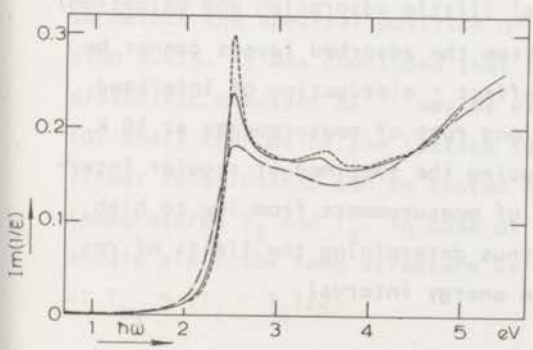

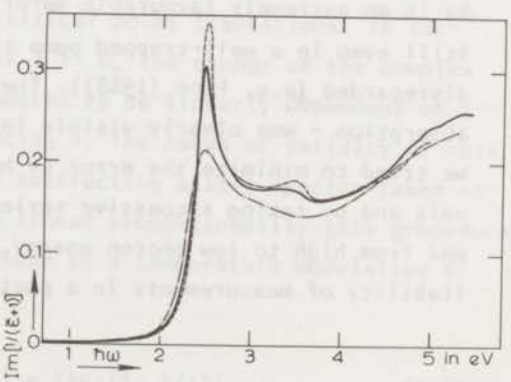

light and possibly causing anomalous absorption and deviations from the Drude theory (see sections 3.5.2., 3.5.3.). It also can cause systematic errors in the determination of the optical constants (Muller (1969b)).

3.4.2. *Experimental results.*

Results are presented in figures 3-3, 4. The shown series are selected from a very extensive "collection" comprising 9 series taken below 295 K, 11 at room temperature and 5 at higher temperature. As some of the older series were intended as calibration measurements of the apparatus, a great variety of experimental conditions (surface preparation, polarizer adjustments, light sources) has been considered in these experiments. The quoted curves must be considered to represent our best data; at some instances (usually qualitative) use will be made of earlier series in order to demonstrate trends or minor effects in the measurements.

Jumps in otherwise smooth series of points are caused by a change of light source (section 5.2.1.) and to a lesser extent by a replacement of detectors (section 5.2.5.) or a change of monochromator slit widths. For a calculation of the random error and discussion of systematic deviations one is referred to section 5.1.5. Photon energies are determined with an accuracy of better than 0.005 eV throughout the whole spectral region (section 5.2.4.); for $\hbar\omega \leq 0.8$ eV the uncertainty decreases to about 0.001 eV.

Especially at low temperatures systematic errors are introduced due to the growth of adsorbed layers on the specimen surface. In this respect Au is an extremely favourable material (little adsorption and oxidation). Still even in a well-trapped pump system the adsorbed layers cannot be disregarded (e.g. Fane (1968)). The effect - a reduction of interband absorption - was clearly visible in long runs of measurements at 40 K. We tried to minimize the error by heating the specimen at regular intervals and by taking successive series of measurements from low to high and from high to low photon energy, thus determining the limits of reliability of measurements in a photon energy interval.

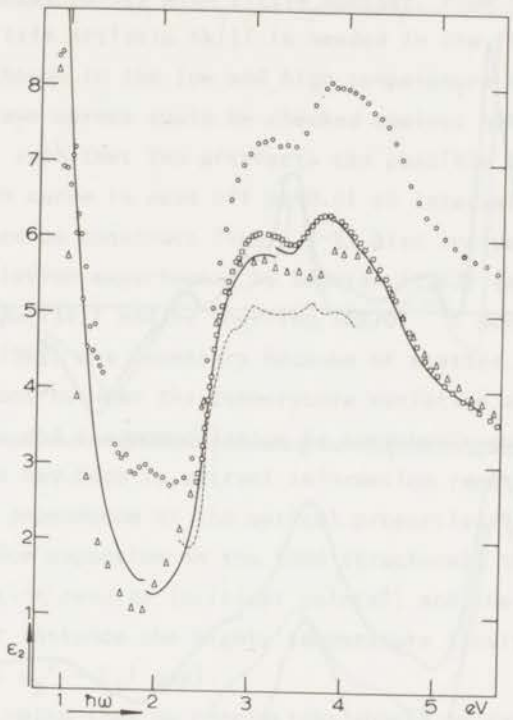

Fig. 3-4: ε_2 - vs. - $\hbar\omega$ at 295 K (solid line) as compared to values from the literature: Fukutani (1966) (broken line), Pells (1969) (○), Irani (1971a) (□), Johnson (1972) (△).

3.5. *Thermovariation.*

As stated in section 2.9.1. modulation spectroscopy is often used to detect the spectral position of critical point transitions. In section 2.6.5. it was concluded that for $T >> \theta_D$ the change of the complex dielectric constant $\Delta\tilde{\varepsilon}^{(b)}$ may be expected to be linearly dependent on T for small changes of the lattice spacing a. The range of validity of this linear relationship can be tested by subtracting static spectra taken at temperatures T_1 and T_2. In case of a linear proportionality this procedure should yield the same structure as found by a temperature modulation ΔT at $T_{av} = (T_1 + T_2)/2$:

$$[\varepsilon_2(T_1) - \varepsilon_2(T_2)]/[T_1 - T_2] = [\Delta\varepsilon_2(T_{av})/\Delta T]_{modulation}. \quad (3\text{-}1)$$

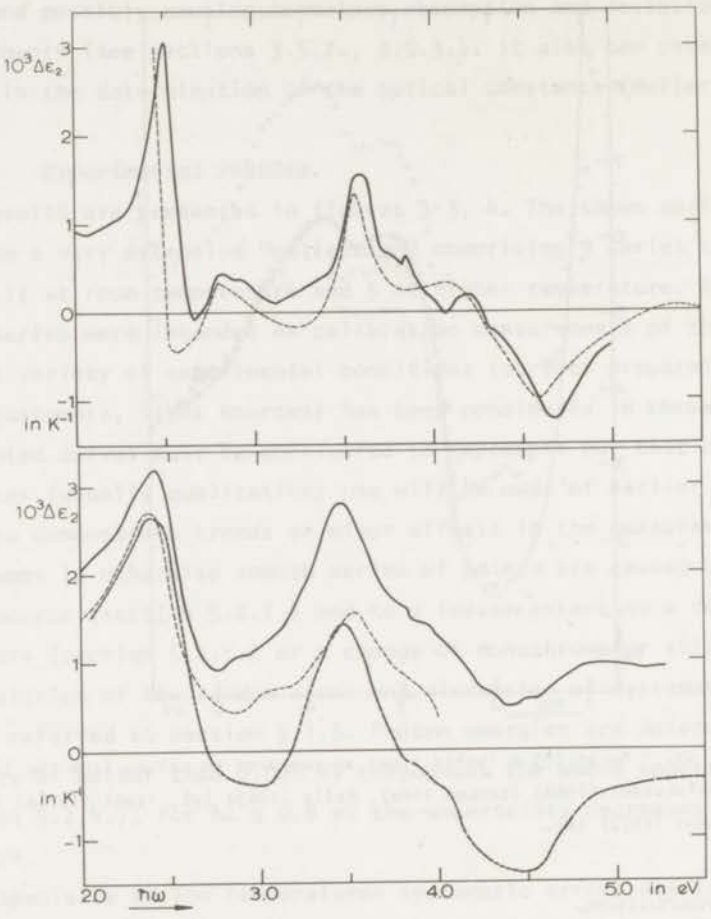

Fig. 3-5: a. $[\varepsilon_2$ (295 K) - ε_2 (40 K)]/255 (solid line) compared to $\Delta\varepsilon_2$ (per degree) as derived from thermoreflectance at 120 K by Scouler (1967) (broken line).
b. $[\varepsilon_2$ (725 K) - ε_2 (295 K)]/430 (solid line) compared to $\Delta\varepsilon_2$ (per degree) as derived from thermoreflectance at 294 K by Sherring (1970) (broken line). Also included $[\varepsilon_2$ (770 K) - ε_2 (295 K)]/475 obtained from measurements by Pells (1969) (dash-dot line).

To distinguish the method from thermomodulation we use the name thermovariation.

In this analysis we plotted the experimental data on a very expanded scale and subsequently drew a smooth curve through the points. Obviously a basic requirement for such a procedure is a large number of closely

spaced experimental points with little scatter. From figure 3-3a it may be seen that little artistic skill is needed in the fit of the 295 K data, somewhat more though in the low and high temperature series. The consistency of the drawn curves could be checked against other series of measurements, however, such that few artefacts can possibly be introduced. The resulting smooth curve is read off at 0.01 eV intervals; the values thus obtained are used to construct figure 3-5. Also included are the results from thermomodulation experiments by Scouler (1967) (as analyzed by Cardona (1969, p. 132)) and by Sherring (1970) [†]. Some smoothing of the data by Pells (1969) was necessary because of scatter.

The agreement between the temperature variation as derived from static measurements and thermomodulation is remarkably good. Thus from such a comparison one may hope to extract information regarding the causes for the temperature dependence of the optical properties (for example the influence of lattice expansion on the band structure), the interpretation of thermomodulation results (critical points?) and the identification of transitions (for instance the highly temperature sensitive $L_4^+ \rightarrow L_4^-$ (nonrelativistic $L_2' \rightarrow L_1$) gap).

It must be noted that no conclusions should be drawn from very localized structure. More specifically the small peak at 3.85 eV in figure 3-5a is a result from the much larger number of experimental points in the 295 K series that allows the observation of a small shoulder in ε_2 at this photon energy. Such detail is possibly lost when a smoothing procedure is used to fit a best curve to fewer data points.

3.6. *Intraband transitions.*

3.6.1. *Intraband data.*

The intraband contribution to the optical properties was investigated using models I (section 2.3.1.1.) and IV (section 2.3.1.4.). In both cases a least-squares fit was performed for all points at wavelengths larger than 0.9 μm. The data are summarized in table 3-1 and figure 3-6. The random error is indicated by vertical bars.

[†] Thanks are due to Dr. C.W. Sherring (Allen Clark Research Centre, The Plessey Company Ltd., Caswell, England) for making available the otherwise unpublished results from his thesis.

Table 3-1

Intraband parameters obtained from a least-squares fit to the experimental data. Unless stated otherwise the data were obtained on well-annealed samples; the short wavelength cut-off in the fitting procedure is set at 0.9 μm. Also included are some values derived from tabulated literature data, and some values taken directly from the literature.

source	ω_{pf} ($10^{16}s^{-1}$)	τ ($10^{-14}s$)	P	B (μm^{-1})	m_o 1)
Model IV					
low temperature					
90 K	1.30	6.2	6.10	1.27	1.11
room temperature					
295 K, before annealing	1.27	1.9	7.44	0.27	1.16
295 K, after annealing	1.30	0.61	6.58	0.35	1.11
Pells (1969)	1.27	1.5	0.47	3.33	1.16
Johnson (1972)	1.38	0.80	12.12	-0.70	0.99
Thèye (1970)[2]:					
best films	1.41	1.00-1.08	∿7.	∿0.2	0.94±0.01
nonannealed films	-	0.64-0.83	∿7.	∿1.5	-
high temperature					
725 K	1.29	0.47	3.76	-0.01	1.13
Pells (1969):470 K[3]					
Pells (1969):670 K	1.23	0.88	-2.17	5.97	1.24
Model II					
295 K	1.33	0.60	1.00	-	1.06
Pells (1969)[3]					
Johnson (1972)	1.31	0.82	1.00	-	1.09
725 K	1.32	0.48	1.00	-	1.08
Model I					
Pells (1969)[2]	1.41	2.40	1.00	-	0.94
Model III					
Johnson (1972)[2]	1.38	0.93±0.09	1.00	-	0.99±0.04

1) In units of electron mass; commonly one omits the unit.

2) Values taken from the literature.

3) It was not found possible to obtain a reasonable fit using these data; deviations and scatter of data points were too large. See also Johnson (1972).

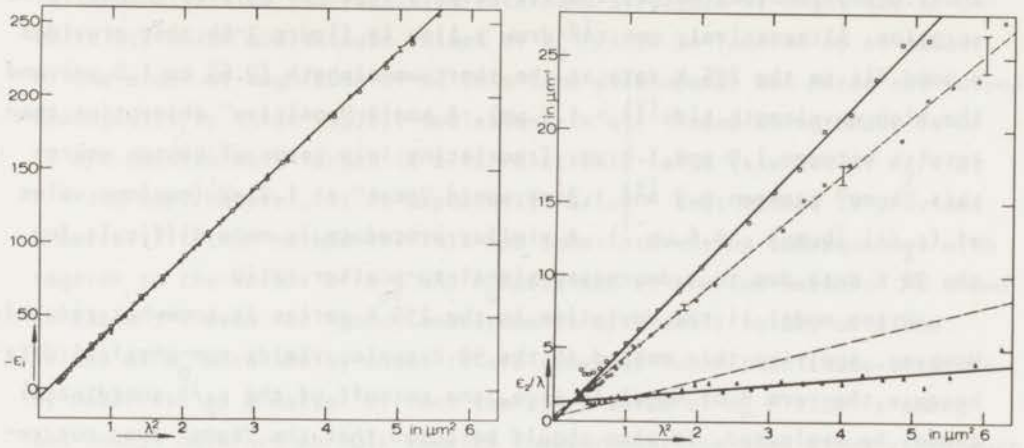

Fig. 3-6: a. $-\varepsilon_1$ - vs. - λ^2 for T = 90 K (Δ), 295 K (o) and 725 K (□).
b. ε_2/λ - vs. - λ^2 for T = 90 K (Δ), 295 K (o) and 725 K (□).
The drawn lines are the results of the least-squares fit of the modified Drude equations 2-4a,c to the experimental data. Also included in b. is the fit to data obtained on a nonannealed specimen at 295 K (dash-dot line).

Great care was taken to minimize jumps in the experimental curves due to changing of detectors or slit widths; experimentally it has been tested during every run by taking a number of overlapping points. Still typical jumps of 2% in ε_1 and 4% in ε_2 are difficult to prevent. The major uncertainty in the measurements is systematic, however, and probably has to be retraced to the nonperfect state of polarization of the light.

On the basis of test points such as explained in section 5.1.2.2. (test (2)) the values of ε_2/λ quoted in figure 3-6b are too high and probably should be lowered by about 10%. The resulting values of τ in table 3-1 must therefore be increased by 10% and should be quoted with this uncertainty. The analogous error in ε_1 is less than 1%, such that an accuracy of 2% in the absolute value of ω_{pf} and m_0 seems reasonable.

3.6.2. *Anomalous absorption?*

Some remarks should be made regarding the intraband analysis. In the 295 K and 90 K series the experimental data in figure 3-6b are systematically lower than the Drude fit using model IV for wavelengths between 0.65

and 1.0 μm. In other words, the fit results in a non-physical negative absorption. Alternatively one can draw a line in figure 3-6b that provides a good fit to the 295 K data at the short wavelength (0.65 to 1.0 μm) and the high wavelength side ($\lambda > 1.5$ μm). A small "positive" absorption then results between 1.0 and 1.4 μm. Translating into terms of photon energy this "bump" between 0.9 and 1.3 eV would "peak" at 1.2 eV (maximum value of (ε_2/λ) (bump) $\simeq 0.6\ \mu m^{-1}$). A similar procedure is more difficult for the 90 K data due to a decreased signal-to-scatter ratio.

Using model II the deviation in the 295 K series is somewhat reduced. However, applying this method to the 90 K series yields non-physical data because the term B of model IV (i.e. the cut-off of the ε_2/λ coordinate) cannot be neglected. It also should be added that the "bump" does not reproduce well in other experimental series.

Summarizing, one is tempted to think of "anomalous" absorption which - as suggested in section 2.4.1. - could be due to specimen conditions (surface roughness, grain boundaries, etc.). However, in view of the experimental and theoretical uncertainty even such a conclusion would be stretching the data too far. As a negative conclusion, no clear evidence is found of a temperature dependence of the bump such as reported by Hodgson (1968), who reports an increase at higher temperature. Additional absorption below the absorption edge has also been reported by a.o. Garfinkel (1966), Beaglehole (1969), Steel (1972a,b), Thèye (1970), Pells (1969). (See also section 2.4.1.).

3.6.3. *Drude fit with a frequency dependent relaxation time.*

As indicated in the preceding section, when B is relatively large as compared to ε_2 it is necessary to use model IV (section 2.3.1.4.) instead of model II. The assumption B = 0 in the latter method then leads to non-physical values of the intraband parameters. In sections 2.3.2. and 2.4.1.1. it was demonstrated that it is difficult to distinguish between a frequency dependence of τ, an additional class of electrons with a very short relaxation time (model V), and an additional broad absorption. In view of the uncertainties involved we have preferred to use model IV throughout the intraband analyses of Au. This somewhat phenomenological procedure has the merit of consistency in providing a good fit. Admittedly, however,

in the analysis of the resulting interband structure it might add an uncertainty which could cause values of $\varepsilon_2^{(b)}/\lambda$ to be lowered by an amount of the order of magnitude of B. This same discrepancy was noted and solved analogously by Thèye (1970). Deviations in $\varepsilon_1^{(f)}$ found using model IV or II are considerably larger if B is relatively large (say 10% of ε_2/λ at λ = 1.5 μm). However, it is especially for $\varepsilon_1^{(f)}$ that method IV provides a better fit than method II. This has some interesting consequences with regards to the values of ω_{pf} and m_0 obtained by the two methods. As shown in table 3-1 even for "good" measurements with small values of B the values of m_0 obtained by model II are somewhat lower than those obtained by model IV. As a matter of fact the 295 K value of m_0 = 1.06 is among the lowest obtained on bulk samples (measurements on good films yield much lower values yet, e.g. Thèye: $m_0 = 0.94 \pm 0.01$) and compares favourably with recent values of the thermal mass: 1.06 (Boerstoel (1971)) and 1.09 (Martin (1968)). Therefore, although experimentally the ε_1 - vs. - λ^2 graph is quite reproducible, considerable care should be taken in the evaluation of ω_{pf} and m_0: the "best" value of m_0 (1.06; model II) does not provide the best fit to our data. In addition it was found that a different choice of the cut-off wavelength for the least-squares fit caused variations in the intraband parameters. In our opinion any analysis using values of m_0 or ω_{pf} should therefore include proper reference to the particle Drude model, the cut-off wavelength and to the experimental uncertainties (see sections 2.3.2, 5.1.1.1., 5.1.5.).

3.6.4. *Conclusions.*

A number of interesting conclusions may be drawn from figure 3-6 and table 3-1.

(1) The intraband plasma frequency ω_{pf} and thus the optical mass m_o are temperature independent: $\omega_{pf} = (1.30 \pm 0.02) \times 10^{16} \text{sec}^{-1}$, $m_o = 1.11 \pm 0.02$. From other measurements on the same specimen it was found that these values are only slightly dependent on surface preparation, annealing, minor misadjustments of the optical system (polarizers, etc.). This temperature independence is in good agreement with the results obtained by Motulevitch (1967, 1969), who showed that the change of the optical mass depends on the difference in the Debye-Waller factors W(T) at the two temperatures.

Using the values of W as calculated by Christensen (1971) the variation of the optical mass of Au on going from 0 K to 800 K can be estimated to be at most 3 percent. As pointed out by Motulevitch, in polyvalent metals this can be considerably more (see also Young (1969)).

(2) Clearly the results on the intraband relaxation time are much more erratic. Any conclusions based on values of τ should therefore be considered with care (section 2.3.2.). Still consistently it is found that annealing of the specimen results in a decrease of τ. Values of $\varepsilon^{(f)}(\omega)$ therefore increase as also observed by Pells (1969). This is contradictory to the expectation of improving conduction that results in a higher value of τ (Thèye (1970)). Quite possibly the roughening of the surface (due to thermal etching) causes a greatly enhanced contribution of surface scattering such that $\tau_{surface}$ may play a dominant role;

$$\tau^{-1} = \tau_{rest}^{-1} + \tau_{surface}^{-1}$$

where τ_{rest} includes all other scattering mechanisms. This suggestion finds support in the work of Palmer (1972). In extreme cases this roughness may cause an increase of the somewhat phenomenological term B, such as observed by Pells. Thèye (1970) and Roberts (1955) have pointed at a possible relation between a deteriorating specimen quality and an increasing B (section 2.3.2.).

(3) For good surface preparation the room temperature value of P is 7 ± 1 ($\delta\varepsilon_1^{(b)} = 6 \pm 1$; eq. 2-16a) in good agreement with the results obtained by Hodgson (1968) and Thèye (1970). P decreases on annealing.

3.7. *Interband transitions.*

The interband contributions to $\varepsilon_1(\omega)$ and $\varepsilon_2(\omega)$ are obtained on subtracting the respective intraband contributions (eq. 2-15). The $\varepsilon_2^{(b)}(\omega)$ spectra are very similar to those of $\varepsilon_2(\omega)$. Shown in figure 3-7 is the interband contribution to ε_1, i.e. $\varepsilon_1^{(b)} + \delta\varepsilon_1^{(b)}$ (see eqs. 2-15,16a).

3.8. *Absorption edge.*

Results on the location of the absorption edge using various defini-

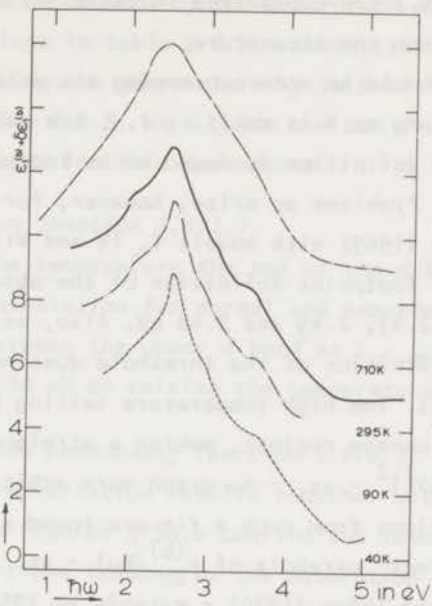

Fig. 3-7: $[\varepsilon_1^{(b)} + \delta\varepsilon_1^{(b)}]$ - vs. - $\hbar\omega$ for T = 40 K (--), 90 K (– –), 295 K (——) and 725 K (— -). The zeroes of the curves are shifted relative to one another as indicated on the right coordinates.

Table 3-2

The absorption edge of Au (in eV) at different temperatures according to various definitions.

definition of the absorption edge	T=40 K	T=90 K	T=295 K	T=725 K
parabolic footpoint of $\varepsilon_2^{(b)}(\omega)$-vs.-$\hbar\omega$	2.495±0.02	2.49 ±0.01	2.455±0.01	2.40±0.04
Nilsson (1967)			2.45 ±0.01	
Thèye (1970)			2.45 ±0.01	
Christensen (1971) RAPW-calc.	2.38(at 0 K)			
Maximum in $\Delta\varepsilon_2^{(b)}(\omega)/\Delta(\hbar\omega)$-vs.-$\hbar\omega$	2.54 ±0.01		2.52 ±0.02	2.48±0.08
Welkowsky (1971)		2.49(at 80 K)	2.44	
Maximum in $\varepsilon_1^{(b)}(\omega)$-vs.-$\hbar\omega$	2.55 ±0.01	2.545±0.01	2.515±0.01	2.47±0.04
Steel (1971)			2.5	

tions (section 2.5.6.) are summarized in table 3-2. Also included are some values taken from the literature.

Some remarks should be made concerning the determination of the absorption edge. As long as B is small, $\lesssim 1.$, the value of the edge according to a chosen definition is found to be independent of the intraband analysis technique. Problems do arise, however, for large B: analizing the 295 K data of Pells (1969) with models I, IV and VII (section 2.3.1.) and using the parabolic footpoint definition of the absorption threshold, we obtained values of 2.43, 2.49 and 2.48 eV. Also, as demonstrated in figure 3-8, this definition of the threshold does not work well at high and low temperatures. The high temperature tailing of the edge extends over larger photon energy regions, making a straight line fit to the results in a $[\varepsilon_2^{(b)}(\hbar\omega)^2]^2$ - vs. - $\hbar\omega$ graph more arbitrary. Similarly at low temperatures deviations from such a fit are found around 2.7 eV, indicating that the "perfect" parabola of $\varepsilon_2^{(b)}(\hbar\omega)$ - vs. - $\hbar\omega$ that - as found by Nilsson (1967) and Thèye (1970) - extends at 295 K to 3.5 eV, is somewhat coincidental (see section 3.8.3.).

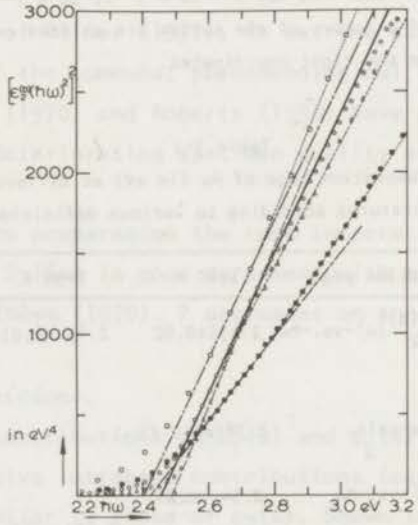

Fig. 3-8: $[\varepsilon_2^{(b)}(\hbar\omega)^2]^2$ - vs. - $\hbar\omega$ for T = 90 K (▲), 295 K (●), 725 K (□). Also included are data obtained at 650 K (■). Emphasizing the region around 2.6 eV the data are fit with straight lines, the footpoints of which give an indication of the value of the absorption threshold. The dotted lines indicate straignt-line fits to the high and low temperature data for photon energies above 2.8 eV.

3.8.1. *Temperature dependence of the absorption edge.*

For all definitions in table 3-2 the absorption edge is temperature dependent: on increasing the temperature it is shifted to lower photon energies. Using section 2.6.5. as a guide one can distinguish a number of possible explanations for this dependence.

(1) *Lattice expansion (section 2.6.1.).*

On increasing the temperature the top of the *d* band is lowered. From Christensen's band calculation for normal and expanded lattices it follows that an energy gap between the upper *d* band at $L_{5^+ + 6^+}$ and the "muffin-tin zero" decreases by 0.40 eV on raising the temperature from 0 K to 920 K.

(2) *Fermi distribution broadening (section 2.6.3.).*

The derived thermovariation results together with the thermomodulation data gathered in figures 3-5a,b confirm the involvement of the Fermi surface in the transitions leading to the absorption edge. As suggested in section 2.7.3.1. $\Delta\varepsilon_2$ (Fermi surface transitions) is expected to increase and sharpen relative to $\Delta\varepsilon_2$ (non-Fermi surface transitions). This pattern is further supported by Rosei (1973) in thermomodulation data taken at 20 K.

(3) *Shift of Fermi level (section 2.6.4.).*

From his expanded lattice calculation Christensen (private communication) obtained a Fermi energy (with respect to the "muffin-tin zero") of 6.76 eV which compares with a value of 7.21 eV at T = 0 K. This downward shift of 0.45 eV is somewhat larger than the analogous change as calculated by the free-electron formulas ($E_F \approx 5.51$ eV; $\Delta E_F \approx -0.14$ eV).

Summarizing, the shift of $E_F(3)$ is almost compensated by the simultaneous displacement of the top of the *d* band (1) such that the calculated shift of the absorption threshold is -0.05 eV. Assuming a completely linear temperature dependence of the lattice expansion this shift of -0.5×10^{-4} eV/K is to be compared with the experimental value of about -1.4×10^{-4} eV/K (table 3-2). According to table 3-2 the shift of the absorption edge is somewhat smaller, approximately -1.0×10^{-4} eV/K. Grobman (1972) reports a shift of the edge of the *d* band relative to E_F of between 2 and 6×10^{-4} eV/K.

This conclusion is in contradiction to that by Pells (1969) who noticed that the edge at approximately 2.5 eV broadens while the central positions remain constant from 295 K to 770 K. Similarly Miller (1969) finds no evidence of a shift. Joos (1954) suggested Fermi distribution broadening to be exclusively responsible for the temperature dependent changes in the absorption edge. However, our findings are supported by recent results from wavelength modulation at various low temperatures (Welkowsky (1971), Stokes (1972)) and from temperature-modulated photoemission (Grobman (1972)). Evidence in favor of a shift of structure is also obtained by Garfinkel (1966) and Cheyssac (1973) who in piezoreflectance measurements find a well-defined variation of $\tilde{\varepsilon}^{(b)}$ for photon energies at the absorption edge. From eqs. 2-28,29b shifts of the type (1) and (2) thus must occur. As a matter of fact completely parallel shifts of the top of the *d* band and of E_F would be very coincidental.

3.8.2. *Tailing of the absorption edge.*

The tailing of the absorption edge to lower photon energies is shown in figure 3-9. Also included are data from some less reliable low-temperature measurements (larger systematic deviations probably due to surface contamination). Below the absorption threshold the data are described quite well by an exponential relation between $\varepsilon_2^{(b)}\omega^2$ and $\hbar\omega$. At low temperatures a fairly sharp change of slope is observed for photon energies above threshold. The smoothing of the curves obtained at higher temperatures probably results to a major extent from the Fermi distribution broadening of the absorption edge.

This tailing has been a source for considerable speculation (see section 2.4.2.). The analysis is troubled by the uncertainty in the lowest values of $\varepsilon_2^{(b)}\omega^2$ that is due to the intraband analysis ($\varepsilon_2^{(f)} > \varepsilon_2^{(b)}$). A downward deviation below the straight lines, that is noticed one decade lower in most series, therefore is not drawn in figure 3-9. However, very interesting evidence regarding the tailing comes from $\varepsilon_1^{(b)}$ - vs. - $\hbar\omega$ spectra as shown in figure 3-7. Especially at low temperatures a broad shoulder is observed at 2.0 eV below which photon energy $\varepsilon_1^{(b)}$ falls off rapidly. Using the interrelations of $\varepsilon_1(\omega)$

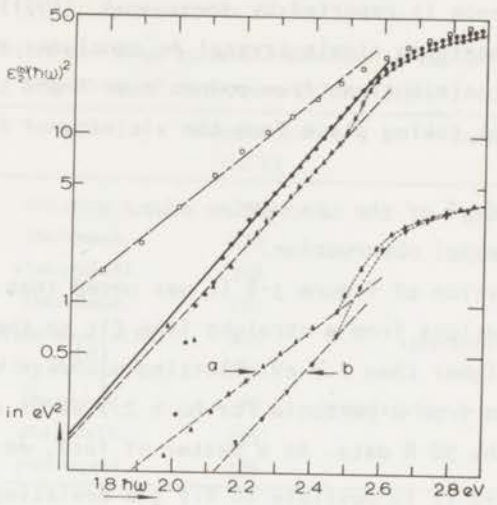

Fig. 3-9: Logarithmic plot of $\varepsilon_2^{(b)}(\hbar\omega)^2$ - vs. - $\hbar\omega$ in the tail region. Experimental points are indicated by ▲: T = 90 K, ●: T = 295 K, □: T = 725 K. A straight-line fit to the tail is drawn for all temperatures (90 K: dash--dash; 295 K: full; 725 K: broken line). Also drawn but shifted down one decade are some other low temperature results (a: T = 90 K; b = 40 K). Above 2.45 eV the low temperature points are connected by a dotted line.

and $\varepsilon_2(\omega)$ as given in section 2.5.2. one indeed expects a change of slope in $\varepsilon_2^{(b)}(\omega)$ at about 2 eV.

This pattern is difficult to explain by any of the suggested causes in section 2.4.2. except for the last one, (6). As a matter of fact Christensen (1971) shows in his figure 21 that a change of slope at these photon energies follows directly from the band calculation. In view of the good agreement between theory and experiment we therefore conclude that the tailing of the absorption edge is largely due to interband transitions. From the band calculation the first transitions occur from band 5 to band 6 (at E_F) in the vicinity of X. This is demonstrated quite clearly in figure 3-11. The calculated onset photon energy is 1.7 eV in fair agreement with the values derived from experiments by Thèye (1070; 1.5 eV) and us (1.7 ± 0.2 eV). Also Kupratakuln (1970) quotes a value of the transition near $X_{7+} \rightarrow E_F$ of 1.89 eV. However, he uses this type of transition to explain some - what we think is - anomalous absorption (e.g. section 3.6.2.).

Further evidence is reported by Szczepanek (1971) who from piezoreflectance measurements on single-crystal Au concludes that the absorption edge consists of contributions from points near X and L with the first interband transitions taking place from the vicinity of X.

3.8.3. *"Splitting" of the absorption edge.*

3.8.3.1. *Experimental observation.*

In the discussion of figure 3-8 it was noted that at low and at high temperatures deviations from a straight line fit to the data occur for photon energies higher than 2.7 eV. Plotting $\varepsilon_2^{(b)}/\lambda$ - vs. - $\hbar\omega$ the curve therefore deviates from a parabola for $\hbar\omega \geq 2.7$ eV as demonstrated in figure 3-10 for the 90 K data. As a matter of fact, as indicated by dotted lines in figure 3-8 it is possible to fit the deviating points by a second parabola.

Checking the literature (table 3-3) only one direct observation is made of structure in this photon energy region. In measurements on non-

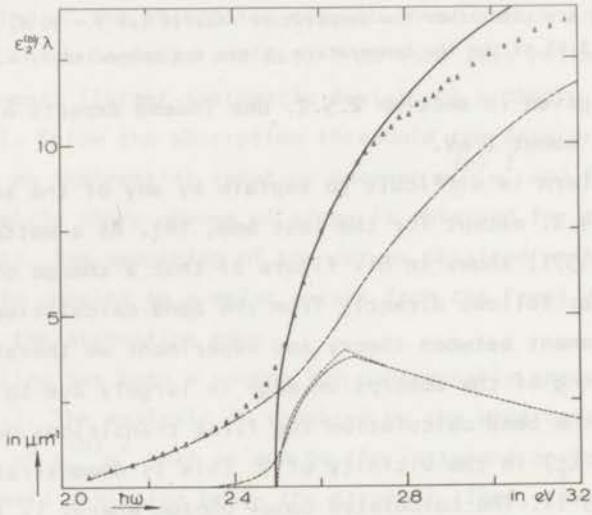

Fig. 3-10: "Splitting" of the absorption edge at 90 K. Experimental data (▲) are fitted by a parabola derived from the data in figure 3-8. Also shown is a term such a proposed by Cooper (1965) et al. to originate from band 5 → band 6 transitions in the vicinity of L (----). Subtracting this broadened (Miloslavskii (1967)) structure (— — —) from the experimental curve one obtains a smoothly sloping structure (— - —).

Table 3-3

Literature review of structure observed in the optical properties of Au between 2.7 and 3.0 eV.

reference	method	temperature (in K)	explanation
Fukutani (1966)	opt.prop!s	295	-
Scouler (1967)	thermomod.	120	-
Buckman (1968)	electrorefl.	295	-
Sherring (1970)	thermomod.	120	-
Erlbach (1971)	alloy modulation	295	spin-orbit splitting
Beaglehole (1972)	alloy modulation	295	-
Rosei (1973)	thermomod.	20	overlapping d-band→FS transitions
Cheyssac (1973)	piezorefl.	295	-
Cheyssac (1973)	thermorefl.	288	-

annealed films Fukutani (1966) obtains a remarkably strong splitting at room temperature (see figure 3-4). No discussion is given of this effect; in later measurements Fukutani (1971) makes no mention of such a splitting. Again this would suggest an effect due to sample conditions (see also section 3.14.). However, confirmation is obtained from modulation spectroscopy, especially so from thermomodulation. As shown in figure 3-5a a very distinct positive structure in $\Delta\varepsilon_2$ is derived from both our and Scouler's data. This observation is strongly supported by Rosei and Cheyssac. Furthermore Erlbach and Beaglehole in alloy modulation experiments obtain a similar positive structure in $\Delta\varepsilon_2$ (Au - AuCu) on adding Cu to Au (up to 2.6 at.%). This structure decreases to a change of slope in measurements on AuAg and AuFe systems.

3.8.3.2. *"Splitting" in photoemission spectra.*

Related evidence may possibly be derived from photoemission experiments. It has been reported a number of times (Nilsson (1969,1970b), Eastman (1970,1972), Smith (1971,1972a,b)) that the major structure observed in the energy distribution curves of initial states around 2.7 eV splits off a second smaller structure. The major peak that remains static for changing incident photon energy has been attributed to nondirect transitions or alternatively to direct transitions from a very flat part of the

d band to the Fermi surface (section 2.7.2.1.). The secondary structure is seen to shift non-proportionally to the photon energy thus providing a strong argument for direct transitions. The data obtained by Smith (1972a, b) using higher-derivative photoemission spectroscopy seem to indicate that on lowering the photon energy the initial state crosses that of the major structure. This results in a bulge on the high energy side of the main peak in the energy distribution curves of the initial states.

At the lowest photon energies structure observed in photoemission experiments is limited to interconduction-band transitions (band 6 → band 7) and to transitions from *d* bands to the lowest conduction band. Part of this conduction band is "masked" due to the influence of the work function (for cesiated surfaces about 1.8 eV). As pointed out by Lindau (1971b) assuming direct transitions photoemission data at the lowest photon energies (e.g. Smith (1972a)) only account for transitions in rather confined regions of the Brillouin zone near the W corners. Checking the band structure (figure 3-1) one might expect additional transitions to occur in the vicinity of K. As a matter of fact the first *d* band transitions observable by photoemission should occur around X. Subsequently at slightly higher photon energies transitions become possible from very flat parts of the *d* band (e.g. Q_{3+4}). Quite possibly therefore the secondary structure observed in photoemission is due to transitions from the highest *d* band to the lowest conduction band in the vicinity of the square Brillouin zone faces with center at X.

3.8.3.3. *Modelling the absorption edge.*

One can attempt to match the observed behaviour with models introduced before. It is widely accepted that the absorption edge in Au is due to transitions from the top of the *d* band to the Fermi surface. As structure observed in optical spectra has long been analyzed using the critical interband point assumption (section 2.7.1.) (e.g. Phillips (1968)), most attention has been paid to models of this type. Especially the Fermi surface transition between band 5 and band 6 in the vicinity of L (Q) has been the objective of model calculations.

Such models have been introduced in section 2.7.2.1. However, although Cooper (1965) and Miloslavskii (1967) both predicted a parabolic

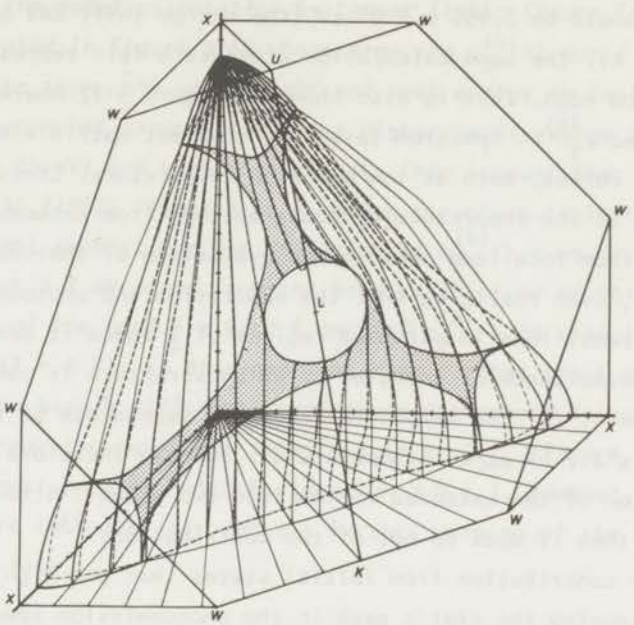

Fig. 3-11: Axiometric plot of sections of the Fermi surface (fine lines) and the surface of constant interband energy $E_{ul} = \hbar\omega_i = 2.38$ eV (heavy lines) for constant azimuthal angles. In the hatched area, the two surfaces coincide. $\underline{k}$ vectors in this region correspond to the states giving the steep increase of the absorption at the interband edge $\hbar\omega_i = 2.38$ eV (from Christensen (1971)).

shape of the absorption edge from the assumption of transitions in localized regions of $\underline{k}$-space, it was not found possible to obtain more than a semi-qualitative fit to the data using reasonable values of the band parameters (gaps, effective masses). Similarly the models of Rosei (1972, 1973) (also Antonangeli (1973)) for calculating the temperature-induced variation of ε_2 yield structure that is confined to photon energy intervals that are too narrow to explain the observed behavior in figure 3-5a.

Most probably the absorption edge is caused by transitions over extended regions of $\underline{k}$-space (section 2.7.3.). Figure 3-11 is taken from the work of Christensen (1971). The hatched area shows the region where the surface of constant interband energy $E_{ul} = 2.38$ eV coincides with the Fermi surface. Apart from a correction of the onset energy that from our

experiment should be 2.455 ± 0.01 eV (the energy shift has been extrapolated to T = 0 K), the band calculation provides a fair representation of the absorption edge. This is also shown in figure 3-12 where we compared the calculated $\varepsilon_2^{(b)}/\lambda$ spectrum (assuming constant matrix elements) with experimental curves, both at low and high temperature. Christensen (1972a) also pointed at the importance of contributions from extended regions rather than from localized ones in the evaluation of photoemission spectra.

However, even realizing that the absorption and photoemission spectra are due to transitions in extended regions of $\underline{k}$-space it must be pointed at (1) the coincidence of energies at which structure is observed in the two experiments; (2) the parabolic frequency dependence of the absorption edge for $\hbar\omega \leq 2.7$ eV at all temperatures. One can therefore attempt a rough division of the extended region into two groups. Structure in optical spectra then is made up out of two contributions [†)].

(1) A major contribution from initial states that are highly localized in energy (causing the static peak in the photoemission spectra). From the band calculations and the derived PJDOS it follows that this structure mainly results from band 5 → band 6 transitions close to the hexagonal zone face in the vicinity of L. This absorption may be described using model calculations; it is expected to reach its maximum height around 2.65 eV (Smith (1972a)).

(2) The remainder of the edge originates from contributions of band 5 → band 6 transitions near the square zone faces in the vicinity of X. At the top of the absorption edge minor contributions are possible from other pairs of bands (6 → 7, 4 → 6, 3 → 6; see figure 3-2).

This separation offers a reasonable explanation for most structure reported. It provides a feasible interpretation of the relevant photoemission spectra in good agreement with the work of Nilsson (1970b). It also gives a fair account of the parabolic onset of the absorption edge. It no longer is necessary to "explain" the total height and width of a parabolic edge that extends to about 3.5 eV, a problem that led to the

[†)] Possible support is reported by Szczepanek (1971; abstract only) who concludes from piezoreflectance data on single-crystal Au that the absorption edge is made up of contributions from points near X and L.

failure of the model calculation by Cooper (1965; figure 11) et al. This is demonstrated in figure 3-10 where from the $\varepsilon_2^{(b)}/\lambda$ curve we subtracted a Cooper-like term: the same height and peak energy as indicated in their figure 11, somewhat narrower due to a higher onset energy (Cooper et al. use $\hbar\omega^* = 2.35$ eV) and broadened to take into account that $T \neq 0$ K (Miloslavskii (1967; figure 3)). A smooth structure is left.

Important support for the deviation of $\varepsilon_2^{(b)}/\lambda$ - vs. - $\hbar\omega$ from a parabola at about 2.7 eV comes from the band calculation of Christensen. An indentation of the band 5 → band 6 partial $\varepsilon_2^{(b)}/\lambda$ is clearly visible in figure 3-2 (T = 0 K); it disappears at high T. That the L and X region contributions have a different temperature dependence is not illogical. The *d* band near the hexagonal zone face (e.g. Q_{3+4}, figure 3-1) was found to shift almost parallel with E_F (section 3.8.1.). However, quite possibly a temperature increase introduces a further warping of the bands near the square zone face.

3.8.3.4. *Thermovariation structure at 2.9 eV.*

As indicated in table 3-3 in most modulation experiments one observes a small positive structure in $\Delta\varepsilon_2$ between 2.7 and 3.0 eV. This is also shown in the low-temperature thermovariation spectrum in figure 3-5a. Christensen (1971) assigns the positive structure in thermomodulation spectra around 2.9 eV to Fermi-level transitions, e.g. Δ_6^2 or $\Delta_7^2 \rightarrow E_F(\Delta_6^3)$. That the structure originates from initial states in the *d* bands is confirmed by the temperature-modulated photoemission experiments of Grobman (1972).

However, somewhat surprising evidence can be derived from the shift of the structure as observed in thermovariation spectra at a higher average temperature. Such spectra are presented in section 3.9., figure 3-14. Although at higher temperatures the small $\Delta\varepsilon_2(\Delta T)$ structure is somewhat difficult to follow, it may be seen to move to higher photon energy (figure 3-15). According to Christensen such a relatively large positive temperature-induced shift is typical for transitions near the X symmetry point. Most probably therefore the structure is associated with the $X_{7+3} \rightarrow X_{6-}$ critical interband point transition (band 5 → band 6) that is calculated to move from 3.01 eV at 0 K to 3.11 eV at 920 K.

This assignment to transitions that do not involve the Fermi surface is supported by the results of Cheyssac (1973) et al. who measured both thermoreflectance and piezoreflectance on the same specimen. A very strong structure in $\Delta\varepsilon_2(\Delta T)$ results from the Fermi distribution broadening of the absorption edge; the corresponding structure in the piezoreflectance experiment is much smaller. However, in the same figure the $\Delta\varepsilon_2$ structures around 3 eV are of the same order of magnitude, possibly even larger in piezoreflectance. This indicates that lattice expansion is the dominant influence such as to be expected for $X_{7+3} \rightarrow X_{6-}$ transitions. In this regard it also can be pointed at the theoretical "piezoreflectance" $\Delta\varepsilon_2$ spectrum as derived from Christensen's band calculation. As shown in figure 3-13 a splitting of the structure below 3.2 eV into two major components is indeed expected.

3.9. *Absorption maximum.*

A strong maximum in ε_2/λ is observed around 4.0 eV (figure 3-3a). The shape and magnitude of this broad peak is found to vary considerably from one experiment to the other. Also the interpretation of the peak in terms of band structure has been the subject of a number of optical studies. As shown in table 3-4 the analyses of (especially modulation) experiments have been concentrated on critical interband point transitions. More specifically structure around 3.6 eV is usually identified with interconduction-band transitions $L_{4-} \rightarrow L_{4+}$ (nonrelativistic: $L_{2'} \rightarrow L_1$). In this regard it is shown that thermovariation can be an important tool in the investigation of such expectedly highly temperature-dependent structure.

In view of the many contributions from different sources and disciplines the analysis becomes somewhat complicated. To prevent repeating ourselves we introduce all relevant data in section 3.9.. Arguments - to be used in subsequent analyses (sections 3.10., 3.11., 3.12.) - are indicated by a number-between-brackets that is placed in the margin.

3.9.1. *Comparison with theoretical spectra.*

(1) *Critical interband points.*

Relativistic band structure calculations predict the following values

Table 3-4

Literature review of critical interband point evaluations of optical spectra of Au between 3.4 and 4.7 eV.

reference	method	photon energy (in eV)	explanation
$\hbar\omega < 4.2$ eV:			
Garfinkel (1966)	piezorefl.	3.5	$X_5 \rightarrow X_4$,
Cooper (1966)	opt.prop!s	3.9	$X_5 \rightarrow X_4$,
Cardona (1969)	thermomod.	3.6	$X_5 \rightarrow X_4$,
Parsons (1969)	electrorefl.	~4.	L_2, $\rightarrow L_1$
Pells (1969)	opt.prop!s	~4.0	L_2, $\rightarrow L_1$
Christensen (1970a,1971)	RAPW calc.	3.72	L_2, $\rightarrow L_1$ ($L_4- \rightarrow L_4+$)
Christensen (1970a,1971)	RAPW calc.	4.24[1]	$X_{7+2} \rightarrow X_{6-}$
Kupratakuln (1970)	RAPW calc.	3.67	L_2, $\rightarrow L_1$ ($L_4- \rightarrow L_4+$)
Smith (1971)	photoemission	3.5	L_2, $\rightarrow L_1$
Szczepanek (1971)[2]	piezorefl.	3.55	$L_4- \rightarrow L_4+$
Welkowsky (1971)	wavelength mod.	3.91	$X_5 \rightarrow X_4$,
Fukutani (1972)	opt.prop!s	3.5	$X_5 \rightarrow X_4$,
Fukutani (1972)	opt.prop!s	4.1	L_2, $\rightarrow L_1$
Smith (1972a)	photoemission	4.0	L_2, $\rightarrow L_1$
Stokes (1972)	wavelength mod.	3.8	M_1 c.i.p. at X
Rosei (1973)	thermomod.	3.6	L_2, $\rightarrow L_1$ ($L_4- \rightarrow L_4+$)
$\hbar\omega > 4.2$ eV:			
Garfinkel (1966)	piezorefl.	4.5	L_2, $\rightarrow L_1$
Pells (1969)	opt.prop!s	~4.55	$X_5 \rightarrow X_4$,
Kupratakuln (1970)	RAPW calc.	4.3	$X_5 \rightarrow X_4$,
Erlbach (1971)	alloy mod.	4.5	$X_5 \rightarrow X_4$,
Szczepanek (1971)[2]	piezorefl.	4.5	$X_{7+} \rightarrow X_{6+}$?
Fukutani (1972)	opt.prop!s	5.0	$X_1 \rightarrow X_4$,

1) Correction to original value; private communication.

2) According to Beaglehole (1972), table I.

of the critical interband point energy gaps that are of interest in this photon energy region (all values in eV).

	Sommers 1969	Connolly*) 1970	Kupratakuln 1970	Ramchandani 1970,1971	Christensen 1971	Smith 1972a
$L_4- \rightarrow L_4+$	3.68	4.22	3.67	4.00	3.72	4.1
$X_{6+2} \rightarrow X_{6-}$	1.90	3.76	4.30	3.49	4.07	4.6*)
$X_{7+2} \rightarrow X_{6-}$	2.08	4.02	4.57*)	3.72	4.24	5.0*)

*) values read from graphs

Also included are results from a non-first-principles calculation by Smith.

Somewhat surprising the deviations between the various authors are larger in the $X_{6+} \rightarrow X_{6-}$ (band 4 → band 6) and $X_{7+} \rightarrow X_{6-}$ (band 3 → band 6) values than in the $L_{4-} \rightarrow L_{4+}$ (band 6 → band 7). The latter transition is renowned for its sensitivity to the choice of crystal potential.

(2) *Calculated* $\varepsilon_2^{(b)}/\lambda$ *spectrum.*

In figures 3-2a,b we showed $\varepsilon_2^{(b)}/\lambda$ - vs. - $\hbar\omega$ as calculated by Christensen for the various pairs of bands that are expected to contribute to the absorption spectrum. Summing all contributions a theoretical $\varepsilon_2^{(b)}/\lambda$ spectrum is obtained that can be compared with the experimental values. Adjusting the scale of the calculated spectrum around 4 eV a fair

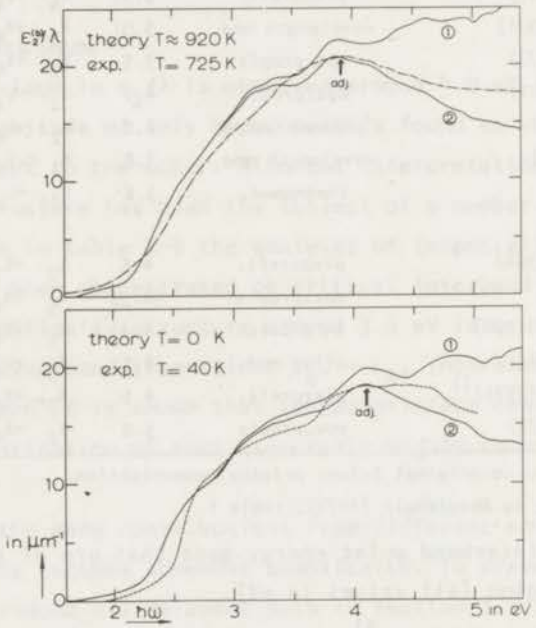

Fig. 3-12: Experimental $\varepsilon_2^{(b)}/\lambda$ - vs. - $\hbar\omega$ (broken line) together with calculated spectra of $\varepsilon_2^{(b)}/\lambda$ with (1) and without (2) contributions from band 3 → band 6 and band 2 → band 6 transitions. The vertical scale of the theoretical curves is adjusted in order to match the experimental curves.

a. Experiment at 725 K, calculation for T = 920 K.

b. Experiment at 40 K, calculation for T = 0 K.

fit is obtained only for lower photon energies (figure 3-12). At higher photon energies the agreement is considerably improved if contributions from lower d bands ($3 \rightarrow 6$, $2 \rightarrow 6$, etc.) are omitted. Similar results are found by Christensen (1971) in the adaptation of measurements by Thèye and by Johnson (1972). Christensen suggests as an explanation a decrease of matrix elements for transitions originating from deeper d bands. This suggestion is supported to some extent by XPS results of Shirley (1972). The XPS density of states is typically 20% lower than the calculated DOS for states that are more than 5 eV below E_F.

(3) *Calculated thermovariation.*

Through subtraction and division by $\hbar\omega$ one can calculate from the partial $\varepsilon_2^{(b)}/\lambda$ spectra in figure 3-2a,b the theoretical $[\varepsilon_2(920\ K) - \varepsilon_2(0\ K)]$ - vs. - $\hbar\omega$ spectra shown in figure 3-13.

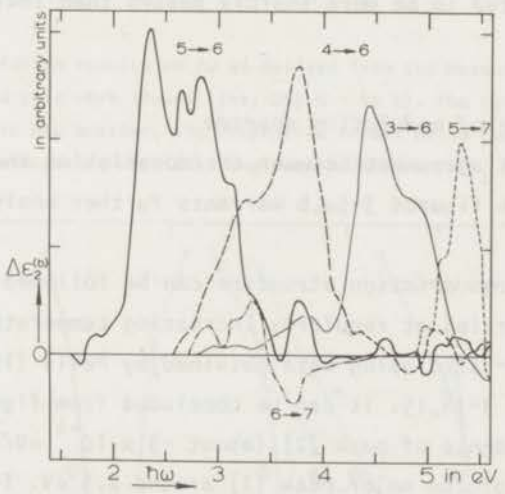

Fig. 3-13: $[\varepsilon_2^{(b)}\ (920\ K) - \varepsilon_2^{(b)}\ (0\ K)]$ - vs. - $\hbar\omega$ for various pairs of bands as calculated from the partial $\varepsilon_2^{(b)}/\lambda$ spectra shown in fig. 3-2. No account has been taken of Fermi distribution broadening; actually therefore this figure is more directly relevant to hydrostatic strain modulation experiments.

(4) *Interconduction-band structure: matrix elements?*

The structure in the calculated $\varepsilon_2^{(b)}/\lambda$ and $\Delta\varepsilon_2^{(b)}(\Delta T)$ due to interconduction band transitions (figures 3-2, 13: band $6 \rightarrow$ band 7) is very

small when compared with for instance that originating from transitions between band 4 to band 6. However, it is known from measurements and calculations on Cu and Ag that matrix elements are very large for interconduction band transitions in the vicinity of L. At their peak energy these transitions account for 20 to 30% of all absorption structure in these metals. If one assumes for Au a similar 30% contribution of the band 6 → band 7 transitions it follows from figure 3-2 that the partial $\varepsilon_2^{(b)}/\lambda$ due to these transitions - and therefore also the calculated $\Delta\varepsilon_2(\Delta T)$ - has to be multiplied by a factor 5. From figure 3-13 it can be seen that even then the $\Delta\varepsilon_2$(band 6 → band 7) is only of the order of $\Delta\varepsilon_2$(band 4 → band 6).

In the case of Cu and Ag it has been shown (e.g. Mueller (1967), Nilsson (1973)) that the matrix elements decrease rapidly on moving away from the L symmetry axis. The interconduction band structure in ε_2 and $\Delta\varepsilon_2(\Delta T)$ thus may be expected to be more sharply peaked than indicated in figures 3-2, 13.

3.9.2. *Analysis of modulation spectra.*

The excellent agreement between thermovariation and thermomodulation as demonstrated in figures 3-5a,b warrants further analysis.

(5) *Shift of thermovariation structure* can be followed using values of the optical properties at regularly increasing temperature intervals. Such an analysis - also using data obtained by Pells (1969) †) - is performed in figures 3-14,15. It can be concluded from figure 3-15 that the temperature dependence of peak [2] (about -3×10^{-4} eV/K) is approximately equal to that of the major peak [1] around 2.5 eV. This latter structure is known to be caused mostly by transitions from band 5 to band 6. Interconduction-band structure is expected (and in Ag also found) to be much more temperature dependent. On the other hand, however, it must be stressed that the shift of [2] follows very closely that predicted by Christensen (1971) for the $L_{4-} \rightarrow L_{4+}$ (nonrelativistic: $L_{2'} \rightarrow L_1$) critical interband point transition.

†) Thanks are due to Dr. G.P. Pells for making available tabulated values of the optical constants of Au and Cu at various temperatures.

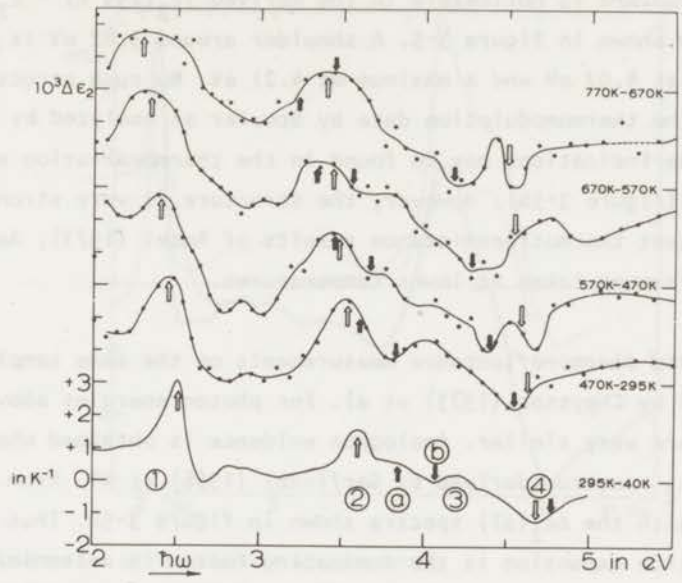

Fig. 3-14: Thermovariation results on Au as derived from the measurements by Pells (1969) and this work (lower line: 295 K - 40 K). The curves are shifted relative to one another, the respective zeroes being indicated on the right coordinate together with the temperature difference $T_2 - T_1$.

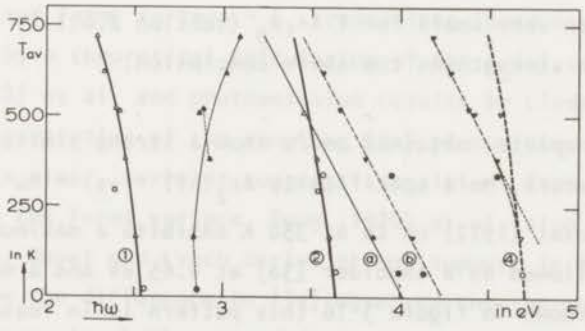

Fig. 3-15: Shift of structure in thermovariation spectra of Au (figure 3-14). The position of extrema in $[\varepsilon_2(T_2) - \varepsilon_2(T_1)]/[T_2 - T_1]$ - vs. - $\hbar\omega$ is plotted as a function of the average temperature $T = \frac{1}{2}[T_2 + T_1]$. Major (or minor) maxima are indicated by △ (respectively ▲), minima similarly by ▽ and ▼. Also included are some data derived from fig. 3-5b (725 K - 295 K: △, ▽) and from thermomodulation experiments by Sherring (1970) (□) and Rosei (1973) (○, ●).

(6) *Fine structure* is noticeable in the derived $[\varepsilon_2(295\ K) - \varepsilon_2(40\ K)]/255$ spectrum shown in figure 3-5. A shoulder around 3.82 eV is followed by a minimum at 4.07 eV and a maximum at 4.21 eV. No such structure is observed in the thermomodulation data by Scouler as analyzed by Cardona and only vague indications may be found in the thermovariation at higher temperatures (figure 3-5b). However, the structure is very strongly supported by recent thermotransmittance results of Rosei (1973), Antonangeli (1973) and Grassano taken at lower temperatures.

(7) *Piezo- and thermoreflectance* measurements on the same sample have been reported by Cheyssac (1973) et al. For photon energies above 3 eV the spectra are very similar. Analogous evidence is obtained when comparing the $\Delta\varepsilon_2$ spectrum derived by Garfinkel (1966) et al. from piezoreflectance with the $\Delta\varepsilon_2(\Delta T)$ spectra shown in figure 3-5b. Thus most probably lattice expansion is the dominating factor in determining the $\Delta\varepsilon_2(\Delta T)$ structure in this region.

This is also supported by Rosei (1973) and Antonangeli (1973). From thermomodulation they found that peak [2] at 3.6 eV progressively disappears on lowering the temperature. As transitions involving the Fermi surface are expected to become more peaked at lower T whereas lattice expansion becomes very small for $T << \theta_D$ (section 2.6.1.), this temperature dependence strengthens the above conclusion.

(8) *Modulation spectra obtained on Cu* show a strong similarity to the analogous Au spectra. More specifically $\Delta\varepsilon_2(\Delta T)$ - vs. - $\hbar\omega$ from thermomodulation by Rosei (1972) on Cu at 350 K exhibits a maximum [2a] at about 4.3 eV followed by a shoulder [3a] at 4.65 eV and a minimum [4a] at 4.95 eV. As shown in figure 3-16 this pattern is in reasonable agreement with thermovariation results as derived from ε_2 values by Pells (1969). Also included are results derived by Gerhardt (1968) from a modulation of hydrostatic volume strain at room temperature.

A major contribution to the understanding of Cu spectra comes from the analysis of this hydrostatic strain and especially the associated uniaxial strain experiments. Gerhardt suggests the peak [2a] to be due to

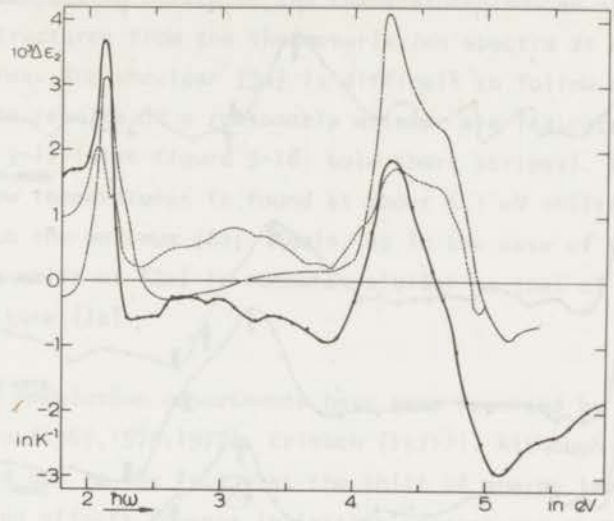

Fig. 3-16: Comparison of "modulation" spectra of Cu.
solid line: $[\varepsilon_2\ (575\ K) - \varepsilon_2\ (77\ K)]/498$ derived from data by Pells (1969);
broken line: thermomodulation at 350 K by Rosei (1972);
dash-dot line: hydrostatic strain modulation by Gerhardt (1968); this $\Delta\varepsilon_2$ structure is scaled to match the maximum-to-minimum value of the thermovariation spectrum.

highly localized Fermi surface → L_1 transitions (band 6 → band 7). This is supported by a theoretical calculation of the $\varepsilon_2(\omega)$ spectrum by Williams (1972) et al. and photoemission results by Lindau (1971b).

The interpretation of the shoulder [3a] plus minimum [4a] around 4.8 eV is less clear. Gerhardt suggests transitions from the bottom of the *d* band to the Fermi surface. Fong (1970) et al. also report evidence in this sense. Rosei and Lynch derive strong support in favor of this explanation from the difference in [3a] observed the thermo- and piezomodulation spectra. It should be noted, however, that the differences are much smaller when comparing Gerhardt's $\Delta\varepsilon_2$ with the thermovariation in figure 3-16. Also Williams et al. and Lindau and Walldèn point at the $L_{2'} \rightarrow L_1$ critical interband point that is expected to cause structure at these photon energies. If indeed the contribution of band 6 → band 7 brings about the strong peak [2a], then the $L_{2'} \rightarrow L_1$ transitions must show up in a pronounced way in the modulation spectra.

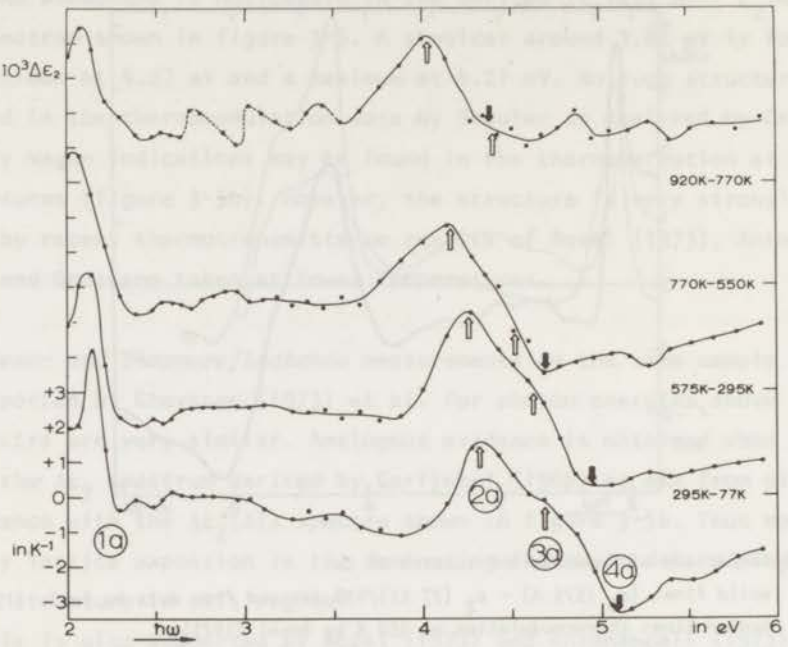

Fig. 3-17: Thermovariation of Cu at various average temperatures as derived from measurements by Pells (1969) and Shiga (see also figure 3-14).

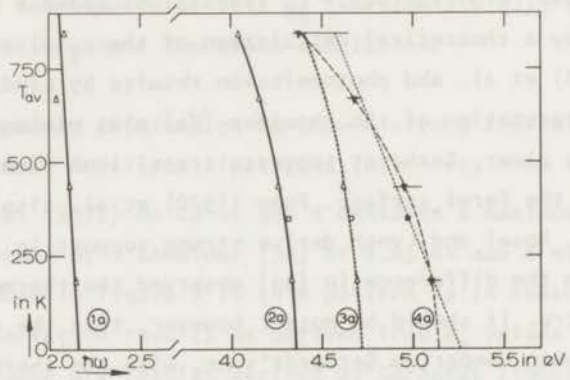

Fig. 3-18: Shift of structure in thermovariation spectra of Cu. (See also figure 3-15.) Also included are some data derived from thermomodulation experiments by Rosei (1972) (□, ■).

One can try to determine the temperature-induced shift of various $\Delta\varepsilon_2(\Delta T)$ structures from the thermovariation spectra at different average temperatures. The shoulder [3a] is difficult to follow at higher temperatures; the results of a reasonable attempt are indicated by open arrows in figure 3-17 (also figure 3-18: bold short stripes). The minimum [4a] that at low temperatures is found at about 5.1 eV shifts very rapidly as compared to the maximum [2a]. Again, as in the case of the Au (figure 3-15), the shift of [2a] is somewhat similar to that of the absorption edge structure [1a].

Alloy modulation experiments have been reported by Beaglehole et al. (Beaglehole (1969,1970,1972), Erlbach (1971)). Although the analysis is complicated due to the fact that the shift of energy levels now is determined by two effects (change in lattice spacing and change in atomic potential), some of the results from alloy modulation spectra are of considerable interest.

(9) Structures [1] and [2] + [4] have different origins. For some alloy systems (Au Fe, Au Ag) [1] is negative whereas [2] + [4] show the maximum--minimum pattern familiar from thermovariation. In other systems (Au Cu) this behavior is reversed.

(10) In our opinion it is important to note that [2] and [4] seem to originate from the same source: if the one is a minimum, the other is a maximum.

(11) *Line shape analysis* of modulation spectra sometimes yields information regarding the origin of structure (see section 2.7). This method has been particularly relevant in critical interband point assignments from semiconductor data.

3.9.3. *Photoemission results.*

(12) *Box model*

Recently evidence of interconduction-band transitions in photoemission work on the noble metals has been analyzed using somewhat more refined versions of the model described in section 2.7.2.2. The rectangular box-like structure in the PJDOS (and therefore also in the energy distribution curves referring to initial states) that was predicted by Koyama

(1970) (see also figure 2-7b) was used to locate the position of the $L_{4-} \rightarrow L_{4+}$ ($L_{2'} \rightarrow L_1$) gap (Smith (1971,1972a), Eastman (1972), Grobman (1972)). The uncertainty of the analysis for Au is demonstrated by the results reported by Smith (1971: 3.5 eV; 1972a: 4.0 eV). However, the latter value - derived from higher derivative photoemission spectra - is supported to some extent by a theoretical calculation of the EDC's and the second derivatives by Christensen (1972a) who found that the second derivative calculated for a photon energy of 3.70 eV (i.e. approximately the calculated band gap $L_{4-} \rightarrow L_{4+}$) agrees only with the experimental second derivative for $\hbar\omega = 4.2$ eV. This discrepancy actually is larger because the band calculation was performed for T = 0 K whereas the experiment was performed at room temperature. The L-gap is known to shift to lower energies on increasing the temperature.

(13) *Temperature-modulated photoemission experiments* are reported by Grobman and Eastman (Grobman (1972)). Some caution should be taken in the analysis of these experiments, for instance little is known about the temperature dependence of the work function. However, it is concluded that the structure due to transitions from initial states in the *d* band region can be associated with an upward shift of all the accessible *d* bands with respect to E_F with increasing lattice constant. In this regard it can be noted that the features obtained by Grobman are in surprising agreement with the "room temperature" thermovariation (470 K - 295 K) shown in figure 3-14 (also figure 3-5b). In the temperature-modulated energy distribution curves of initial states Grobman finds the following sequence of structures below E_F (the photon energy values of the analogous structure in $\Delta\varepsilon_2(\Delta T)$ are indicated between brackets): a large positive peak at -2.1 eV ([1]: 2.45 eV), a shoulder at -2.6 eV (2.95 eV), a minimum at -3.2 eV ($\sim$ 3.1 eV), a maximum at -3.6 eV ([2]: 3.53 eV), a maximum at -4.1 eV ([3]: 4.0 eV), a minimum at -4.3 eV ([4]: 4.55 eV), a maximum at -4.7 eV ($\sim$ 4.7 eV?).

3.10 *$L_{4-} \rightarrow L_{4+}$ at 3.6 eV?*

The critical interband point $L_{4-} \rightarrow L_{4+}$ (nonrelativistic: $L_{2'} \rightarrow L_1$) is known to be highly sensitive to changes in the lattice spacing. Trans-

itions taking place at this energy gap thus have received a good deal of attention in the interpretation of modulation spectra. This is also clearly reflected in table 3-4. Using the arguments given in the preceding sections one can analyze the pros and cons of the assignment of structure in $\Delta\varepsilon_2$ spectra at 3.6 eV to the $L_{4-} \rightarrow L_{4+}$ energy gap.

3.10.1. *Pro.*

(7) Lattice expansion rather than Fermi distribution broadening has a dominating influence on peak [2]. Alternative explanations show that the peak can be attributed to a shift of band 4 → band 6 absorption (section 3.11) or to the onset of band 6 → band 7 transitions ($E_F \rightarrow \sim L_{4+}$; section 3.12). These types of transitions both involve the Fermi surface as final respectively initial state. However, as pointed out in section 3.11.2. the influence of Fermi distribution broadening may be limited for band 4 → band 6 transitions.

(9) An advantage over this latter type of explanation stems from (9): band 4 → band 6 and band 5 → band 6 transitions are expected to react more or less analogously to alloying. This is not necessarily so for $L_{4-} \rightarrow L_{4+}$ transitions.

(1) The $L_{4-} \rightarrow L_{4+}$ assignment at 3.6 eV is in agreement with the band calculations by Sommers, Kupratakuln and Christensen. Although the calculations by Ramchandani and Smith are subject to doubt (section 3.2.), Connolly also finds a value for the L-gap that is too large, about 4.2 eV.

(5) Similarly the support from the close agreement of the theoretical and experimental temperature dependence of the assumed L-gap structure is questionable. Rather inspection of figure 3-15 and the evidence from Ag and Cu results contradict the assignment.

Positive evidence can possibly be seen in the small peak in ε_2/λ at 3.5 to 3.6 eV that has been reported by Fukutani and by Johnson (see figure 3-4). This structure is tentatively identified by Johnson and Christy as being due to $L_{4-} \rightarrow L_{4+}$ transitions (see also section 3.14).

3.10.2. *Contra.*

Apart from the discussion of (1) and (5) in the preceding section a

number of arguments can be given against the assignment of 3.6 eV structure to $L_{4-} \rightarrow L_{4+}$ transitions.

(11) As shown in section 2.7.2.2. $L_{4-} \rightarrow L_{4+}$ is a critical interband point transition of the type M_2. It is known from band calculations that the $L_{4-} \rightarrow L_{4+}$ gap decreases at higher temperatures. The corresponding shift of $\Delta\varepsilon_2(\Delta T)$ is in the right direction. However, major problems arise in an attempted line shape analysis using figure 2-5. For a decreasing value of E_0 the expected structure of $\partial\varepsilon_2/\partial E_0$ is strongly negatively peaked in contradiction to the experimental data. We find it somewhat surprising that in the analysis of the various modulation experiments (table 3-4) this very obvious discrepancy has not been noted before.

(12) On the basis of photoemission analyses the energy gap $L_{4+} - L_{4-}$ should be larger than 3.6 eV. The analysis by Smith should be treated with some caution though; as shown by Nilsson (1973) and Eastman an 2-OPW model is not completely adequate to describe the "box" structure in the band 6 → band 7 PJDOS of Ag (see also (4)). Independent support comes from Christensen (1972a) though.

(2,3,4) Major problems arise from the magnitude of the calculated interconduction band structure. The evidence from figure 3-13 is weak and open to alternative interpretations (sections 3.11,3.12.). However, even making the (reasonable) assumption that the matrix elements in Au are of the same order of magnitude as in Cu and Ag, it still is difficult to account for such a large peak in $\Delta\varepsilon_2(\Delta T)$ as being due to the $L_{4-} \rightarrow L_{4+}$ critical interband point.

(8) The band structure of Au and Cu near L_{4-} and L_{4+} is rather analogous. It was pointed at the similarity in the thermovariation and modulation spectra. Noteworthy in this respect is the generally accepted assignment of the large positive peak [2a] in the various Cu spectra as being due to transitions from E_F to band 7 near L_{4+}. Even if peak [2] in Au is due to $L_{4-} \rightarrow L_{4+}$ transitions, one would expect a (possibly even larger) positive peak to precede [2]. Again no indication of these $E_F \rightarrow \sim L_{4+}$ transitions is observed though.

(6) The situation for the "fine" structure around 4 eV is less clear. Rosei suggests that on lowering the temperature the $\Delta\varepsilon_2(\Delta T)$ peak at 4.2 eV splits off into two different components. The first at 4 eV tends to

increase and is therefore attributed to a *d* band → Fermi surface transition (presumably band 4 → band 6). The second peak at 4.3 eV is of uncertain origin. A more complete explanation along these lines cannot be excluded. Referring to (2) and (3) it would involve very large matrix elements of the band 6 → band 7 transitions as compared to those of band 4 → band 6 transitions at the same photon energy. Furthermore a satisfactory analysis should also account for the minimum [4] that is probably related to [2]. Christensen (1971) suggests transitions from the third *d* band to the Fermi surface (e.g. $(Q_3 + Q_4)^3 \rightarrow E_F$) to account for this structure. On the basis of figure 3-13 and alloy modulation experiments this is highly improbable.

3.10.3. *Comments.*

If the $L_{4-} \rightarrow L_{4+}$ assignment of the major peak in the thermovariation spectra is correct, the extrapolation in figure 3-19 locates the maximum of $\Delta\varepsilon_2(\Delta T)$ at T = 0 K at 3.64 eV. In view of the uncertainty of the line shape analysis (section 3.10.2. (9)) it is not possible to determine the energy gap at T = 0 K with a higher accuracy than $L_{4+} - L_{4-} = (3.64 \pm 0.07)$ eV. The corresponding value at room temperature is (3.56 ± 0.07) eV.

A further discussion of the merits of this explanation is given in section 3.12.4.

3.11. *Shift of band 4 → band 6 structure.*

Recently the optical properties and photoemission have been interpreted as originating from extended regions of $\underline{k}$-space rather than from localized critical points (section 2.7.3.; also Christensen (1972a)).

3.11.1. *Pro.*

Such an explanation is quite strongly suggested by the calculated thermovariation in figure 3-13. A strong positive peak around 3.76 eV is seen to originate from a shift of the band 4 → band 6 (2^{nd} *d* band → conduction band) contribution to $\varepsilon_2^{(b)}$. Comparing figures 3-13,14 it is clear that a line shape analysis of structure around 3.6 eV yields correct results.

(11)

(5) The explanation also is supported by the similarity of the temperature dependence of [2] and [1] (also section 3.11.2.:(7)). The latter structure is generally attributed to band 5 → band 6 transitions. This
(13) similarity of temperature-induced shifts is also noted by Grobman and Eastman. Although - until a more complete analysis is given of the experimental technique - their results should be treated with care, they indicate that the 3.6 eV maximum is due to structure in the density of states of the *d* bands.

3.11.2. *Contra.*

(9) As already indicated in section 3.10.1 one of the strongest arguments against this interpretation comes from alloy modulation experiments. Whereas in thermovariation [1] and [2] are positive peaks, it is found that on alloying (AuFe, AuAg, AuCu) these peaks can have an opposite sign. It is most difficult to reconcile this with the expected similarity of the influence of alloying on band 4 → band 6 and band 5 → band 6 transitions.

(7) Further strong evidence against this assignment stems from piezoreflectance and low temperature thermomodulation results that indicate lattice expansion to be the dominating influence on [2]. Partially the absence of a pronounced effect of Fermi distribution broadening in the thermomodulation spectra can be explained from the fact that band 4 is not as flat as band 5 (band 4 lower effective mass; see figure 3-1). Especially in the vicinity of L - the region that was found to contribute most to the absorption edge, i.e. to the onset of the band 5 → band 6 $\varepsilon_2^{(b)}/\lambda$ - band 4 is more warped. Consequently the onset of band 4 → band 6 structure in the calculated $\varepsilon_2^{(b)}/\lambda$ (figure 3-2) is spread out over a larger photon energy interval and thus the expected influence of the Fermi distribution broadening on [2] is not so strong as on [1]. However, this explanation can by no means account for the large difference between the 2.5 eV and the 3.6 eV structures that is observed in piezoreflectance measurements. Again these data strongly suggest that the thermovariation peaks have different origins, thus spoiling the important argument (5) given in the preceding section.

(8) A third negating argument is found in the similarity of the thermovariation spectra of Au and Cu. The major maximum [2a] in $\Delta\varepsilon_2(\Delta T)$ of Cu was attributed to highly localized transitions from E_F to band 7 in the vicinity of L. Conclusive evidence in this regard can possibly be obtained from experiments on Au analogous to those performed on Cu by Gerhardt (uniaxial and hydrostatic strain).

(10) The calculated $\Delta\varepsilon_2^{(b)}$ spectrum (figure 3-13) does not exhibit the expected minimum [4] around 4.5 eV. Speculatively one can point at the assumption of constant matrix elements in the calculated $\varepsilon_2^{(b)}/\lambda$ - vs. - $\hbar\omega$ spectra. It was suggested in section 3.9.1. (2) that in order to improve the agreement between experiment and theory the band 3 → band 6 transition probably had to be very small. From the band structure (figure 3-1) one would logically expect this decrease of the matrix elements to have a pronounced influence on the band 4 → band 6 transitions too, more specifically so on those from initial states further below E_F. Thus especially the high energy side of the band 4 → band 6 contribution to $\varepsilon_2^{(b)}/\lambda$ could drop more rapidly than shown in figure 3-2. A shift of this structure to lower photon energies would then give a reasonable explanation to the minimum [4]. A calculation of the wave-functions such as has been performed for Cu (e.g. Williams (1972)) is necessary in this respect.

(5) Figure 3-14 can be checked for a temperature dependence of [4]. Assuming the minimum [4] as observed at low temperatures to shift at the same rate as the maximum [2] (see figure 3-15) leads to locations at higher temperatures such as indicated by open downward arrows in figure 3-14. Clearly the agreement with experiment is not very good; our own measurements at high temperatures suggest however that part of the discrepancies is due to scatter in the ε_2 data of Pells.

3.11.3. *Comments.*

Undoubtedly band 4 → band 6 transitions contribute to modulation and thermovariation spectra. However, from the arguments in section 3.11.2. it is improbable that the major structure [2] and [4] is due to this type of transitions.

3.12. *Shift of band 6 → band 7 transitions: $L_{4-} \rightarrow L_{4+}$ at 4.3 eV?*

In the literature the interconduction band structure of Cu and Ag is often treated by a "box" model of the PJDOS such as shown in a simplified way in section 2.7.2.2. The high energy side of the box originates from the type M_2 critical interband point $L_{4-} \rightarrow L_{4+}$, whereas the low energy side is due to the onset of transitions at the Fermi surface. To our knowledge this type of analysis has never been used in case of Au. This is somewhat surprising as the relevant band structure of Au is very similar to that of Cu. The analysis will be shown to have good possibilities.

3.12.1. *Pro.*

(8) In this explanation we stress the analogy with Cu

3.12.1.1. *Thermovariation of Cu.*

In modulation spectra of Cu a strong positive peak [2a] is observed at 4.3 eV followed by a broad shoulder [3a] around 4.8 eV and a minimum [4a] at 5.1 eV. The peak [2a] is usually attributed to the onset of transitions from E_F (band 6) to band 7 in the vicinity of L_{4+}. The $L_{4-} \rightarrow L_{4+}$ energy gap has recently been determined to be about 4.8 eV. The relevant band structure is shown in figure 3-19. A corresponding partial ε_2 structure is chosen such as to account in a satisfactory way for the observed $\Delta\varepsilon_2$ spectra (e.g. $\Delta\varepsilon_2$ (295 K - 77 K) in figure 3-17). The proposed ε_2 pattern is very similar to that given by Lindau and Walldèn (Lindau (1971b), figure 18).

At a higher temperature band 7 is expected to move down, thus decreasing the energy gap at L. However, at the same time the Fermi surface is lowered (e.g. section 3.8.1.). As shown in figure 3-19e the result is a narrowing of the box. The temperature dependence of [2a] thus is expected to be smaller than that of [4a]. Indeed such a pattern is observed in the analysis of the thermovariation spectra in figure 3-17. The position of [2a] (indicated by an open upward arrow) shifts at roughly -3.6×10^{-4} eV/K, [4a] (black arrows) considerably faster (see figure 3-18). Admittedly this last shift is somewhat arbitrary. Alternatively a good fit to the data can be obtained by taking the positions of [4a] as suggested by the almost straight dotted line in figure 3-18. The temperature dependence then is approximately -8.1×10^{-4} eV/K.

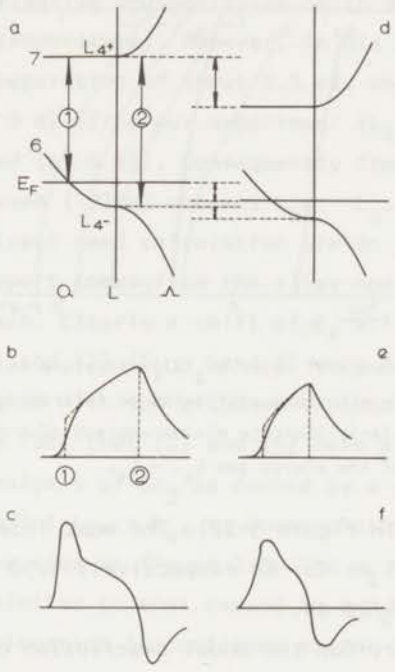

Fig. 3-19: Interconduction band transitions:
a. band structure; b. a possible ε_2 spectrum; c. the corresponding $\Delta\varepsilon_2$;
d., e., f. same as a., b., c. at higher temperature.
The effect of Fermi distribution broadening on the onset of the "box" is tentatively included in b. and e.

3.12.1.2. *Thermovariation of Au.*

(5) Turning to Au a similar situation if found on following the movement of the maximum [2] and the minimum [4] in $\Delta\varepsilon_2(\Delta T)$ on increasing the temperature (figure 3-14). The analogy with Cu is quite pronounced as can be seen in figure 3-20. An estimate of the $L_{4^-} \rightarrow L_{4^+}$ energy gap at an average temperature $T_{av} = \frac{1}{2}(T_1 + T_2)$ can be obtained from the photon energy at which $\Delta\varepsilon_2(T_2 - T_1) = 0$. However, this analysis is considerably complicated by the very large uncertainty of this zero-level as demonstrated in figures 3-14,17. Still from the expected line shape and the temperature dependence of [4], that is thought to be very similar to that of the L gap, it is possible to estimate the value of $L_{4^-} \rightarrow L_{4^+}$ at various temper-

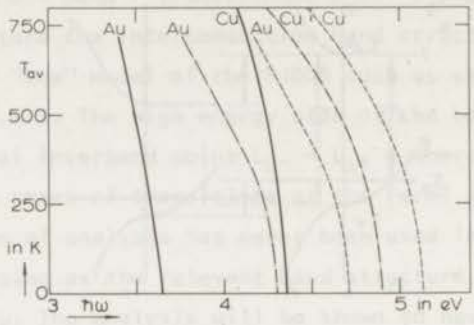

Fig. 3-20:Temperature dependence of major $\Delta\varepsilon_2(\Delta T)$ structure in Au and Cu. Solid lines indicate maxima in structure attributed to interconduction-band transitions; broken lines similarly indicate minima whereas dash-dot lines refer to the estimated value of the energy gap $L_{4-} \rightarrow L_{4+}$.

atures (dash-dot line in figure 3-20). The most interesting values are those at 0 K and at 295 K: for Cu respectively 4.90 and 4.81 eV, for Au respectively 4.30 and 4.20 eV.

Qualitative support for the model description of interconduction-band transitions in the vicinity of L at low and high temperatures (figure 3-19a,d) can be derived from Christensen's band calculations. Some results calculated from the difference between the 920 K and 0 K calculations are shown in table 3-5 together with some values derived from figure 3-15. Again the shift of [4] is used to estimate the temperature dependence of the $L_{4-} \rightarrow L_{4+}$ energy gap. Although the absolute values deviate, the shift of the $L_{4-} \rightarrow L_{4+}$ gap is indeed seen to be about twice that of the E_F (band 6) $\rightarrow \sim L_{4+}$ (band 7) gap. This is largely due to the decrease of E_F with respect to L_{4-}.

Table 3-5

Comparison of theoretical and experimental shifts of interconduction-band energy gaps.

	theory (920K-0K)	experiment (700K-0K)
$E_F(6) \rightarrow \sim L_{4+}(7)$:	-0.17 eV	-0.23 eV
$L_{4-} \rightarrow L_{4+}$:	-0.35 eV	-0.52 eV
$L_{4-} \rightarrow E_F$:	-0.20 eV	
$E_F \rightarrow L_{4+}$:	-0.15 eV	

(12) From higher-derivative photoemission Smith determined the L gap to be 4.0 eV (at room temperature). However, in his box model analysis he assumes a $L_{4-} \rightarrow E_F$ separation of about 0.5 eV, whereas Christensen calculated 0.72 eV (at 0 K) (from our experiment $(L_{4+} - L_{4-}) - (\sim L_{4+} - E_F) = 4.30 - 3.64 = 0.66$ eV (at 0 K)). Consequently from theoretically second derivatives Christensen (1972a) obtains $L_{4+} - L_{4-} = 4.2$ eV, somewhat to his dismay as the direct band calculation yields 3.72 eV (at 0 K).

Very strong support comes from the alloy modulation experiments by (9) Beaglehole and Erlbach. Clearly a shift of E_F will influence the peaks [1] (mainly band $5 \rightarrow E_F$) and [2] ($E_F \rightarrow$ band 7) very differently. Indeed Beaglehole et al. agree with the proposed explanation of [2]. Important, (10) however, also is the fact that [2] and [4] have associated origins.

(11) A line shape analysis of $\Delta\varepsilon_2$ as caused by a shift of the type M_2 critical interband point $L_{4-} \rightarrow L_{4+}$ to lower photon energy ($\delta E_0 < 0$) causes no problems as can be seen in figure 2-5. The ε_2 structure due to $E_F \rightarrow \sim L_{4+}$ transitions is similar to that caused by a M_0 critical interband point; again the explanation is confirmed by the line shape of $\Delta\varepsilon_2$.

It should also be noted that it is virtually impossible to think of (5) any other reasonable explanation for the large temperature dependence of [4]. The critical point L_{4+} is known to be very sensitive to lattice expansion.

3.12.2. *Contra.*

(3,4) More or less sensational would be the influence of matrix elements on the optical properties. The transition probability for band 6 $\rightarrow$ band 7 transitions near L is known to be large for Ag and Cu. However, even if their contribution of $\varepsilon_2^{(b)}/\lambda$ is as large as 30% of the total absorption structure one would still expect to see a very strong $\Delta\varepsilon_2(\Delta T)$ structure due to band 4 $\rightarrow$ band 6 transitions (figure 3-13). One must therefore assume a considerable reduction of this structure relative to that originating from band 6 $\rightarrow$ band 7 transitions. Again matrix elements would be the culprit.

(7) As a matter of fact this supposition is confirmed by the measurements of Garfinkel (1966) and Cheyssac (1973). On the basis of figure 3-13

piezoreflectance structures due to band 5 → band 6 and band 4 → band 6 transitions are expected to be of approximately the same magnitude. However, in actual experiment peak [2] is three to four times stronger than [1]. This latter structure is definitely associated with band 5 → band 6 transitions (section 3.8). Thus band 4 → band 6 transitions would only account for 25 to 35% of the peak value of [2]. The remaining 65% must be attributed to interconduction-band transitions.

(2) In this context it can be remarked that any agreement between the calculated and experimental $\varepsilon_2^{(b)}/\lambda$ spectra such as suggested by Christensen (1971) and Johnson (1972) (figure 3-12) must be considered to be fortuitous. Either the calculated piezoreflectance spectrum (figure 3-13) is in error (and consequently also the $\varepsilon_2^{(b)}/\lambda$ spectra) or one has to include the large effect of matrix elements also in the $\varepsilon_2^{(b)}/\lambda$ spectra which would therefore be changed quite considerably between 3 and 5 eV. Referring to figure 3-2 and the discussion in section 3.11.2 (10) we suggest that the $\varepsilon_2^{(b)}/\lambda$ structure originating from band 4 → band 6 transitions is reduced through the influence of matrix elements. On the other hand the absorption maximum around 4 eV will have strong contributions from interconduction-band transitions.

(5) The proposed explanation does not account for the fine structure that is observed in low temperature $\Delta\varepsilon_2(\Delta T)$ spectra (figure 3-5a). Information regarding the minor up-and-down structure between [2] and [3] is limited. Tentatively one can search figure 3-14 for evidence of a temperature-induced shift. The minimum - indicated by [b] in figure 3-14 - can be seen to move to lower photon energies on increasing the temperature. At high temperatures it is very difficult to follow. This is even more so for the maximum [a] that has merged with peak [2] at room temperature already. Our best guess for the shifts is indicated by black arrows in figure 3-14. As shown in figure 3-15 the shifts are similar to those attributed to interconduction-band structure, thus suggesting an assignment in this sense.

It can be noted that alternative explanations failed. The shift to lower photon energies is too large for band 4 → band 6 transitions. It was not found possible to match the observed behavior with a shift of structure to higher photon energies such as would be possible for struc-

ture originating from transitions at the $X_{6+2} \rightarrow X_{6-}$ or $X_{7+2} \rightarrow X_{6-}$ critical interband points (Christensen (1971), figure 18).

In figure 3-13 it is indicated that quite probably the band 6 → band 7 contribution to $\Delta\varepsilon_2$ spectra is not so smooth as indicated in figure 3-19. A possible agreement of the observed pattern with the calculated spectra will not be stressed here in view of the expected influence of matrix elements.

(4)

(7) Major difficulties are caused by the attribution of peak [2] in $\Delta\varepsilon_2(\Delta T)$ to a lattice expansion effect rather than to transitions involving the Fermi surface. Clearly this is in striking contradiction with the proposed explanation. It should be noted that this same problem must arise in the analysis of peak [2a] in Cu. Unfortunately Rosei (1972) and Lynch do not present any results from low temperature thermomodulation in the relevant photon energy interval.

Speculatively one can account for this difficulty by assuming that part of peak [2] in Au is due to band 4 → band 6 transitions. This contribution is expected to be mainly due to lattice expansion (section 3.11.2. (7)); it will therefore decrease at low temperatures. However, its peak energy is also expected to be somewhat less temperature dependent than that of band 6 → band 7 structure. Two overlapping maxima at higher temperatures thus can be separated at low temperatures. This would provide a possible explanation to the thermomodulation results obtained by Rosei (1973), Antonangeli (1973) and Grassano. A large amount of guess-work is involved though and other solutions are conceivable.

Clearly better experiments with less scatter in the data are necessary to calculate more reliable thermovariation spectra at high temperatures. Possibly from such results one can more accurately derive the shift of the up-and-down structure [a][b] and thus obtain information regarding its origins. Important evidence also may come from uniaxial strain modulation on Au single crystals such as have been performed on Cu by Gerhardt (1968).

3.12.3. *Comments.*

Of all explanations this one is the most empirical. It rests heavily on the expected analogy with Cu and little on theoretically calculated spectra. Deviations from such spectra are attributed to the k-dependence

of matrix elements. Actually therefore for a conclusive decision on this model one needs a "wave function band structure", i.e. a calculation of the $\underline{k}$-dependence of the wave function. Perhaps this will also provide more justification to the assumed shape of the "box" (figure 3-19b,e) that differs considerably from that presented in figure 2-7. Nilsson (1973a) and Eastman have shown for Ag that matrix elements do have a strong influence on the box. Any change in the box, however, will not interfere with the fundamental quality of the explanation: the relation between the maximum and the minimum in $\Delta\varepsilon_2(\Delta T)$.

(1) The only band calculation that yields a gap in good agreement with our proposed value is that of Connolly ($\sim$ 4.2 eV). In this respect it should be repeated that it is the L_{4+} level that is extremely sensitive to the choice of the crystal potential in band calculations. In chapter 4 it will be shown that in the case of Ag the theoretically calculated $L_{4+} - L_{4-}$ = 3.49 eV (Christensen (1972b)) has to be raised to about 4.25 eV on the basis of experimental data. Thus the discrepancy between Christensen's 3.72 eV and the proposed 4.30 eV is no conclusive evidence against this explanation.

3.12.4. *Conclusions.*

If one compares the pros and cons of the proposed explanation with those given in section 3.10. in regard to the assignment of peak [2] to transitions at the $L_{4-} \rightarrow L_{4+}$ critical interband points the following points are of major concern.

The $L_{4-} \rightarrow L_{4+} \simeq 3.6$ eV explanation rests heavily on argument (7): the experimental evidence indicates that lattice expansion is the primary factor in determining the "size" of [2]. Major difficulties arise from the analogy with Cu results (8); more specifically the explanation does not account for the highly temperature dependent minimum [4] ((5),(8),(9), (10)). Further evidence against this interpretation stems from photoemission (12) and possibly a line-shape analysis (11).

The $L_{4-} \rightarrow L_{4+} \simeq 4.3$ eV explanation given in the preceding sections, on the other hand, is mostly troubled by (7). The positive points are exactly those that negated the alternative explanation. Especially noteworthy is the fact that the proposed model provides a good explanation

for $\Delta\varepsilon_2(\Delta T)$ spectra not only of Au but also of Cu. The box model analysis has been used with good success by Lindau (1971b) and Walldèn in the interpretation of photoemission work on the latter metal; to our knowledge it has not been used to account for modulation spectra (the box proposed by Gerhardt (1968) is too narrow). Although better measurements of the optical properties are necessary to get more certainty, the minor up-and--down structure [a] + [b] probably also originates from interconduction--band transitions (5).

From the gathered evidence we therefore conclude that most probably the box model explanation of the interconduction-band structure is correct. The results of this analysis are summarized in figure 3-20 and table 3-6. The values for the energy gap $L_4^- \rightarrow L_4^+$ are expected to be accurate to within ±0.1 eV for temperatures below 350 K and to ±0.2 eV at higher temperatures. In the estimation of the gap $E_F \rightarrow L_4^+$ it was assumed that the relevant part of band 7 is perfectly flat in the directions parallel to the Brillouin zone face. According to Christensen's band calculations for Au the induced error due to this assumption is small; the quoted values should perhaps be lowered by about 0.02 eV. Consequently this would increase the values of $L_4^- \rightarrow E_F$ by the same amount.

Table 3-6

Energy gaps at L for conduction bands near E_F.

	Au			Cu		
temperature	0 K	295 K	700 K	0 K	295 K	700 K
$L_4^- \rightarrow L_4^+$	4.30	4.20	3.81	4.90	4.81	4.40
$E_F \rightarrow L_4^+$	3.64	3.57	3.41	4.36	4.31	4.14
$L_4^- \rightarrow E_F$	0.66	0.63	0.40	0.54	0.50	0.26

3.13. *Minor structure in $\varepsilon_2^{(b)}/\lambda$ between 3.5 and 5.0 eV.*

Weak structure in the absorption spectra is observed at 3.75 eV and between 4.3 and 4.7 eV. As the evidence is weak, the discussion will be limited.

3.13.1. *Fine structure around 3.75 eV.*

Speculatively a small shoulder is observable in most series of measurements at a photon energy of about 3.75 eV. Although best results are obtained at low temperatures and 295 K, the structure seems to persist up to the highest temperatures. Probably therefore it can be assigned to transitions originating from the *d* bands. Tentatively it can be pointed at a small shoulder in the band 5 → band 6 partial $\varepsilon_2^{(b)}/\lambda$. As shown in figure 3-2 this shoulder is observed at about 3.8 eV for both the T = 0 K and the T ≈ 920 K calculation. However, band 4 → band 6 transitions are also known to contribute to $\varepsilon_2^{(b)}/\lambda$ in this photon energy range.

New structure at 3.75 eV is also reported by Weiss (1972) and Muldawer (abstract only). No details on these measurements are known as yet.

3.13.2. *Shoulder between 4.3 eV and 4.7 eV.*

A broad weak shoulder in ε_2/λ is observed at all temperatures for photon energies between 4.3 and 4.7 eV (also Pells (1969)). A shoulder is also obtained at 4.5 eV below E_F in a number of EDC's of initial states in recent XPS work (Shirley (1972a), Lindau (1972)) in agreement with the density of states derived from band calculations (Kupratakuln (1970), Christensen (1971), Smith (1972a,b), Connolly (see Shirley (1972a))). Thus one is led to think of an absorption reflecting this *d* band structure.

In this respect Kupratakuln points at transitions from $X_{6+2} \rightarrow X_{6-}$ (nonrelativistic $X_5 \rightarrow X_{4'}$) in support of the identification by Pells. Further evidence for this critical interband points assumption is derived from modulation experiments again (table 3-4). Comparing with Scouler's thermomodulation results Christensen suggests transitions from the third *d* band to the Fermi surface, for instance $(Q_3 + Q_4)^3 \rightarrow E_F$. However, in section 3.12. it was suggested that such structure would be weak.

Speculatively we rather refer to section 3.11.2. Quite possibly the shoulder in $\varepsilon_2^{(b)}/\lambda$ is associated with a shoulder in the density of states of band 4. The effect could become more pronounced through the influence of matrix elements that "cuts off " part of the structure at higher energies. This explanation would be in reasonable agreement with the XPS

results. The identification with transitions at the X critical interband points $X_{6+2} \rightarrow X_{6-}$ or $X_{7+3} \rightarrow X_{6-}$ is doubtful. Both transitions are expected to shift to higher photon energy on increasing the temperature (Christensen (1971)). Again, more accurate measurements of the optical properties at regularly spaced temperatures are necessary to determine a possible shift of fine structure in thermovariation spectra (see section 3.11.2. (5)).

3.14. *Dependence of ε_2/λ on specimen structure.*

In order to explain the discrepancy between the absorption spectra as reported in the literature it often has been pointed at the influence of specimen structure (e.g. Pells (1969), Johnson (1972)). As shown by Devant (1967) and Thèye (1970) the interband absorption in thin films is little affected by the size of the composing crystallites. However, for samples containing many structural defects interband structure is decreased and broadened, not displaced in photon energy. This is demonstrated in figure 2 of Ripken (1972). The structure dependence also is very obvious from the influence of surface treatment on bulk samples. The effect of annealing of mechanically polished Au specimens or thick films once again is an increase of $\varepsilon_2^{(b)}/\lambda$ as shown very clearly by Köster (1967). This observation has been corroborated in our own measurements. Thus measurements on evaporated and bulk samples indicate that $\varepsilon_2^{(b)}/\lambda$ is rather sensitive to structural defects. More specifically the influence of annealing of bulk samples suggests an appreciable influence of internal strain.

In this regard it can be pointed out that the absorption maximum (between 3.5 and 4.8 eV) is considerably more dependent on the quality of the sample than the absorption edge (2.0 to 3.5 eV) (e.g. Köster (figures 4a,5), Ripken). The larger decrease and broadening of the maximum may be understood by modelling the "deformed" lattice as a mixture of regions with an expanded and regions with a compressed lattice (also section 4.11). The relevant "band structure" correspondingly can be thought of as such a mixture. It was concluded in section 3.12 that band 6 → band 7 transitions contribute an important part of all structure at the absorption maximum. The energy gaps for these transitions are highly sensitive to lattice changes. A smearing of the interconduction-band structure due to

internal strains satisfactorily accounts for the observed behavior. On annealing the lattice "straightens out" and the absorption maximum becomes much better defined. Thus the shape and size of the absorption maximum (relative to the size of the absorption edge) provides a criterion for the quality of the sample and therefore for a comparison of experimental data.

In our opinion a good example may be found in the work on thick non-annealed films by Fukutani (1966) (see figure 3-4). In addition to the decrease of the maximum in ε_2 Fukutani also obtained a very large splitting of the absorption edge. It was suggested in section 3.8.3. that this splitting reflects structure in the *d* bands and that it is susceptible to lattice changes. Thus - although the internal strain in the specimen has to be very large - this model provides a possible explanation of the differing behavior observed by Fukutani. Whether the positive structure in ε_2 at 3.6 eV is a remnant of the moving interconduction-band structure or is due to some other mechanism is impossible to say. A similar, somewhat less pronounced structure has to our knowledge only been reported by Johnson and Christy (Johnson (1972)). From figure 3-4 it may be seen that their ε_2 values in the region of the absorption maximum are intermediate between those of Fukutani and ours (also Irani (1971a)).

3.15. *Summary.*

The results obtained on Au can be summarized as follows.

3.15.1. *Intraband absorption.*

(1) In our opinion only qualitative arguments can be derived from experiments of this type (section 3.6.).

(2) The derived data are dependent on the model used in the analysis (section 3.6.).

(3) The optical mass is nearly independent of temperature (section 3.6.4.).

(4) Surface scattering of electrons may play an important role in determining $\varepsilon_2^{(f)}/\lambda$ (section 3.6.4.).

3.15.2. *Interband transitions.*

3.15.2.1. *Absorption edge.*

(1) The absorption edge shifts to lower photon energies on increasing the

temperature (section 3.8.1.).

(2) The low-energy tail is due to interband transitions (band 5 → band 6) in the vicinity of X (section 3.8.2.).

(3) At all temperatures the absorption edge (i.e. $\varepsilon_2^{(b)}/\lambda$ - vs. - $\hbar\omega$) is parabolic up to $\hbar\omega \simeq 2.7$ eV. Tentatively this can be explained by assuming a "parabolic" contribution to $\varepsilon_2^{(b)}/\lambda$ (Cooper (1965), Miloslavskii (1967)) from band 5 → band 6 transitions in the vicinity of L to be superimposed on a continuous background contributed by transitions in extended regions of $\underline{k}$-space (mostly in the neighborhood of X) (section 3.8.3.).

(4) Structure around 2.9 eV as observed in modulation experiments is attributed to transitions near the $X_{7+3} \rightarrow X_{6-}$ - critical interband point (band 5 → band 6) (section 3.8.3.4.).

3.15.2.2. *Absorption maximum.*

(1) Structure between 3.5 and 4.8 eV as observed in modulation spectra is due to interconduction-band transitions (band 6 → band 7) in the vicinity of L. More specifically at T = 0 K the critical interband point energy gap $L_{4-} \rightarrow L_{4+} = 4.30 \pm 0.10$ eV, at T = 295 K $L_{4-} \rightarrow L_{4+} = 4.20 \pm 0.10$ eV. The energy gap $E_F \rightarrow L_{4+} = 3.64 \pm 0.10$ eV at T = 0 K (section 3.12.). The value of $L_{4-} \rightarrow L_{4+}$ gap is considerably larger than those obtained in most relativistic band calculations.

(2) The $\underline{k}$-dependence of transition matrix elements - especially those for interconduction-band transitions - cannot be disregarded (section 3.12.). The coincidence of the calculated $\varepsilon_2^{(b)}/\lambda$ spectrum (Christensen (1971)) with the experimental spectrum is to a major extent coincidental.

(3) The height (relative to other structure) and width of the absorption maximum provide a good criterion for judging the quality of the sample (section 3.14.).

3.15.2.3. *Copper.*

The analysis also yields relevant information on Cu. More specifically at T = 0 K $L_{4-} \rightarrow L_{4+} = 4.90 \pm 0.10$ eV, at T = 295 K 4.81 ± 0.10 eV. The onset of interconduction-band transitions $E_F \rightarrow \sim L_{4+}$ occurs at 4.36 ± 0.10 eV (T = 0 K). These values are in good agreement with those proposed by Lindau (1971b) and Walldèn on the basis of photoemission work (section 3.12.).

CHAPTER 4: SILVER

4. *Silver.*

4.1. *Motivation.*

Relativistic band calculations of Ag (Christensen (1972b)) indicated a major displacement of the $L_{4^-} \rightarrow L_{4^+}$ (nonrelativistic: $L_{2'} \rightarrow L_1$) energy gap from the values predicted by previous nonrelativistic calculations. As a matter of fact transitions near this gap were expected to cause a minor absorption structure around 3.5 eV, i.e. below the absorption edge that in Ag is around 4.0 eV. No convincing evidence was known for such

structure; however, possibly it could be "hidden" in the intraband contribution to ε_2/λ.

Measurements of the temperature dependence of the optical properties of Ag have two advantages. First, at low temperatures the intraband contribution is reduced such that any interband structure will show up more clearly. Second, the interconduction-band structure is expected to be highly temperature dependent. Changes in the absorption spectrum therefore are expected to be pronounced. As in the case of Au thermovariation thus may yield valuable information.

4.2. *Band structure.*

As noted in section 2.2.2. relativistic corrections are smaller for Ag than for Au. Still in view of the success of the RAPW calculation in the preceding section we will not consider the numerous nonrelativistic band calculations that have appeared in the literature (Chatterjee (1966, 1967,1968), Jacobs (1968), Lewis (1968), Snow (1968), Ballinger (1969), Bhatnagar (1969), Christensen (1969), Cooper (1969,1971)). Rather the RAPW calculation of Christensen (1972b) will be used. This calculation

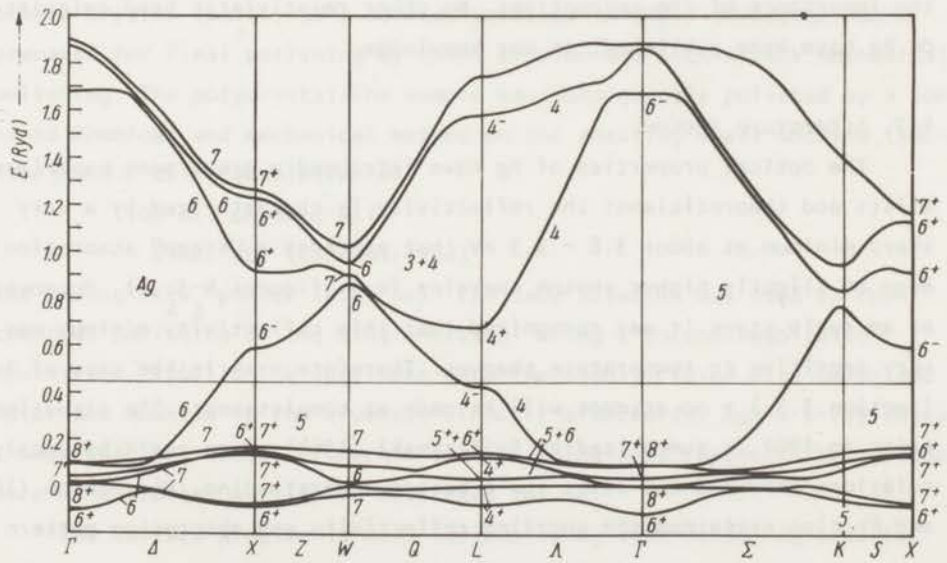

Fig. 4-1: RAPW energy band of Ag (at T = 0 K) (after Christensen (1972b)).

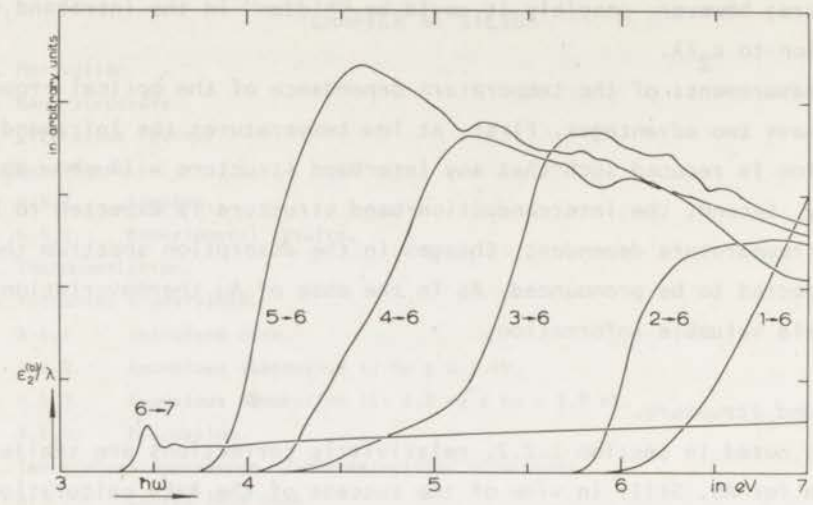

Fig. 4-2: Partial $\varepsilon_2^{(b)}/\lambda$ - vs. - $\hbar\omega$: contributions from the various pairs of bands calculated assuming constant matrix elements (after Christensen †).

predicts a greatly reduced value of the $L_{4-} \rightarrow L_{4+}$ gap, 3.48 eV, compared to the analogous nonrelativistic $L_{2'} \rightarrow L_1$ gap, 4.34 eV, indicating once again the importance of the corrections. No other relativistic band calculations on Ag have been published, to our knowledge.

4.3. *Literature review.*

The optical properties of Ag have intrigued a great many experimentalists and theoreticians: the reflectivity is characterized by a very sharp minimum at about 3.8 - 3.9 eV that precedes a "steep" absorption edge at slightly higher photon energies (e.g. figures 4-3c,a). Moreover at an early stage it was recognized that this reflectivity minimum was very sensitive to temperature changes. Therefore - as in the case of Au (section 3.3.) - no attempt will be made at completeness. The situation prior to 1962 is summarized by Suffczynski (1964). Once again band calculations provided the basis for a better understanding. Ehrenreich (1962) and Philipp explained the puzzling reflectivity and absorption pattern as

†) Again we wish to express our gratitude to Dr. N.E. Christensen for making available tabulated values of the results of his band calculation.

being due to the combined effects of a volume plasma resonance and interband absorption. Since that time much work has been reported on the assignment of the various structural details in optical or photoemission spectra to specific interband transitions. References to the literature will be given whenever relevant.

As stated above the temperature dependence of the optical properties of Ag has interested physicists for a long time. A summary of the early work has been given by Pennington (1932). More interesting in regard to band structure were the results reported by Joos (1954) and Klopfer at temperatures between 20 K and 428 K. Their interpretation was rendered out of date, however, by the experiments of Liljenvall (1970b) and Mathewson between 298 K and 773 K in a photon energy interval between 2.8 and 4.3 eV.

4.4. *Experiment.*

4.4.1. *Samples.*

Following the procedures outlined for Au (section 3.4.1.) polycrystalline Ag sample (purity 5N+; average grain diameter 0.5 mm) and an Ag single crystal (purity 3N+; surface polished in (321) direction) were prepared for final polishing by spark erosion and etch-attack mechanical polishing. The polycrystalline sample was subsequently polished by a combined chemical and mechanical method on the rotating wheel machine (section 5.3.1.) using a solution of

100 ml. chromic acid
8 ml. HCl (concentrated)

and adding Al_2O_3 powder (0.05 μm). The same solution was used in the chemical polishing of the single-crystal using a cotton swab (also Levinstein (1962)). The specimens were thoroughly rinsed with deionized water and mounted in the cryostat directly afterwards. Again X-ray tests showed that all traces of mechanical polishing were removed. The surfaces were of a similar quality as described for Au.

The surface problem is more serious in Ag than in Au. Ag adsorbs, oxidizes and sulfidizes very easily. The surfaces of the samples-as--polished therefore can not be characterized as "clean" (e.g. Matsuoka

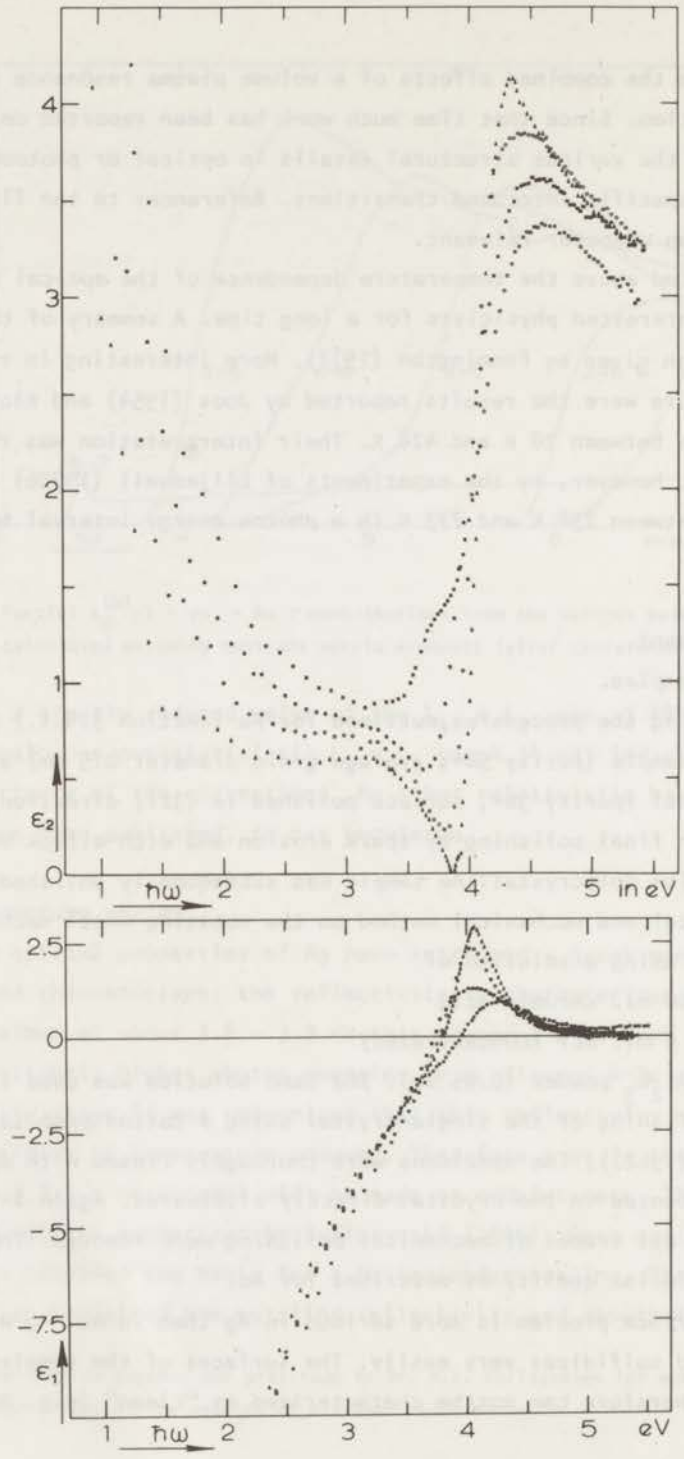
4
3
2
1
0
ε_2
1
$\hbar\omega$
2
3
4
5 in eV
2.5
0
-2.5
-5
-7.5
ε_1
1
$\hbar\omega$
2
3
4
5
eV

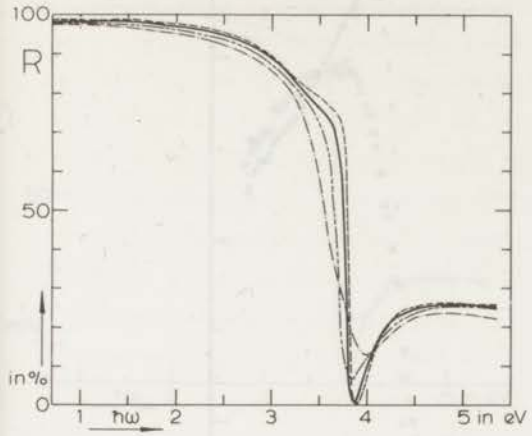

Fig. 4-3: Optical properties for T = 90 K (△), 295 K (○), 515 K (■) and 795 K (□):

a. ε_2/λ - vs. - $\hbar\omega$

b. $-\varepsilon_1$ - vs. - $\hbar\omega$

for T = 90 K (---), 295 K (——), 515 K (— - -) and T = 795 K (– – –):

c. R - vs. - $\hbar\omega$

d. n - vs. - $\hbar\omega$

e. k - vs. - $\hbar\omega$

f. $\mathrm{Im}(1/\tilde{\varepsilon})$ - vs. - $\hbar\omega$

g. $\mathrm{Im}[1/(\tilde{\varepsilon}+1)]$ - vs. - $\hbar\omega$

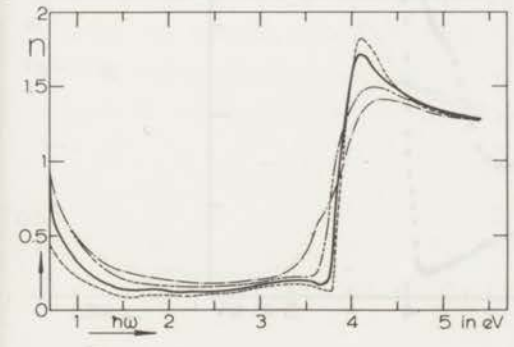

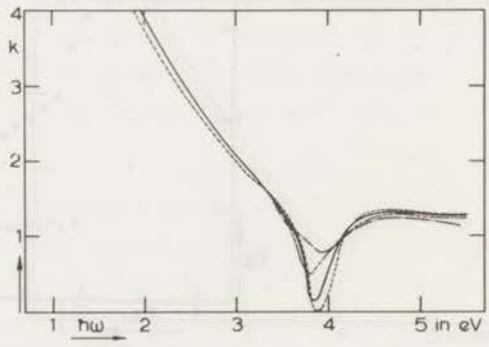

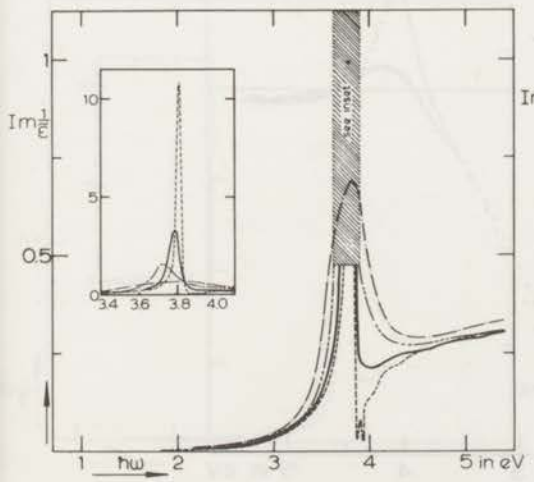

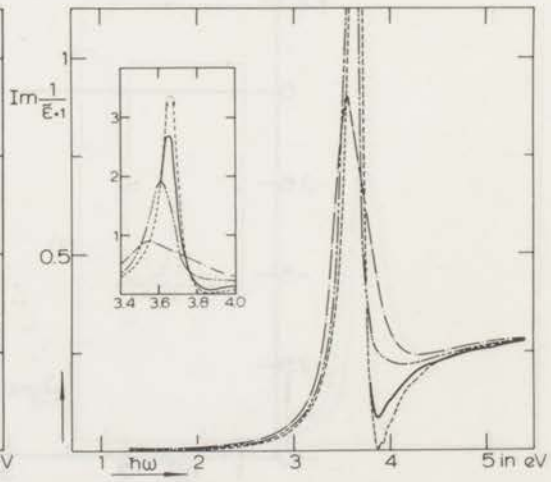

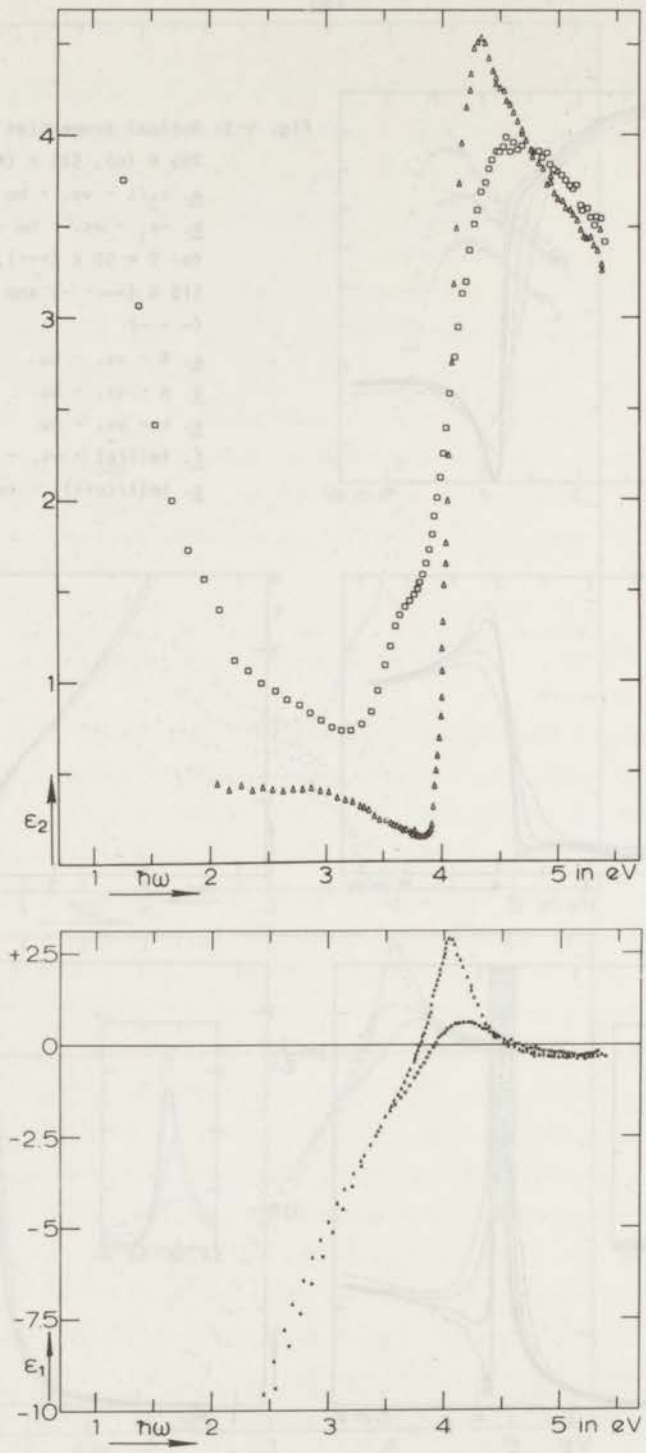
4
3
2
1
ε_2
1
$\hbar\omega$
2
3
4
5 in eV
+2.5
0
-2.5
-5
-7.5
ε_1
-10
1
$\hbar\omega$
2
3
4
5 in eV

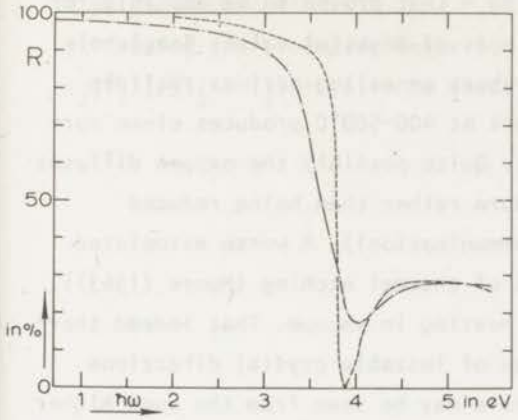

Fig. 4-4: Optical properties of Ag single crystal for T = 90 K (▵) and 840 K (▫):

a. ε_2/λ - vs. - $\hbar\omega$

b. $-\varepsilon_1$ - vs. - $\hbar\omega$

for T = 90 K (---) and 840 K (— - —):

c. R - vs. - $\hbar\omega$

d. n - vs. - $\hbar\omega$

e. k - vs. - $\hbar\omega$

f. $\mathrm{Im}(1/\tilde{\varepsilon})$ - vs. - $\hbar\omega$

g. $\mathrm{Im}[1/(\tilde{\varepsilon}+1)]$ - vs. - $\hbar\omega$

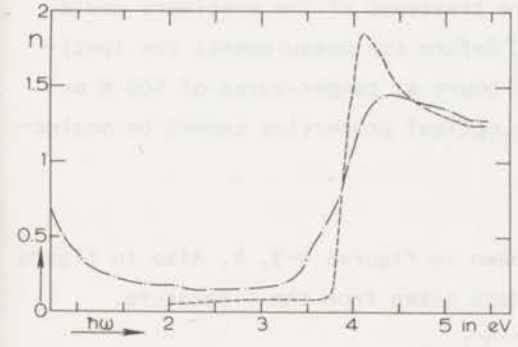

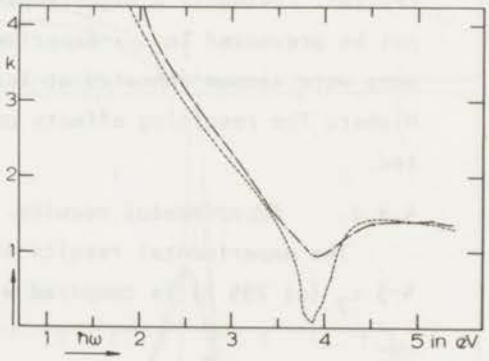

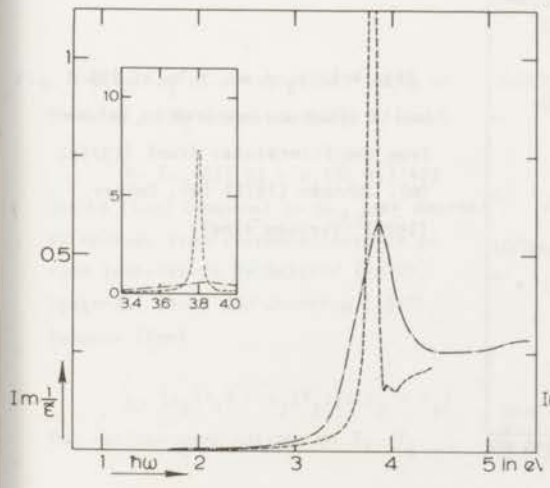

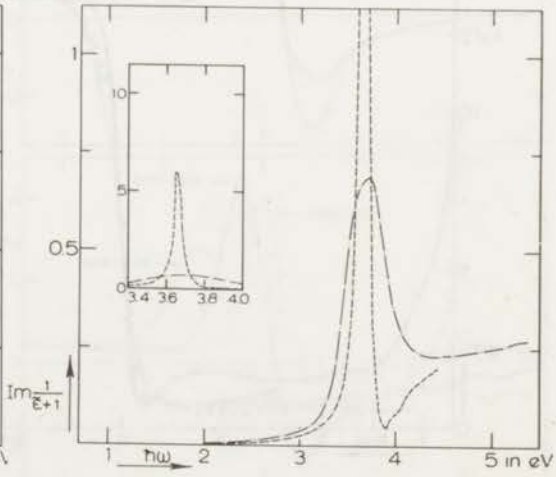

(1969), Muller (1969b)). Heat cleaning - that proved to be possible for Cu (Roberts (1960), Kostyuk (1970)) - is of doubtful value: Beaglehole (1972) reports negative results for short annealing periods; Walldèn (1970), however, states that 4-7 hours at 400-500°C produces clean surfaces as shown in photoemission work. Quite possibly the oxygen diffuses into the material during this procedure rather than being reduced (Haneman (1961); De Geus (private communication)). A worse associated effect of heating is the high degree of thermal etching (Moore (1963)). Surfaces "roughen" immediately upon heating in vacuum. That indeed thermal faceting and possibly transitions of instable crystal directions (Muller (1969b)) play an important role may be seen from the much higher roughness of the polycrystalline sample as compared to that of the single crystal. Obviously a high-temperature treatment of the specimens could not be prevented in our experiments. Before the measurements the specimens were vacuum-annealed at least 4 hours at temperatures of 500 K or higher. The resulting effects on the optical properties cannot be neglected.

4.4.2. *Experimental results.*

The experimental results are shown in figures 4-3, 4. Also in figure 4-5 ε_2 (at 295 K) is compared with data taken from the literature.

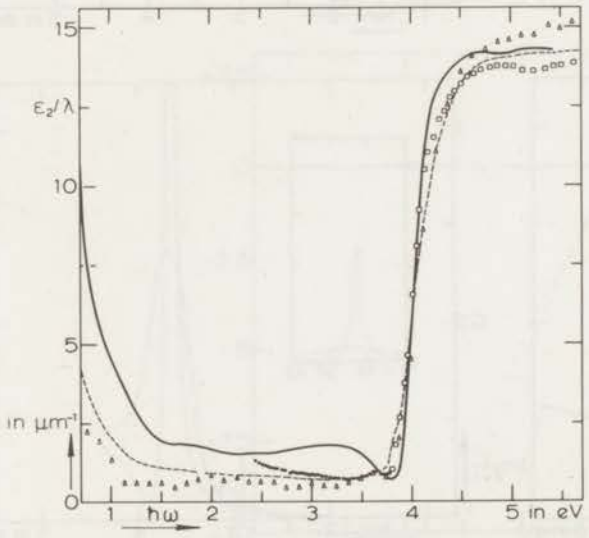

Fig. 4-5: ε_2 - vs. - $\hbar\omega$ at 295 K (solid line) as compared to values from the literature: Irani (1971a) (□), Johnson (1972) (△), Decker (1971)[†] (broken line).

[†] Thanks are due to Dr. D.L. Decker for making available his data.

4.5. *Thermovariation.*

Using the procedure described in section 3.5.1. the $[\varepsilon_2(T_2) - \varepsilon_2(T_1)]/[T_2 - T_1]$ - vs. - $\hbar\omega$ spectra were obtained. The results are

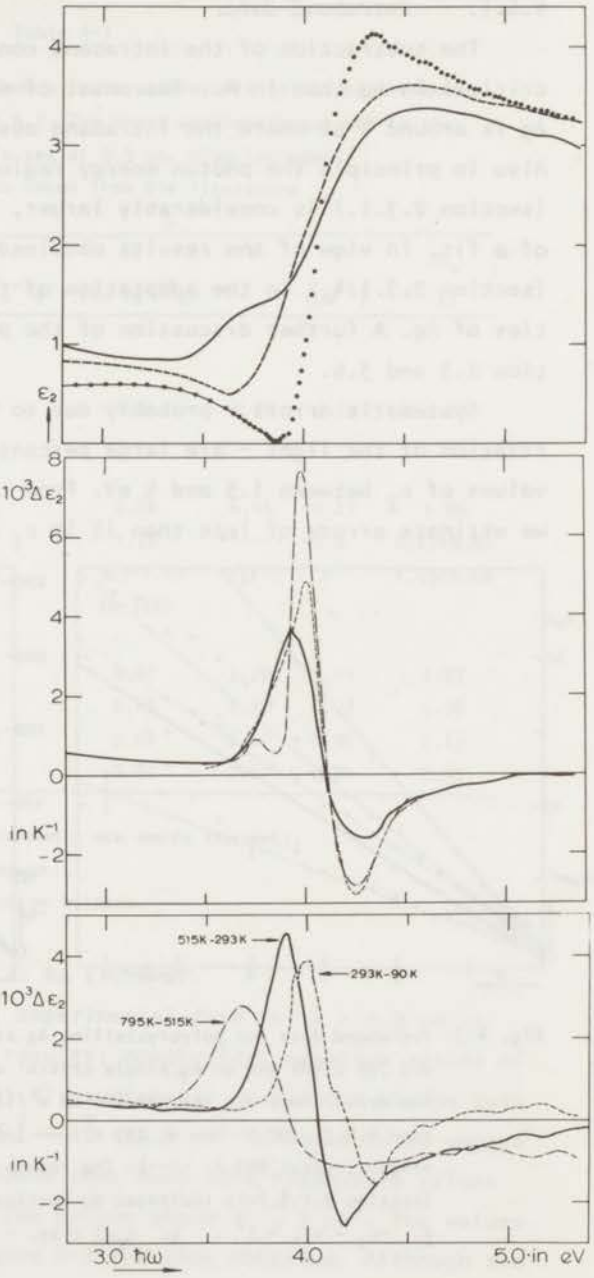

Fig. 4-6: a. ε_2 of polycrystalline Ag at 90 K (●), 515 K (---) and 795 K (——).

b. $[\varepsilon_2(515\ K) - \varepsilon_2(90\ K)]/425$ (solid line) compared to $\Delta\varepsilon_2$ (per degree) as derived from thermoreflectance at room temperature by Baldini (1970) (dash-dot line) and Sherring (1970) (broken line).

c. $[\varepsilon_2(T_1) - \varepsilon_2(T_2)]/[T_1 - T_2]$ for various combinations of T_1, T_2.

compared in figure 4-5 with $[\Delta\varepsilon_2(T_{av})/\Delta T]_{modulation}$ data from thermomodulation experiments by Baldini (1970) and Sherring (1970).

4.6. *Intraband transitions.*

4.6.1. *Intraband data.*

The subtraction of the intraband contribution (eq. 2-15) is less critical in Ag than in Au. The onset of major interband absorption in Ag is around 4 eV where the intraband absorption is very small already. Also in principle the photon energy region for fitting a Drude model (section 2.3.1.) is considerably larger, thus increasing the accuracy of a fit. In view of the results obtained on Au we used method IV (section 2.3.1.4.) in the adaptation of the intraband optical properties of Ag. A further discussion of the pros and cons is given in section 2.3 and 3.6.

Systematic errors - probably due to the non-perfect state of polarization of the light - are large percentage-wise due to the small values of ε_2 between 1.5 and 4 eV. From test points (section 5.1.1.1.) we estimate errors of less than 1% in ε_1 and typically 5 to 10% in ε_2.

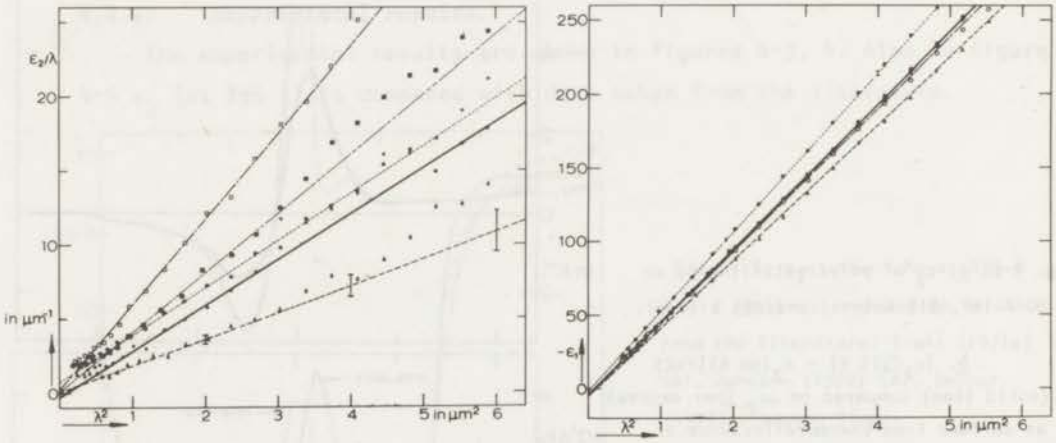

Fig. 4-7: Intraband data for polycrystalline Ag at T = 90 K (Δ), 293 K (o), 515 K (■), and 795 K (□) and an Ag single crystal at 840 K (●).
The drawn lines are the results of a fit to the data as described in section 4.6.2. (90 K: — — —; 293 K: ——— ; 520 K: ——— -- ; 795 K: ——— - ——— ; single crystal 840 K: ----). The random error in the experimental data (section 5.1.5.) is indicated by vertical bars.
a. $-\varepsilon_1$ - vs. - λ^2 ; b. ε_2/λ - vs. - λ^2.

However, in the 90 K series this was considerably higher, about 20%. Still in absolute values around 2.5 eV this is equivalent to a rather small uncertainty of $\Delta\varepsilon_2 \approx 0.2$.

Table 4-1

Intraband parameters obtained from a least-squares fit to the experimental data as described in section 4.6.2. The short wavelength cut-off in the fitting procedure is set at 0.9 μm. Also included are some values taken from the literature

	ω_{pf} (in $10^{16}s^{-1}$)	τ (in $10^{-14}s$)	P	B (μm^{-1})	m_o 1)
Method IV					
low temperature					
90 K	1.27	1.4	3.55	0.14	1.17
room temperature					
293 K	1.33	0.86	4.45	-0.27	1.06
Dujardin (1971)[2]	1.47	1.75	.....	≈0.5	0.87±0.01
Ehrenreich (1962)[2)3]	1.35	3.7-1.6 (0-3eV)	.....	-	1.03±0.06
high temperature					
515 K	1.32	0.65	3.70	0.14	1.07
705 K	1.32	0.45	3.36	0.27	1.08
795 K	1.29	0.68	2.62	0.98	1.13
840 K, single crystal	1.39	0.91	2.21	0.74	0.97

1) In units of electron mass; commonly one omits the unit.

2) Values taken from the literature.

3) Values determined by alternative methods.

4.6.2. *Anomalous absorption I: $\hbar\omega \leq 0.7$ eV.*

Using method IV to fit all experimental data for $\lambda > 0.9$ μm we obtained rather unsatisfactory results: nonphysical negative values of B for all series (except T = 795 K), systematic deviations of the data below the fitted line for 1.8 $\mu m^2 < \lambda^2 < 3.4\ \mu m^2$ followed by an upward deviation at lower λ^2. It was found that much more reasonable values could be obtained by excluding the points above $\lambda^2 \approx 3\ \mu m^2$. The values summarized in table 4-1 and figure 4-7 are thus obtained. Although the

low-wavelength fit now makes much more sense, as a consequence we have to conclude to an anomalous absorption for $\lambda \gtrsim 1.7$ μm ($\hbar\omega \lesssim 0.7$ eV). This absorption is mostly found for samples that were annealed at high temperatures (thermally etched!); very little difference is seen in the single-crystal data. The indications therefore once again suggest surface roughness and/or specimen defects as the probable cause (sections 2.3., 2.4.1.). On the basis of our measurements it is not possible to determine whether the anomalous absorption occurs in the form of a distinct peak or can be explained with a two-or-more relaxation time model (sections 2.3.1.5., 2.4.1.). In view of the roughness and distinct grain boundaries the latter suggestion is rather tempting. For further discussion in this regard one is referred to the sections 3.6.2. and 3.6.4. (2) on Au.

It should be noted that the values of ω_{pf} and m_o are very much the same, independent of the inclusion or exclusion of the data at higher wavelength (see figure 4-7a).

4.6.3. *Anomalous absorption II: 2.0 eV ≤ ħω ≤ 3.8 eV.*

All experimental data in figure 4-8b deviate systematically from the Drude fit for wavelengths smaller than 1 μm. Obviously therefore the argument used in section 4.6.1. and also regularly in the literature (higher accuracy due to larger fitting region) is doubtful. At best one can say that in Ag it is easier to see where the Drude model goes wrong.

Referring to section 2.4.1. and figures 4-3a,b it is highly probable that surface plasmons cause anomalous absorption in the photon energy range between 2.0 and 3.8 eV: $\varepsilon_1 \simeq -1$ and ε_2 is small. Indeed as seen in figure 4-3g $\mathrm{Im}[1/(\tilde{\varepsilon} + 1)]$ peaks sharply in this interval. The circumstances thus are exceptionally favorable for such absorption in Ag, leading to a great number of specialized studies in this field.

As indicated in sections 4.1. and 4.2. absorption in this photon energy range is of considerable interest. In order to reduce the effect of thermal etching we therefore performed series of measurements on a single crystal specimen. The relevant results shown in figure 4-8 indicate a decreased absorption. Visual inspection of the sample together

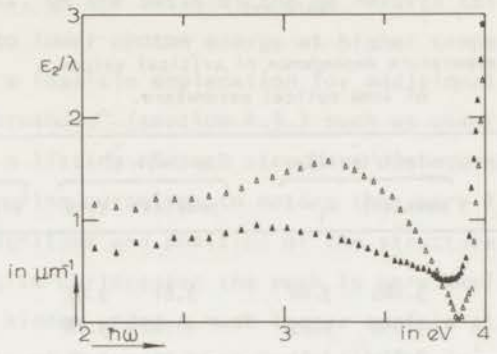

Fig. 4-8: ε_2/λ - vs. - $\hbar\omega$ for polycrystalline (▵) and single crystal (▲) Ag at 90 K between 2 and 4 eV.

with the observation of a much smaller light scattering of the obliquely incident light beam confirm the influence of the sample surface. In this regard it is interesting to note that thermal etching occurs preferentially in different crystal directions, that is for different surface orientations of the crystallites. This leads to a "sawah"- like structure of the surface: some less-evaporated crystallites stick out relative to more-evaporated crystallites such that steps along grain-boundaries become rather pronounced. The much larger light scattering on the polycrystalline sample seems to be due to the influence of grain boundaries. It cannot be excluded that the surface roughness due to the etching is quite different for various crystal orientations too. A more systematical research - making use of X-ray orientation studies and especially an accurate surface roughness meter - is necessary to ascertain the importance of this possibility, and also to determine the optimal crystal direction for single-crystal measurements. Still in view of the very large differences observed in figure 4-8 it is reasonable to assume the major part of the absorption between 2.0 and 3.85 eV to be due to the influence of grain boundaries of defects in the sample (see section 4.9.1.).

As is very obvious from figure 4-3g,4g the shape of the surface plasmon peak is highly temperature dependent. Some care should be taken with the indicated values of the height of the peak in the inset. Even

Table 4-2

Temperature dependence of critical values of some optical parameters.

	$Im[1/(\tilde{\varepsilon}+1)]$		$Im[1/\tilde{\varepsilon}]$		R
	peak(eV)	$\varepsilon_1=-1$	peak(eV)	$\varepsilon_1=0$	minimum(eV)
polycr. sample					
90 K	3.665	3.66	3.81	3.81	3.90
293 K	3.645	3.65	3.785	3.78	3.88
515 K	3.61	3.61	3.73	3.74	3.84
705 K	3.57	3.58	3.70	3.80	3.96
795 K	3.56	3.59	3.82	3.85	3.97
single crystal					
90 K	3.65	3.65	3.80	3.80	3.89
840 K	3.67	3.73	3.85	3.92	3.99

with closely spaced experimental points such as shown in the 90 K data it is not possible to extrapolate accurately for very sharp structure. Still the location of the peak as a function of temperature can be obtained with good accuracy. Results are given in table 4-2. It is beyond the scope of this thesis to go into detail concerning the surface plasma resonances. However, checking table 4-2 - that suggests a temperature dependence proportional to the lattice expansion - it is probable that temperature could be a valuable tool in the investigation of these properties. Whether such temperature dependence is determined by "expansion" of the surface roughness etc. or simply reflects the variation of ε_1 is not clear (see table 4-2; section 4.7.). Very rough tests of the temperature dependence (110 K, 290 K) by Jasperson (1969) and Schnatterley yielded negative results; however, a very definite shift is reported by Welkowsky (1971).

In section 2.4.1. it has been noted that various alternative explanations have been given for absorption in this photon energy region. From our point of view the most interesting is that of a small interband absorption. Christensen (1972b) obtained a minor peak due to critical point transitions from $L_{4^-} \rightarrow L_{4^+}$ (nonrelativistic $L_{2'} \rightarrow L_1$) around 3.49

eV (at T = 0 K). On the basis of the Au results this peak must be expected to shift to lower photon energy at higher temperatures. Therefore it would provide a feasible explanation for additional absorption below the absorption "threshold" (section 4.9.) such as observed in almost all experiments. As a listing of such structure consequently would be very extensive, we confine ourselves to noting that very little uniformity is obtained in magnitude and position of the structure.

According to Christensen the peak is very small and narrow. It thus may easily be hidden under a much larger surface plasmon contribution. Therefore it is of interest that Otter (1961b) in measurements on the temperature dependence of the optical properties of vacuum-grown-and--measured single-crystals observes no additional absorption peak. This was supported by Dujardin (1971) in measurements on very smooth thin films. The evidence for such a peak as possibly could be derived from piezoreflectance (Garfinkel (1966), Nilsson (1970c)) is not sufficiently convincing (e.g. Schmidt (1971), Kofman (1972)). The same is true for thermoreflectance structure in view of the observed temperature dependence of the surface plasma resonance (table 4-2).

Summarizing, although due to the magnitude of the expected structure it is not possible to exclude a below-the-absorption-edge interband absorption peak with certainty, there is little positive evidence for such assumption. On the basis of the negative evidence (Otter, Dujardin, also section 4.10.) and knowing the highly critical dependence of the calculated L-gap on the choice of crystal potential we do not believe in such an interband absorption peak. Also see section 4.9.2..

4.6.4. *Discussion.*

The experimental data for Ag allow even fewer conclusions to be drawn than in the case of Au. It was found that in three initial series measurements (705 K, 515 K, 293 K) ε_1 does not change to a great extent, $\omega_{pf} = 1.32 \pm 0.01$, $m_o = 1.07 \pm 0.01$ and $P = 4 \pm 1$. In later series (90 K, 795 K) the results are out of line. The reason is not clear. Mathewson (1972) et al. found that the optical mass is independent of temperature in the range 145 - 575 K.

As in the case of Au the derived value of the optical mass m_o is much larger than that obtained from measurements on films (Dujardin (1971): 0.87, Mathewson (1972):0.85 ± 0.01). Our 295 K value of m_o = 1.06 compares fairly well with others obtained on bulk specimens (a.o. Ehrenreich (1962): 1.03 ± 0.06; Stokes (1972): 1.09). Our 840 K single crystal value is much lower, m_o = 0.97. Possibly this large difference can be retraced to the influence of grain boundaries and defects in the solid such as suggested by Hunderi (1973c) (see also sections 4.6.3., 4.7.3.) and supported to some extent for the case of Au by Thèye (1970) (section 3.6.4.). On the other hand Dujardin (1971) finds an optical mass of 0.87 regardless of film structure.

In view of the uncertainties involved in the data and in the analysis we abstain from any further discussion of the relaxation time τ and B.

4.7. *Temperature dependence of characteristic structures.*

4.7.1. *Energy loss peak.*

Peaks in $\mathrm{Im}(1/\tilde{\varepsilon}) = \varepsilon_2/(\varepsilon_1^2 + \varepsilon_2^2)$ are usually associated with volume plasma resonances or (to a lesser extent) with interband transitions. The peak energy of $\mathrm{Im}(1/\tilde{\varepsilon})$ such as observed in figures 4-3f,4f is named the plasma energy $\hbar\omega_p$. Although it can directly be measured by electron energy loss experiments $-\mathrm{Im}(1/\tilde{\varepsilon})$ is consequently named the energy loss function - the spectrum can also be calculated from the optical properties.

As this subject has been the goal of much specialized research, little will be said about our findings. From figures 4-3f,4f it is obvious that energy loss peak is highly temperature dependent. As going to high T ε_2 increases, it is damped and broadened, whereas the shift of $\varepsilon_1 = 0$ is reflected in the position of the peak. This is demonstrated in table 4-2. The results are in good agreement with the work on films in a more limited temperature range as performed by Schulz (1968) and Kretschmann (1969a).

The high temperature data clearly exhibit the effect of the splitting of the absorption edge. After an initial decrease of the peak energy roughly proportional to the lattice expansion one observes a subsequent increase at T ≳ 500 K. The relevant energy loss peaks are rather asymmetrical with a shoulder at the low energy side. Thus one may conclude

that part of the $\mathrm{Im}(1/\tilde{\varepsilon})$ spectrum is determined by interband transitions (section 4.10.) and as such is not directly relevant to volume plasma resonances.

In the low temperature $\mathrm{Im}(1/\tilde{\varepsilon})$ spectra (figures 4-3f,4f) a wavy structure is observed at the high energy side of the plasma energy $\hbar\omega_p$. Although a resonance-like structure just above $\hbar\omega_p$ due to optically excited longitudinal volume plasmons has been predicted and recently also observed for very thin films (thickness $\sim$ 100 to 150 Å) (Lindau (1970,1971c) plus references cited there) it can hardly be expected to be observable in data obtained on non-smooth non-parallel thick bulk samples. Probably the "waves" are a direct result of the interband transitions.

4.7.2. *Reflectivity minimum.*

In a century of work on the optical properties one of the most surprising findings has been the high temperature dependence of the reflectivity minimum (transmission maximum, emission maximum) of Ag as compared to that of the other noble metals. A summary of the older work has been given by Pennington (1932) who quotes nearly linear shifts of the transmission maximum ranging from -1.0×10^{-4} to -2.3×10^{-4} eV/degree for temperatures between 4 K and 340 K. Using a quantummechanical model due to Kronig he supposes lattice expansion to be the only cause for this temperature dependence. Mohler (1931) showed the absorption minimum to shift at about -5×10^{-4} eV/degree between 20 K and 490 K. This is in good agreement with later values such as reported by Joos (1954) and Klopfer and Taft (1961) and Philipp. In measurements extending to higher temperatures such as ours and those of Liljenvall the reflectivity minimum is seen to split into a highly temperature sensitive (shifts of typically -8×10^{-4} eV/degree for $T > 300$ K) and a very stable part [†]. Our findings are given in table 4-2. For a further discussion one is referred to section 4.10..

[†] As a consequence of this splitting the X-point as observed in the reflectivity of the noble metals (see section 2.8.) can be understood to be directly associated with transitions originating from initial states in the upper *d* bands (Winsemius (1973b)).

4.8. *Interband transitions.*

The interband contributions to $\varepsilon_1(\omega)$ and $\varepsilon_2(\omega)$ are obtained on subtracting the respective intraband contributions (eq. 2-15). As in the relevant photon energy range the latter contributions are small, the results are not shown graphically.

4.9. *Absorption edge.*

From figures 4-3a,4a it is obvious that at low temperatures the absorption edge in Ag is very well-defined. Results on the location of the edge using various definitions (section 2.5.6.) are summarized in table 4-3. Also included are some values taken from the literature.

Table 4-3

The absorption edge of Ag at different temperatures according to various definitions. Unless stated otherwise the data refer to polycrystalline Ag.

definition of the absorption edge	T= 90K	T=293 K	T=515 K	T=705 K	T=795K
parabolic footpoint of $\varepsilon_2^{(b)}(\omega)$-vs.-$\hbar\omega$	4.02	3.98	3.91	3.94	3.98
single crystal	4.02				3.93(840K)
Christensen (1972b) RAPW calc.	3.98(0 K)				
maximum in $\Delta\varepsilon_2^{(b)}/\Delta(\hbar\omega)$-vs.-$\hbar\omega$	4.06	4.05	4.05	4.06	4.07
single crystal	4.06				4.10(840K)
Welkowsky (1971)	3.93				
secondary maximum in $\Delta\varepsilon_2^{(b)}/\Delta(\hbar\omega)$	....	3.97	3.90	3.70	3.56
single crystal	3.94				3.55(840K)
Welkowsky (1971)	3.77				
maximum in $\varepsilon_1^{(b)}(\omega)$-vs.-$\hbar\omega$	4.06	4.03	3.92	4.06	4.05
single crystal	4.06	4.04			4.04(840K)
Morgan (1968)		4.03			
linear extrapolation of $\varepsilon_2^{(b)}(\omega)$-vs.-$\hbar\omega$	3.96	3.87	3.70	3.62	3.57
single crystal	3.96				3.55(840K)
Dujardin (1971)		3.86±0.01			
Schmidt (1971)		3.87			

4.9.1. *Anomalous absorption III: $\hbar\omega \simeq 3.91$ eV.*

At the very onset of the absorption edge of the 90 K data on the polycrystalline sample a very minor structure may be noticed (figure 4-3a,8). This mini-peak that was found to be reproducible shows up very clearly in the $\mathrm{Im}(1/\tilde{\varepsilon})$ and $\mathrm{Im}[1/(\tilde{\varepsilon}+1)]$ spectra (figures 4-3f,g) at 3.91 eV. Furthermore it was found in a series of (unpublished) AgCu (8 at.%) measurements at 40 K (figure 4-9). Interestingly, however, very little confirmation is obtained from the low temperature measurements on the single-crystal specimen, whereas the effect is considerably reduced in measurements on a second somewhat more homogeneous AgCu (10 at.%) sample. A literature review of anomalous structure in this photon energy range is given in table 4-4.

Discussion of the structure is limited. Although shown very clearly Fukutani (1966) does not discuss the shoulder in ε_2 and $\mathrm{Im}(1/\tilde{\varepsilon})$. It should be noted that his films were nonannealed. Similarly no mention is made of the minor spike obtained by Beaglehole (1972; figure 17) on a 1.75 at.% AgCu sample. The annealed specimen is measured in air. Huebner obtained a jump in the otherwise smooth series of n values for films exposed to air.

From these observations the absorption may be thought to originate from sample conditions again. Summarizing our own results, structure is found for measurements of well-annealed polycrystalline samples, hardly any for single crystals. Also the structure is considerably reduced for improving AgCu samples (nonannealed). By micro-X-ray and microscope analysis the major improvement was found to be in the homogeneity of the

Table 4-4

Literature review of anomalous absorption structure for photon energies above the absorption threshold.

reference	method	photon energy	explanation
Huebner (1965)	opt.prop!s	3.73	films measured in air
Fukutani (1966)	opt.prop!s	3.86	
Welkowsky (1971)	wavelength mod.	3.77	overlapping interband transitions
Dujardin (1971)	opt.prop!s	3.4-3.8	poorly crystallized films
Beaglehole (1972)	alloy modulation	3.91	-

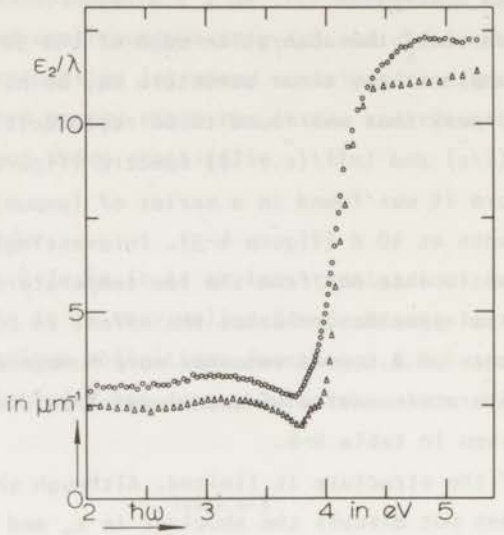

Fig. 4-9: ε_2/λ - vs. - $\hbar\omega$ for AgCu (8 at.%) at 40 K (Δ) and 295 K (o).

sample at the grain boundaries: the first sample contained narrow regions of lower Cu concentration (approx. 6 at.%) and in addition a large number of small holes ("cracks"). As stated before (section 4.6.3.) the steps along the grain boundaries in the polycrystalline Ag sample become very pronounced upon high temperature annealing. There is little reason to expect a very large difference in surface roughness for the polycrystalline and the single-crystal sample. Therefore the indications once again suggest grain boundaries to be the cause for the structure. The importance of grain boundaries and defects inside the grains rather than surface roughness is strongly supported by Dujardin (1971; p. 2039). It should be added that an alternative explanation is possible for the structure observed in AgCu alloys. Nilsson et al. (1973c) suggest the growth of a shoulder at the bottom of the absorption edge on adding Cu, presumably due to interband transitions. This is somewhat conflicting with our interpretation. Also ε_2/λ is rather large in the alloy; a plasma resonance effect is thus expected to be damped to a large extent.

Obviously interesting in this regard is the theoretical model of grain boundary plasma resonance proposed by Hunderi (1973a,b,c). Hunderi

(1973b) used this model amongst other things to explain the structure found by Welkowsky (1971) in wavelength modulation experiments. In our opinion this assignment is doubtful. A distinct change of slope of ε_2 just above the onset of the absorption edge is seen in our single-crystal data and also in Decker's curve (figures 4-4a,5). This structure - that causes a well-defined peak in a derived $\Delta\varepsilon_2/\Delta(\hbar\omega)$ spectrum - we definitely attribute to interband transitions (section 4.10.). It is located at 3.94 eV, however, whereas Welkowsky quotes a value of 3.77 eV. In this regard it can be pointed at a possible spread of structure such as will be discussed in section 4.11.. Interestingly exactly Welkowsky's feature has been reported by Fukutani (1972, figure 5) who points at the fulfilment of the condition for plasma resonance absorption ($\varepsilon_1 = 0$)[†)] at this photon energy and the dependence on the angle of incidence. Therefore we find it difficult to conclude whether the shoulder reported by Welkowsky is associated with grain boundary plasma resonance, volume plasma resonance, or interband absorption.

In our opinion a better illustration of the grain boundary plasma resonance probably is found in the results on poorly crystallized films by Dujardin (1971; figure 6) that show the two types of anomalous absorption (section 4.6.3.; this section) that are predicted by Hunderi (1973b). The model also provides strong support for our conclusion that the anomalous absorption between 2.0 and 3.8 eV is mostly due to the influence of grain boundaries and defects in the sample (section 4.6.3.).

A weak point of the explanation using this model stems from the great variation in shape etc. of the grain boundaries in a bulk specimen. Expectedly this would cause a rather spread-out absorption structure instead of the well-defined shoulder observed. Alternatively therefore it cannot be excluded that the shoulder is due to internal strains at the grain boundaries. Such a possibility has been suggested with regard to Fukutani's somewhat "anomalous" results on Au (section 3.14.). The shoulder then results from the shift of a part of the interband structure, possibly that causing the tailing of the absorption edge as calculated by Christensen (band 5 → band 6 in the vicinity of X) (section 4.9.2.).

[†)] In our experiment at 3.91 eV $\varepsilon_1 \approx 1$.

Although this explanation is tempting, difficulties arise due to the expected influence of such strain on band 6 → band 7 transitions (section 4.11.). We therefore hesitate to draw any conclusions in this sense.

4.9.2. *Tailing of the absorption edge.*

In view of the anomalous absorptions little can be said about the tailing of the absorption edge. Even in the single crystal data some slight structure is seen below the absorption edge. In measurements on very smooth thin films Dujardin (1971) observes an approximately exponential tailing, that has a smaller intensity and extends over a larger energy interval (down to about 2.1 eV) than in the case of Au (section 3.8.3.). Again it is tentatively attributed to an Auger broadening of the absorption edge, due to the finite lifetime of the hole created at the top of the flat narrow $\bar{d}$ band (section 2.4.2.).

In section 3.8.3. it was pointed at the possible satisfactory explanation of the tailing in Au as being due to interband transitions in the vicinity of X. Although the analogous tailing is predicted by Christensen (1972b) it can by no means account for the "length" of the tail obtained by Dujardin.

The tail recently has received considerable attention especially in experiments on alloys (Green (1965,1970), Morgan (1968), Morris (1969), Nilsson (1970a,c), Flaten (1973)). Notably Flaten and Stern suggest that the onset of interconduction-band transitions (section 4.10.2.) in pure Ag occurs at approximately 3.3 eV in good agreement with the relativistic calculation of Christensen (1972b)(3.37 eV). The peak due to the $L_{4-} \rightarrow L_{4+}$ (nonrelativistic: $L_{2'} \rightarrow L_1$) critical point transition - predicted at 3.48 eV - is not found by Flaten. Rather the interconduction-band structure is found to peak at 4.2 eV with a low maximum of about 0.4 in ε_2. Clearly this interband absorption tail is even more difficult to exclude than the theoretically predicted below-the-absorption-edge absorption peak (section 4.6.3.). Alternative explanations have been proposed though, for instance it has been been pointed at indirect transitions in alloys (e.g. Morris) and at tailing due to crystallographic clustering and broadening due to resonance scattering of the conduction electrons (Nilsson (1970a)).

Further discussion of the tailing is put off to section 4.11..

4.10. *Absorption maxima.*

It is generally recognized that (at room temperature) the strong maximum in $\varepsilon_2^{(b)}/\lambda$ is due to overlapping contributions from band 5 → band 6 (upper d band to conduction band) and band 6 → band 7 (interconduction-band) transitions. Experimental evidence in this respect is given in a number of articles quoted in table 4-5 together with relevant photoemission work. As in the case of Au attention has often been concentrated on transitions in the vicinity of L; the absorption spectrum

Table 4-5

Literature review of the assignment of optical structure to transitions in the vicinity of L.

reference	experiment	$L_{5^+6^+}\rightarrow E_F$ ($L_3\rightarrow E_F$)	$L_4\rightarrow E_F$ ($L_2\rightarrow E_F$)	$E_F\rightarrow L_{4^+}$ ($E_F\rightarrow L_1$)	$L_{4^+}\rightarrow L_{4^-}$ ($L_2\rightarrow L_1$)
Berglund (1964)	photoemission	4.3	0.3		4.2
Cooper (1965)	opt.prop!s	3.97	0.3		
Morgan (1968)	alloys	3.97	0.30	4.09	4.24
Morris (1969)	piezorefl.alloys		∿0.1	4.07	4.15
Green (1970)	alloys	4.4	0.2	3.88	4.1
Nilsson (1970c)	piezorefl.			3.8	4.1
De Chatel (1970)	piezorefl.			3.9	4.1
Liljenvall (1970b)	T-dependence				4.14
Schmidt (1971)	piezomod.	3.92		3.98	4.25
Welkowsky (1971)	wavelength mod.	(3.77)			4.42
Smith (1971)	photoemission		0.3		4.2
Fukutani (1971)	alloys	∿4.			6.2
Christensen (1972b)	RAPW calc.	3.98	0.16	∿3.3	3.48
Stokes (1972)	calc.				4.27
Beaglehole (1972)	alloy mod.	3.9			4.15
Walldèn (1972)	photoemission		0.31		4.17
Flaten (1973)	alloys			onset:	3.3
				peak :	4.2

around 4 eV is tentatively described by combining the models introduced in section 2.7.2.. However, again the band calculation by Christensen (1972b) indicates that transitions in extended rather than localized regions of $\underline{k}$-space contribute to the absorption spectrum. The relevant partial ε_2/λ 's are shown in figure 4-2. A comparison of the theoretical-

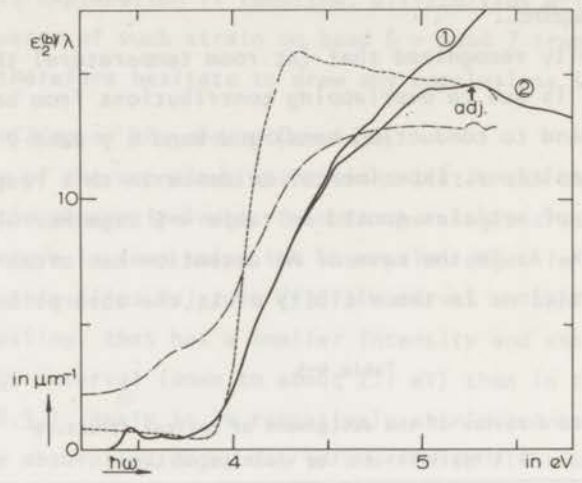

Fig. 4-10: Experimental $\varepsilon_2^{(b)}/\lambda$ - vs. - $\hbar\omega$ for Ag single crystal at 90 K (---) and 840 K (— - —) together with calculated spectra of $\varepsilon_2^{(b)}/\lambda$ with (1) and without (2) contributions from band 3 → band 6 and band 2 → band 6 transitions. The theoretical spectra are derived from Christensen's band calculation (T = 0 K) assuming constant matrix elements. The vertical scale of these curves is adjusted to the 90 K spectrum at $\hbar\omega$ = 5.25 eV.

ly calculated $\varepsilon_2^{(b)}/\lambda$ spectrum with the experimental results is given in figure 4-10. Clearly the agreement is poor. A further discussion is given in section 4.10.4.

In view of the results obtained in the preceding chapter in separating the expectedly more temperature dependent interconduction-band structure from the band 5 → band 6 structure, the analysis will follow the same lines.

4.10.1. *Thermovariation.*

As shown in figure 4-6 the thermovariation (thermomodulation) pattern is rather simple: a well-defined positive structure is immediately followed by a smaller negative structure. Thermovariation spectra derived from values of ε_2 obtained by Liljenvall (1970b) and Mathewson[†)] confirm our findings. The temperature dependence of $\Delta\varepsilon_2(\Delta T)$ structure is shown in figure 4-11 that also includes values derived from Liljenvall's

[†)] We thank Prof. H.P. Myers for making available tabulated values of these data.

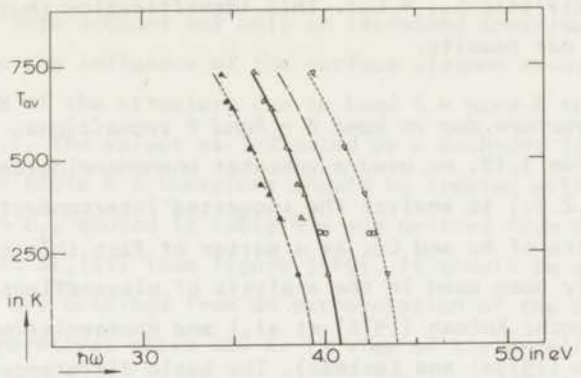

Fig. 4-11: Temperature induced shift of structure observed in the thermovariation of Ag. The positions of the onset of $\Delta\varepsilon_2(\Delta T)$ structure, the maximum and the minimum are shown as derived from our data (respectively ▲, △, ▽) and from those of Liljenvall (1970) (▲, △, ▽). Also included are some results derived from thermomodulation data by Baldini (1970) (o) and Sherring (1970) (□). The meaning of the lines is given in the text.

data and some thermomodulation results. Not included are values derived from $\Delta\varepsilon_2(\Delta T)$ modulation spectra by Cheyssac (1972) et al. Although the spectrum obtained at room temperature is somewhat analogous to that of Baldini, their $\Delta\varepsilon_2(\Delta T)$ at 77 K is completely different from thermovariation spectra at these temperatures. As these low-temperature results are not substantiated by recent measurements of Rosei (private communication) they were not included in figure 4-11.

When comparing with the results obtained on Au and Cu (figures 3-5, 15,16,18) it is noted that the temperature dependence of the Ag structure is very much the same as that of the structures associated with the $L_4^- \rightarrow L_4^+$ gap in Au and Cu. The shift of the positive structure in $\Delta\varepsilon_2(\Delta T)$ of Ag is characterized by a value of -8.5×10^{-4} eV/K for T > 300 K. For the suggested interconduction-band transitions in Au and Cu the analogous values typically are about $-8. \times 10^{-4}$ eV/K (section 3.12.). The shift of structure that originates from initial states in the *d* bands is considerably smaller in both Au and Cu. Liljenvall attributes the new structure in ε_2/λ - vs. - $\hbar\omega$ (figure 4-6a) that at high temperatures "grows" at the bottom of the absorption edge to transitions near $L_4^- \rightarrow$

L_{4+} (nonrelativistic:$L_{2'} \rightarrow L_1$). This identification thus is strongly supported by our results.

4.10.2. *Structure due to band 6 → band 7 transitions.*

In section 3.12. we used a somewhat phenomenological box model (section 2.7.2.2.) to analyze the suggested interconduction-band structure in spectra of Au and Cu. As a matter of fact this type of model has frequently been used in the analysis of piezoreflectance (e.g. Morris (1969) and Lynch; Kofman (1972) et al.) and photoemission experiments. (e.g. Nilsson (1973a) and Eastman). The basic difference with the corresponding situation in Au and Cu is in the energy gap between L_{4-} ($L_{2'}$) and E_F which in Ag is calculated to be 0.16 eV (Christensen (1972b)), much smaller than in Au ($\sim$ 0.7 eV) and Cu ($\sim$ 0.5 eV). Therefore the ensuing ε_2 and $\Delta\varepsilon_2$ structures are expected to be confined to smaller photon energy intervals such as for instance indicated in figures 3-19d, e,f (section 3.12.1.1.).

Comparing the temperature dependence of the thermovariation structure an important difference is observed between Ag on the one side and Au and Cu on the other (section 3.12.1.2., figure 3-20). On increasing the temperature the maximum and minimum in $\Delta\varepsilon_2(\Delta T)$ of Ag are found to shift approximately at the same rate whereas in Au and Cu the peak is considerably less temperature dependent than the negative structure. Two alternative explanations are possible.

4.10.2.1. *$L_{4-} \rightarrow L_{4+}$ at $\sim$ 4.25 eV?*

In section 3.12.1.2. it was suggested that the smaller shift of the peaks [2] and [2a] in $\Delta\varepsilon_2(\Delta T)$ of Au and Cu is due to the relative lowering of the Fermi energy with respect to L_{4-}. Quite possibly the corresponding effect is smaller in the case of Ag where L_{4-} is much closer to E_F. This assumption seems reasonable in view of the still larger lowering of upper conduction bands at L at high temperatures.

As in section 3.12.1. one can extract a value of the $L_{4-} \rightarrow L_{4+}$ energy gap at an average temperature $T_{av} = \frac{1}{2}(T_1 + T_2)$ from the photon energy at which $\Delta\varepsilon_2(T_2 - T_1) = 0$. The choice is somewhat arbitrary as

one has to take into account not only an intraband contribution to $\Delta\varepsilon_2(\Delta T)$ but also the influence of the surface plasmon absorption (section 4.6.3.) and of the structure due to band 5 → band 6 transitions (section 4.10.3.). The values as indicated by a dash-dot line in figure 4-11 and also in table 4-6 therefore should be treated with care. The values of $E_F \rightarrow \sim L_{4+}$ quoted in table 4-6 are derived from the position of the maximum in $\Delta\varepsilon_2(\Delta T)$ (see figure 3-19). It should be added that the T = 90 K values are obtained from an extrapolation of the curves as determined at temperatures above 200 K. In view of the excellent agreement with the shift of thermovariation structure of Au and Cu in this high-temperature range (figure 3-20) we used these curves in the extrapolation. The accuracy of the suggested values of the energy gaps is estimated to be ±0.06 eV; due to the extrapolation procedure at low temperatures this should be ±0.10 eV.

Table 4-6

Energy gaps (in eV) at L for conduction bands near E_F.

model	box (section 4.10.2.1.)		inverted box (section 4.10.2.2.)	
temperature	0 K	295 K	0 K	295 K
$L_{4-} \rightarrow L_{4+}$	4.25	4.11	3.92	3.79
$E_F \rightarrow \sim L_{4+}$	4.01	3.86	4.25	4.11
$L_{4-} \rightarrow E_F$	0.24	0.25	0.33	0.32

4.10.2.2. *$L_{4-} \rightarrow L_{4+}$ at 3.92 eV?*

Alternatively one may assume that the interband effective mass of bands 6 and 7 in the direction normal to the ΓL symmetry axis is positive. In other words, moving away from L(Q) the gap between bands 6 and 7 increases. One thus obtains an "inverted box" model: the onset of interconduction-band absorption now is due to transition $L_{4-} \rightarrow L_{4+}$ whereas the cut-off of the structure is caused by $E_F \rightarrow \sim L_{4+}$. It should be noted that actually the cut-off will not be sharp as band 6 → band 7 transitions also occur along the ΓL(Λ) symmetry axis, thus causing a

"tail" at the high energy side of the box (see e.g. figure 4-2). Therefore it will be very difficult to distinguish this box from the one in section 3.10.2.1.

In the proposed alternative the $L_{4-} \rightarrow L_{4+}$ critical interband point is of the type M_o. The value of the energy gap $L_{4-} \rightarrow L_{4+}$ now is determined from the position of the onset of highly temperature-sensitive absorption structure. Again allowing for a certain amount of arbitrariness we determined the values as indicated by a dash-dot line in figure 4-11. The temperature dependence of the assumed gap is approximately equal to that of the maximum in $\Delta\varepsilon_2(\Delta T)$. As shown in figure 4-11 again the agreement with the values obtained by Liljenvall and Mathewson is very good. Typical results are given in table 4-6.

As can be seen in table 4-5 this interpretation is in complete contradiction to almost all analyses found in the literature. To our knowledge only Kofman (1972), Richard and Saïssy have suggested an "inverted box", i.e. $(L_{4+} - L_{4-}) < (\sim L_{4+} - E_F)$, in the explanation of piezoreflectance measurements. However, it should be stated that most experiments will not be able to differentiate between the models presented in this section and in section 4.10.2.1. The PJDOS is very much the same for both models and little conclusive evidence must be expected to come from photoemission (e.g. Walldèn (1972)) or modulation spectroscopy. An exception possibly must be made for low-temperature thermomodulation: Fermi distribution effects become more pronounced than those due to lattice expansion.

From our point of view the most positive feature of this inverted box model is that it provides a feasible explanation for the observed temperature dependence of the peak in $\Delta\varepsilon_2(\Delta T)$ in very good agreement with the results obtained on Au and Cu for the $L_{4-} \rightarrow L_{4+}$ gap. The position of the broad minimum in figure 4-6b,c is much more difficult to determine, especially at high temperatures. Evidence against this model stems from band calculations (e.g. Christensen (1972b)) that indicate $(L_{4-} \rightarrow L_{4+} > E_F \rightarrow \sim L_{4+})$ However, again the differences are small and the uncertainty especially with regard to band 7 is relatively large. Still, although the inverted box cannot be excluded on the basis of our measure-

ments, the theoretical evidence in our opinion turns the scale in favor of the "normal" box model explanation given in section 4.10.2.1.

4.10.3. *Absence of Fermi distribution broadening effects?*

A highly remarkable feature in the thermovariation spectra is the virtual absence of the highly peaked structure due to Fermi distribution broadening. In Cu and Au this broadening is thought to give rise to the large positive peak in $\Delta\varepsilon_2(\Delta T)$ at the absorption edge (e.g. section 3.9.2.). No such effect is observed in Ag (figure 4-6); only minor shoulders are observable for instance in the $[\varepsilon_2(293\ K) - \varepsilon_2(90\ K)]/203$ spectrum. Especially at high temperatures, where the interconduction-band structure has shifted sufficiently far to low photon energies, one would expect to see more than these very weak structures. Our findings were corroborated by results derived from Liljenvall's data.

The experimental evidence is too weak to determine any temperature induced shift of $\Delta\varepsilon_2(\Delta T)$ structure. However, from the static spectra it is probable that the structure attributed to transitions from the upper d band to E_F (band 5 → band 6) is very little affected by the temperature changes (figures 4-3,4,10).

As the information from experimental data is limited, an explanation of this effect - or rather the absence of an effect - is most difficult. From a model calculation (section 2.7.2.1. (2); also Rosei (1973), Antonangeli (1973)) Rosei (private communication)[†] shows that $\Delta\varepsilon_2(\Delta T)$ structure due to Fermi distribution broadening is confined to a rather limited photon energy interval and that it is not a very dramatic effect. Also Christensen (private communication) points out that possibly the $\Delta\varepsilon_2(\Delta T)$ peaks reported for Au and Cu are not *entirely* due to a Fermi broadening of the final states. Also temperature effects on the initial states must be considered, and the "feed-back" to the final s-p-like states via the (sp)-d hybridization. This hybridization probably is stronger in Cu and Au than in Ag because the d bands in Ag lie twice as far from the Fermi level as the d bands in Au and Cu. Also the

[†] We thank Dr. R. Rosei for making available some of his results prior to publication and for valuable comments regarding our work.

Ag *d* states are more localized; any temperature effect therefore possibly is smaller than for Au and Cu. Thus *d* states may play an important role in the broadening of the absorption edge of Au and Cu, more so than in Ag.[††)]

One is tempted to think of partially compensating effects such as for instance a broadening of the edge (resulting in an up-and-down pattern in $\Delta\varepsilon_2(\Delta T)$) coupled to a shift of the edge to higher or lower photon energy (causing a minimum respectively a maximum in $\Delta\varepsilon_2(\Delta T)$). Adding the contributions a negative (respectively positive) $\Delta\varepsilon_2(\Delta T)$ structure would result. A perfect balancing would be very coincidental, however.

Again it can be referred to the results obtained on Au. The strong peak [1] in $\Delta\varepsilon_2(\Delta T)$ at the absorption edge was suggested to arise from transitions in a localized region of the Brillouin zone near L (section 3.8.3.3.). It generally is assumed that the very steep absorption edge in Ag is mostly due to band 5 → band 6 (E_F) transitions near L, or, in other words transitions of the type $L_{5^+ \to 6^-} \to E_F(\sim L_{4^-})$ (figure 4-1). From the band calculations of Jacobs (1968) for a normal and an expanded lattice one expects a large downward shift of $L_{5^+ \to 6^+}$ (nonrelativistic L_{32}) on increasing the temperature. Even a minor shift of the more or less parabolic $\varepsilon_2^{(b)}/\lambda$ structure due to these transitions (section 2.7.2.1. (2)) results in a pronounded $\Delta\varepsilon_2(\Delta T)$ feature. Therefore the downward shift of the upper *d* band near L must be compensated by an equally large shift of E_F, a supposition that we find somewhat too speculative.

Rather we think that the absorption edge arises mostly from transitions in extended regions of k-space. In sections 3.8.3.4., 3.8.11. and 3.8.12. it was suggested that transitions of this type give rise to a much smaller structure in the $\Delta\varepsilon_2(\Delta T)$ spectra of Au. Contributions to $\varepsilon_2^{(b)}/\lambda$ from extended regions possibly are less sensitive to temperature changes than those originating from localized regions. Firstly, the influence of Fermi distribution broadening may be spread out over a larger photon energy interval and secondly, on summing all contributions to

[††)] We are grateful to Dr. N.E. Christensen for pointing out this possible difference between Ag and the other noble metals.

$\Delta\varepsilon_2(\Delta T)$ caused by shifts of initial or final states the effect of large changes in localized regions may be smoothed out. A shift of a smooth, not very steeply sloping $\varepsilon_2^{(b)}/\lambda$ structure will yield a smooth, broad positive or negative contribution to $\Delta\varepsilon_2(\Delta T)$. This type of structure obviously cannot be discerned in the thermovariation spectra. The proposed explanation is supported to some extent by the observation in section 4.10.4. that the steepness of the absorption edge is largely due to interconduction-band structure; the remaining structure increases much more gradually. An analogous assumption is made by Nilsson (1970c) in the interpretation of piezoreflectance spectra. It was also used in the analysis of $\Delta\varepsilon_2(\Delta T)$ structure due to band 4 → band 6 transitions in Au (sections 3.8.11., 3.8.12.).

It can be noted that the demonstrated absence of band 5 → band 6 structure negates some interpretations of spectra found in the literature. As a matter of fact the shoulder at the high energy side of the peak in $\Delta\varepsilon_2$, that led De Chatel (1970) and Schmidt (1971) to propose overlapping contributions from band 5 → band 6 and band 6 → band 7 transitions, is very adequately explained in our box model (figure 3-19f).

Summarizing, the absence of any significant structure in the thermovariation spectra originating from band 5 → band 6 transitions is most unexpected. One is led to think in terms of contributions from transitions in extended regions of $\underline{k}$-space. In addition the broadening of initial and final states may be smaller in Ag than in Au and Cu.

4.10.4. *Magnitude of interconduction-band structure.*

In figure 4-10 it was demonstrated that the calculated and the experimental $\varepsilon_2^{(b)}/\lambda$ spectra do not agree very well. It goes without saying that in order to have any alikeness the contributions of transitions from the three lowest *d* bands to the theoretical spectra have to be neglected (also Christensen (1972b), figure 5). As in the case of Au (section 3.1, 3.12.2.) we attribute the remaining discrepancy to the underestimation of interconduction-band structure. Some indication in this sense may be obtained from the 840 K data that are also included in figure 4-10 where the band 6 → band 7 structure has shifted to lower photon energies. The experimental and theoretical absorption edges now are much more similar.

A rough estimate indicates that about 25% of the 90 K $\varepsilon_2^{(b)}/\lambda$ peak is contributed by the interconduction-band transitions. From figure 4-2 it is obvious that the assumption of constant matrix elements is incorrect (see also Nilsson (1973a) and Eastman). As a consequence the close agreement of theory and experiment such as suggested by Christensen is fortuitous; most probably it results from a considerable broadening of the interconduction-band structure in measurements on poor specimens (section 4.11.).

4.11. *Dependence of ε_2/λ on specimen structure.*

A pronounced dependence of $\varepsilon_2^{(b)}/\lambda$ on structural defects is noticeable in Ag. As a rule the better the specimen, the higher and narrower the room temperature peak in the $\varepsilon_2^{(b)}/\lambda$ spectrum. Evidence for this "rule" may be derived from a comparison of the polycrystalline and single-crystal data (figures 4-3a,4a): the single-crystal is expected to be less strained. This is supported by Otter (1961a). Dujardin (1971) notes a minor decrease of the peak for films with very small grains (i.e. more strained). As in the case of Au the influence of annealing of mechanically polished samples is a sharpening and raising of the peak in $\varepsilon_2^{(b)}/\lambda$ (e.g. Köster (1967)). Differences can also be observed in figure 4-5: the absorption edge in our very highly annealed samples is very steep.

In Ag it is more obvious than in Au (section 3.14.) to suspect the interconduction-band absorption to be the cause of this structure dependence. This absorption is known to contribute about 25% of the maximum value of $\varepsilon_2^{(b)}/\lambda$ and it also is known to be highly sensitive to strain. If it is assumed that the temperature variation is entirely due to lattice expansion, the shift of structure with dilation can be obtained by dividing the temperature coefficient (in this case -8×10^{-4} eV/K) by the coefficient of lattice expansion. Using literature values of the latter (Pandey (1964)) one thus derives a shift of roughly -0.4 eV for a 1% change in the lattice spacing. Interestingly already in 1929 Margenau (1929) noted that a cold-deformation of an Ag sample such as caused by mechanical polishing has the same effect on the reflectivity as an increase of temperature.

Again one can use the model that was introduced in section 3.14. to account for the structure dependence of the absorption maximum of Au. Actually this model is rather analogous to the local dilatation model described in detail by Bardeen (1950) and Shockley. A deformed specimen is thought to consist of regions with different lattice spacings. The optical spectra then are representative of such a mixture. More specifically the $\varepsilon_2^{(b)}/\lambda$ structure due to band 6 → band 7 transitions will be smeared out, the compressed parts causing a shift to higher photon energies and the expanded parts leading to a shift to lower energies. Thus the footpoint of the absorption edge will be masked whereas the top of the ε_2/λ peak is lowered. On annealing the specimen becomes more homogeneous and the band 6 → band 7 absorption structure is expected to narrow and to peak. This is indeed observed experimentally.

On the basis of these results one can attempt to explain some of the discrepancies between various spectra reported in the literature (e.g. figure 4-5). For instance thin films are known to have a lower density than bulk specimens. The band 6 → band 7 absorption therefore is shifted to lower photon energies, causing a more gradual onset of the absorption edge or - as often quoted - a lower absorption threshold. Non-annealed films are known to contain internal strains. However, this is also expected to be the case for well-annealed films (Morgan (1968)), especially so at low temperatures. In our opion this accounts for the observed differences between data obtained on films and bulk samples. In films the absorption edge generally is broadened and the peak value is decreased. This effect has been noted by Johnson (1972) and Christy when comparing their ε_2 spectrum which obtained on bulk Ag by Taft (1961) and Philipp. See also figure 4-5. It also could explain the agreement of the theoretical and experimental spectra (see section 4.10.4.) that Christensen (1972b) quotes. If the interconduction-band structure is sufficiently broadened that it adds an almost structureless contribution to $\varepsilon_2^{(b)}/\lambda$, then one expects to get a good agreement of the positions of the theoretical and the experimental maxima in $\varepsilon_2^{(b)}/\lambda$ - vs. - $\hbar\omega$ (figure 4-10). Essentially they both reflect structure originating from the *d* bands (figure 4-2). The proposed effect also casts doubts on low-temper-

ature measurements on films. In this regard it can be pointed for instance at the very low values of the absorption edge as reported by Welkowsky from wavelength-modulation experiments at 80 K (table 4-3).

The unexpectedly large strain dependence raises the question whether this effect could possibly explain the tailing of the absorption edge. As stated in section 4.9.2. this tailing is observed over a wide photon energy interval, too wide for any of the "normal" explanations (with the possible exception of an Auger-type broadening of the edge; see section 2.4.2.). The tail has received particular attention in the analysis of Ag alloy data. On adding an impurity the lattice can reasonably be expected to become strained which would give a qualitative explanation for the rapid growth of the tail. As a matter of fact the explanation agrees very well with the suggested onset of interconduction-band structure at 3.3 eV by Flaten (1973) and Stern. However, difficulties arise in the case of AgAu alloys (e.g. Nilsson (1970c)) where the lattice spacings of the two components are almost equal and the changes therefore are expected to be small. The experimental evidence is against this expectation.

An interesting consequence of the above model is the possible disagreement in the position of the band 6 → band 7 structure as determined from different experiments. For instance photoemission is known to be more a surface effect than optical properties (the escape depth of the emitted electrons generally is smaller than the penetration depth of the light). The density of the lattice is expected to be smaller near the surface, for instance Paasch (1972) et al. calculate an increase of the lattice constant at the surface of about 1% (in the case of simple metals). Such a change will influence the experimentally observed structure. This effect must be of special importance in for instance electroreflectance experiments that sample only a few atomic layers at the very surface.

It should be added that the sensitivity of the interconduction-band structure in Ag and Au to strain etc. could very well be related to the structure-dependence of the interband peak at 1.5 eV in Al (O'Shea (1972)).

4.12. *Summary*.

The results obtained on Ag can be summarized as follows:

4.12.1. *Anomalous absorption.*

Anomalous absorption is found in three photon energy regions: $\hbar\omega \lesssim 0.7$ eV, $2.0 \lesssim \hbar\omega \lesssim 3.8$ eV and $\hbar\omega \simeq 3.91$ eV. In the latter two cases measurements on a Ag single-crystal sample suggest a major influence of structural disorder (grain boundaries) (sections 4.6.3., 4.9.1.).

4.12.2. *Interband absorption.*

(1) At low temperatures the absorption edge is composed of contributions from band 5 → band 6 and band 6 → band 7 transitions.

(2) Structure observed in piezo- and thermomodulation spectra is due to interconduction-band transitions (band 6 → band 7) in the vicinity of L. On the basis of experimental evidence it is not possible to distinguish between a "normal" box model (section 4.10.2.1.) and an "inverted box" model (section 4.10.2.2.). Band calculations suggest a preference for the normal box ($E_F \rightarrow \sim L_{4+} < L_{4-} \rightarrow L_{4+}$) which would locate the critical interband point energy gap $L_{4-} \rightarrow L_{4+}$ at 4.25 ± 0.10 eV fot $T = 0$ K and 4.11 ± 0.06 eV for $T = 295$ K. These values are considerably larger than those obtained by Christensen (1972b) in a RAPW band calculation (3.48 eV). No positive evidence for interband structure is found near the latter photon energy (section 4.6.3.).

(3) The temperature dependence of the $L_{4-} \rightarrow L_{4+}$ energy gap in Ag is about the same as that of the corresponding gap in Au and Cu.

(4) The $\underline{k}$-dependence of transition matrix elements - especially those for interconduction-band transitions - cannot be disregarded (section 4.10.4.). As in the case of Au the agreement of the calculated $\varepsilon_2^{(b)}/\lambda$ spectrum (Christensen (1972b)) with the experimental spectrum is to a major extent coincidental.

(5) Shifts and broadening of absorption structure due to band 5 → band 6 transitions cause no significant structure in thermovariation spectra. Tentatively this is explained by assuming that the relevant absorption originates from transitions in extended regions of $\underline{k}$-space. In addition the broadening of initial and final states may be small in Ag (section 4.10.3.). The absorption edge due to this type of transitions is hardly sensitive to temperature (section 4.9.).

(6) The steepness and height of the absorption edge together with the location and the width of the absorption peak provide a good criterion for judging the quality of the sample (section 4.11.).

CHAPTER 5: EXPERIMENT

"The student who uses home-made apparatus, which is always going wrong, often learns more than one who has the use of carefully adjusted instruments which he is apt to trust, and which he dares not take to pieces".

This quote from Maxwell, that was used by P.A. Zeeman (Ph.D. thesis, University of Leiden, 1893) as his 12th proposition, heads the chapter on experimental techniques. Carefully adjusted instruments - the so--called black boxes -, that we bought because of the known quality of their known services and that we did not dare to take to pieces, will be mentioned, not treated. Those parts or techniques, that we forced to study, will be treated extensively. The result of such an approach may seem unbalanced to some people. However, it is our hope that others may profit from our experiences in these selected fields.

It is of importance to note that from an experimental point of view our principal aim has been precision. This choice is mainly determined by the decision to use bulk specimens rather than evaporated films. In

the latter case it is possible to perform measurements on a large number of samples as the preparation is a matter of "minutes". The metallurgy and polishing of bulk samples, however, is most demanding. Rather than "number" we therefore chose "perfection". As a consequence the random error in our data is small thus allowing reliable use of analytic methods such as thermovariation.

5.1. *Method of Beattie.*

In Appendix A measurable parameters (intensity, angle of incidence) are related via "ellipticity" parameters (reflection amplitude coefficients, phase shifts) to the optical properties (complex dielectric constant). In a great many ways the optical properties can be extracted from experiment. It is beyond the scope of this thesis to go into greater detail in the description and comparison of the various methods. An excellent guide to the literature is provided by Bennett (1967, chapter 6-9) and Bennett. Further reviews are given by Noskov (in Sokolov (1967, section 9 f.f.)), Lavin (1971), Hummel (1971, chapter 7), Bell (1967) and Fan (1959).

Originally designed for direct measurement of the optical properties in the near infrared (Beattie (1955a,b)) the adopted method has been used with good results also in the visible and near ultraviolet regions of the spectrum (e.g. Roberts (1959,1960), Lenham (1967a), Myers (1968), Pells (1969), Liljenvall (1970), Steel (1972a,b), Mayer (1972)). Alterations and other work of interest have been reported by Hodgson (1955), Prishivalko (1961), Roberts (1964), Dold (1965), Noskov (in Sokolov (1967), p. 61 f.f.) and Miller (1969). A short survey of the pros and cons of Beattie's method relative to other techniques is given in section 5.1.6..

5.1.1. *Basic relations*[†].

Ellipsometry is the measurement of Δ and ψ. With a knowledge of the angle of incidence θ one can calculate the optical properties

[†] For definitions and derivations see Appendix A.

$$\varepsilon_1 = n^2 - k^2 = \sin^2\theta\tan^2\theta\,\frac{\cos^2 2\psi - \sin^2\Delta\sin^2 2\psi}{(1 + \cos\Delta\sin 2\psi)^2} + \sin^2\theta\,, \quad \text{(A-12a)}$$

$$\varepsilon_2 = 2nk = \sin^2\theta\tan^2\theta\,\frac{\sin\Delta\sin 4\psi}{(1 + \cos\Delta\sin 2\psi)^2}\,. \quad \text{(A-12b)}$$

In Beattie's method Δ and ψ are determined using eqs. A-10,11b:

$$I'(\psi_P,\psi_A) = \tfrac{1}{2}I[r_s^2\sin^2\psi_P\sin^2\psi_A + r_P^2\cos^2\psi_P\cos^2\psi_A + \tfrac{1}{2}r_s r_P\sin 2\psi_P\sin 2\psi_A\cos\Delta]\,.$$

Fixing the analyzer setting at $\psi_A = 45°$ one measures the intensity at 4 polarizers settings †)

$$I_1 = I'(\ 0°,45°) = \tfrac{1}{2}I\ R_s\ \tan^2\psi \quad \text{(5-1a)}$$

$$I_2 = I'(\ 90°,45°) = \tfrac{1}{2}I\ R_s \quad \text{(5-1b)}$$

$$I_3 = I'(\ 45°,45°) = \tfrac{1}{2}I\ R_s[\tfrac{1}{2}(1 + \tan^2\psi + 2\cos\Delta\tan\psi)] \quad \text{(5-1c)}$$

$$I_4 = I'(-45°,45°) = \tfrac{1}{2}I\ R_s[\tfrac{1}{2}(1 + \tan^2\psi - 2\cos\Delta\tan\psi)] \quad \text{(5-1d)}$$

The ellipticity parameters now are determined from eqs. 5-1a,b:

$$\tan\psi = \rho = (I_1/I_2)^{\frac{1}{2}} \quad \text{(5-2a)}$$

and from eqs. 5-1c,d

$$\cos\Delta = (\sin 2\psi)^{-1}\ [(I_3 - I_4)/(I_3 + I_4)]\,. \quad \text{(5-2b)}$$

From eq. A-9 it can be seen that alternatively the polarizer can be set at a fixed $\psi_P = 45°$, whereas the analyzer is rotated. Also other combinations of $I'(\psi_P,\psi_A)$ can be used to extract Δ and ψ (e.g. Prishivalko

†) The numbering of the four intensities differs from that introduced by Beattie. Rather it follows the convention used by Prishivalko (1961).

(1961), Noskov (in Sokolov (1967), p. 61 f.f.). For a further discussion in regard to the use of eqs. 5-1,2 one is referred to the original article by Beattie (1955b).

5.1.1.1. *Test points.*

(1) $I_1 + I_2 = I_3 + I_4$,

(2) $I_1 = I'(\ 0°,45°) = I'(180°,45°) = I_5$,

$I_2 = I'(\ 90°,45°) = I'(270°,45°) = I_6$,

$I_3 = I'(\ 45°,45°) = I'(225°,45°) = I_7$,

$I_4 = I'(-45°,45°) = I'(135°,45°) = I_8$.

In case of a correct adjustment of the optical system these criteria should be satisfied to within 0.5%. As a matter of fact from experience we learned that an experimental point with a larger deviation is "off the curve" made up of points that do fulfil these requirements. To allow a fair evaluation of the measurements we therefore incorporate a calculation of the deviation of test (1) in our computer program. In "smoothing" the data in the derivation of the thermovariation spectra (sections 3.5.1., 4.5.1.) and in the analysis of fine structure (sections 3.9.2.(6), 3.13., 4.9.1.) we occasionally used these tests as an indication of the reliability of an experimental point. Test (2) is more difficult to apply. Ideally at all wavelength settings I_1 through I_8 should be measured. This doubles the measuring time, however. As a rule we therefore measured I_5 through I_8 at every fifth wavelength setting.

Most difficulties were usually encountered at both extremes of our wavelength interval for test (2); test (1) was troublesome only in the ultraviolet. The deviations are associated with a non-ideal homogeneity or state of polarization of the light beam. With the number of components in our optical system it is most difficult to indicate the culprit, or to provide a fool-proof remedy. From very extensive test series we found a strong influence of the light source (type: geometrical orientation; see section 5.1.2.), of the monochromator (adjustment on the image of

the entrance slit) and of the detector (orientation with respect to the exit slit of the monochromator;see section 5.2.5.). Most important, however, was the adjustment (section 5.1.4.) and especially the orientation of the polarizer and analyzer. This latter fact and the quoted wavelength--dependence of the deviation suggest the wavelength-dependent asymmetry of the angular polarized field of the polarizers (section 5.2.3.) to be the major cause of these difficulties. This is supported to some extent by a positive change when limiting the opening angle of the light beam by masking part of a mirror.

It should be noted that at some instances we found $I_1 + I_2 = I_3 + I_4$ and $I_5 + I_6 = I_7 + I_8$ to be satisfied simultaneously to better than 0.2%. Still at the same time test (2) was in no way fulfilled. The systematic deviation between the values of ε_2/λ as derived from I_1 through I_4 and those obtained from I_5 through I_8 should not be underestimated; especially in the infrared it is of importance as values of the intraband relaxation time τ are calculated from ε_2/λ. As indicated in section 3.6.1. the uncertainty in our values due to this cause must be estimated at about 10%; the corresponding deviations in test (2) are approximately 0.4%. The error in ε_1 (and therefore ω_{pf} and m_o) is smaller, about 1%.

Concluding we believe that for a fair appraisal of (especially intraband) optical properties determined by Beattie's method it is necessary to measure occasional test points I_5 through I_8.

5.1.2. *Experimental arrangement* (with drs. J.G. Smits).

5.1.2.1. *Optical system.*

Essentially our set-up is a perfected version of that by Beattie. The optical system is shown schematically in figure 5-1. An image is formed on slit S' (amplification 1x), then again on the specimen S (amplification 2x); because of symmetry the amplification of the image on the entrance slit of the monochromator is 1. For quick reference the components in the optical system are given below; the sections indicated between brackets refer to a more extensive or non-standard treatment.

light source L (section 5.1.2.):

for $\hbar\omega \lesssim 4$ eV: tungsten ribbon filament (6 V, 16 A) (Philips type W 2KGV12i),

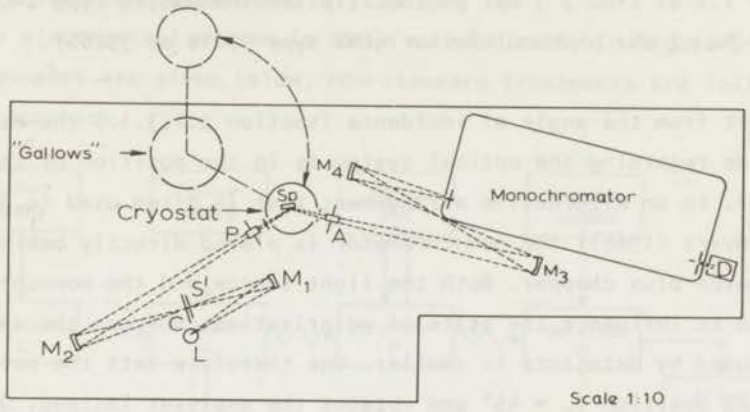

Fig. 5-1: Optical arrangement. Further information regarding the various components is given in the text.

for $\hbar\omega \geq 3$ eV: deuterium discharge lamp (55 V, 0.5 A) (Hilger & Watts type DF3H);

mirrors M_1, M_2, M_3, M_4 (section 5.2.2.):

front surface aluminized, overcoated with silicon-oxide,

M_1, M_4: radius of curvature 370 mm, outer diameter 66 mm,

M_2, M_3: radius of curvature 465 mm, outer diameter 56 mm;

slit S' (section 5.1.2.);

chopper C:

10 to 20 cps;

polarizer P, analyzer A (section 5.2.3.)

double Glan-Taylor prism (Karl Lambrecht),

open diameter 20 x 20 mm;

cryostat windows (section 5.2.7.)

silica (Heraeus Suprasil I or Quartz & Silice Pursil Ultra)

open diameter 22 mm, thickness 2.5 mm;

specimen Sp;

monochromator (section 5.2.4.):

double prism Van Cittert-type (Kipp model L35),

effective aperture f/6, usually natural quartz prisms;

detector D (section 5.2.5.):

for $\hbar\omega \leq 1.4$ eV: thermopile (Hilger type FT19 with CaF_2 window),

for 1.1 eV $\leq \hbar\omega \leq$ 3 eV: photomultiplier (Hamamatsu type R406),
for $\hbar\omega \geq$ 2 eV: photomultiplier (EMI type 9781B or 9526S).

Apart from the angle of incidence (section 5.1.3.1.) the main choice to be made regarding the optical system is in the position of the monochromator. In an alternative arrangement that is often used (e.g. Pells (1967), Myers (1968)) the monochromator is placed directly behind the light source plus chopper. Both the light source and the monochromator are found to influence the state of polarization, whereas the analogous error caused by detectors is smaller. One therefore sets the polarizer at a fixed position $\psi_p = 45°$ and rotates the analyzer instead. Quite possibly this arrangement is easier on the experimentalist; serious difficulties in the adjustment of our system probably were caused by a large extent by the polarization of the light from the deuterium lamp (section 5.1.2.). An additional advantage of the alternative set-up also is a smaller heat input during the low temperature measurements. On the other hand the larger intensity of the light at most places in our system facilitates the visual alignment. More important, however, the placement of the monochromator directly in front of the detector minimizes the amount of stray light reaching the detector.

The use of mirrors rather than lenses was dictated by the original demand of working at wavelengths larger than 2.7 μm. Most "normal" lens materials are absorbing here. A disadvantage of mirror optics is the introduction of aberrations (Born (1965) and Wolf, chapter 5) due to the positioning of the spherical mirrors relative to the optical axis. However, these effects are reduced to a minimum by the small angle of incidence on the mirror and the symmetry of the optical path relative to the specimen Sp. Similarly the polarization introduced by the mirrors is minimal due to the small angles of incidence and the high reflectivity of the mirrors. Disadvantages of lens systems are apart from the wavelength limitation the chromatic aberration, back reflections on both surfaces (stray light) and strain-induced polarization effects. An important advantage of the use of lenses undoubtedly is the much easier alignment of the various components (the so-called optical train).

5.1.2.2. *Electronical system.*

The electronical system is shown schematically in figure 5-2. Again the components are given below; non-standard treatments are indicated between brackets.

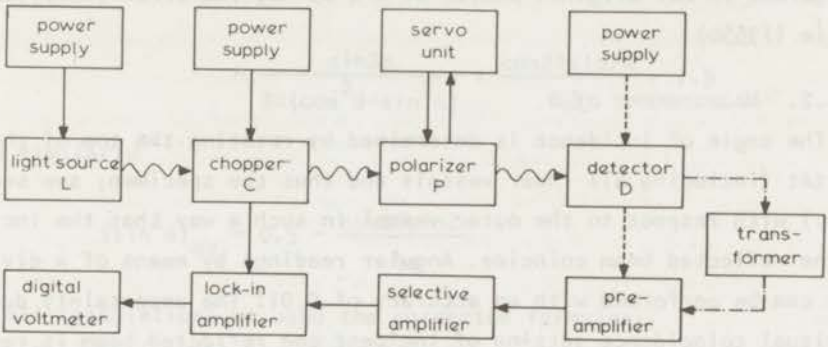

Fig. 5-2: Arrangement of electronical components with regard to the optical path. Details are given in the text.

power supply of the light source L:

for the tungsten ribbon lamp Hewlett-Packard Model 6264A,

for the deuterium discharge lamp Hewlett-Packard Model 6448B;

power supply of the chopper C:

Hewlett-Packard 204C oscillator,

Hewlett-Packard 467A power amplifier;

servo-unit for the rotation of the polarizer P (section 5.2.3.);

power supply of the detector D:

for the photomultipliers: PAR 280;

transformer:

for the thermopile: transformer ratio 1:79;

preamplifier: PAR 213 + 221 (for photomultipliers)
selective amplifier: PAR 210
lock-in amplifier: PAR 220
} in PAR 200 NIMBIN;

digital voltmeter: Oltronix DPM 319.

5.1.3. *Angle of incidence.*

5.1.3.1. *Choice of* θ.

The choice of the angle of incidence θ is determined by the expected values of the optical properties that one wants to measure. We were guided in our original choice of $\theta \approx 69°$ by the error analysis of Beattie (1955b).

5.1.3.2. *Measurement of* θ.

The angle of incidence is determined by rotating the top of the cryostat (including all inner vessels and thus the specimen; see section 5.2.6.) with respect to the outer vessel in such a way that the incident and the reflected beam coincide. Angular readings by means of a divided scale can be performed with an accuracy of 0.01°. The uncertainty due to the visual coincidence setting of incident and reflected beam is reduced by repeating the measurements a number of times. The estimated accuracy of the measured θ typically is 0.03° corresponding to a systematic error of about 0.6% in ε_2 and between 0.6% (in the intraband region) to 2% (in the interband region) in ε_1 (section 5.1.5.).

5.1.3.3. *"Effective" angle of incidence.*

A converging light beam is imaged on the specimen surface. If the opening angle of the beam is 2α, the maximum angle of incidence of any single ray is $(\theta + \alpha)$, the maximum angle $(\theta - \alpha)$. As pointed out by for instance Hodgson (1955) and Hunter (1965) the use of a straight mean for the value of θ in eqs. A-12 will lead to certain errors, especially for large values of θ. Hunter calculated the reflectance at for instance 70° by averaging the reflectance from 68° through 72° taken every 0.2°. The averaging procedure tacitly assumes that the light beam is uniform, i.e. rays of any angle of incidence in the interval between $(\theta - \alpha)$ and $(\theta + \alpha)$ are equally represented in the beam. If this is not the case, further corrections must be made.

The use of the computer has greatly facilitated such a procedure. Writing eqs. A-12 in the form.

$$\varepsilon_1 = A \sin^2\theta\tan^2\theta + \sin^2\theta \quad \text{and} \quad \varepsilon_2 = B \sin^2\theta\tan^2\theta,$$

one has to replace $\sin^2\theta\tan^2\theta$ and $\sin^2\theta$ by their averages

$$(\sin^2\theta\tan^2\theta)_{av} = \frac{1}{(\theta+\alpha)-(\theta-\alpha)} \int_{\theta-\alpha}^{\theta+\alpha} \sin^2\theta'\tan^2\theta' d\theta'$$

$$= \frac{\sin 2\alpha}{2\alpha(\cos^2\theta-\sin^2\alpha)} + \frac{\cos 2\theta \sin 2\alpha}{4\alpha} - 1.5 \qquad (5\text{-}3a)$$

and similarly

$$(\sin^2\theta)_{av} = 0.5 - \frac{\cos 2\theta \sin 2\alpha}{4\alpha} \qquad (5\text{-}3b)$$

In all calculations we used the corrected formulas.

Calculating $(\sin^2\theta\tan^2\theta)_{av}/(\sin^2\theta\tan^2\theta)$ one can estimate the importance of this correction on for instance ε_2. The angle α is found by determining which element on the optical system serves as the aperture stop (Born (1965) and Wolf, p. 186). From this one can calculate the angular aperture 2α of the effective incident light beam. In our experiment generally $\alpha \simeq 1°$. The correction to ε_1 and ε_2 then is about + 0.5%. This systematic deviation increases rapidly for larger angles θ or α.

5.1.4. *Adjustment of polarizer-analyzer assembly.*

Various methods have been proposed for the correct adjustment of the polarizer-analyzer assembly relative to the specimen surface. We have experimented with methods due to Lenham (private communication), Archer (1968, p. 5), Dignam (1970), Liljenvall (1970a), Steel (1971) and a "wiggle method" of our own. Every method has some aspects that are directly associated with a specific experimental set-up (variation of θ allowing "90° incidence" of the light, i.e. straight through the polarizer--analyzer assembly such that P and A can be crossed with ease; fine adjustments of ψ_P and ψ_A; motordriven rotation of P and A). Discussion therefore is limited.

In our earlier measurements we used *Liljenvall's* method. Although it worked well for the noble metals the correct adjustment was more troublesome for Rh as in the most appropriate wavelength one has $\Delta > 90°$.

A disadvantage that this technique shares with most other ones is that it essentially is an extinction method. Moreover best results are obtained at certain wavelengths such that the accuracy often is limited by the noise in the detected I' signal.

For the majority of the measurements reported in this thesis we therefore used the method proposed by *Steel*. It satisfies most criteria for practical use (fixed angle of incidence, alignment at high signal--to-noise ratio (no extinction!)). In our arrangement an uncertainty is possibly introduced by the necessity of crossing P and A. After various tests this error was minimized; the time required for adjustment (approximately an hour) still is a handicap though.

The importance of correct azimuthal alignment in ellipsometry has been pointed out frequently. For instance Dignam (1970) and Moskowits show that a small error can have a large effect on the measured optical properties.

5.1.5. *Error calculation.*

The basic formulas are eqs. A-12 and 5-1,2 (section 5.1.2.1.) that relate ε_1 and ε_2 to the experimental parameters I_1, I_2, I_3, I_4, θ, ψ_P and ψ_A. The measured value of the dielectric constant $\tilde{\varepsilon}'$ can be expressed as the sum of the "real" value $\tilde{\varepsilon}$ and a deviation $\delta\tilde{\varepsilon}$

$$\tilde{\varepsilon}' = \tilde{\varepsilon} + \delta\tilde{\varepsilon}$$

One can expand $\delta\tilde{\varepsilon}$ in a Taylor series which, considering only first-order terms, yields the following formula for the mean error:

$$\Delta\tilde{\varepsilon} = \left[\sum_{i=1}^{4}(a_i^2+b_i^2)\left\{(\delta I_i)^2+\left(\frac{\partial I_i}{\partial \psi_P}\right)^2(\delta\psi_P)^2+\left(\frac{\partial I_i}{\partial \psi_A}\right)^2(\delta\psi_A)^2+\left(\frac{\partial I_i}{\partial I}\right)^2(\delta I)^2\right\}\right.$$
$$\left.+\left(\frac{\partial\tilde{\varepsilon}}{\partial\theta}\right)^2(\delta\theta)^2\right]^{\frac{1}{2}} \qquad (5\text{-}4)$$

In this expression

$$a_i = \frac{\partial\tilde{\varepsilon}}{\partial\psi}\frac{\partial\psi}{\partial I_i} \qquad \text{and} \qquad b_i = \frac{\partial\tilde{\varepsilon}}{\partial\Delta}\frac{\partial\Delta}{\partial I_i} \qquad (5\text{-}4a)$$

and δI_i ($i = 1,2,3,4$), $\delta\psi_P$, $\delta\psi_A$, δI and $\delta\theta$ are the estimated errors in the respective experimental parameters.

The equations given by Loescher for the derivatives of ε_1 and ε_2 with respect to ψ, Δ and θ are in error. Correctly these expressions - as derived from eqs. A-12 - should be:

$$\frac{\partial\varepsilon_1}{\partial\psi} = -2\varepsilon_2\left[\frac{1+\sin^2\Delta}{\sin\Delta} + \frac{(\varepsilon_1-\sin^2\theta)(1+\sin2\psi\cos\Delta)\cot\Delta}{\sin^2\theta\tan^2\theta\sin2\psi}\right] , \qquad (5\text{-}5a)$$

$$\frac{\partial\varepsilon_1}{\partial\Delta} = \frac{\varepsilon_2}{\cos2\psi}\left[-\cos\Delta\sin2\psi + \frac{(\varepsilon_1-\sin^2\theta)(1+\sin2\psi\cos\Delta)}{\sin^2\theta\tan^2\theta}\right] , \qquad (5\text{-}5b)$$

$$\frac{\partial\varepsilon_1}{\partial\theta} = \frac{4(\varepsilon_1-\sin^2\theta)(1+\cos^2\theta)}{\sin2\theta} + \sin2\theta , \qquad (5\text{-}5c)$$

$$\frac{\partial\varepsilon_2}{\partial\psi} = 4\varepsilon_2\left[\cot4\psi - \frac{\cos2\psi\cos\Delta}{1+\sin2\psi\cos\Delta}\right] , \qquad (5\text{-}5d)$$

$$\frac{\partial\varepsilon_2}{\partial\Delta} = \varepsilon_2\left[\cot\Delta + \frac{\varepsilon_2(1+\sin2\psi\cos\Delta)}{\sin^2\theta\tan^2\theta\cos2\psi}\right] , \qquad (5\text{-}5e)$$

$$\frac{\partial\varepsilon_2}{\partial\theta} = \frac{4\varepsilon_2(1+\cos^2\theta)}{\sin2\theta} . \qquad (5\text{-}5f)$$

5.1.5.1. *Random error.*

The random error in our experiment is determined by all "moving" components. At a well-defined wavelength one therefore has to consider the scatter in the intensity readings I_1 through I_4 (eqs. 5-1), the inaccuracy of the polarizer setting ψ_P and the drift of the incident intensity I. Thus in eq. 5-4 one may set $\delta\psi_A = \delta\theta = 0$.

From eqs. 5-1 one can derive the partial derivatives of Δ and ψ with respect to I_1, I_2, I_3, I_4. A long but straightforward calculation yields

$$\frac{\partial\psi}{\partial I_1} = \frac{\sin 2\psi}{4I_1} \quad , \qquad \frac{\partial\psi}{\partial I_2} = -\frac{\sin 2\psi}{4I_2} \quad ,$$

$$\frac{\partial\Delta}{\partial I_1} = \frac{\cot\Delta\cos 2\psi}{2I_1} \quad , \qquad \frac{\partial\Delta}{\partial I_2} = -\frac{\cot\Delta\cos 2\psi}{2I_2}$$

$$\frac{\partial\Delta}{\partial I_3} = -\frac{1-\cos^2\Delta\sin^2 2\psi}{\sin\Delta\sin 2\psi I_3} \quad , \qquad \frac{\partial\Delta}{\partial I_4} = \frac{1-\cos^2\Delta\sin^2 2\psi}{\sin\Delta\sin 2\psi I_4} \quad .$$

The inaccuracy of the polarizer setting is noticed as an error in the intensity readings. From eq. A-10

$$\partial I'(\psi_P, 45°)/\partial\psi_P = \tfrac{1}{2}I[\tfrac{1}{2}\sin 2\psi_P(r_s^2 - r_p^2) + r_s r_p \cos 2\psi_P \cos\Delta].$$

Thus

$$\frac{\partial I_1}{\partial\psi_P} = \frac{\cos\Delta}{\tan\psi} I_1 \quad , \qquad \frac{\partial I_2}{\partial\psi_P} = -\cos\Delta\tan\psi I_2 \quad ,$$

$$\frac{\partial I_3}{\partial\psi_P} = \frac{\cos 2\psi}{1+\cos\Delta\sin 2\psi} I_3 \quad , \qquad \frac{\partial I_4}{\partial\psi_P} = -\frac{\cos 2\psi}{1-\cos\Delta\sin 2\psi} I_4 \quad .$$

Finally from eqs. 5-1 $\partial I_i/\partial I = I_i/I$ for all I_i.
Substituting all partial derivatives in eq. 5-4 one obtains

$$\Delta\tilde{\varepsilon} = \{[(\frac{\partial\tilde{\varepsilon}}{\partial\psi}\frac{\sin 2\psi}{4})^2 + (\frac{\partial\tilde{\varepsilon}}{\partial\Delta}\frac{\cot\Delta\cos 2\psi}{2})^2][(\frac{\delta I_1}{I_1})^2 + (\frac{\delta I_2}{I_2})^2 + 2(\frac{\delta I}{I})^2] +$$

$$[\frac{\partial\tilde{\varepsilon}}{\partial\Delta}\frac{1-\cos^2\Delta\sin^2 2\psi}{\sin\Delta\sin 2\psi}]^2[(\frac{\delta I_3}{I_3})^2 + (\frac{\delta I_4}{I_4})^2 + 2(\frac{\delta I}{I})^2] +$$

$$[(\frac{\partial\tilde{\varepsilon}}{\partial\psi}\frac{\cos\Delta}{2})^2 + (\frac{\partial\tilde{\varepsilon}}{\partial\Delta}\frac{\cos 2\psi}{\sin\Delta\sin 2\psi})^2(\cos^4\Delta + 2\cos^2\Delta\sin^2 2\psi + 2)](\delta\psi_P)^2\}^{\frac{1}{2}}. \qquad (5\text{-}6)$$

The random error, $\delta I'$, in the intensity is estimated from the instability of the last digit on the digital voltmeter. On a maximum reading of 15.00 V the deviation generally is ±0.01 V. This number increases, however, for spectral regions with smaller signal-to-noise ratio; i.e. the ultraviolet and the infrared. Especially in the latter case the ratio $\delta I_3/I_3$ can become quite appreciable as I_3 is very small.

The error $\delta\psi_p$ is determined from tests to be ±1'(section 5.2.3.3.). For typical Au (295 K) measurements the resulting relative error in ε_1 is of the order of 1°/oo or smaller and thus can be neglected. The relative error in ε_2 is more wavelength-dependent ranging from 1°/o in the intraband to less than 1°/oo in the interband region. It should be noted that even for such a highly accurate polarizer setting this error is the source of the largest random deviation in the infrared.

In our actual calculation we assumed $\delta I/I = 0$. In other words, we neglected a change of the intensity due to "long-term" instabilities of the light source or the electronics (chopper, detector, etc.) that can influence the intensity reading in the time that is usually required to complete a measurement at one wavelength setting (2 to 5 minutes). After some initial difficulties we essentially eliminated such influences in our set-up. The induced random error is more serious when "atmospheric" conditions can affect the working conditions of specific components (draught on open light sources such as a Nernst glower; varying strongly light - e.g. sunshine - on detectors).

The use of the computer allows the routine calculation of these errors for all data points. Results indicate that for the Au (295 K) data in the intraband region $(\Delta\varepsilon_1/\varepsilon_1) \lesssim 0.5\%$ and $(\Delta\varepsilon_2/\varepsilon_2) \simeq 2\%$. In the for our purposes more interesting interband region $(\Delta\varepsilon_1/\varepsilon_1)$ is between 0.5 and 1.5% and $(\Delta\varepsilon_2/\varepsilon_2) \simeq 0.3\%$ or - translating in absolute values - $|\Delta\varepsilon_2| \lesssim 0.02$.

An earlier error calculation (not including $\delta\psi_p$) was reported by Prishivalko (1961), who also demonstrated the application of this type of calculation to other experimental methods. Such calculations allow a comparison to be made of the sensitivity of the various techniques in different spectral regions. Using a somewhat different approach Böhme (1968) derived related formulas for this type of work. A more limited

calculation (for ellipsometrical methods where Δ, ψ, and θ are directly measured) is presented by Loescher (1971). It should be noted that apart from the formulas 5-5 also the vertical scale of his figure 1 is in error.

Random errors in the measurement of the photon energy (i.e. the "horizontal" coordinate of the spectra) are determined by the accuracy of the reading of the monochromator setting. Additional random errors due to erroneous reading of calibration graphs or interpolating of tables are eliminated through the use of a computer calibration of the monochromator (section 5.2.4.). Thus we estimate the random error in the photon energy to be ± 0.002 eV, possibly somewhat smaller in the ultraviolet and infrared regions of the spectrum.

5.1.5.2. *Systematic error.*

The most important single source of discrepancies between the optical properties of a specific metal as presented in the literature undoubtedly is in the preparation of the sample. Numerous times in this thesis we pointed at surface roughness, grain boundaries, mechanical deformation, differing density, adsorbed layers, etc. as possible strong influences on the structure in optical spectra. As suggested in for instance sections 3.6. and 4.6. these causes can give rise to anomalous absorption; however, also other structure (interconduction-band absorption!) is considerably reduced and broadened. In view of these different effects it is not possible to give even an estimate of the deviation due to sample conditions. Reasonable criteria for judging the quality of the sample from the observed interband absorption structure have been given in sections 3.14. and 4.11.

Almost every component in our optical system is a potential source of systematic errors, some of which are most difficult to eliminate or even minimize. These sources are not expected to introduce new structure. However, important wavelength-dependent deviations can cause misleading changes of slope whereas the interchanging of optical components may bring about jumps in the observed spectra. The most important of these errors plus suggested solutions and references are brought forward in the treatment of the various components (section 5.2.).

5.1.6. *Pros and cons.*

The pros and cons of Beattie's method with respect to other commonly used methods can be sketchily assessed.

5.1.6.1. *Ellipsometric extinction methods* (Drude (1959, p. 255), Archer (1968), Bennett (1967), chapter 9)) yield more accurate values of the optical constants in limited wavelength intervals in the visible. Whenever the signal-to-noise ratio of the intensity measurement decreases (ultraviolet, infrared) these methods become less useful. Furthermore they are hampered by the use of phase compensators (generally limited to the visible) and the necessity of measuring at $\theta \approx \overline{\theta}$, the principal angle of incidence (Holl (1967)). Beattie's method, however, requires the use of linear detectors in order to give correct values of the ratios of the intensities (section 5.2.5.).

5.1.6.2. *Non-normal incidence reflection measurements* can be subdivided into two major groups.

(1) R, R_p or R_p/R_s are determined at *two* (or more) *angles of incidence* and ε_1 and ε_2 are extracted from these data by means of eqs. A-13b,14b, 15b. An important advantage of the $R(\theta_1,\theta_2)$ method (Tousey (1939), Simon (1951)) is that it does not involve the use of polarizers. Therefore it is virtually the only technique that allows direct measurement of the optical properties in the vacuum ultraviolet ($\lambda < 0.18$ μm) without taking resort to Kramers-Kronig analysis (see c.). An advantage that the $R_p/R_s(\theta_1,\theta_2)$ method (Avery (1952) shares with Beattie's method is that no measurement of the incident intensity is necessary; a number of experimental errors cancel by taking the ratio of reflected intensities.

Highest accuracy is achieved when $\theta_1 \approx \theta_B'$, the pseudo-Brewster angle of incidence (Holl (1967)). For strongly absorbing materials $\theta_B' \approx 90°$; this grazing incidence condition essentially eliminates these methods from the infrared region (e.g. Beattie (1955a)). The reflectometers become rather complicated (e.g. Lavin (1971), p. 44). The second angle θ_2 is much smaller, typically about 16° (Miller (1970,1971)), The differing beam geometry may lead to errors such as arise from the variation of the effective specimen surface, the angle-dependent influence of surface irregularities and the homogeneity of detectors.

(2) The second class of techniques involves one reflection measurement plus the measurement of a "special" angle of incidence. Best known are $R_p/R_s(\theta')$ (Humphreys-Owen (1961), Potter (1964)) and $R_p/R_s(\bar{\theta})$ (Swindell (1968)). Again the wavelength range is limited as in the infrared θ_D' and $\bar{\theta}$ are close to 90°. Good results have been obtained in the visible and near-ultraviolet though.

For more critical reviews of these methods (2) one is referred to the literature (e.g. Humphreys-Owen (1961), Hunter (1965), Miller (1970, 1971), Lavin (1971)).

5.1.6.3. *Normal incidence reflectivity* is determined from measurement of I and I'(see sections A.3. and A.4.). At normal incidence p and s components of the light are indistinguishable such that - also using eq. 2.8. -

$$R(\theta=0°) = \tilde{r}_s^* \tilde{r}_s = r_s^2 \text{ with } \tilde{r}_s = r_s \exp i\delta_s = (1-n+ik)/(1+n-ik).$$

The optical constants follow upon inversion (writing $r = r_s$, $\delta = \delta_s$)

$$n = (1 - r^2)/(r^2 + 2r\cos\delta + 1) \quad ,$$

$$k = 2r\sin\delta/(r^2 + 2r\cos\delta + 1) \quad .$$

Clearly $R(\theta = 0°)$ yields insufficient information about δ. One has to resort to the Kramers-Kronig dispersion relations, that in their most practical form in this respect will give the phase shift at a certain angular frequeny ω_o as a function of $r(\omega)$ over all other frequencies (Stern (1963), p. 336)

$$\delta(\omega_o) - \pi = (\omega_o/\pi)\int_0^\infty \{[\ln R(\omega) - \ln R(\omega_o)]/[\omega_o^2 - \omega^2]\}d\omega \quad (\omega \neq \omega_o) \tag{5-7}$$

Measurements of R over the whole frequency range thus provides the necessary information for obtaining the optical constants.

Experimentally these methods offer some very favorable conditions. The experiment is relatively easy (e.g. Bennett (1967), Lavin (1971))

and produces data (continuous curves) over a large wavelength region in a short time. Also the method is hardly sensitive to errors due to problematic experimental parameters such as the state of polarization of the light, the exact angle of incidence and the opening angle of the beam. Fewer difficulties than at non-normal incidence are caused by specimen conditions such as surface roughness and adsorbed layers.

However, the experimentally unsolvable problem is the determination of $R(\theta = 0°)$ for all frequencies. The use of limited frequency ranges in eq. 5-7 may yield misleading results (e.g. Bowlden (1963)). Especially in "abnormal" studies such as those involving temperature dependence of alloy samples the use of extrapolation procedures is problematic. Theoretical models for the optical properties become increasingly difficult under these circumstances, whereas usually no reliable literature values are available for extrapolation purposes. A further disadvantage of the use of dispersion relations is that errors in one part of the spectrum influence all data in other regions.

5.1.6.4. *Comments.*

Summarizing, the major advantage of Beattie's method undoubtedly is that it allows a direct determination (i.e. without Kramers-Kronig analysis) of ε_1 and ε_2 over a relatively large wavelength interval while using a fixed angle of incidence and pre-selected settings of the polarizer. The use of the method is limited to $\lambda \geq 0.2$ μm by the requirement of high-quality polarizers and at the infrared side of the spectrum by the exceedingly large differences in the measured intensities (see section 5.1.1.) that necessitate very accurate, linear detection techniques.

5.2. *Components.*

5.2.1. *Light sources.*

5.2.1.1. *Demands.*

A rather thorough review of light sources has been presented by Cann (1967,1969). The following source requirements were of major importance in our experiments.

(1) Spectral range: 2.7 - 0.22 μm (0.46 - 5.6 eV).

(2) Uniformity: in order for the light beam to be considered homogeneous, a high degree of uniformity is necessary, both across the source (i.e. also over its image; the required size of the uniform part of the source is determined by the dimensions of the monochromator slit, in our case for ease of adjusting 0.5 mm wide and 5 mm high) and as a function of angle (the opening angle of the beam at the light source is about 4°). Cann requires a variation of brightness smaller than ±5%.

(3) Stability: drift (long term) smaller than 0.1% over 5 minutes; random fluctuations and ripple (short term) smaller than 1% over 5 minutes.

(4) Polarization: none. (This demand was not made by Cann; however for ellipsometric measurements it may be seen to provide an important source of error.)

5.2.1.2. *Realization.*

(1) *Tungsten ribbon incandescent lamps.*

Highly stable and reproducible sources for the visible and near-infrared (0.4 - 2.7 μm) will be found in the tungsten ribbon filament lamps. Their spectral radiance can be estimated from the emissivity curves of tungsten at different temperatures such as given by De Vos (1954) which must be multiplied by the appropriate blackbody relations. The comparison made by Cann shows that the radiance is smaller than that obtainable with competitive sources in this region (high pressure arc discharges (Hg, Xe, A), low current carbon arc). However this is compensated by a superior stability and uniformity, properties which make these lamps widely used as standards of radiance.

Using vacuum or gas-filled lamps (Philips types W2KVV12i or W2KGV12i) with a Hewlett-Packard Model 6264A d.c. power supply (long and short term stability better than 0.05%) we measured a drift smaller than 0.2% per hour, a total noise smaller than 0.15%. The ribbon is about 10 mm long and 2 mm wide, easily large enough to select a uniform central part by means of a slit. The uniformity of the emitted beam is further increased by using a horn-shaped bulb such that very few reflections from the glass envelope will pass through the plane-parallel quartz window. The opening

angle of the beam is 18.5°; no uniformity problems are to be expected in the small part used in our experiments (Worthing (1926), De Vos (1954)). Obviously the problem can become serious when using coiled filament lamps.

This last statement is true even more so for the degree of polarization of coiled filament lamps. As a more complete report is published elsewhere (Lengkeek (1973) and Winsemius), we refrain from detailed accounts of this work. The degree of polarization is commonly defined (Shurcliff (1962), p. 12) by

$$V = (I_d - I_i)/(I_d + I_i) \qquad (5\text{-}8)$$

where I_d is the maximum intensity of the light in any direction of vibration (i.e. the intensity of the dominant component) and I_i is the intensity associated with the orthogonally polarized inferior component. For our lamps $V \approx 0.5\%$ in the central part of the ribbon, increasing to about 1.5% at the sides. These undesired contributions were eliminated by placing slit S' at the first focus of the beam.

(2) *Deuterium lamps.*

These lamps produce a strong continuum from .165 to .450 μm and a spectrum of lines superimposed on a continuous background for longer wavelengths. Spectral radiances are shown by Cann and Pitz (1969); the output of a D_2-lamp is claimed to be between 1.4 and 2.5 times higher than that obtainable with its precessor, the hydrogen arc. Cann shows that other types of lamps (Xe or A discharges; low current carbon arc) produce much higher intensities. As was the case with the tungsten lamp, however, considerations of stability and uniformity were thought to be of greater importance (Cann (1967, Table XIII), Liebmann (1969), Breeze (1972)).

It should be pointed out, in this respect, that it not always is advantageous to have lamps that cover a very wide spectral range. The measured signal in an optical system is produced by the combination of light source, optics and detecting system. In addition to the signal within its passband the monochromator (see section 5.2.4.) allows a

fraction of the incident light of other wavelengths to stray onto the detector. Thus if in a specific wavelength interval the emitted intensity is small relative to its peak value in another spectral range, the stray signal - and therefore the optical noise - may become a serious problem. This is especially true for ultraviolet light sources with intensity peaks in the visible where usually detectors (photomultipliers) have their peak detectivity values.

A thorough discussion of the construction of deuterium lamps is given by Kern (1954). We experimented with various types. Best results were obtained with the Hilger & Watts type DF3H lamp. This lamp differs from the others that we tried in that its emitting area is rectangular rather than circular. It therefore is recommended for illuminating optical slits. The rectangular area (actually the hole in the cathode) is 6.0 mm high and 0.7 mm wide. These dimensions are of major importance in view of the rather poor uniformity of this type of light source (Pitz (1969), Lengkeek (1973)). The deviations in the uniformity - up to 20% of the maximal intensity - are expected to be wavelength dependent being more pronounced at shorter wavelengths (Cann (1967), p. 25 on Xe--arcs). Kern showed that due to construction the angular distribution of the emitted light is not homogeneous. In addition to these problems the position of the arc may change; the mechanical stability of the anode --cathode assembly is uncertain (Dr. Kern GmbH, Göttingen, Germany, produces a special lamp where through extra precautions the movement of the arc is limited to less than 0.005 mm). These effects may have been the cause for a number of unpleasant experiences when working with circular sources. Obviously circular sources producing a high intensity light spot of 1 mm diameter cannot fulfil the uniformity demand of a height of 5 mm.

Not many data are known on the stability of deuterium lamps. Manufacturers quote ripple and noise as 0.1% peak to peak. Our own tests on the Hilger and Watts lamp DF3H showed the drift to be less than 0.4% per hour. Short term instabilities had peak-to-peak values of the order of 0.4%. These figures have to be taken as maximum values as the data were taken on a well-used lamp with a rather low output intensity. With the point-by-point measurements using Beattie's method only a limited period

of time is needed to complete the data at a certain wavelength (typically 2-5 minutes). An important advantage of this method therefore is that one need not worry about long term drift of the emitted intensity.

The power supply for these lamps consists of two parts. Most commercial sources can be handled, when a voltage of maximal 6 V and a current of 10 A is available for heating the electron-source filament, whereas a well-stabilized d.c. supply is required for the striking (typically at 200-300 V) and the running (40-100 V at 0.3-1.0 A) of the arc. These last demands are very adequately met by the Hewlett-Packard Model 6448B, which is capable of producing 1-600 V and 0-1.5 A. Ripple and noise are of the order of 1%, drift less than 0.05% in 5 minutes. Incorporating this instrument one easily obtains a reliable power supply that provides excellent versatility.

The extremely difficult alignment of circular sources suggested a rather high degree of polarization of the emergent light. As very little was known on this subject we developed a rather simple technique to evaluate V. A thorough discussion of this technique (photographing the image of the light source through a polarizer and consequently analyzing the negatives) is given by Lengkeek (1973) together with the most relevant results. We will therefore abstain from details. It was found that with the rectangular source it is possible to select (by means of a slit S') a central region of 5 by 0.5 mm where $V \leq 7\%$. With an accurate adjustment system on the lamp holder this is sufficient for a correct alignment of the light source. This is found to be virtually impossible for circular sources. Similar problems most certainly will be encountered with the usual incandescent coiled filament lamps.

A more definitive solution of the polarization problem has been introduced by Roberts (1964) who employed an additional polarizer that is placed directly behind the lamp. Clearly the perfectly polarized light source, that is thus created, is easier to control than a normal source. The method of taking data of course will differ from the usual Beattie procedure, as will be the calculation of the optical properties. Some loss of light occurs due to the extra polarizer, especially in the ultraviolet.

5.2.2. *Mirrors and mirror holders.* (with Mr. H. van Zanten and Mr. H.R.A. Nater).

5.2.2.1. *Demands.*

(1) Reflectance better than 90% between 0.2 and 3.0 μm.

(2) The holders should allow separate horizontal and vertical translations and also separate rotations around a horizontal and a vertical axis (accuracy 2.5'). Such a rotation corresponds to a beam displacement of 0.4 mm at a distance of 300 mm.

5.2.2.2. *Realization.*

The mirrors were polished at this laboratory. Deviations from sphericity are smaller than 1/8th of the wavelength of the Na D-line, i.e. smaller than 750 Å. A reflective coating of aluminium was evaporated using conventional techniques (Al purity ≥ 99.99%, vacuum 10^{-5} to 10^{-6} mm Hg). A protective silicon oxide film was evaporated according to the "recipe" given by Bradford (1963,1965) to a thickness of about 1400 Å; the deposition rate was 2.5 Å/sec at an oxygen pressure of approximately 1.5×10^{-4} mm Hg. When irradiated with a strong ultraviolet light source (Philips type HPLR 400 watt quartz mercury burner of which the outer envelope was removed) for a prolonged time (5 hours at a distance of 28 cm) the mirrors have a reflectance of more than 90% for wavelengths between 0.2 and 8.0 μm. SiO-films exhibit absorption between photon energies of 3 and 8 eV (0.4 to 0.15 μm). However, when SiO is slowly deposited at rather high oxygen pressures and the layer is subsequently irradiated with strong ultraviolet light, this ultraviolet absorption completely disappears. Similar results have been obtained on annealing in air or argon. Various suggestions and explanations have been given for this somewhat surprising effect (Cremer (1962), Garski (1964), Bradford (1965), Philipp (1971)), especially the latter being noteworthy. Further recent work of interest is due to Bradford (1970), Hodgkinson (1970) and Nagasima (1972).

The required translations are performed with the aid of dovetail mounts, the rotation with a fine motion tangent adjustment. Any unwanted mechanical movement is prevented by the use of springs. The use of such precision apparatus was found to be very profitable, almost essential in

the routine alignment of the optical system. The holders were made by students of the Leiden Instrumentmakers' School.

5.2.3. *Polarizers.*

5.2.3.1. *Demands.*

(1) Spectral range: 2.7 - 0.22 μm (0.46 - 5.6 eV).

(2) Extinction coefficient (defined as the ratio of extinguished and transmitted components of incident natural light) $\leq 5 \times 10^{-5}$.

(3) Minimal deviations of the transmitted beam.

(4) Large angle of divergence between the two components.

(5) Aperture ≥ 15 mm.

(6) Angular polarized field ≥ 6° for all wavelengths.

(7) Angular setting of the polarizer in eight steps of 45° with an accuracy and reproducibility of 1'.

(8) Translations and rotations as in the case of mirror holders (section 5.2.2.).

5.2.3.2. *Realization.*

A review of polarizers is given by Schulz (1928, p. 373 f.f.). Requirement (4) is of importance as the specimen is closely behind the polarizer; it eliminates Rochon, Senarmont, Thompson, Wollaston and Abbe-types polarizers. It should be noted that in alternative optical arrangements one can use for instance Rochon-type polarizers (e.g. Pells (1967)). The allowable deviation of the transmitted beam (3) is mostly determined by the homogeneity of the light source; if poor, as in the case of deuterium lamps (section 5.1.2.2.), any movement of the non-uniform image on the entrance slit of the monochromator or on the detector is apt to introduce errors. This demand cannot be fulfilled by Wollaston, Dove, Abbe, Nicol, Foucault and Hartnack type polarizers. More important, however, is the elimination of the otherwise "ideal" Glan-Thompson polarizers that due to the use of ultraviolet absorbing cements transmit down to about 0.3 μm (4 eV). The use of special ultraviolet Glan-Thompson polarizers is advised against by the manufacturer because of a considerably deteriorating performance upon ageing. Actually this elimination procedure limits the choice to a Glan type or double Glan-Taylor polarizers.

The most serious source of difficulties in our experiment probably has been the angular polarized field (or angular aperture). The angular polarized field by the critical angles of incidence θ_o and θ_e of respectively the ordinary and extraordinary rays at the calcite-cement interfaces. If the angle of incidence $\theta' > \theta_e$ the two rays are totally reflected, if on the other hand $\theta' < \theta_o$ both are transmitted. The angles θ_o and θ_e are related to angles of incidence α_o and α_e of the light on the front surface of the prism polarizer. Thus these angles determine the angular polarized field that is characterized by an angle α:

$$\alpha = \alpha_o + \alpha_e \quad .$$

Very importantly the refractive indices n_o and n_e of calcite are not constant, dispersion being especially high in the ultraviolet. The wavelength-dependence of θ_o and θ_e - and therefore of α_o and α_e - is different and the angular polarized field is not symmetrical with respect to the rotational axis of the polarizer. In our type of experiments therefore the useable (symmetrical) polarized field is determined by whichever is the smallest of α_o and α_e

$$\alpha_{eff} = 2 \min (\alpha_o, \alpha_e) \quad .$$

That this distinction between α_{eff} and α is of considerable importance is shown by Archard (1948) and Taylor for a modified Glan-Foucault (also Glan-Taylor):

at $\lambda = 0.2006$ µm: $\alpha_e = 0°58'$, $\alpha_o = 13°30' \Rightarrow \alpha = 14°28'$, $\alpha_{eff} = 1°56'$
at $\lambda = 0.3612$ µm: $\alpha_e = 4°27'$, $\alpha_o = 4°19' \Rightarrow \alpha = 8°46'$, $\alpha_{eff} = 8°38'$
at $\lambda = 0.9047$ µm: $\alpha_e = 5°32'$, $\alpha_o = 2°12' \Rightarrow \alpha = 7°44'$, $\alpha_{eff} = 4°24'$.

Obviously in the ultraviolet this polarizer does not fulfil requirement (6); some gain can be made by adapting the cutting angle of the polarizer prisms and thus α_o and α_e, however, this goes at the expense of α_{eff} in the infrared.

This problem is considerably minimized when using the double-Glan-Taylor polarizers designed by Roberts (1964) and Marple. These polari-

zers have a much larger useable angular polarized field, according to the manufacturer $\alpha_{eff} = 12°$ at 0.214 μm and 16° at 2.3 μm. Still highly accurate rotational and translational adjusting facilities on the polarizer holder are required to obtain the "perfect" coincidence of the geometrical axis of the polarizer and the optical axis of the beam. Although ideally for this type of polarizer $\alpha_{eff} = \alpha$ the adjustment for $\lambda \leq 0.28$ μm was found to be much easier when the polarizer axis was set at an angle with the optical axis, thus probably indicating an asymmetry of the polarized angular field. Generally, however, such a procedure led to difficulties in other wavelength regions as indicated by systematic deviations in tests (1) and (2) in section 5.1.1.1..

From a comparison of manufacturer's literature it is found that for measurements at photon energies below 4 eV ($\lambda > 0.3$ μm) the best choice of polarizer undoubtedly is the Glan-Thompson type. It has a lower extinction ratio (2), smaller deviation (3), an α that is about twice as large and a lower price than a double-Glan-Taylor polarizer. For experiments at higher photon energies the latter type has the best prospects: for our polarizers extinction ratio 5×10^{-5}, deviation $\leq 4'$, aperture 20 x 20 mm.

The demand on the extinction ratio $\leq 5 \times 10^{-5}$ was determined from an error calculation. If this requirement is fulfilled, the corresponding error is always smaller than the random error (section 5.1.5.1.). In other photon energy regions (the vacuum ultraviolet range and the infrared) no suitable polarizers are available and corrections must be made for the non-"perfect" state of polarization of the light (e.g. Haas (1968), Graves (1971)).

5.2.3.3. *Polarizer holders* (with Mr. J.A.G. Verkuyl and Mr. H.R.A. Nater).

The divided scale of the polarizer holder is readable with an accuracy of $\frac{1}{2}'$. A complete account of the servo-driven angular setting is published elsewhere (Verkuyl (1973), Lengkeek and Winsemius) and will not be repeated here. The accuracy and reproducibility of the setting is better than $\pm 1'$. In the interband region of Au and Ag the corresponding systematic and random errors in ε_1 and ε_2 may be neglected compared to

other sources of error. This is not necessarily so in the intraband region (see section 5.1.5.1.).

The complicated mechanical part of the polarizer holder, that was almost essential in the ultraviolet adjustment of the polarizer, was very ably made by students of the Leiden Instrumentmakers' School.

5.2.4. *Monochromator.*

5.2.4.1. *Demands.*

(1) Spectral range: 2.7 - 0.22 μm (0.46 - 5.6 eV).

(2) Resolution of the monochromator should be such, that under normal operating circumstances the Rayleigh criterion of resolution (Bousquet (1971), p. 10) is fulfilled for two intensity peaks that are separated by 0.005 eV.

(3) Measurement of the selected photon energy throughout the whole wavelength region with an accuracy better than 0.005 eV.

(4) At all wavelengths the "signal-to-noise" ratio of the optical system (including light source, polarizer, detector, etc.) must be larger than 1500. As the monochromator serves as the "optical fitter" of the system, this means that the ratio of the transmitted energy in a chosen wavelength interval (i.e. the optical system) and the total energy of the stray light (i.e. the optical noise) must be appreciably larger than 1500.

(5) The emerging light should be homogeneous in intensity and spectral composition. The monochromator should not influence the state of polarization of the incident light.

5.2.4.2. *Realization.*

A general treatise of monochromators is given by Bousquet (1971). The Kipp model L35 monochromator is based on principles outlined by Van Cittert (1923,1926) (see also Christensen (1963)). It is composed of two identical prism monochromators (Wadsworth mounting). The first monochromator serves as the dispersive instrument. The half-width of the passband (i.e. the passed interval of wavelengths) is determined by the dispersion of the prism material $dn/d\lambda$, the widths of the slits S and a number of instrumental parameters (Bousquet (1971), p. 140); in our case

$$\Delta\lambda \simeq 2.5 \times 10^{-6}\ S/(dn/d\lambda)\ \mu m$$

(S and λ also expressed in μm). For optimal resolution all slit-widths are set equal (Christensen (1963)); typical in our measurements for $\lambda <$ 0.35 μm S = 0.20 mm, for λ between 0.35 and 1 μm S = 0.10 mm and for $\lambda >$ 1 μm S = 0.30 mm. The demand on the Rayleigh criterion of $\Delta(\hbar\omega) \leq$ 0.005 eV can alternatively be written as $\Delta\lambda \approx (\Delta(\hbar\omega))\lambda^2/1.24 \leq 4 \times 10^{-3}$ λ^2 μm. Theoretical estimates of $dn/d\lambda$ show that with the given slit widths quartz prisms produce satisfactory resolution throughout the whole required spectral range. Although in practice various factors (aberrations, line curvature (Van Heel (1950), p. 371)) have a negative influence, this conclusion was substantiated in experimental tests of the splitting of spectral lines.

The mean wavelength of the passband is selected through a rotation of the prisms. A drum read-out gives quantitative information on the angular position of the prisms. In principle the calibration of the drum reading as a function of wavelength or photon energy can be performed with the aid of spectral lamps. A smooth dispersion curve then can be drawn in the ensuing graph. However, the optical system of the monochromator is such that it allowed the calibration data to be computer fitted to a model dispersion formula that is made up of some instrumental parameters together with a classical dispersion formula. This computer calibration method is described in more detail in Appendix B. It is shown that the uncertainty in the measurement of the selected photon energy is less than 0.004 eV for all photon energies.

Because of the inversion images ("lens action") on passing from the first monochromator into the second and the form of symmetry between the two, the dispersion of the second prism is in opposition with that of the first (Bousquet (1971), p. 141). In absence of the common central slit the second half would mix the spectrum again and completely "white" light would emerge from the exit slit. Thus the second monochromator does not influence the resolving power of the total instrument. However, very importantly the amount of stray light passing through the double monochromator is greatly reduced: $a^2/100\%$ as compared to a% for a single monochromator. This then is the main advantage of the Van Cittert type monochromator.

Apart from the homogeneity of the spectral composition of the emerging light condition (5) is not satisfied with our monochromator. This possibly can lead to errors in the measurement of intensity with non-uniform detectors (section 5.2.5.2.).

5.2.5. *Detectors.*

An excellent introduction to the terminology involved with and the evaluation of detectors has been given by Limperis (1965). The fundamental parameter in performance rating is the spectral D-star

$$D^*(\lambda, f_o) = (A\Delta f)^{\frac{1}{2}} D_\lambda \quad (\text{in cm } (\text{cps})^{\frac{1}{2}} \text{w}^{-1})$$

where A is the responsive area (in cm^2), f_o the chopping frequency, Δf the electrical bandwidth and the spectral detectivity $D_\lambda = 1/NEP_\lambda$ (in $watt^{-1}$) is the reciprocal of spectral noise equivalent power. This NEP_λ (in watt) in turn is defined as that value of monochromatic incidence rms signal power of wavelength λ required to produce an rms signal to rms noise ratio of unity.

5.2.5.1. *Demands.*

One is referred to a listing of 10 primary requirements to the system designer given by Limperis (p. 460). Of specific importance to our experiments are

(1) Spectral response: 2.7 - 0.22 μm (0.46 - 5.6 eV).

(2) Responsive area: minimal 5 mm high, 0.5 mm wide.

(3) NEP_λ: at least a factor 1500 smaller than the incident signal (i.e. signal-to-(electrical) noise ratio > 1500).

(4) Homogeneity of the detector.

5.2.5.2. *Realization.*

(1) *Photomultipliers.*

The photon energy range between 1.1 and 5.6 eV can be covered by photomultipliers with S1 (1.1 - 2.5 eV) and S5 or S11 (2 - 6 eV) response. Values of $D(\lambda, f_o)$ are of the order of 10^{10} to 10^{16} $watt^{-1}$ such that optical noise rather than electrical noise determines the random variation

of the measured intensity. Even in the ultraviolet ($\hbar\omega > 4$ eV) little gain is made by substituting detectors with higher $D^*(\lambda, f_o)$. Therefore only a few remarks will be made on this subject[†].

Frequently it has been pointed at jumps in the overlap of measurements performed with different photomultipliers (e.g. Lettington (1966), section 3.6.1.). Possible causes have been indicated such as reflections inside the photomultiplier (Beaglehole (1968)) or the influence of the shape of the receiver on its sensitivity to radiation of differing states of polarization (Archard (1952), Conn (1954)). Thus latter effect has been substantiated for some side-on photomultipliers. Although we did not perform any systematic research, the influence of the geometrical orientation of the photomultipliers with respect to the exit slit of the monochromator was very obvious. Most notably with the Hamamatsu R406 side-on detector we measured maximal intensities at two vertical positions relative to the exit slit of the monochromator. Good overlap with data obtained when using the thermopile - where no such effects were found - was only possible at an intermediate position. As a rule the position of the Hamamatsu detector therefore was "calibrated" on thermopile measurements; subsequently measurements obtained with the Hamamatsu were used in adjusting the ultraviolet photomultiplier. Still in our opinion this highly bothersome effect warrants some further investigation.

Bennett (1966a) indicated the importance of employing detectors with a sufficient linearity in measurements such as ours. An apparatus such as developed by Bennett was not finished in time to perform tests of the linearity of our detectors. Systematic errors might be introduced, especially at lower photon energies where $I_3 \ll I_4$ (section 5.1.1.).

The chopping frequency in our experiments (about 18 cps) is somewhat low for photomultiplier use causing a possible increase of the NEP_λ (Limperis, p. 469). However, as stated before, optical noise generally is the limiting factor in this energy range.

[†] We had some very unpleasant experiences with an EMI 9781B side-on photomultiplier that exhibited a strong overshoot (up to 30%) if the light signal was drastically changed. It sometimes took up to 4 or 5 minutes to reach an equilibrium value. The reason probably is so-called photomultiplier hysteresis (RCA Photomultiplier Manual (1970), p. 51).

The performance of the perfect light source and the perfect detector are independent of wavelength. However for instance in the visible the emitted energy of filament lamps decreases with decreasing wavelength. Even a small percentage of the emitted energy of longer wavelength, that strays onto the detector, will make measurements misleading. This effect can be greatly amplified by the strongly wavelength-dependent sensitivity of photomultipliers. Thus - as was pointed out before in regard to light sources - the best photomultiplier is not always the one that covers the largest spectral range.

(2) *Thermopile* (with drs. J.G. Smits and Mr. H. van Zanten).

For the spectral range from 0.8 to 2.7 μm (0.46 - 1.5 eV) we selected a Schwarz-Hilger vacuum thermopile, the principles of which are adequately outlined by Conn (1960) and Avery (p. 83 f.f.). The choice of a thermopile ($D^*(2\,\mu m, 11cps) \approx 10^{10} cm(cps)^{\frac{1}{2}}w^{-1}$) rather than a photodetector - for instance a PbS cell that is useable up to 3.5 μm and has a much higher $D^*(2\mu m, 250cps) \approx 10^{11} cm(cps)^{\frac{1}{2}}w^{-1}$ (Limperis (1965) - was determined mostly by historical reasons: measurements were planned at higher wavelengths. The very small responsive area of the thermopile (in our case 2 x 0.2 mm) necessitates the use of an additional mirror system behind the exit slit of the monochromator. The Cassegrainian system constructed for this purpose yields a reduction of the object (i.e. the exit slit) to the image (the responsive area of the thermopile) of a factor 5 thus fulfilling requirement (2). A disadvantage of our set-up remains, however, the more complicated piece of equipment and its adjustment.

A major advantage of thermopiles over photoconductive cells is the much higher homogeneity. As shown for instance by Limperis (p. 510 f.f.) the latter are found to be very poor in this respect which as suggested previously can be the cause of serious errors.

5.2.6. *Cryostat* (with Mr. H.R.A. Nater and Mr. J. Turenhout).

Temperature-induced changes of the optical properties at low temperature were not expected to be very drastic (see section 2.6.5.). No ex-

treme demands therefore were made regarding the lowest attainable temperature. Consequently the design of the "cold finger" type cryostat is rather standard and the description can be limited.

5.2.6.1. *Demands.*

(1) Vacuum better than 5×10^{-7} mmHg; pump-down to these pressures should be rapid.

(2) Temperature controllable between 20 and 700 K to within 1% for prolonged periods of time (10 to 16 hours).

(3) Rapid and easy mounting of specimen.

(4) Radiation shields surrounding the specimen must shield against both heat and contamination.

5.2.6.2. *Realization*[†]).

The stainless steel cryostat consists of three cylindrical vessels: an inner liquid He reservoir the contours of which are closely followed by a liquid N_2 reservoir. The outer casing of the cryostat consists of two parts: an upper part that surrounds the N_2 reservoir and a lower part that contains the optical windows. The specimen holder is suspended at the bottom of the reservoir (the so-called cold finger).

The common vacuum space is pumped through an opening (diameter 100 mm) at the bottom of the cryostat. The pumping system is close to standard. As the oil diffusion pump (Philips 250l/sec three stage fractionating plus liquid N_2 baffle) is mounted almost directly underneath the cryostat high pumping speeds are obtained. Typically in a well-cleaned cryostat that is only opened to mount a specimen (approximately 5 minutes) a vacuum of about 3×10^{-7} mmHg is reached in one or two hours. This pressure is measured by means of a Balzers IMR3 ionization gauge at the bottom of the cryostat. It can be further reduced by cryopumping.

The specimen holder has a number of special features. The back of the holder can be swung open to a horizontal position around a hinge at the bottom. The sample is laid down face-up and subsequently the back of the holder (now plus specimen) is returned to its original position. The

†) Many thanks are due to Dr. G.P. Pells for valuable suggestions and information, also during later stages of these experiments.

specimen is softly clamped against the front part of the holder by means of a tungsten spring (the use of other spring materials was prohibited because of high-temperature annealing). The mounting procedure thus takes a very short time only. Importantly very little mechanical force is exerted on the sample in this spring-loaded system; in the large temperature range of our experiments a rigid clamping system (e.g. Pells (1967)) can lead to serious strains on the specimen due to differing expansion coefficients.

The orientation of the front surface of the sample is determined by an auxiliary ring that can be positioned with three tiny screws relative to the rigid part of the holder. Thus the specimen surface can be adjusted with respect to the incident light beam. Once a correct alignment is obtained, the position of the ring is locked. Because of the spring--loaded mounting system every following sample is directly correctly positioned.

The heater - the principles and merits of which are outlined in a separate publication (Winsemius (1973a) and Lengkeek) - consists of a layer of colloidal graphite that is painted on a fused silica disc (thickness 1 mm). Initially we used Acheson "dag" 660, however, more recently we obtained excellent results with Acheson DAG S 5102-D. Due to a lower specific resistivity the layer then was painted in a zig-zag pattern. The heater is attached to the back of the specimen holder; it is electrically insulated from the specimen by another thin fused silica disc or mica. With this rather good heat contact a power of about 40 watt suffices to heat a specimen to about 800 K. Temperature is measured by means of thermocouples that are attached onto the auxiliary copper ring. Using test specimens it was found that in an equilibrium situation the temperature measurement is accurate to within 5 degrees Kelvin. Clearly there is some room for improvement here.

The specimen holder is surrounded by two copper radiation shields, one of which is attached to the reservoir and the other to the N_2 vessel. In order to mount the sample the part of both shields, that corresponds with the back of the specimen holder, is removed by a rotation around a vertical axis. Directly after mounting the shields are locked in their normal position.

In order to measure the angle of incidence (section 5.1.3.2.) we incorporated a rotating system between the top flanges of the N_2-reservoir and the outer vessel. In principle the rotation is made possible through the use of a ball bearing in V-shaped grooves that are located opposite each other in both flanges. The diameter of the balls was chosen such that the smallest of openings is left between the flanges. The vacuum seal is secured by two rubber quad-rings situated in grooves in the lower flange. A rough vacuum can be obtained between the two rings by pumping through a narrow tube that ends in the V-groove. This system - designed and constructed by Mr. E.S. Prins - allows a 360° rotation of the N_2 and He reservoirs (and thus also the specimen) around a vertical axis, while even at the best vacuum no inleak is indicated by the ionization gauge.

To increase the ease of mounting and aligning the specimen the upper part of the outer vessel (and therefore also the inner vessels) can be lifted by means of a "gallows", the position of which is shown in figure 5-1. This gallows - actually a vertical column with a horizontal arm permits a vertical movement of about 50 cm. Also it can be rotated around a vertical axis that is about 40 cm distant from the central axis of the cryostat. Thus the cryostat can be lowered to a position beside the optical table. After mounting the sample the upper part of the cryostat is re-positioned on the lower part that remained on the optical table and pump-down can start immediately. These degrees of freedom proved very helpful in actual practice.

5.2.7. *Windows.*

The windows are conventionally clamped between an O-ring (vacuum side) and a soft rubber ring (outside). With a window thickness of 2.5 mm (fused silica) and an open diameter of 22 mm the results were quite satisfactory. In various tests (with-without windows, no vacuum-vacuum) no indication was found of strain birefringence (e.g. Archer (1968, p. 12), McCrackin (1970), Azzam (1970)). The materials were selected to be free from fluorescence effects; no signs of solarization were observed (Bennett (1967), p. 47). Errors, that could not be excluded with certainty, are due to multiple reflections (Archer (1968), p. 9) and to scattering (Bennett (1947), p. 46).

5.3. *Auxiliary equipment.*

5.3.1. *Polishing apparatus* (with drs. H.P. Lengkeek).

Although occasionally alternative methods such as swab polishing (Levinstein (1962)) were used, best results were generally obtained with combined electrolytical-plus-mechanical (Reinacher (1957)) or chemical--plus-mechanical polishing. For these purposes we developed a "rotating wheel machine" that is similar in design to the acid polishing machines of Young (1961) and Dyer (1963); the adaptation of Young's machine to electrolytical polishing is described by Snouse (1965). Similar to the apparatus described by Dyer our machine has an axial tilt device to facilitate the orientation of single-crystal specimens. As the mechanical contact between sample and polishing cloth is very light only, the resulting surfaces are relatively free of dislocations, scratches, etc.. The inclusion of mechanical polishing was given in by the need of flat surfaces that are free of etch pits. As shown by Reinacher this is of special importance in the polishing of alloys.

Appendix A. *Ellipsometry.*

A.1. *Introduction.*

In actual experiments a medium will have finite dimensions and the electromagnetic radiation will be incident from another medium. To obtain information on the quantities of interest - $\tilde{\varepsilon}_r(\omega)$ or $\tilde{n}(\omega)$ - one has to study the light, that is transmitted or reflected at the boundary between the two media.

The theoretical problem is greatly simplified by assuming:

(a) the first medium is a vacuum;

(b) the second medium - the specimen - has a perfectly clean and flat surface, that has exactly the same physical properties as the "bulk" of the specimen.

For some experiments involving thin films one measures the intensity of the light that is transmitted through the sample. Since we work with non-transmitting bulk samples, however, we are only interested in suitable expressions that relate the reflected intensity (together with other measurable parameters such as the angle of incidence and the polarizer setting) to the optical properties of the metal.

A rather complete derivation of basic formulas starting from Maxwell's equations 2-1 is given by Stern (1963, chapter 2). We therefore abstain from repeating these parts and rather refer to the definitions and derivations in this review article. Due to the slightly different convention used by Stern minor deviations in the formulas are possible (see section 2.2.1.).

A.2. *Coordinate system.*

Any field vector can be resolved into a s-component that is normal to the plane of incidence and a p-component in the plane of incidence. Throughout this thesis we will use the traditional convention (Bennett (1967), p. 71) in which the direction of the polarization vector is measured by an observer, who is looking against the direction of propagation of the light. The polarization vector makes an angle ψ_p with the plane of incidence, where positive angles ψ_p are measured in a counter-clockwise direction starting from the right-hand half of the plane of incidence. In this coordinate system (with unit vectors for the incident

wave $\underline{\hat{e}}_s$, $\underline{\hat{e}}_p$ and for the reflected wave $\underline{\hat{e}}_s'$, $\underline{\hat{e}}_p'$) one can decompose a polarized vector at angle ψ_p

$$\underline{\tilde{E}}_o = \underline{\tilde{E}}_{os} + \underline{\tilde{E}}_{op} = \tilde{E}_{os}\underline{\hat{e}}_s + \tilde{E}_{op}\underline{\hat{e}}_p = \tilde{E}_o \sin\psi_p \underline{\hat{e}}_s + \tilde{E}_o \cos\psi_p \underline{\hat{e}}_p \qquad \text{(A-1)}$$

It should be pointed out, that the choice of the coordinate systems is not without criticism. Especially the direction of $\underline{\hat{e}}_p'$ has been the cause of a great deal of confusion, as a 180°-shift (i.e. "the opposite direction") is physically more plausible. More extensive treatment are found in the literature (e.g. Sokolov (1967, p. 30 f.f.), Friedmann (1965)). Many text-books use the formulae as derived here (Muller (1969a), table 6). Also azimuth circles (i.e. read-out of angular setting) of polarizers etc. usually show the same sense of rotation for incident and reflected beam. This somewhat pragmatic argument makes the alternative chosen here a strongly favored choice in the Modified Muller Nebraska Convention (section 2.1.1.).

A.3. *Amplitude reflection coefficients.*

A reflected wave (with polarization vector $\underline{\tilde{E}}_0'$) may be described in terms of the incident wave (with polarization vector $\underline{\tilde{E}}_0$) by means of the complex amplitude reflection coefficients $\tilde{r}_s$ and $\tilde{r}_p$:

$$\tilde{E}_{os}' = \tilde{r}_s \tilde{E}_{os} \quad , \quad \tilde{E}_{op}' = \tilde{r}_p \tilde{E}_{op} \quad . \qquad \text{(A-2)}$$

Generally one decomposes $\tilde{r}_s$ and $\tilde{r}_p$

$$\tilde{r}_s = r_s \exp(i\delta_s) \quad , \quad \tilde{r}_p = r_p \exp(i\delta_p) \qquad \text{(A-3)}$$

where $r_s(r_p)$ is a measure of the attenuation of the amplitude (i.e. intensity) upon reflection and $\delta_s(\delta_p)$ is the phase-shift of the s(p) component of the electric vector.

Using the boundary equations one can express $\tilde{r}_p$ and $\tilde{r}_p$ in terms of the complex relative dielectric constant $\tilde{\varepsilon}$ and the angle of incidence θ (Stern (1963), p. 320):

$$\tilde{r}_s = [\cos\theta-(\tilde{\varepsilon} - \sin^2\theta)^{\frac{1}{2}}]/[\cos\theta+(\tilde{\varepsilon} - \sin^2\theta)^{\frac{1}{2}}] \quad ,$$

$$\tilde{r}_p = [\tilde{\varepsilon}\cos\theta-(\tilde{\varepsilon} - \sin^2\theta)^{\frac{1}{2}}]/[\tilde{\varepsilon}\cos\theta+(\tilde{\varepsilon} - \sin^2\theta)^{\frac{1}{2}}] \quad \dagger) . \tag{A-4}$$

A.4. *Reflectivity.*

The light intensity of a wave was defined (eq. 2-11)

$$I = |\underline{\tilde{E}}|^2|\underline{K}_1|/2\omega\mu_0.$$

In vacuum therefore one obtains for the incident wave, using eqs. 2-2,6:

$$I = \tfrac{1}{2}(\varepsilon_0/\mu_0)^{\frac{1}{2}}(|\tilde{E}_{os}|^2 + |\tilde{E}_{op}|^2) \tag{A-5a}$$

and for the reflected wave, also using eq. A-2

$$I' = \tfrac{1}{2}(\varepsilon_0/\mu_0)^{\frac{1}{2}}(r_s^2|\tilde{E}_{os}|^2 + r_p^2|\tilde{E}_{op}|^2) \quad . \tag{A-5b}$$

Combining these equations one can define the reflectivity

$$R = I'/I \quad . \tag{A-6}$$

Substitution of eq. A-4 and $\theta = 0°$ yields the formula 2-13 for the reflectivity at normal incidence.

A.5. *Reflection of polarized light.*

In a completely unpolarized beam one places an ideal polarizer that is set to transmit at an angle ψ_p with the plane of incidence, such that the transmitted intensity

$$I(\psi_p) = \tfrac{1}{2}I \quad . \tag{A-7a}$$

For the polarization vector of the light transmitted by the polarizer, one may write

$$\underline{\tilde{E}}_0(\psi_p) = \tilde{E}_0(\psi_p)\underline{\hat{e}}(\psi_p) = \tilde{E}_0(\psi_p)\sin\psi_p\underline{\hat{e}}_s + \tilde{E}_o(\psi_p)\cos\psi_p\underline{\hat{e}}_p \quad ,$$

which shows that

$$I(\psi_p) = \tfrac{1}{2}(\varepsilon_0/\mu_0)^{\frac{1}{2}}|\tilde{E}_0(\psi_p)|^2 \quad . \tag{A-7b}$$

On reflection the s- and p-components of the amplitude are multiplied by their respective reflection coefficients. The polarization vector now becomes

$$\underline{\tilde{E}}_0'(\psi_p) = \tilde{r}_s\tilde{E}_0(\psi_p)\sin\psi_p\underline{\hat{e}}_s' + \tilde{r}_p\tilde{E}_0(\psi_p)\cos\psi_p\underline{\hat{e}}_p' \; ;$$

using eqs. A-7 the intensity after reflection of the polarized light is

$$I'(\psi_p) = \tfrac{1}{2}I[r_s^2\sin^2\psi_p + r_p^2\cos^2\psi_p] \quad . \tag{A-8}$$

Some simple relations of practical interest can be derived. When the electric field is polarized perpendicular to the plane of incidence ($\psi_p = 90°$), or in that plane ($\psi_p = 0°$), one finds from section A.4. respectively

$$R_s = \tilde{r}_s^*\tilde{r}_s = r_s^2 \qquad \text{and} \qquad R_p = \tilde{r}_p^*\tilde{r}_p = r_p^2 \quad . \tag{A-9a}$$

Thus the reflectivity of natural light can be expressed as

$$R = \tfrac{1}{2}(R_s + R_p) \quad . \tag{A-9b}$$

A.6. *Reflection in polarizer-sample-analyzer system.*

When in addition to the polarizer in the incident beam one places another polarizer - the so-called analyzer - in the reflected beam, the equations are modified again. Suppose the analyzer is set at an angle ψ_A with respect to $\underline{\hat{e}}_p'$, the direction of the transmission being indicated by the unit vector $\underline{\hat{e}}(\psi_A)$. The polarization vector of the light, that is passed by the analyzer, now is

$$\underline{\tilde{E}}_0'(\psi_p,\psi_A) = \tilde{E}_0'(\psi_p,\psi_A)\underline{\hat{e}}(\psi_A) = [\tilde{r}_s\tilde{E}_0(\psi_p)\sin\psi_p\sin\psi_A +$$

$$\tilde{r}_p\tilde{E}_0(\psi_p)\cos\psi_p\cos\psi_A]\underline{\hat{e}}(\psi_A) \quad .$$

The intensity, that is transmitted through the whole polarizer-specimen--analyzer system, therefore is

$$I'(\psi_p,\psi_A) = \tfrac{1}{2}(\varepsilon_0/\mu_0)^{\frac{1}{2}}|\tilde{E}_0(\psi_p)|^2[\tilde{r}_s^* \tilde{r}_s \sin^2\psi_p \sin^2\psi_A + \tilde{r}_p^* \tilde{r}_p \cos^2\psi_p \cos^2\psi_A$$

$$+ (\tilde{r}_s^* \tilde{r}_p + \tilde{r}_p^* \tilde{r}_s)\sin\psi_p \sin\psi_A \cos\psi_p \cos\psi_A] \quad .$$

Using eqs. A-3, 7a, 7b this expression can be simplified:

$$I'(\psi_p,\psi_A) = \tfrac{1}{2}I[r_s^2 \sin^2\psi_p \sin^2\psi_A + r_p^2 \cos^2\psi_p \cos^2\psi_A +$$

$$+ \tfrac{1}{2} r_s r_p \sin 2\psi_p \sin 2\psi_A \cos(\delta_p - \delta_s)] \quad . \qquad \text{(A-10)}$$

A.7. *Elliptic polarization.*

In the analysis of reflected light the parameter of greatest interest is the ratio of the complex amplitude reflection coefficients (eqs. A-3)

$$\tilde{r}_p/\tilde{r}_s + (r_p/r_s) \exp i(\delta_p - \delta_s) = \tan\psi \exp i\Delta \; .$$

Here we introduced the relative amplitude attenuation

$$\tan\psi = r_p/r_s \quad \text{†)} \qquad \text{(A-11a)}$$

and the relative phase change

$$\Delta = \delta_p - \delta_s \quad , \qquad \text{(A-11b)}$$

that occur for the p- and s-components of the incident light upon reflection. More specifically these two parameters determine the shape of the vibrational ellipse of the reflected light, i.e. at a given angle of incidence they contain all information on the optical properties of a specimen. For a more elaborate treatment one is referred to text-books for instance Born and Wolf (1965, p. 25 f.f., 617 f.f.).

†) Alternatively one finds in the literature: $\rho = r_p/r_s$.

A.8. *Ellipticity parameters related to* $\tilde{\varepsilon}$.

Knowledge of ψ, Δ and θ allows the determination of ε_1 and ε_2 by taking a closer look at

$$\frac{1 - (\tilde{r}_p/\tilde{r}_s)}{1 + (\tilde{r}_p/\tilde{r}_s)} = \frac{1 - \tan\psi\exp(i\Delta)}{1 + \tan\psi\exp(i\Delta)} = \frac{\cos2\psi - i\sin\Delta\sin2\psi}{1 + \cos\Delta\sin2\psi} .$$

However, using eqs. A-4 one can also write

$$\frac{1 - (\tilde{r}_p/\tilde{r}_s)}{1 + (\tilde{r}_p/\tilde{r}_s)} = \frac{(\tilde{\varepsilon} - \sin^2\theta)^{\frac{1}{2}}}{\sin\theta\tan\theta} .$$

Equating real and imaginary parts of these expressions yields

$$\varepsilon_1 = n^2 - k^2 = \sin^2\theta\tan^2\theta \, \frac{\cos^2 2\psi - \sin^2\Delta\sin^2 2\psi}{(1+\cos\Delta\sin2\psi)^2} + \sin^2\theta \quad , \quad \text{(A-12a)}$$

$$\varepsilon_2 = 2nk = \sin^2\theta\tan^2\theta \, \frac{\sin\Delta\sin4\psi}{(1+\cos\Delta\sin2\psi)^2} . \quad \text{(A-12b)}$$

Alternatively the optical properties can also be used to calculate the "ellipticity" parameters. To simplify the calculation Pfeiffer (König; 1928) substituted

$$(\tilde{\varepsilon} - \sin^2\theta)^{\frac{1}{2}} = a - ib \quad ,$$

which is equivalent to

$$\varepsilon_1 = a^2 - b^2 + \sin^2\theta \quad , \qquad \varepsilon_2 = 2ab.$$

Eq. A-4 now becomes

$$\tilde{r}_s = r_s\exp i\delta_s = r_s\cos\delta_s + ir_s\sin\delta_s = (\cos\theta - a + ib)/(\cos\theta + a - ib),$$

which gives the prompt results

$$\tan\delta_s = \frac{-2b\cos\theta}{a^2 + b^2 - \cos^2\theta} , \quad \text{(A-13a)}$$

$$R_s = \tilde{r}_s^* \tilde{r}_s = \frac{a^2 + b^2 + \cos^2\theta - 2a\cos\theta}{a^2 + b^2 + \cos^2\theta + 2a\cos\theta} \quad . \tag{A-13b}$$

Similarly one obtains the somewhat more complicated formulas

$$\tan\delta_p = \frac{-2b\cos\theta(a^2+b^2-\sin^2\theta)}{[(a^2-b^2+\sin^2\theta)^2+4a^2b^2]\cos^2\theta-(a^2+b^2)} \quad , \tag{A-14a}$$

$$R_p = \tilde{r}_p^* \tilde{r}_p = \frac{[(a^2-b^2+\sin^2\theta)^2+4a^2b^2]\cos^2\theta-2a(a^2+b^2+\sin^2\theta)\cos\theta+a^2+b^2}{[(a^2-b^2+\sin^2\theta)^2+4a^2b^2]\cos^2\theta+2a(a^2+b^2+\sin^2\theta)\cos\theta+a^2+b^2} \quad , \tag{A-14b}$$

and

$$\tan\Delta = \frac{-2b\sin\theta\tan\theta}{a^2 + b^2 - \sin^2\theta\tan^2\theta} \quad , \tag{A-15a}$$

$$R_p/R_s = \frac{(a - \sin\theta\tan\theta)^2 + b^2}{(a + \sin\theta\tan\theta)^2 + b^2} \quad . \tag{A-15b}$$

Numerical calculations of the interrelationship between the ellipticity parameters and the optical properties have been published in tabulated and graphical form by Holl (1963, 1967). Obviously it also is possible to determine the "ellipticity" parameters from known values of the optical properties.

Appendix B. *Calibration procedure of the Kipp Model L35 monochromator* (with drs. S.N.M. Ruysenaars).

The optical system of the Kipp monochromator is such that only the rays, which have traversed the prisms at minimum deviation, pass through the exit slit. If 2ϕ is the refracting angle of the prism and the (wavelength dependent) minimum deviation is $2\delta(\lambda)$, then the angle of incidence of a parallel beam on the prism is $\phi + \delta(\lambda)$ (Born (1965) and Wolf, p. 178 f.f.). The prism tables are simultaneously rotated by means of a spindle in such a way that a drum read-out D may be assumed to be linearly proportional to the angular position of the tables, i.e. to $\phi + \delta(\lambda)$ †). An increase in D corresponds to a decrease in $\delta(\lambda)$:

$$C_6 - C_7 D = \phi + \delta(\lambda). \qquad \text{(B-1)}$$

C_6 is the angle of incidence of the beam at drum-setting D = 0, and C_7 is a constant representing the mechanical coupling of drum and prism table.

Writing the condition for minimum deviation

$$\sin[\phi + \delta(\lambda)]/\sin\phi = n(\lambda)$$

($n(\lambda)$: refractive index of the prism material)

and introducing $C_8 = \sin\phi$, i.e. another apparatus constant, one obtains

$$D = \{C_6 - \arcsin[n(\lambda)C_8]\}/C_7 . \qquad \text{(B-2)}$$

This same procedure was followed by Ho (1971).

In order to relate the drum reading D to the wavelength λ of the passed light, it now suffices to substitute in eq. B-2 the appropriate

†) In fact, as a translational movement of the (horizontal) drum spindle is converted into a rotational movement of the prism tables (around a vertical axis), the proportionality between D and the angular position of the prism tables is not exactly linear, a deviation being noticeable in the ultraviolet. However, the corresponding deviation in the photon energy is found to be less than 0.004 eV, i.e. smaller than the demanded accuracy (section 5.1.5.). The use of the exact formulas - although possible in principle - is much more complicated.

dispersion formula of the prism material. For a number of prism materials these formulas, relating n to λ, are given in the literature (Streiff (1965), Ho (1971)). However, little is known about the temperature dependence of the dispersion. We therefore used the procedure described by Fryer (1967) who substituted an adapted version of Selmeier's dispersion formula (e.g. Born (1965) and Wolf, p. 94 f.f.)

$$n^2 = C_5 + C_1\lambda^2/(\lambda^2 - C_2) + C_3\lambda^2/(\lambda^2 - C_4) \ . \qquad \text{(B-3)}$$

This formula is a good approximation if λ is not too close to the mean wavelength of the neighboring absorption bands respectively $\lambda_{uv} = C_2^{\frac{1}{2}}$ and $\lambda_{ir} = C_4^{\frac{1}{2}}$. Combination of eqs. B-2,3 gives the desired relation between D and λ:

$$D = \{C_6 - \arcsin\{C_8[C_5 + C_1\lambda^2/(\lambda^2 - C_2) + C_3\lambda^2/(\lambda^2 - C_4)]^{\frac{1}{2}}\}\}/C_7 \qquad \text{(B-4)}$$

Through inversion one obtains an expression for λ as a function of D.

Eq. B-4 contains eight constants: C_{1-5} originating from the dispersion formula B-3 and C_{6-8} because of the specific mechanism of the monochromator (rotation prism table, shape of the prisms). These parameters now should be adapted in such a way that eq. B-4 gives a best fit to a number of experimental calibration points. For this purpose Fryer used a least-squares estimation of non-linear parameters, i.e. the constants are adjusted to minimize squares of the errors in the fit. An algorithm for this estimation is given by Marquardt (1963); a computer program written in Fortran IV G by Baumeister and Marquardt - available from the IBM Share Library (T. Baumeister III, D.W. Marquardt; "Least Squares Estimation of Nonlinear Parameters", IBM Share Library Program Number 7040-G2 3094) - requires only minor adaptations. Estimates of the constants C_1, C_2, C_3, C_4 may be deduced from a graph where one plots n^2 vertically versus λ^2 horizontally, using the values of n and λ derived from a rough recalculation of experimental calibration points. According to eq. B-3 one now is able to decompose this "experimental" curve in an ultraviolet term and an infrared term (e.g. Born and Wolf). The ultraviolet term has as horizontal and vertical asymptotes C_1 resp. C_2; the

infrared term C_3 and C_4. These values admittedly are crude, however as pointed out by Fryer, the convergency of the approximation is such that they may differ by a factor ten of the final values found by the computer. From classical dispersion theory an initial value $C_5 = 1$ is reasonable.

Three prism sets were available with the Kipp-monochromator: natural quartz, flint glass and NaCl. The initial values of C_6 were estimated from rough measurements; C_7 was determined with the aid of a number of microscope readings of the rotation of the first prism table (accuracy about 30 seconds of arc). Values of C_8 of course can be calculated from data given by the manufacturer; due to repolishing of the prisms (a.o. because of the hygroscopic nature of the NaCl) these values are not completely accurate.

Calibration points were taken over the wavelength-region of interest by means of a number of spectral lamps, mainly making use of the identifications by Zwerdling (1961) and also with the aid of a calibrated grating-monochromator (McPherson Model 218) in series with the Kipp monochromator. This proved to be very helpful in obtaining reliable calibration points in regions of few spectral lines (e.g. the near infrared). As an example in the case of quartz 134 calibration points were taken at wavelengths between 0.2265 and 2.750 μm; for flint glass 83 points between 0.4358 and 1.7 μm. In principle the computer iteration can be carried on until the accuracy of the fit is sufficient, that is until the standard deviation of the residuals is sufficiently small. More detailed information in this regard is given by Fryer.

Results obtained for quartz indicated that nearly all calibration points are within the bounds set by the requirement of $\Delta(\hbar\omega) < 0.005$ eV (section 5.2.4.1.). A few points in the region of lowest dispersion ($\lambda \approx 1$ μm) did not fulfil the requirement and were subsequently discarded. In this wavelength region the deviation between the experimental calibration curve and the computer fit is smaller than 0.004 eV. This value is smaller yet in the ultraviolet and especially in the infrared range.

As pointed out by Ho an important advantage of this calibration procedure is due to the linearity of eq. B-1. Suppose the calibrated monochromator is set to transmit light of wavelength $\lambda(1)$. The drum setting

then is T(1), the minimum deviation $\delta(1)$, and the angle of incidence of the beam on the prism is $\phi + \delta(1)$. If the prisms now are temporarily removed from the monochromator, a non-perfect kinematic mounting might cause the angle of incidence to become $\phi + \delta(2)$. At the same T(1) the prism passes another wavelength $\lambda(2)$ that corresponds to minimum deviation $\delta(2)$. In order to transmit the original $\lambda(1)$ again the prism has to be rotated until the angle of incidence is $\phi + \delta(1)$ once more. The drum-setting then is T(2) however. Both C_7 and ϕ are apparatus constants. From eq. B-1 it is obvious, that C_6 (the angle of incidence at T = 0) has changed:

$$C_6(2) - C_6(1) = C_7[T(2) - T(1)] .$$

On remounting the prisms one calibration point will suffice to obtain the corrected value of C_6. All values of T are simply shifted by an amount $\Delta C_6/C_7$.

Comments.

This computer calibration method offers a number of significant advantages over the more conventional graphical methods. In order to be sufficiently accurate a calibration graph becomes excessively large. Requiring an accuracy of the reading of photon energy of better than 0.005 eV and of the drum-setting of 0.01 drum numbers (the total wavelength region of a set of prisms is covered by about 40 drum numbers) a plot of D versus photon energy typically would be 4 x 1.2 m. Reading errors will produce random errors. Fryer claims an increase in accuracy by as much as an order of magnitude over that of the graphical method. All information on the calibration is stored in eight parameters. With the aid of an auxiliary computer program the calibration data can be printed, giving the wavelength or the photon energy of the transmitted light for any desired spacing of drum number.

However, in our opinion the main advantage of our method over those that make use of dispersion values from the literature (e.g. Sidran (1966), Ho (1971)) or those that employ empirical means to obtain a relation between the drum-setting D and the refractive index n (e.g. Fryer (1967) plus references cited here) is that it yields results that are representative for the specific monochromator at the specific circumstances that it is used.

References.

Abelès, F. (editor)(1966); "Optical Properties and Electronic Structure of Metals and Alloys" (North-Holland, Amsterdam; 1966).

Abelès, F. (1966a); in Abelès (1966) p. 533.

Abelès, F.; 1966b, J. Phys. 27, C2-72.

Abelès, F. (editor)(1972); "Optical Properties of Solids" (North-Holland, Amsterdam; 1972).

Abelès, F. (1972a); in Abelès (1972), p. 93.

Agranovich, V.M., Ginzburg, V.L.; "Spatial Dispersion in Crystal Optics and the Theory of Excitations" (Interscience, London; 1966).

Altmann, S.L.; "Band Theory of Metals, The Elements" (Pergamon, Oxford; 1970).

Andersen, O.K.; 1971, Phys. Rev. B2, 883.

Antonangeli, F., Grassano, U.M., Rosei, R.; 1973, Istituto di Fisica G. Marconi (University of Rome), Rept. No. 433.

Archard, J.F., Taylor, A.M.; 1948, J. Sci. Instrum. 25, 407.

Archard, J.F., Clegg, P.L., Taylor, A.M.; 1952, Proc. Phys. Soc. B65, 758.

Archer, R.J. (1968); "Manual on Ellipsometry" (Gaertner, Chicago; 1968).

Avery, D.G.; 1952, Proc. Phys. Soc. B65, 425.

Azzam, R.M.A., Bashara, N.M.; 1971, J. Opt. Soc. Am. 61, 600, 773.

Baldini, G., Nobile, M.; 1970, Solid State Comm. 8, 7.

Ballinger, R.A., Marshall, C.A.W.; 1969, J. Phys. C2, 1822.

Bardeen, J., Shockley, W.; 1950, Phys. Rev. 80, 72.

Bassani, G.F. (1966); in Tauc (1966), p. 33.

Batz, B. (1972); in Willardson (1972), p. 315.

Beaglehole, D.; 1965, Proc. Phys. Soc. 85, 1007.

Beaglehole, D.; 1966a, Proc. Phys. Soc. 87, 461.

Beaglehole, D. (1966b); in Abelès (1966), p. 175.

Beaglehole, D.; 1968, Appl. Optics 7, 2218.

Beaglehole, D., Hendrickson, T.J.; 1969, Phys. Rev. Letters 22, 133.

Beaglehole, D., Erlbach, E.; 1972, Phys. Rev. B6, 1209.

Beaglehole, D., Erlbach, E.; 1970, Solid State Comm. 8, 255.

Beattie, J.R., Conn, G.K.T.; 1955a, Phil. Mag. 46, 222.

Beattie, J.R.; 1955b, Phil. Mag. 46, 235.

Bedeaux, D., Vlieger, J.; 1973, Physica, to be published.

Bell, E.E. (1967); in "Handbuch der Physik", Vol. XXV/2a: "Licht und Materie Ia" (ed. L. Genzel; Springer, Berlin; 1967), p. 1.

Bennett, H.E., Porteus, J.O.; 1961, J. Opt. Soc. Am. 51, 123.

Bennett, H.E., Bennett, J.M. (1966); in Abelès (1966a), p. 175.

Bennett, H.E.; 1966a, Appl. Optics 5, 1265.

Bennett, H.E., Bennett, J.M. (1967); in "Physics of Thin Films" (ed. G. Hass, R.E. Thun; Academic, New York; 1967), Vol. IV, p. 1.

Bennett, H.E., Bennett, J.M., Ashley, E.J., Motyka, R.J.; 1968, Phys. Rev. 165, 755.

Bennett, L.H. (editor) (1971); "Electronic Density of States" (Nat. Bur. Stand. (U.S.), Special Publ. 323, Dec. 1971).

Berglund, C.N., Spicer, W.E.; 1964, Phys. Rev. 136, A1044.

Berreman, D.W.; 1970a, Phys. Rev. B1, 381.

Berreman, D.W.; 1970b, J. Opt. Soc. Am. 60, 499.

Bhatnagar, S.; 1969, Phys. Rev. 183, 657.

Bispinck, H.; 1970, Z. Naturforsch. 25a, 70.

Boerstoel, B.M., Zwart, J.J., Hansen, J.; 1971, Physica 54, 442.

Böhme, H.; 1968, Z. angew. Phys. 25, 208.

Born, M., Wolf, E. (1965); "Principles of Optics" (Pergamon, Oxford; 3rd ed., 1965).

Bousquet, P. (1971); "Spectroscopy and Its Instrumentation" (Hilger, London; 1971).

Bowlden, H.J., Wilmshurst, J.K.; 1963, J. Opt. Soc. Am. 53, 1073.

Bradford, A.P., Hass, G.; 1963, J. Opt. Soc. Am. 53, 1096.

Bradford, A.P., Hass, G., McFarland, M., Ritter, E.; 1965, Appl. Optics 4, 971.

Bradford, A.P., Hass, G., Heaney, J.B., Triolo, J.J.; 1970, Appl. Optics 9, 339.

Breeze, R.H., Ke, B.; 1972, Rev. Sci. Instrum. 43, 82.

Brown, H.R., Morgan, G.J.; 1971, J. Phys. F1, 132.

Buckman, A.B., Bashara, N.M.; 1968, Phys. Rev. 174, 719.

Callaway, J. (1964); "Energy Band Theory" (Academic, New York; 1964).

Cann, M.W.P.; 1967, NASA Report CR-854 (August 1967).

Cann, M.W.P.; 1969, Appl. Optics 8, 1645.

Cardona, M. (1969); "Modulation Spectroscopy" (Solid State Physics, Suppl. 11, Academic, New York; 1969).

Carlan, A.; 1969, Ann. Phys. 4, 5.

Chatterjee, S., Sen, S.K.; 1966, Proc. Phys. Soc. 87, 779.

Chatterjee, S., Sen, S.K.; 1967a, Proc. Phys. Soc. 91, 749.

Chatterjee, S., Chakraborty, D.K.; 1967b, Indian J. Phys. 41, 134.

Chatterjee, S., Sen, S.K.; 1968, J. Phys. C1, 759.

Cheyssac, P., Garrigos, R., Kofman, R., Pénavaire, L., Richard, J., Saïssy, A.; 1972, Thin Solid Films 13, 275.

Cheyssac, P., Garrigos, R., Kofman, R., Pénavaire, L., Richard, J., Saïssy, A. (1973); in Seraphin (1973).

Ching, W.Y., Callaway, J.; 1973, Phys. Rev. Letters 30, 441.

Christensen, N.E.; 1969, Phys. Stat. Sol. (b) 31, 635.

Christensen, N.E., Seraphin, B.O.; 1970a, Solid State Comm. 8, 1221.

Christensen, N.E.; 1970b, thesis (Technical University of Denmark, Lyngby, Report No. 75).

Christensen, N.E., Seraphin, B.O.; 1971, Phys. Rev. B4, 3321.

Christensen, N.E.; 1972a, Phys. Stat. Sol. (b) 52, 241; 1972, Technical University of Denmark, Lyngby, Report No. 101.

Christensen, N.E.; 1972b, Phys. Stat. Sol. (b) 54, 551.

Christensen, R.L., Potter, R.J.; 1963, Appl. Optics 2, 1049.

Conn, G.K.T., Eaton, G.K.; 1954, J. Opt. Soc. Am. 44, 484.

Conn, G.K.T., Avery, D.G. (1960); "Infrared Methods" (Academic, New York; 1960).

Connolly, J.W.D., Johnson, K.H.; 1970, M.I.T. Solid-State and Molecular Theory Group Semi-Annual Progress Report No. 72 (Jan. 15, 1970), p. 19.

Cooper, B.R., Ehrenreich, H., Philipp, H.R.; 1965, Phys. Rev. 138, A494.

Cooper, B.R., Kreiger, E.L., Segall, B.; 1969, Phys. Letters 30A, 333.

Cooper, B.R., Kreiger, E.L., Segall, B.; 1971, Phys. Rev. B4, 1734.

Cottin, N., Wolter, H.; 1967, Z. Physik 204, 474.

Corruccini, R.J., Gniewek, J.J.; 1961, Nat. Bur. Stand. Monograph 29.

Cremer, E., Pulker, H.; 1962, Monatsh. Chem. 93, 491.

Das, S.G.; 1973, Phys. Rev. B7, 2238.

Daudé, A., Savary, A., Robin, S.; 1972, J. Opt. Soc. Am. 62, 1.

Davis, H.L., Faulkner, J.S., Joy, H.W.; 1968, Phys. Rev. 167, 601.

De Chatel, P.F.; 1970, Solid State Comm. 8, 1807.

Decker, D.L., Stanford, J.L.; 1971, J. Opt. Soc. Am. 61, 679A.

Devant, G., Theye, M.-L.; 1967, Proc. 2nd Coll. on Thin Films, Budapest, p. 306.

Dignam, M.J., Moskowits, M.; 1970, Appl. Optics 9, 1868.

Dobberstein, P., Hampe, A., Sauerbrey, G.; 1968, Phys. Letters 27A, 256.

Dold, B.; 1965, Optik 22, 519.

Dresselhaus, G., Dresselhaus, M.S., Beaglehole, D. (1971); in Bennett (1971), p. 33.

Drude, P. (1959); "The Theory of Optics" (Dover, New York, 1959).

Dujardin, M.-M., Theye, M.-L.; 1971, J. Phys. Chem. Solids 32, 2033.

Dyer, L.D.; 1963, Rev. Sci. Instrum. 34, 1114.

Eastman, D.E., Cashion, J.K.; 1970, Phys. Rev. Letters 24, 310.

Eastman, D.E.; 1971, Phys. Rev. Letters 26, 1108.

Eastman, D.E., Grobman, W.D.; 1972, Phys. Rev. Letters 28, 1327.

Eastman, D.E. (1972a); in "Measurements of Physical Properties, Part 1: Some Special Properties" (ed. E. Passoglia; Wiley, New York; 1972), p. 411.

Economou, E.N.; 1969, Phys. Rev. 182, 539.

Ehrenreich, H., Cohen, M.H.; 1959, Phys. Rev. 115, 786.

Ehrenreich, H., Philipp, H.R.; 1962, Phys. Rev. 128, 1622.

Ehrenreich, H., (1966); in Tauc (1966), p. 106.

Elson, J.M., Ritchie, R.H.; 1971, Phys. Rev. B4, 4129.

Endriz, J.G., Spicer, W.E.; 1971, Phys. Rev. B4, 4144, 4159.

Erlbach, E., Beaglehole, D. (1971); in L.H. Bennett (1971), p. 545.

Fan, H.Y. (1959); in "Methods of Experimental Physics", Vol. 6 Solid State Physics Part B (ed. K. Lark-Horovitz, V.A. Johnson; Academic, New York; 1959), p. 249.

Fane, R.W., Neal., W.E.J.; 1968, Proc. 4th Int. Vacuum Congress.

Feinleib, J.; 1966, Phys. Rev. Letters 16, 1200.

Flaten, C.J., Stern, E.A.; 1973, to be published.
Fletcher, G.C. (1971); "The Electron Band Theory of Solids" (North-Holland, Amsterdam; 1971).
Fong, C.Y., Cohen, M.L., Zucca, R.R.L., Stokes, J., Shen, Y.R.; 1970, Phys. Rev. Letters 25, 1486.
Friedel, J. (1972); in Abelès (1972), p. 1.
Friedman, G., Sandhu, H.S.; 1965, Am. J. Phys. 33, 135.
Fryer, R.E.; 1967, Appl. Optics 6, 275.
Fukutani, H., Sueoka, O. (1966); in Abelès (1966), p. 565.
Fukutani, H., Kuwabara, G.; 1972, J. Phys. Soc. Japan 33, 989.
Fukutani, H.; 1971, J. Phys. Soc. Japan 30, 399.

Galeener, F.L.; 1971, Phys. Rev. Letters 27, 421.
Garfinkel, M., Tiemann, J.J., Engeler, W.E.; 1966, Phys. Rev. 148, 695.
Garski, H.; 1964, Z. Naturforsch. 19A, 1219.
Gerhardt, U.,; 1968, Phys. Rev. 172, 651.
Givens, M.P.; 1958, Solid State Phys. 6, 313.
Graves, R.H.W.; 1971, Appl. Optics 10, 2679.
Green, E.L.; 1965, Frankford Arsenal Rept. R-1765 (Frankford Arsenal, Philadelphia, Pa.).
Green, E.L., Muldawer, L.; 1970, Phys. Rev. B2, 330.
Grobman, W.D., Eastman, D.E.; 1972, Phys. Rev. Letters 28, 1038.
Gurzhi, R.N.; 1966, Sov. Phys. JETP 22, 654.

Haas, H.; 1968, Feingerätetechnik 17, 6.
Haga, E., Okamoto, H.; 1965, J. Phys. Soc. Japan 20, 1610.
Hagstrum, H.D. (1971); in Bennett (1971), p. 349.
Haidemenakis, E.D. (editor) (1970); "Optical Properties of Solids" (Gordon and Breach, New York; 1970).
Haneman, D.; 1961, Phys. Rev. 121, 1093.
Ho, S.-Y.; 1971, Appl. Optics 10, 584.
Hodgkinson, I.J.; 1970, Appl. Optics 9, 1577.
Hodgson, J.N.; 1955, Proc. Phys. Soc. B68, 593.
Hodgson, J.N.; 1968, J. Phys. Chem. Solids 29, 2175.
Hodgson, J.N. (1970); "Optical Absorption and Dispersion in Solids (Chapman and Hall, London; 1970).

Holl, H.B.; 1963, U.S. Army Missile Command, Red Stone Arsenal, Alabama; Rept. No. RF-TR-63-4; March 15, 1963, Vol. I, II.

Holl, H.B.; 1967, J. Opt. Soc. Am. 57, 683.

Holstein, T.; 1954, Phys. Rev. 96, 535.

Hopfield, J.J.; 1965, Phys. Rev. 139, A419.

Huebner, R.H., Arakawa, E.T., Hamm, R.N., MacRae, R.A.; 1965, Oak Ridge National Laboratory Rept. No. ORNL-TM-1104.

Hüfner, S., Wertheim, G.K., Smith, N.V., Traum, M.M.; 1972, Solid State Comm. 11, 323.

Hummel, R.E. (1971); "Optische Eigenschaften von Metallen und Legierungen" (Springer, Berlin; 1971).

Humphreys-Owen, S.P.F.; 1961, Proc. Phys. Soc. 77, 949.

Hunderi, O., Beaglehole, D.; 1970, Phys. Rev. B2, 321.

Hunderi, O.; 1973a, Solid State Comm. 12, 237.

Hunderi, O.; 1973b, Phys. Rev. B7, 3419.

Hunderi, O., Myers, H.P.; 1973c, to be published.

Hunter, W.R.; 1965, J. Opt. Soc. Am. 55, 1197.

Irani, G.B., Huen, T., Wooten, F.; 1971a, J. Opt. Soc. Am. 61, 128.

Irani, G.B., Huen, T., Wooten, F.; 1971b, Phys. Rev. B3, 2385.

Irani, G.B., Huen, T., Wooten, F.; 1972, Phys. Rev. B6, 2904.

Jacobs, R.L.; 1968, J. Phys. C1, 1296, 1307.

Jasperson, S.N., Schnatterley, S.E.; 1969, Phys. Rev. 188, 759.

Johnson, P.B., Christy, R.W.; 1972, Phys. Rev. B6, 4370.

Joos, G., Klopfer, A.; 1954, Z. Physik 138, 251.

Kane, E.O.; 1966, Phys. Rev. 146, 558.

Kasowski, R.V.; 1969, Phys. Rev. 187, 885, 891.

Kennard, E.B., Koskimaki, D., Waber, J.T., Mueller, F.M. (1971); in Bennett (1971), p. 795.

Kern, J.; 1954, Z. angew. Phys. 6, 536.

Kittel, C. (1968); "Introduction to Solid State Physics" (Wiley, New York; 3rd ed., 1968).

Kofman, R., Richard, J., Saïssy, A.; 1972, Solid State Comm. 10, 1237.

König, W. (1928); in "Handbuch der Physik" (ed. H. Geiger, K. Scheel; Springer, Berlin; 1928), Vol. 20, p. 242.

Köster, W., Stahl, R.; 1967, Z. Metallkde 58, 768.

Kostyuk, V.P., Shkliarevskii, I.N.; 1970, Opt. and Spectrosc. 29, 102.

Koyama, R.Y., Smith, N.V.; 1970, Phys. Rev. B2, 3049.

Kretschmann, E.; 1969a, Z. Physik 221, 357.

Kretschmann, E.; 1969b, Z. Physik 227, 412.

Kronig, R. de L.; 1929, Proc. Roy. Soc. A124, 409.

Kronig, R. de L.; 1931, Proc. Roy. Soc. A133, 255.

Kupratakuln, S., Fletcher, G.C.; 1969, J. Phys. C2, 1886.

Kupratakuln, S.; 1970, J. Phys. F3, 109.

Landau, L.D., Lifshitz, E.M. (1960); "Electrodynamics of Continuous Media" (Pergamon, Oxford; 1960).

Latyev, L.N., Chekhovskoi, V.Ya., Shestakov, E.N.; 1970, Phys. Stat. Sol. 38, K149.

Lavin, E.P. (1971); "Specular Reflection" (Hilger, London; 1971).

Lenham, A.P., Treherne, D.M.; 1966, J. Opt. Soc. Am. 56, 1076.

Lenham, A.P.; 1967a, J. Opt. Soc. Am. 57, 473.

Lenham, A.P., Treherne, D.M.; 1967b, J. Opt. Soc. Am. 57, 476.

Lengkeek, H.P., Winsemius, P.; 1973, to be published.

Lettington, A.H. (1966); in Abelès (1966), p. 147.

Levinstein, H.J., Robinson, W.H.; 1962, J. Appl. Phys. 33, 3149.

Lewis, P.E., Lee, P.M.; 1968, Phys. Rev. 175, 795.

Liljenvall, H.G., Mathewson, A.G.; 1970a, Appl. Optics 9, 1489.

Liljenvall, H.G., Mathewson, A.G.; 1970b, J. Phys. C3, Suppl. Metal Phys. S341.

Limperis, T. (1965); in "Handbook of Military Infrared Technology" (ed. W.L. Wolfe, U.S. Government Printing Office, Washington; 1965), Chapter 11.

Liebmann, P.A., Entine, G.; 1969, Appl. Optics 8, 1502.

Lindau, I., Nilsson, P.-O.; 1970, Phys. Letters 31A, 352.

Lindau, I., Walldèn, L.; 1971a, Solid State Comm. 8, 1147.

Lindau, I., Walldèn, L.; 1971b, Physica Scripta 3, 77.

Lindau, I., Nilsson, P.-O.; 1971c, Physica Scripta 3, 87.
Lindau, I., Wilson, L.; 1972, Phys. Letters 42A, 279.
Loescher, D.H.; 1971, Appl. Optics 10, 1031.
Lorentz, H.A. (1935); "H.A. Lorentz, Collected Papers" (editors P.A. Zeeman, A.D. Fokker; Nijhoff, The Hague; 1935).
Loucks, T.L. (1967); "Augmented Plane Wave Method" (Benjamin, New York; 1967).

Margenau, H.; 1929, Phys. Rev. 33, 1035.
Marquardt, D.W.; 1963, J. Soc. Industr. Appl. Math. 11, 431.
Martin, D.L.; 1968, Phys. Rev. 170, 650.
Mathewson, A.G., Aronsson, H., Bernland, L.G.; 1972, J. Phys. F2, L39.
Matsuoka, M., Brown, F.; 1969, Bull. Am. Phys. Soc. 14, 27.
Mayer, H., Hietel, B. (1966); in Abelès (1966), p. 47.
Mayer, H., Hietel, B.; 1972, Z. Physik 254, 232.
McCrackin, F.L.; 1970, J. Opt. Soc. Am. 60, 57.
Melnyk, A.R., Harrison, M.J.; 1970, Phys. Rev. B2, 835, 851.
Meessen, A,; 1968, Ann. Soc. Sci. Bruxelles 82, 315.
Meessen, A.; 1972, J. Phys. 33, 371.
Miller, J.C.; 1969, Phil. Mag. 20, 1115.
Miller, R.F., Taylor, A.J., Julien, L.S.; 1970, J. Phys. D3, 1957.
Miller, R.F., Julien, L.S., Taylor, A.J.; 1971, J. Phys. D4, 1100.
Miloslavskii, V.K., Yarovaya, R.G.; 1966, Opt. and Spectroscop. 21, 388.
Miloslavskii, V.K.; 1967, Sov. Phys. Solid State 8, 1633.
Mitra, T.K.; 1969, J. Phys. C2, 52.
Mohler; 1931, Bur. Stand. J. Res. 8, 357.
Moore, A.J.W. (1963); in "Metal Surfaces" (ed. W.D. Robertson, N.A. Gjostein; American Society for Metals, Metals Park, Ohio; 1963), Chapter 5.
Morgan, R.M., Lynch, D.W.; 1968, Phys. Rev. 172, 628.
Morris, C.E., Lynch, D.W.; 1969, Phys. Rev. 182, 719.
Mott, N.F., Jones, H. (1958); "The Theory of the Properties of Metals and Alloys" (Dover, New York; 1958).
Motulevitch, G.P.; 1967, Sov. Phys. JETP 24, 1287.

Motulevitch, G.P.; 1969, Sov. Phys. Uspekhi 12, 80.
Mueller, F.M., Phillips, J.C.; 1967, Phys. Rev. 157, 600.
Muller, R.H.; 1969a, Surface Sci. 16, 14.
Muller, R.H., Steiger, R.F., Somorjai, G.A., Morabito, J.M.; 1969b, Surface Sci. 16, 234.
Myers, H.P., Walldèn, L., Karlsson, A.; 1968, Phil. Mag. 18, 725.

Nagasima, N.; 1972, J. Appl. Phys. 43, 3378.
Nilsson, P.-O., Persson, A., Nordén, H.; 1967, Ark. Fysik 35, 165.
Nilsson, P.-O.; 1968, Appl. Optics 7, 435.
Nilsson, P.-O., Norris, C., Walldèn, L.; 1969, Solid State Comm. 7, 1705.
Nilsson, P.-O.; 1970a, Phys. Kondens, Mat. 11, 1.
Nilsson, P.-O., Norris, C., Walldèn, L.; 1970b, Phys. Kondens. Mat. 11, 220.
Nilsson, P.-O., Sandell, B.; 1970c, Solid State Comm. 8, 721.
Nilsson, P.-O. (1970d); in Haidemenakis (1970), p. 145.
Nilsson, P.-O., Eastman, D.E.; 1973a, to be published.
Nilsson, P.-O.; 1973b, Solid State Phys., to be published.
Nilsson, P.-O.; et al.; 1973c, EPS Conf. on Disordered Metallic Systems, Strasbourg, France; private communication.
Nix, F.C., MacNair, D.; 1941, Phys. Rev. 60, 597.
Nudelman, S., Mitra, S.S. (editors)(1969); "Optical Properties of Solids" (Plenum, New York; 1969).

O'Shea, K.R., Fane, R.W.; 1972, Solid State Comm. 10, 1185.
O'Sullivan, W.J., Switendick, A.C., Schirber, J.E.; 1970, Phys. Rev. B1, 1443.
Otter, M.; 1961a, Z. Physik 161, 163.
Otter, M.; 1961b, Z. Physik 161, 539.

Paasch, G., Eschrig, H., John, W.; 1972, Phys. Stat. Sol. (b) 51, 283.
Palmer, R.E., Schnatterley, S.E.; 1971, Phys. Rev. B4, 2329.
Palmer, R.E.; 1972, J. Opt. Soc. Am. 62, 144.
Pandey, H.D., Dayal, B.; 1964, Phys. Stat. Sol. 5, 273.
Parsons, B.J.; 1969, Phys. Rev. 182, 975.

Pells, G.P.; 1967, J. Sci. Instrum. 44, 997.
Pells, G.P., Shiga, M.; 1969, J. Phys. C2, 1835.
Pennington, J.V.; 1932, Phys. Rev. 39, 953.
Philipp, H.R.; 1971, J. Phys. Chem. Solids 32, 1935.
Phillips, J.C.; 1966, Solid State Phys. 18, 55.
Phillips, J.C.; 1968, J. Appl. Phys. 39, 755.
Pitz, E.; 1969, Appl. Optics 8, 255.
Potter, R.F.; 1964, J. Opt. Soc. Am. 54, 904.
Powell, C.J.; 1970, J. Opt. Soc. Am. 60, 78.
Prishivalko, A.P.; 1961, Opt. and Spectrosc. 11, 131.

Ramchandani, M.G.; 1970, J. Phys. C3 Suppl. Metal Phys. No. 1, S1.
Ramchandani, M.G.; 1971, J. Phys. F3, 169.
Rasigni, M., Rasigni, G.; 1972, C.R. Acad. Sci. Paris B275, 955.
Rayne, J.A.; 1961, Phys. Rev. 121, 456.
RCA Multiplier Manual (1970); RCA Technical Series PT-61 (RCA, Harrison, N.J.; 1970).
Reinacher, G.; 1957, Z. Metallkde 48, 162.
Ripken, K.; 1972, Physik 250, 228.
Roberts, S.; 1955, Phys. Rev. 100, 1667.
Roberts, S.; 1959, Phys. Rev. 114, 104.
Roberts, S.; 1960, Phys. Rev. 118, 1509.
Roberts, S.; 1964, Misc. Publ. Nat. Bur. Stand. 256, 119.
Rosei, R., Lynch, D.W.; 1972, Phys. Rev. b5, 3883.
Rosei, R., Antonangeli, F., Grassano, U.M. (1973); in Seraphin (1973).
Rouard, P., Bousquet, P.; 1969, Optica Acta 16, 675.

Sak, J.; 1968, Phys. Stat. Sol. 25, 155.
Samuels, L.E. (1971); "Metallographic Polishing by Mechanical Methods" (Pitman, Melbourne; 2nd ed., 1971).
Schlosser, H.; 1970, Phys. Rev. B1, 491.
Schmidt, B.F., Lynch, D.W.; 1971, Phys. Rev. B3, 4015.
Schulz, D., Zurheide, M.; 1968, Z. Physik 211, 165.
Schulz, L.G.; 1957, Adv. Phys. 6, 102.

Schulz, H. (1928); in "Handbuch der Experimentalphysik" (ed. W. Wien, F. Harms; Akademische Verlagsgesellschaft, Leipzig; 1928), Vol. XVIII, p. 365.

Scouler, W.J.; 1967, Phys. Rev. Letters 18, 445.

Seraphin, B.O. (1970); in Haidemenakis (1970), p. 213.

Seraphin, B.O.; in Abelès (1972), p. 163.

Seraphin, B.O. (1973); Proceedings of the First international Conference on Modulation Spectroscopy, Tucson, Arizona, Nov. 1972; 1973, Surface Sci. 37, to be published.

Sham, L.J., Ziman, J.M.; 1963, Solid State Phys. 15, 221.

Sherring, C.W.; 1970, thesis, University of Exeter.

Shirley, D.A.; 1972a, Phys. Rev. B5, 4709.

Shirley, D.A. (editor) (1972); "Electron Spectroscopy" (North-Holland, Amsterdam; 1972).

Shkliarevskii, I.N., Yarovaya, R.G.; 1966, Opt. and Spectroscop. 21, 115.

Shurcliff, W.A. (1962); "Polarized Light" (Harvard University Press, Cambridge; 1962).

Sidran, M., Stalzer jr., H.J., Hauptman, M.H.; 1969, Appl. Optics 5, 1133.

K.Siegbahn et al. (1967); "ESCA" (Almqvist & Wiksell, Uppsala; 1967).

Simon, I.; 1951, J. Opt. Soc. Am. 41, 336.

Sissingh, R.; 1885, Comm. Lab. Phys. Leiden 1, 3.

Smith, N.V.; 1969a, Phys. Rev. 183, 634.

Smith, N.V., Spicer, W.E.; 1969b, Opt. Commun. 1, 157.

Smith, N.V.; 1970, Phys. Rev. B2, 2840.

Smith, N.V.; 1971, Phys. Rev. B3, 1862.

Smith, N.V.; 1972a, Phys. Rev. B5, 1192.

Smith, N.V., Traum, M.M.(1972b); in Shirley (1972), p. 541.

Snouse, T.W.; 1965, Rev. Sci. Instrum. 36, 866.

Snow, E.C.; 1968, Phys. Rev. 172, 708.

Sokolov, A.V. (1967); "Optical Properties of Metals" (Blackie, London; 1967).

Sommers, C.B., Amar, H.; 1969, Phys. Rev. 188, 1117.

Spicer, W.E. (1972); in Abelès (1972), p. 755.

Stahl, R., Spranger, H.-J., Aubauer, H.-P.; 1969, Z. Metallkde 60, 933.

Stanford, J.L.; 1970, J. Opt. Soc. Am. 60, 49.

Steel, M.R.; 1971, Appl. Optics 10, 2370.

Steel, M.R., Treherne, D.M.; 1972a, J. Phys. F2, 199.

Steel, M.R.; 1972b, J. Phys. F2, 605.

Stern, F.; 1963, Solid State Phys. 15, 299.

Stern, E.A.; 1967, Phys. Rev. 162, 565.

Stokes, J., Shen, Y.R., Tsang, Y.W., Cohen, M.L., Fong, C.Y.; 1972, Phys. Letters 38A, 347.

Stratton, J.A. (1941); "Electromagnetic Theory" (McGraw-Hill, New York; 1941).

Streiff, M.L., Ferriso, C.C.; 1965, Appl. Optics 4, 1668.

Suffczyński, M.; 1964, Phys. Stat. Sol. 4, 3.

Swindell, W.; 1968, Appl. Optics 7, 943, 1455.

Szczepanek, P.S., Beaglehole, D.; 1971, Bull. Am. Phys. Soc. 16, 636.

Taft, E.A., Philipp, H.R.; 1961, Phys. Rev. 121, 1100.

Tauc, J. (editor) (1966); "The Optical Properties of Solids" (Academic, New York; 1966).

Theye, M.-L.; 1970, Phys. Rev. B2, 3060.

Tousey, R.; 1939, J. Opt. Soc. Am. 29, 235.

Van Baarle, C.; 1967, Physica 33, 424.

Van Cittert, P.H.; 1923, Rev. d'Opt. 2, 57.

Van Cittert, P.H.; 1926, Z. Instrumentenkde 46, 557.

Van Heel, A.C.S. (1950); "Inleiding in de Optica" (Nijhoff, The Hague; 3rd.ed., 1950).

Velický, B.; 1961, Czech. J. Phys. B11, 787.

Verch, J., Schley, U.; 1967, PTB-Mitteil. 77, 371.

Verkuyl, J.A.G., Lengkeek, H.P., Winsemius, P.; 1973, J. Phys. E6, 322.

De Vos, J.C.; 1954, Physica 20, 669, 690.

Walldèn, L.; 1970, Phil. Mag. 21, 571.

Walldèn, L., Gustafsson, T.; 1972, Physica Scripta 6, 73.

Watson, R.E., Ehrenreich, H., Hodges, L.; 1970, Phys. Rev. Letters 24, 829.

Weiss, D.E., Muldawer, L.; 1972, Bull. Am. Phys. Soc. 17, 367 (abstract only).

Welkowsky, M., Braunstein, R.; 1971, Solid State Comm. 9, 2139.

Willardson, R.K., Beer, A.C. (editors) (1972); "Semiconductors and Semimetals, Volume 9: Modulation Techniques" (Academic, New York; 1972).

Williams, A.R., Janak, J.F., Moruzzi, V.L.; 1972, Phys. Rev. Letters 28, 671.

Winsemius, P., Lengkeek, H.P.; 1973a, Rev. Sci. Instrum. 44, 229.

Winsemius, P.; 1973b, to be published.

Wooten, F. (1972); "Optical Properties of Solids" (Academic, New York; 1972).

Worthing, A.G.; 1926, J. Opt. Soc. Am. 13, 635.

Yarovaya, R.G., Shkliarevskii, I.N.; 1965, Opt. and Spectrosc. 18, 465.

Yoshida, S., Yamaguchi, T., Kinbara, A.; 1971, J. Opt. Soc. Am. 61, 62, 463.

Young, C.-Y.; 1969, J. Phys. Chem. Solids 30, 2765.

Young, F.W., Wilson, T.R.; 1961, Rev. Sci. Instrum. 32, 559.

Ziman, J.M. (1960); "Electrons and Phonons" (Oxford University, London; 1960).

Ziman, J.M.; 1961a, Adv. Phys. 10, 1.

Ziman, J.M.; 1961b, Phys. Rev. 121, 1320,

Ziman, J.M. (1965); "Principles of the Theory of Solids" (Cambridge University, Cambridge; 1965).

Zwerdling, S., Theriault, J.P.; 1961, Spectrochimica Acta 17, 819.

Samenvatting.

Het kennen van de energieniveaus van elektronen is van fundamenteel belang voor het begrijpen van de eigenschappen van metalen. Berekeningen van de bandenstruktuur van de edele metalen Cu, Ag en Au worden veelal getoetst met behulp van gegevens uit optische metingen (dielektrische konstante, fotoemissie, modulatie experimenten). Van bijzonder belang zijn in dit verband de breedte en plaats (ten opzichte van de Fermi energie) van de *d* banden en de energieniveaus van de geleidingsbanden bij symmetrie punten binnen de Brillouin zone. Uit bandenberekeningen is gebleken dat vooral de energieverschillen tussen de laagste geleidingsbanden bij L (relativistisch: $L_{4-} \rightarrow L_{4+}$; niet relativistich: $L_{2'} \rightarrow L_1$) uitermate gevoelig zijn voor veranderingen in de kristalpotentiaal.

Het door ons beschreven onderzoek van de temperatuur-afhankelijkheid van de optische eigenschappen is gericht geweest op het bepalen van dit soort veranderingen ten gevolge van uitzetting van het rooster. De hiermee korresponderende verschuivingen in de absorptiespektra, ε_2/λ - vs. - $\hbar\omega$, zijn vaak zeer klein. Het bleek echter dat de effekten duidelijk naar voren komen in een analyse van het verschil tussen statische spektra zoals gemeten bij temperaturen T_1 en T_2: $[\varepsilon_2(T_2) - \varepsilon_2(T_1)]/(T_2 - T_1)$ - vs. - $\hbar\omega$. Deze "thermovariatie" spektra vertonen een bijzonder goede overeenstemming met resultaten verkregen uit thermomodulatie metingen. Deze modulatie experimenten moeten in verband met de noodzakelijke geringe warmtekapaciteit worden verricht aan dunne opgedampte laagjes, waardoor de hoogste bereikbare temperatuur ongeveer 400 K is. Tevens is voor de uitwerking van de resultaten kennis vereist van de statische spektra. De door ons beschreven thermovariatie-analyse biedt daarom belangrijke voordelen. Een absolute noodzaak voor het waarnemen van de kleine effekten is echter een geperfektioneerde apparatuur. Met name de toevallige fout - d.w.z. de spreiding in de meetresultaten - dient zoveel mogelijk beperkt te worden. De uitgebreide beschrijving in het laatste hoofdstuk van de hoofdlijnen en de foutenbronnen in dit soort experiment zal - naar wij hopen - de taak verlichten van andere onderzoekers van de optische eigenschappen van metalen.

De belangrijkste resultaten beschreven in dit proefschrift kunnen als volgt worden samengevat.

(1) De sterke stijging van de interband-absorptie in Au tussen 2.4 en 3.2 eV - de z.g. absorptiekant ("absorption edge") - wordt bij lage temperaturen "gesplitst". Deze splitsing kan wellicht worden verklaard uit een superpositie van een parabolisch deel (t.g.v. lokale overgangen van de hoogste d band bij L naar de laagste geleidingsband) op een vrij struktuurloze achtergrond (t.g.v. overgangen in uitgestrekte delen van de Brillouin zone). Deze verklaring vindt (geeft) steun bij (aan) vroegere pogingen tot verklaring van de absorptiekant (o.a. Cooper, Ehrenreich en Philipp (1965)).

(2) Zeer verrassend in de thermovariatie spektra van Ag is de afwezigheid van enige struktuur die zou worden veroorzaakt door overgangen van de d band naar het Fermi niveau. Algemeen wordt aangenomen dat de absorptiekant in Ag vooral het gevolg is van dergelijke overgangen dicht bij L; een verbreding van de Fermi verdeling zou voor deze lokale overgangen moeten resulteren in een nadrukkelijke thermovariatie-struktuur. Mogelijk dient daarom te worden gedacht aan absorptie ten gevolge van overgangen in uitgestrekter delen van de Brillouin zone.

(3) De absorptie struktuur ten gevolge van overgangen tussen de laagste geleidingsbanden bij L kan in Au, Ag en ook Cu goed beschreven worden met behulp van het z.g. "box" model. Hoewel de gevonden waarden voor het energieverschil bij de overgang $L_{4-} \rightarrow L_{4+}$ voor Cu en Ag (bij 295 K resp. 4.81 eV en 4.11 eV) in goede overeenstemming zijn met gepubliceerde resultaten, is de waarde in het geval van Au aanzienlijk hoger (4.20 eV) dan in het algemeen op grond van experimenten en relativistische berekeningen wordt voorgesteld. Voor temperaturen boven 300 K neemt het energieverschil $L_{4-} \rightarrow L_{4+}$ voor alle drie metalen af met ongeveer -8×10^{-4} eV/K. Uit de bijdrage van de intergeleidingsband-absorptie tot ε_2/λ blijkt voorts dat zowel in Au als in Ag het niet toegestaan is de overgangsmatrixelementen konstant te veronderstellen.

Studieoverzicht.

september 1960: aanvang studie te Leiden.
juni 1963: kandidaatsexamen natuur-en wiskunde met bijvak scheikunde (d').
oktober 1963: aanvang van de werkzaamheden in de werkgroep Mt-IV (leiding: Prof. dr C.J. Gorter, dr. G.J. van den Berg) van de werkgemeenschap "Metalen F.O.M. - T.N.O."; assistentie van dr. C. van Baarle bij het onderzoek betreffende de thermospanning en de warmtegeleiding van metaallegeringen.
zomer 1965: aanvang van een literatuur onderzoek betreffende de optische eigenschappen van metalen en legeringen.
september 1966: doktoraal examen experimentale natuurkunde; aanvang van experimenteel onderzoek betreffende de optische eigenschappen van metalen.
december 1970: eerste metingen van optische eigenschappen van Au.
vanaf oktober 1965: assistentie bij diverse natuurkunde praktika.

Velen hebben bijgedragen aan het tot stand komen van dit proefschrift. Dank is verschuldigd aan drs. J.G. Smits, drs. F.F. van Kampen, drs. H.P. Lengkeek en C.G. van Went voor samenwerking en vriendschap tijdens de lange - soms donkere - dagen van voorbereiding en uitvoering van de experimenten. Evenzo zij gememoreerd de vooral ook morele steun en het ondervonden vertrouwen van dr. G.J. van den Berg en de stimulerende invloed van dr. C. van Baarle, dr. J.B. Diamond en dr. W.M. Star. Bijdragen van de "theoretici" drs. S.N.M. Ruysenaars, R. Houtappel en drs. C.P. Louwerse waren onmisbaar bij het opstellen van computerprogramma's.

Het is niet doenlijk al degenen te noemen die hebben bijgedragen tot de ontwikkeling van de apparatuur. Bewondering heb ik steeds gehad voor de kreativiteit en de positieve instelling van de heren H.R.A. Nater, J. Turenhout, H. van Zanten en J.A.G. Verkuyl: vakmanschap is meesterschap. De medewerking van vele leerlingen van de Leidse Instrumentmentmakers School was onontbeerlijk. De preparaten werden vervaardigd door de heren C.E. Snel, H.J. Tan en T.J. Gortenmulder.

In een gebied van onderzoek, dat "nieuw" is voor het Kamerlingh Onnes laboratorium, is het kontakt met "buitenlandse" kollega's van groot belang geweest. Speciaal de hulp van dr. P. de Chatel (Universiteit van Amsterdam), dr. N. Egede Christensen (Technical University of Denmark, Lyngby) en dr. G.P. Pells (A.E.R.E., Harwell) was van grote waarde.

Veel respect heb ik voor de inzet en de zorg bij het vervaardigen van de tekeningen door de heer W. Brokaar en bij het typewerk door mevr. E. de Haas-Walraven (Inzendbureau Knollenland). Het fotografische werk werd verzorgd door de heer W.F. Tegelaar.

Ik dank mijn gezin en mijn ouders voor de betrokkenheid en de stimulans, die het klimaat hebben geschapen om het werk - beschreven in dit proefschrift - te voltooien.